

**Wet chemical deposition of transparent conducting
coatings made of redispersable crystalline ITO
nanoparticles on glass and polymeric substrates**

Dissertation

zur Erlangung des Grades

des Doktors der Ingenieurwissenschaften

der Naturwissenschaftlich- Technischen Fakultät III

Chemie, Pharmazie und Werkstoffwissenschaften

der Universität des Saarlandes

Vorgelegt von

Naji Al-Dahoudi

Saarbrücken

2003

Gedruckt mit Unterstützung des Deutschen Akademischen Austauschdienstes

Tag des Kolloquiums: 18.07.2003
Dekan: Professor Dr. Horst Vehoff
Berichterstatter: Professor Dr. Michel A. Aegerter
Berichterstatter: Professor Dr. Wulff Possart
Vorsitzender: Professor Dr. Michael Veith
Beisitzer Dr. Andreas Rammo

Acknowledgment

I want to express my gratitude to all people who supported my work for this thesis. Most important of course Prof. Dr. M. A. Aegerter who continuously encouraged and supported this work and who provided intensive supervision, valuable suggestion and good proof reading of my thesis.

I am most grateful to the Deutsche Akademische Austauschdienst (DAAD) for the financial support of my study and stay in Germany.

I am very grateful to all my colleagues at the Institute für Neue Materialien (INM), Christian Göbbert, Harish Bisht, Dr. J. Pütz and Dr. S. Heusing who were always willing to help and discuss. The atmosphere has always been a perfect source of motivation. Special thanks for Mrs. M. Bonnard who helped me during many difficult times.

I would also like to thank Dr. T. Krajewski and Dr. D. Hoebbel who made interesting characterizations and fruitful discussions.

I want to thank my wife Nisreen for her patience, understanding and continuous support during all the years of my study. This enabled me to concentrate on the work for this thesis. I could not forget my children Momen, Hanin and Mazen who were the mainspring of this work.

Last but not the least, I shall remain indebted to my parents, brothers and sisters for their love and constant care during my life.

List of abbreviations:

a.u.	arbitrary units
AES	Auger Electron Spectroscopy
AFM	Atomic Force Microscopy
Aq.	aqueous solution
ASTM	American Standard Method
at. %	atomic per cent
BET	Brunauer-Emmett-Teller
CVD	Chemical Vapor Deposition
DBG	Diethyleneglycole-monobutylether
DIN	Deutsche Industrie Norm
DTA	differential thermal analysis
e.g.	exempli gratia (for instance)
ED	electron diffraction
EDX	Energy Dispersive X-ray
EG	ethylene glycole
ESCA	Electron Spectroscopy for Chemical Analysis
et al.	et alli (and others)
etc.	et cetera
EXAFS	Extended X-ray Absorption Fine Structure
Fig.	Figure
FTIR	Fourier Transform Infrared
FWHM	full width of half maximum
GIXR	Grazing Incidence X-ray Reflectivity
GPTS	3-Glycidoxypropyltrimethoxysilane
HRTEM	High Resolution Transmission Electron Microscopy
i.e.	Idest
IBSCA	Ion Beam Spectrochemical Analysis
IR	Infrared
ITO	indium tin oxide
JCPDS	Joint Committee on Powder Diffraction Standards
LC	laser calorimetry
Min.	minute
MPTS	3-methacryloxy propyltrimethoxysilane
NMR	Nuclear Magnetic Resonance
NRA	Nuclear Reaction Analysis
PC	polycarbonate

PE	polyethylene
PET	polyethylene terephthalate
PMMA	polymethyl methacrylate
ppm	part per milion
PTD	Photothermal Deflection techniques
PVC	polyvinyl chloride
RBS	Rutherford Back Scattering
Ref.	Reference
RT	room temperature
SAXS	Small Angle X-ray Scattering
SEM	Scanning Electron Microscopy
SIMS	Secondary Ion Mass Spectroscopy
SNMS	Secondary Neutral Mass Spectroscopy
TDOS	3,6,9- Trioxadecanoic acid
TEOS	tetraethoxysilane
TG	thermo gravimetry
UPA	ultrafine particle analyzer
UV	ultra violet
UV-VIS-NIR	ultra violet-visible-near infrared
VASRA	Variable Angle Specular Reflectance Accessory
vol. %	volume per cent
WDX	Wavelength Dispersive X-ray
WLI	White Light Interferometer
wt.%	weight percent
XRD	X-Ray Diffraction
XRF	X-Ray Fluorescence

List of symbols and units :

Symbol	Meaning	Units
α	absorption coefficient	cm^{-1}
σ	conductivity	$(\Omega.\text{cm})^{-1}$
ρ	density	g/cm^{-3}
ε	dielectric constant	
m^*	effective mass	g
e	electric charge	C
ρ	electrical resistivity	$\Omega.\text{cm}$
E_g	energy gap	eV
Φ	Figure of merit	Ω^{-1}
μ	mobility	$\text{cm}^2/\text{V.s}$
h	Planck constant	J.s
R	reflectance	%
R_{\square}	sheet resistance	Ω_{\square}
γ	surface tension	mN/m
σ	surface energy	mN/m
h	thickness	nm
T	transmission	%
η	viscosity	Pa.s
λ	wavelength	nm
ϕ	work function	eV
ζ	Zeta potential	volt
ω	angular frequency	Hertz (Hz)
A	absorbance	%
n	concentration of charge carriers	cm^{-3}
T	temperature	$^{\circ}\text{C}$
t	time	s
v	velocity	cm/s

Abstract

Stable suspension made of fully redispersable $\text{In}_2\text{O}_3:\text{Sn}$ (ITO) conducting nanoparticles were developed to obtain single thick transparent conducting films (up to 500 nm) on different substrates using wet chemical deposition methods. The coatings can be processed at high sintering temperature process on glass substrates up to 1000 °C to get electrical resistivity as low as $1.7 \times 10^{-3} \Omega \cdot \text{cm}$ and transmit more than 87 % of the visible spectrum. The processing of transparent conductive coatings on polymeric (PC, PMMA, PVY, PE, PET, foils, etc.) and glass substrates at low processing temperature was realized by using a modified ITO suspension in which a polymerisable inorganic-organic binder was added. The coatings can be cured by UV-irradiation and / or by a low temperature heat treatment ($T < 130 \text{ °C}$) in air or reducing atmosphere. The electrical, optical, textural, mechanical and surface properties of the coatings are reported. Transparent conducting coatings with a single 570 nm thick layer exhibiting stable electrical resistivity of $9.2 \times 10^{-2} \Omega \cdot \text{cm}$ have been made by spin and dip coating process. A high transmission of about 87 % is observed in the visible range. The adhesion and the abrasion resistance of the coatings pass the DIN or ASTM tests: DIN 58196-K2, ASTM D 3359, DIN 53151-Gt0, DIN 58196-G10 and DIN 58196-H25 and the hardness measured using the Pencil test ASTM D 3363-92a is 1H. UV-irradiation through a mask allows to easily pattern the coatings.

Eine stabile Suspension, die aus völlig redispersierbaren nanokristallinen $\text{In}_2\text{O}_3:\text{Sn}$ (ITO) leitfähigen Teilchen besteht, wurde hergestellt und entwickelt, um dicke transparente leitfähige Einzelschichten (bis zu 500 nm) auf unterschiedlichen Substraten mittels naß-chemischen Abscheidungsverfahren zu erhalten. Die Schichten können bei hohen Temperaturen (bis 1000 °C) auf Glassubstraten abgeschieden werden, um einen spezifischen Widerstand von $1.7 \times 10^{-3} \Omega \cdot \text{cm}$ erzeugen und um mehr als 87 % des sichtbaren Spektrums zu übertragen. Die Entwicklung von transparenten leitfähigen Schichten auf unterschiedlichen Kunststoffsubstraten (PC, PMMA, PVC, PE, PET, Folien, etc.) bei niedriger Bearbeitungstemperatur wird realisiert, indem man die ITO-Suspension durch die Zugabe von polymerisierten Bindemitteln modifiziert. Die Schichten werden durch UV-Strahlung und/oder durch niedrige thermische Behandlung ($T < 130 \text{ °C}$) in Luft oder in reduzierender Atmosphäre gehärtet. Berichtet wird über die elektrischen, optischen, morphologischen, mechanischen und Oberflächen-Eigenschaften der Schichten. Der Flächenwiderstand der Schichten ist stark abhängig von der UV-Behandlung und der Reduzierung unter Formiergas. Als bester Wert wurde der niedrigste beständige spezifische Widerstand von $\rho = 9 \times 10^{-2} \Omega \cdot \text{cm}$ gefunden. Die Transmission der Schichten im sichtbaren Bereich liegt bei 87%. Die Schichten zeigten gute Haftung und gute Beständigkeit gegen Abrieb nach DIN 58196-K2, ASTM D 3359, DIN 53151-Gt0, DIN 58196-G10 and DIN 58196-H25 und Härte 1H nach ASTM D 3363-92-a. Mittels UV-Strahlung durch eine Maske können die Schichten leicht strukturiert werden.

Zusammenfassung

Bei der Kontrolle der Oberflächenmodifizierung und dem Wachstumsprozess wurden leitfähige kristalline Zinn-dotierte Indium-Oxid (ITO) Partikel erfolgreich hergestellt. Die Partikel sind hochdicht, ihre Größe wächst mit den Sintertemperaturen, und sie haben eine Teilchengröße von 20-35nm.

Die Pulver, die bei Temperaturen niedriger als 350 °C gesintert werden, sind erfolgreich in Wasser oder organischen Lösungsmitteln wie Ethanol redispergiert worden. Die Beschichtungssole, die aus diesen Partikeln bestehen, sind über ein Jahr stabil. Die Partikelgrößenverteilung ist monomodal, und die Teilchengröße der Partikel betrug 15-40 nm. Die Zugabe von anorganisch-organischen Bindern wie MPTS verschiebt die Partikelgrößenverteilung zu einem höheren Wert, allerdings sind die hergestellten Sole noch stabil.

Die stabile Suspension, die aus völlig redispergierbaren nanokristallinen $\text{In}_2\text{O}_3:\text{Sn}$ (ITO) leitfähigen Teilchen besteht, wurde verwendet, um dicke transparente leitfähige Einzelschichten (bis zu 500 nm) auf unterschiedlichem Glas oder polymetrischen Substraten mittels naß-chemischen Abscheidungsverfahren herzustellen. Die Dicke der Schichten nimmt bei Zunahme des Feststoffanteils der Teilchen in dem Sol zu, da auch die Viskosität in dem Sol zunimmt. Die TEOS, GPTS oder MPTS modifizierten ITO-Sole produzieren dickere Schichten.

Die aus reiner ITO-Suspension hergestellten Schichten können bei hohen Temperaturen (bis 1000 °C) auf Glassubstraten abgeschieden werden. Die Schichten zeigen eine Abnahme des spezifischen Widerstandes mit der Zunahme der Ausheiztemperatur. Der spezifische Widerstand nimmt von $4.8 \times 10^{-2} \Omega \cdot \text{cm}$ (550°C) auf $1.2 \times 10^{-2} \Omega \cdot \text{cm}$ (1000°C) ab. Durch eine nachträgliche Reduzierung unter Formiergas bei 350°C kann der spezifische Widerstand noch weiter bis auf $1.5 \times 10^{-3} \Omega \cdot \text{cm}$ reduziert werden. Die Sintertemperatur führt zu besserem Kontakt zwischen den leitfähigen Partikeln und zur Abnahme der Porosität der Schichten. Die Schichten übertragen mehr als 88 % des sichtbaren Spektrums und zeigen Reflexion bis 70 % im IR-Bereich.

Die Entwicklung von transparenten leitfähigen Schichten auf unterschiedlichen Kunststoffsubstraten (PC, PMMA, PVC, PE, PET, Folien etc.) bei niedriger Bearbeitungstemperatur wird realisiert, indem man die ITO-Suspension durch die Zugabe von polymerisierten Bindemitteln modifiziert. Die Schichten werden durch UV-Bestrahlung

und/oder durch niedrige thermische Behandlung ($T < 130\text{ °C}$) in Luft oder in reduzierender Atmosphäre gehärtet. Der Flächenwiderstand der Schichten ist stark abhängig von der UV-Behandlung und der Reduzierung unter Formiergas.

Bei der Untersuchung verschiedener organischer oder organisch-anorganischer Bindemittel zeigte sich, daß die funktionalisierten Silane, besonders 3-Methacryloxypropyltrimethoxysilane(MPTS), zur Verbindung guter elektrischer und mechanischer Eigenschaften der Schichten auf Kunststoffsubstraten am besten geeignet sind. Als bester Wert wurde der niedrigste beständige spezifische Widerstand für eine 570 nm dicke Einzelschicht von $\rho = 9 \times 10^{-2}\ \Omega\text{cm}$ gefunden.

Die FTIR- und NMR Spektroskopie von MPTS/ITO-Schichten zeigt, dass die UV-Behandlung zu besseren und homogeneren Verbindungen zwischen den leitfähigen Teilchen führt. Neben dem Polymerisationsprozeß von MPTS beeinflusst die UV- und reduzierende Behandlung die Konzentration des chemisorbierten Sauerstoffs auf der Oberfläche der ITO-Partikel, die als freie Elektronenfallen dienen. Dieses führt zu einer Zunahme der Ladungsträgerdichte und infolgedessen zu einer Verringerung des spezifischen Widerstandes.

Die Transmission der Schichten auf polymerischen Substraten liegt im sichtbaren Bereich bei 87%, und die Reflexion der Schichten betrug 40 % im IR-Bereich. Die Schichten zeigten gute Haftung und gute Beständigkeit gegen Abrieb nach DIN 58196-K2, ASTM D 3359, DIN 53151-Gt0, DIN 58196-G10 and DIN 58196-H25 und Härte 1H nach ASTM D 3363-92-a. Mittels UV-Bestrahlung durch eine Maske können die Schichten leicht strukturiert werden.

Table of Contents

Acknowledgment	I
List of abbreviations	II
List of symbols and units	III
Abstract	V
Zusammenfassung	VI
1 Objective	1
2 Fundamental	3
2.1 Thin film technology	3
2.1.1 Properties of thin films	3
2.1.2 Substrate Cleaning.....	5
2.2 Deposition techniques	6
2.2.1 Vapor deposition techniques.....	6
2.2.2 Wet chemical deposition techniques	8
2.3 Transparent conducting coatings	14
2.4 Transparent conducting oxides (TCO)	15
2.4.1 Transparent semiconducting materials	15
2.4.2 Electrical properties.....	18
2.4.3 Optical properties.....	21
2.4.4 Application of transparent conducting oxides	25
2.5 Coatings deposited at low temperature	28
2.6 Nanostructured materials technology	30
2.6.1 Introduction	30
2.6.2 Synthesis of Nanomaterials via Sol-Gel Technology.....	31
2.6.3 Colloidal suspension.....	33
3 TCO coatings: state of the art	35
3.1 Transparent conducting coatings on Glass substrates	35
3.1.1 Vapor deposition of TCO coatings on glass.....	35
3.1.2 Wet chemical deposition of TCO on glass	38
3.2 Transparent conductive coatings on plastic substrates (low temperature)	41
3.2.1 Physical deposition	42
3.2.2 Wet chemical deposition of TC coatings on plastics.....	44

4	Experimental methodology and procedure	46
4.1	Preparation of conducting ITO nanopowders	46
4.2	Preparation of ITO coating solution	47
4.2.1	Pure ITO sol	47
4.2.2	Modified ITO sols	47
4.3	Deposition methods	48
4.3.1	Coatings on glass	48
4.3.2	Coatings on polymeric substrates	48
4.4	Post-treatment of the coatings	49
4.4.1	Heat treatment	49
4.4.2	UV-irradiation	49
4.4.3	Plasma treatment	50
4.4.4	Combination of treatments	50
4.5	Shelf life under different atmospheres	50
4.6	Patterning of ITO coatings	50
4.7	Conclusion	51
5	Results and discussions	52
5.1	Structural and physical properties of ITO powders	52
5.1.1	Phase structure (XRD)	52
5.1.2	Particle density and specific BET surface area	54
5.1.3	Conclusion	56
5.2	Characterization of the coating sols	56
5.2.1	Zeta potential	56
5.2.2	Sol morphology (TEM)	57
5.2.3	Particle size distribution (UPA)	59
5.2.4	Rheology	59
5.2.5	Thermal analysis (DTA/TG)	60
5.2.6	Stability of the coating sols (Liquid-NMR-Spectroscopy)	61
5.2.7	Conclusion: sol characterization	64
5.3	Coating thickness	65
5.3.1	Dip coated ITO films	65
5.3.2	Spin coated ITO films	67
5.3.3	Conclusion	68
5.4	Transparent conducting coatings deposited on glass substrates	68

5.4.1	Structural and morphological Properties	68
5.4.2	Electrical properties	70
5.4.3	Optical properties.....	78
5.4.4	Mechanical properties.....	83
5.4.5	Conclusion	84
5.5	Transparent conducting coating cured at low temperature.....	85
5.5.1	Microstructure of the coatings (XRD).....	85
5.5.2	Electrical properties	85
5.5.3	Coatings on other polymeric substrates.....	90
5.5.4	Time evolution of the electrical properties	92
5.5.5	Optical properties.....	96
5.5.6	FTIR spectroscopy.....	99
5.5.7	Solid-state NMR spectroscopy	102
5.5.8	Structural and morphological properties	103
5.5.9	Mechanical properties.....	107
5.5.10	Conclusion	111
5.6	Patterning ITO coatings with a low temperature process.....	112
5.7	Surface properties	113
5.7.1	Work function.....	113
5.7.2	Contact angle and surface energy	115
5.7.3	Conclusion	118
6	Summary and Conclusion	119
	Appendices	122
	A. Methods of Characterization.....	122
	A.1 Powder and Suspension	122
	A.1.1. Crystalline phase and crystallite size	122
	A.1.2. Particles density and specific BET surface area.....	122
	A.1.3. Hydrodynamic size distribution	123
	A.1.4. Morphology of the suspension	123
	A.1.5. Thermal analysis (DTA/TG).....	123
	A.1.6. Zeta potential measurements.....	123
	A.1.7. Viscosity.....	124
	A.1.8. Liquid NMR-Spectroscopy	124
	A.2 Coatings procedure	125
	A.2.1 Cleaning of the substrates.....	125

A.2.2 Coatings methods	125
A.3 Coatings characterization	126
A.3.1 Film thickness.....	126
A.3.2 Electrical properties.....	126
A.3.3 Optical properties	128
A.3.4 Structural and morphological properties	128
A.3.5 Mechanical properties	130
A.3.6 Surface properties.....	131
B List of used chemicals	132
C List of equipments	133
D XRD spectrum	135
E FTIR spectroscopy	135
F NMR spectroscopy	137
G Topography and morphology of the coatings.....	138
H Patterning of ITO coatings.....	139
References	140
List of Publications	156

Chapter 1

Objective

Nanomaterials are defined by a length scale of less than 100 nm, either in one dimension (thin films), two dimensions (nanowires) or in 3 dimension (nanoparticles). This thesis is focused on the production and characterization of transparent conducting coatings using sol-gel made tin doped indium oxide nanoparticles dispersed in a solvent. It shows how nanomaterial properties can be tailored by either size effect or via the modification of the surface of the nanoparticles.

In general, coatings made by the sol-gel technique need to be calcined at high temperature (usually above 400 °C), a process not adequate for many substrate materials. In addition, the film thickness obtained by this method in a single step is usually very small (< 100 nm), so that multicoating process involving the sequence “deposition – drying - sintering”, should be repeated several times in order to obtain a thickness adequate to obtain certain properties. This makes the procedure very complicated and not interesting for many industrial applications.

One of the aim of this work was to develop a technique to produce thick transparent conductive film in a single step using sol-gel deposition methods on different glass substrates. The basic idea to solve this task was to prepare stable sols containing a high amount of dispersed crystalline indium tin oxide (ITO) conducting nanoparticles. Such particles have been made using the so-called controlled growth technique and redispersed using a dispersant agent in a solvent like alcohol or water to obtain highly stable suspension. This suspension was used as the coating solution to produce transparent conductive coatings with thickness up to 600 nm in a single step procedure. The properties of the particles and sols have been studied as a function of the crystallite size and the doping concentration.

To obtain good electrical, optical and mechanical properties, the coatings were heated up to 550 °C (borosilicate glass) and up to 1000 °C (fused quartz). The structural, electrical, optical and mechanical properties of the densified coatings at different sintering temperatures have been characterized.

The second aim of this work was to find a way to deposit such coatings on substrates which don't withstand a heat treatment step at high temperature, such as polymeric substrates (PC, PMMA, PVC, PET, foils) and already preformed glasses.

The basic idea to solve this task was to modify the above coating solution by blending the ITO particles with an inorganic-organic hybrid matrix which can be polymerized at low temperature ($T < 130$ °C) or by UV-irradiation. The properties that such modifier should offer are:

1. Adsorption on the surface of the ITO particles at low temperature without affecting the stability of the suspension.

2. Low temperature polymerization to bring the particles in contact together with a high degree of organic cross linking, which encapsulate the conducting particles.
3. The polymerization and the condensation at low temperature should also enhance the adhesion of the particles to the substrate and improve the mechanical resistance of the coatings.
4. The concentration of the modifiers in the coating solution should be low enough to prevent the formation of very large agglomerates in the deposited film and have the lowest possible effect on the optical quality and the electrical properties of the coatings.

Patterning such coatings on polymeric and glass substrate at low temperature process was the third aim of this work. The coatings were patterned by selective UV irradiation through a mask. The exposed part strongly adheres to the substrate and the non-exposed part is easily washed in ethanol.

The structural, electrical, optical, mechanical and surface properties of the transparent conductive films and the patterns have been studied and the different parameters affecting the deposition, the curing processes and the properties have been determined and discussed.

Chapter 2

Fundamental

2.1 Thin film technology

In recent years the thin films technology has grown world-wide into a major research area. The importance of coatings and the synthesis of new materials for the industry have also resulted in a tremendous increase of innovative thin film processing technologies. Coatings today serve important roles in many applications, including microelectronics (1), catalysis (2), corrosion protection (3), and chemical sensors (4), displays, etc.

A thin film is a two dimensional material created ab initio by the process of condensation and growth of atoms, molecules or ions (5). Their properties are usually different from those of corresponding bulk materials due to their physical dimension, geometry and microstructure. They are largely affected by the high surface-to-volume ratio and influence a number of phenomenas such as gas adsorption, diffusion, and catalytic activity.

The substrate material has also a significant effect and many factors should be taken into consideration (6). For example, the cleaning, the surface energy and the roughness of the substrate affect decisively the adhesion of the film on the substrate. Also the stability of the substrate with the temperature variations as well as at the different aging processes affect their properties. The crystal structure, strength and the internal tension of the substrate material should be taken into account before the deposition process.

Independent of the film material, the mechanical characteristics, optical properties, film thickness, etc of coatings are strongly influenced by the deposition parameters and conditions and are therefore strongly related to the coating technologies. To produce efficiently coatings for a certain application, it is necessary to know all the parameters that influence a desired film property during the deposition process. For example, for films produced by the sol-gel process (dip coating technique), the relevant parameters which must be taken into consideration are the composition of the solution, the withdrawing speed, the temperature, the interaction with the surrounding atmosphere during the withdrawal of the substrate and the reaction with the substrate during densification.

2.1.1 Properties of thin films

The properties of film can be divided into macroscopic and microscopic ones. Among the macroscopic properties are the refractive index, the optical absorption and reflection, the film thickness, the adhesion, the stress, the density, the scattering of light and the hardness. The microscopic quantities are the composition and chemical bonding between the elements, stoichiometry, topography, roughness of the surface, state and formation of interfaces, crystalline or amorphous state, and also the crystalline structure.

There are various analytical tools available to characterize these properties and some of them are summarized in Table 1 (the list of abbreviations is given at Page II). These characterization techniques use different probes such as photons, electrons, ions, and also forces as in Atomic Force Microscopy (AFM). These probes interact with the sample which then emits electrons, photons, ions, etc which are collected by a detector to give information to describe the film (7).

Table 1: Techniques used to characterise thin films

Film Properties	Characterization method
Macroscopic	
<i>Density</i>	GIXR, RBS
<i>Stress</i>	Bending
<i>Adhesion</i>	Tape test, Cutting
<i>Optical quantities</i>	UV-VIS-NIR Spectroscopy
<i>Hardness</i>	Scratching (Pencil test)
<i>Thickness</i>	TEM, SEM, Stylus
<i>Thermal conductivity</i>	PTD, LC
Microscopic	
<i>Composition</i>	
<i>-surface composition</i>	ESCA, AES, XPS
<i>-film composition</i>	EDX, WDX, RBS, NRA, XRF, SMNS, ESCA
<i>-interface composition</i>	TEM/EDX
<i>State of oxidation</i>	ESCA, AES, SIMS, Raman, EXAFS
<i>Structure and texture</i>	XRD, ED, FTIR, SAXS
<i>Roughness of surface</i>	AFM, GIXR, WLI
<i>Formation of interface</i>	TEM, GIXR
<i>Grain and crystalline size</i>	XRD, TEM
<i>Surface topography</i>	AFM, SEM, WLI, GIXR

The structural properties of the deposited films are very important. The arrangement of atoms in a material is determined by the strength and the directionally of the interatomic bonds. The arrangement of the atoms may be regular (crystalline) or irregular (polymeric or glassy). The degree of crystallinity of films can be determined precisely by X-ray and electron diffraction techniques. With electrons, one can investigate very thin layers. Electron diffraction method gives a better determination of hydrogen atoms or ions, which is not possible by x-ray diffraction (8).

The surface properties of thin films affect the quality of these films. Szanyi (9) have studied the origin of haze in CVD tin oxide thin films, where the surface quality of these films are of great importance in the production of solar control architectural glazing. The haze were correlated with the surface roughness and the concentration of internal voids. The surface

chemical composition, impurities concentration, roughness and defects can be determined using many techniques such as SEM, AFM, XPS, AES, UPS, SIMS etc.

The mechanical properties of films are affected by the growth process, structure, chemical composition and incorporated impurities. They are also influenced by the state of cleaning of the substrate. The state of stress of the films is also very important and is related to the structure and microstructure properties as well as to the substrate and the heat treatment. It can be measured using the bending-beam method. The obtention of crack-free layer depends on the thermal expansion of the film and substrate and is characterized by critical thickness, i.e. the maximum achievable thickness without crack formation for single step deposition. Additives incorporated to the sols help to increase the critical thickness of sol-gel coatings (10).

The adhesion and hardness of films are also important properties to be tested. The film density influences the hardness of the film. It is also important to test the influence of weathering (temperature, humidity) on the coatings. Humidity and salt water are of special importance in tropical areas and at sea level. All of these factors and tests should be taken into consideration.

The optical properties of thin films may drastically change the reflectance, transmission and absorption of the substrate. They are determined by measuring their optical constants, i.e the extinction coefficient and the refractive index and they depend strongly on the film thickness and the substrate surface conditions. The most common applications related with the optical properties are the antireflective coatings, reflection coatings, interference filters, beam splitters and waveguides (5).

2.1.2 Substrate cleaning

The cleaning of the surface of the substrate is a very important issue in thin film deposition technology. It is a difficult and delicate operation to achieve highly clean surface. The exposure of the substrate surface to the atmosphere generates gaseous, liquid or solid contaminations which should be removed before the deposition process. When the substrates are not clean, the deposited film will usually not adhere well and the desired film properties will be affected by the impurities on the surface of the substrate.

Different cleaning processes are used to remove the contaminations from the substrate surface. The most common methods are (8):

a- Cleaning with solvents: Various cleaning solvents are used, such as bidistilled water to which detergents, diluted acids or bases as well as non-aqueous solvents such as alcohols and ketones can be added. The type of the solvents to be used depends on the nature of the contaminants.

b- Rubbing and immersion cleaning: This method is considered as a precleaning operation. It is done by rubbing the surface with a cotton cloth or a brush dipped in a mixture of precipitated chalk or fine powder of CeO_2 or Al_2O_3 and alcohol or ammonia. The substrates

can be also immersed in acids with different strength, where a chemical reaction can be exploited for cleaning process.

c. Ultrasonic cleaning: This method is effective for breaking loose contaminants by ultrasonic waves propagating in a cleaning fluids.

A combination of several methods is usually used to achieve an optimum cleanliness of the substrate surface.

Cleaning of polymeric substrates requires special methods and handling because of their low thermal and mechanical stability. Proper cleaning fluids and short cleaning time should be carefully selected. Polymeric substrates can be also pretreated through the activation of their surface energy using corona, plasma or UV-irradiation (11-13).

2.2 Deposition techniques

The deposition techniques play a very important role to achieve desired film properties since the deposition of the same material by different deposition methods usually leads to different coating properties. Every method has its own advantages and disadvantages. The techniques can be broadly classified under two main categories:

- (1) Vapour deposition and
- (2) Wet chemical deposition

Each process has its own parameters which control the formation and the growth of the films. For a given material the microstructure and the morphology depend on the kinetics of the growth, the deposition rate, the deposition atmosphere and the substrate temperature. Producing thin films with specific and high quality properties needs an optimisation of the corresponding parameters. The most commonly used techniques for deposition of thin films are described below.

2.2.1 Vapor deposition techniques

Vapor deposition techniques can be classified into two main classes: (a) Physical vapor deposition (PVD) and (b) Chemical vapor deposition (CVD).

Physical Vapor Deposition (PVD)

These techniques have been described in details in many text books (see e.g (14)). The deposition of a vapor from a source onto a substrate takes place under low pressure conditions in a chamber. The creation of the vapor from a source can be achieved by thermal evaporation (Vacuum evaporation) or by bombarding (Sputtering) the surface of a target by high energetic particles, usually Ar^+ .

In thermal evaporation the source material is heated to a given temperature to obtain a vapor pressure of about 10^{-3} Torr and the vapor condenses onto a cooler substrate to form a film. The evaporation source can be made of a resistance-heated device, such as a tungsten wire, a metal sheet, a sublimation furnace, a crucible, or an electron beam evaporation device (7).

Activated reactive evaporation can be realized by introducing a gas or a plasma into the chamber during the evaporation. This method is characterized by a high evaporating rate and leads to better adhesion, a precise control of the stoichiometry and denser microstructure; however it usually needs a high substrate temperature (15). Various parameters control these techniques, such as substrate temperature, deposition pressure, chemical composition of the source, deposition rate and they are all important to optimize the film properties.

In sputtering processes the vapor is created by bombarding the surface of a solid material source (target) by energetic gas ions such as Ar^+ . The ejected atoms are condensed on a substrate to form a film. These methods can be classified into three main classes:

DC Sputtering: The target is the cathode and the substrate is the anode. The energetic ions are produced by a plasma ignited between the electrodes when a high dc voltage is applied between them. The sputtering chamber should be pumped down to high vacuum and then filled to about 10 to 100 Torr by a gas, usually Argon. This method is generally simple, relatively easy to use and good uniformity of the film thickness can be obtained over large area; however its use is confined to materials possessing a significant electrical conductivity, since insulators quickly lose their negative potential required for sputtering with positive ions (8).

RF Sputtering: A high frequency alternating voltage applied between the electrodes is adequate to sputter conducting as well as insulating materials. In rf sputtering, the application of a high frequency (13.5 MHz) alternating field causes the electrons to oscillate in the so-called “negative glow”. In this way they acquire enough energy to cause ionizing collisions. The discharge is therefore less sensitive to the emission of secondary ions and self-sustained.

Magnetron Sputtering: In this technique a magnetic field is superimposed on the electric field close to the target (7). This increases the percentage of secondary electrons that cause ionizing collisions and it helps to confine electrons near the target. This method is commonly used in industrial production as very high deposition rates can be obtained under low deposition pressure and low substrate temperature. The technique has been scaled up to very large target (up to 4 m width).

Chemical Vapor Deposition (CVD)

Chemical vapor deposition is a technique allowing to deposit reactive gases at the surface of a substrate without requiring vacuum (5). Gaseous precursors are flown over a substrate at elevated temperatures. The conditions at the substrate surface are selected to promote chemical reactions (pyrolysis, reduction, oxidation, etc.) of the precursors. The CVD sources are gases, volatile liquids, sublimable solids or a combination of these materials. These materials should be stable at room temperature, sufficiently volatile and the reaction temperature should be lower than the melting point of the substrate. This method allows high growth rates and the deposition of materials hard to evaporate can be achieved. However it is a complex process and require usually a high temperature.

CVD techniques are nevertheless widely used and have the ability to produce a large variety of films and coatings, like metals, semiconductors, oxide and compounds in crystalline phase or amorphous state with high purity and at relatively low cost. It has been scaled up for large production for a few compounds such as deposition of $\text{SnO}_2\text{:F}$ on float furnaces.

There are three basic CVD techniques (8, 14): (1) thermal CVD, (2) plasma CVD (PCVD) and (3) laser CVD (LCVD). LCVD and thermal CVD use high temperatures, where thermodynamic processes govern the nature of the resulting deposit. In PCVD the chemical reactions are enhanced by the production of a plasma and occur at lower temperatures. The deposition processes are governed by the partial pressure of reactants, rf power and substrate temperature. It is a suitable technique to coat sensitive substrate materials with high deposition rate because of the lower deposition temperature.

2.2.2 Wet Chemical Deposition Techniques

Wet chemical deposition are techniques in which the material species to be deposited are dispersed in a liquid medium. These techniques have the ability to produce coatings with high optical quality on transparent substrates like glass and polymeric substrates as well as homogeneous coatings on non transparent substrates. The resulting coatings should be usually heated at high temperatures but curing at low temperatures is possible and depends on the coating solutions.

Wet chemical methods are used to deposit multifunctional coatings on glass and polymeric substrates, such as coatings for automotive glasses and CRTs (16), water repellent coatings (17), antistatic and antireflective coatings (18), hard coating on plastics (19), transparent conductive coatings (20-22), surface protective films imparting corrosion or abrasion resistance (3, 23), porous films for specific goals (24, 25), metallic mirrors and many other applications.

To obtain high homogeneous coatings with a desired optical property, the solution must possess special physical and chemical characteristics which can be obtained, according to Schröder (26), when the four following requirements are fulfilled:

1. The solubility of the starting solution is high and it must have the tendency to crystallize during the solvent evaporation.
2. The solution must have a sufficiently small contact angle with the substrate. The smaller the contact angle is, the higher is the wettability of the solution. Wettability can be improved in some cases by the addition of a wetting agent to the coating solution or by an appropriate pretreatment of the substrate.
3. The solution must have an adequate durability under certain conditions. The colloidal stability is an important factor affecting the coating quality. The durability of the coating solution could be enhanced by using stabilizers.
4. The drying and the heating process must be carried out carefully in order to obtain reproducible solid and homogeneous coatings.

The main wet chemical deposition methods are the spray and the sol-gel coatings:

Spray Pyrolysis

Spray pyrolysis is one of the most used methods to coat substrates (e.g. with oxide materials) in a mass production with low effective cost (27). The process consists in generating fine droplets which are then thermally decomposed (pyrolysis) on a hot substrate. The atomization can be realized by applying pressure, by using a nebuliser, ultrasonic or electrostatic methods. Each method results on different droplet size distribution, atomization rate and droplet velocity, which in turn determine the growth kinetics and hence the quality of the obtained films. For instance, the drop size depends on the nozzle type and the applied pressure. An increase in the applied pressure reduces the drop size and vice versa. The kind of the precursors strongly influences the microstructure, the crystallinity and the morphology of the films. The film formation depends on the substrate temperature which should be high enough to decompose the precursor's droplet, but not too high to avoid the formation of a powder.

The process is easy to carry out and do not need complicated equipments and it is possible to coat large substrates with different geometries.

Sol-Gel Deposition

The sol-gel process is a versatile process using chemical solutions. In general, the sol-gel process involves the transition of a system from a liquid "sol" (mostly colloidal) into a solid "gel" phase. This method allows to fabricate ceramic or glass materials in a wide variety of forms, ultra-fine or spherical shaped powders, coatings, ceramic fibers, microporous inorganic membranes, monolithic ceramics and glasses and extremely porous materials (aerogel) (28).

The sol-gel method has many advantages for the synthesis of a large variety of thin films and coatings and involve chemical and physical processes such as hydrolysis, polymerization, drying and densification. It consists first in preparing a solution of inorganic or organometallic precursors or metal oxide particles dispersed in a solvent. The sol can be spread across the substrate by different techniques. The chemical precursors play a decisive role in the deposition methods and affect directly the structural, optical and mechanical properties and other performance characteristics of the resultant coating. We shall only discuss the two most widely used techniques.

Dip coating method

The dip coating technique is a good method to prepare thin films with high optical quality and homogeneity. It is simple, cheap and allows to coat complex shapes like curved substrates, tubes and even large substrates on both sides in one step at room temperature. This method does not require vacuum and no complicated instrumentation is required.

Dip coating is a process where a clean substrate is immersed in a liquid and then withdrawn at a given speed under controlled temperature and atmospheric conditions. The environmental conditions (temperature and humidity) affect the quality of the coating.

The thickness of the coating depends on the viscosity of the solution, the rate of solvent evaporation, and the angle at which the substrate is taken out. It can be determined using the Landau-Levich equation (29) .

$$h = 0.94 \frac{(\eta \cdot v)^{2/3}}{\gamma_{LV}^{1/6} (\rho \cdot g)^{1/2}} \quad [1]$$

where h is the film thickness, η is the sol viscosity, v is the withdrawal speed, γ_{LV} is the liquid-vapour surface tension, ρ is the density, and g is the gravity. The above equation showed that the faster the substrate is withdrawn, the thicker is the deposited film.

Fig. 1 shows the scheme of the different stages of the dip coating process: Immersion (dipping), formation of the wet layer where boundary layer is formed and then the drainage and evaporation stage. The evaporation depends on the solvents used and usually accompanies the start up, deposition and drainage stages. This lead to aggregation and gelation of the wet layer and once it has collapsed fully, a dense film remains on the substrate.

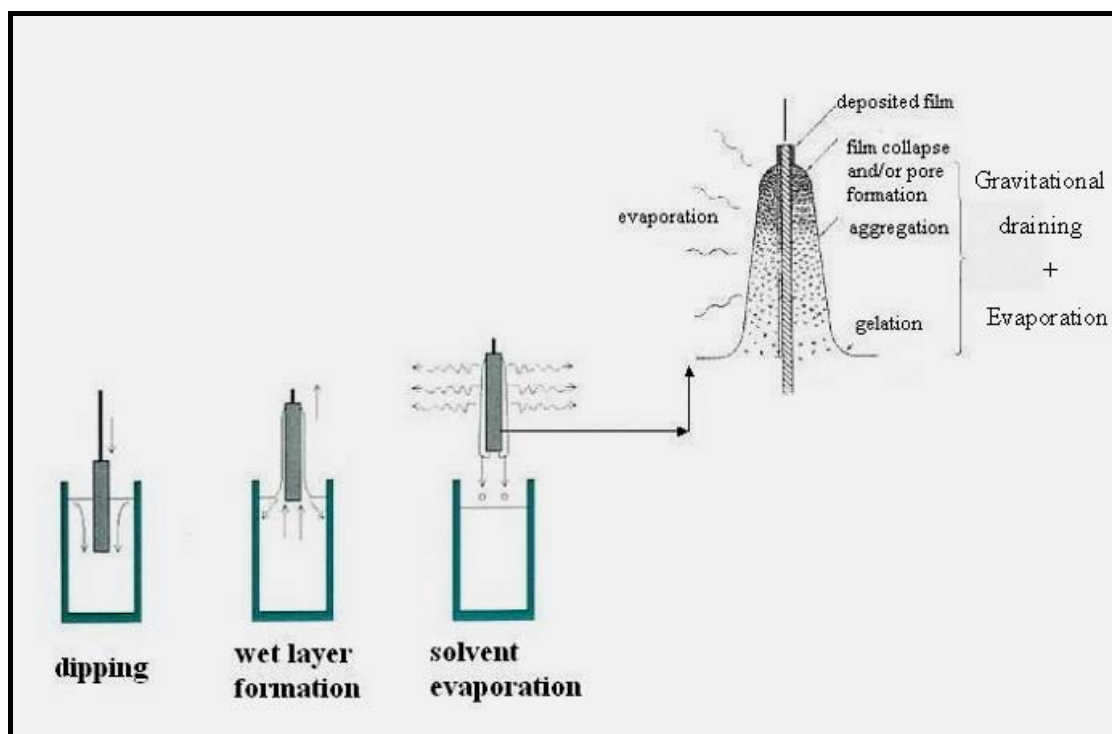


Fig. 1: Schematics of the different stages of the dip coating process (30).

Dip coating can be made either by lifting the substrate from the coating solution (withdrawing) or by lowering the solution, a process in which the substrate remains at rest and the liquid level of the solution is lowered by draining. The withdrawal process is the more economically applicable.

When the substrate is drawn out of the coating solution under a well defined angle of inclination, the process is called angle dependent dip coating (ADDC) (31, 32). Both surfaces are coated simultaneously and the thickness of the film being dependent on the angle between the substrate and the liquid surface, different thickness can be obtained on each side of the substrate (see Fig. 2) (32). This method has some advantages against the conventional dip coating method, as smaller number of layers or coating steps are required to obtain the desired optical properties (33). Production time and costs are therefore reduced.

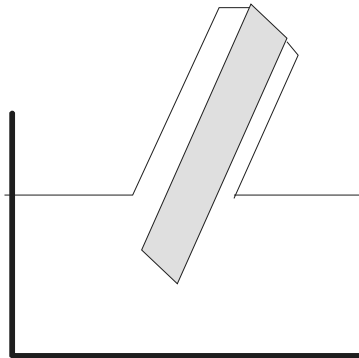


Fig. 2: Scheme of angle dependent dip coating process (ADDC).

Spin coating method

Spin coating is used for many applications in different technological fields. Thin films can be obtained by depositing drops of the solution on the surface of a flat substrate and then spun it to leave a uniform layer for subsequent processing stages and ultimate use. The stages of forming thin films are described as the followings below (34) (Fig. 3):

Stage 1: The first stage is started by pouring a filtrated coating solution or spraying it on the substrate. The solution should wet the surface completely during this stage.

Stage 2: The second stage is started when the substrate is accelerated up to a desired rotation speed. During this rotation, spiral vortices are formed as a result of the twisting motion caused by the inertia of the top of the fluid layer while the substrate below rotates faster and faster.

Stage 3: In this stage the substrate is spinning at a constant rate and fluid viscous forces dominate the fluid thinning behavior. Edge effects are often seen because the fluid flows uniformly outward and it forms droplets at the edge to be flung off.

Stage 4: The last stage occur when the solvent evaporation dominates the coatings thinning. At this point the coatings is effectively transformed into a gel.

After spinning is stopped the coating may be sintered at high temperatures to densify it or be cured at low temperatures or using UV or infra red irradiation depending on the desired application.

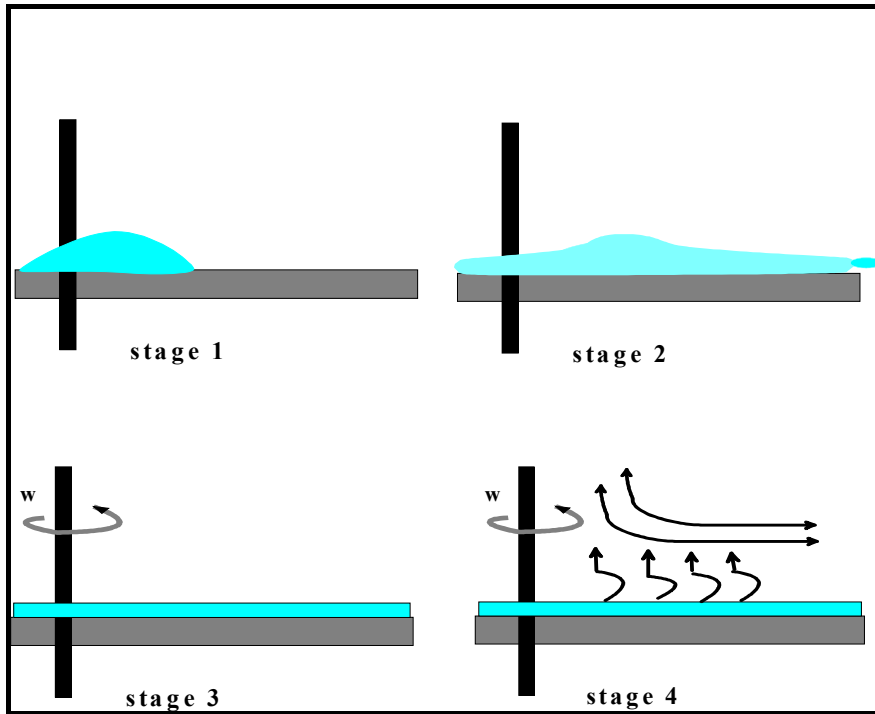


Fig. 3: Scheme of the different stages of the spin coating process.

The thickness of the films made by the spin coating method depends mainly on the rotation speed, time of spinning, viscosity and liquid concentration. It was modeled by Emslie, Bonner, and Peck (35) based on the balance between the centrifugal and viscous force. Assuming that the film is uniform, the time variation of the film thickness is given by:

$$h(t) = \frac{h_0}{\sqrt{1 + 4Kh_0^2 t}} \quad [2]$$

where h_0 is the film thickness at zero time, and K is a system constant defined as:

$$K = \frac{\rho\omega^2}{3\eta} \quad [3]$$

where ρ is the liquid density, ω is the rotation rate, and η is the viscosity of the solution. Both viscosity and density are expected to increase as the solvent evaporation progresses, so that the film thinning will be an important factor. The thinning rate is given by:

$$\frac{dh}{dt} = -2Kh^3 \quad [4]$$

The effect of solvent evaporation was discussed by Meyerhofer (36) who added a constant evaporation term, e , to the above equation:

$$\frac{dh}{dt} = -2Kh^3 - e \quad [5]$$

By assuming that the evaporation rate and the viscous flow rate become equal and that the air flow above the spinning substrate is laminar, Meyerhofer predicted that the final thickness is given by:

$$h_f = c_0 \left(\frac{e}{2(1-c_0)K} \right)^{\frac{1}{3}} \quad [6]$$

where c_0 is the solid concentration in the solution, and e is related to the spinning speed as:

$$e = C\sqrt{\omega} \quad [7]$$

The proportionality constant C depends on the experiment conditions.

As shown above the evaporation rate and the flow process are critical in determining the film thickness and the coating quality. Other factors may affect the quality of the coatings which may formed like the orange peel appearance (37), striations, chuk marks and Marangoni-effect (34). Like the dip coating method the spin coating is sensitive to ambient environment (temperature changes, humidity).

Sintering process

Sol-gel coatings are typically sintered by heat treatments at high temperatures (normally 500°C) or cured at low temperatures ($T < 200^\circ\text{C}$), using IR or UV irradiation in order to make more compact and smoother surfaces. The sintering process leads to a decrease of the film thickness due to the removal of the solvents (80- 250 °C), the combustion of the organic materials (250-300 °C) and the reduction of the porosity ($T > 300^\circ\text{C}$). However the thickness of the film may also increase at high temperatures due to the growth of the crystallites. The heating rate is an important factor affecting the growth of the layer in certain systems.

The sintering atmosphere is playing a decisive factor on the physical and chemical properties of the deposited films. In certain cases the electrical and the optical properties of coatings are enhanced when the sintering process is performed in vacuum or in the presence of protective gases. For example, a TiO_2 film backed in air at 500°C has an index of refraction of 2.1; however the same film has an index of 2.4 if the backing is performed in vacuum (38). Steckl et al (39) studied the effect of ambient atmosphere in the annealing of indium tin oxide films. A reduction in the sheet resistance and increase in the infrared reflection of transparent conducting ITO thin films were observed when the films were annealed in inert or reducing atmosphere.

In certain cases surface treatments of thin films are extremely important to improve some properties of the coatings. The common surface treatments methods are plasma treatment and UV-irradiation. For example, a SF_6 plasma and UV-irradiation treatment of indium tin oxide surface has improved the power efficiency and the stability of the organic light emitting diode (40, 41). Surface treatment reaction may involve changes in the surface structure as well as in the surface chemical composition.

2.3 Transparent conducting coatings

Because of the simultaneous combination of high electrical conductivity and high transparency in the visible region, transparent conductive films are very interesting materials and have today a great importance in a wide range of applications.

There are a variety of materials which exhibit both properties. Beside the transparent conducting oxides which are discussed in details in the next section, two other groups of materials, very thin metallic films (silver, gold, copper) and conducting polymers (polyaniline, polypyrrole, PEDT), can be used for this purpose.

Metallic thin films: Thin conductive metallic film are used for the fabrication of microelectronic devices and even recently for low-E window panes. Typical materials are gold, aluminum, silver and copper. Most materials are deposited via physical (PVD) or chemical (CVD) vapor deposition methods. The transparency and the conductivity of the metallic films are strongly dependent on the film thickness. To reach a high transparency, ultrathin films ($h \sim 10$ nm) should be deposited; however the resistivity of such films may be high as the films often consist of isolated islands and are consequently discontinuous (42). The resistivity rapidly decreases when the thickness of the film increases as continuous films are formed.

Conducting polymers: Polymers find a widespread use as structural and functional materials. The development of intrinsically conducting polymers is driven by the hope to replace the inorganic conductors used in electronic devices (43). The most important conducting polymers which has been developed in the past 20 years are those based on polyanilines, polypyrroles, polythiophenes, polyphenylenes, and poly(p-phenylene vinylene)s compounds (43-45). The conductivity of these polymers is due to the extended π -conjugated system which is formed by the overlap of carbon Pz orbitals and alternating carbon-carbon bond lengths along the polymer chain. These polymers become conductive upon exposure to acids or adequate oxidation or reduction (called doping) carried out by chemical or electrochemical means.

A low sheet resistance of conductive polymers requires a thick layer. For example a conductive polymer core-shell system (46) consisting of polyurethane particles surrounded with polypyrrole shows antistatic properties with sheet resistance around $10^8 \Omega_{\square}$ for a thickness of 100 nm. Lower sheet resistance of $10^4 \Omega_{\square}$ is achieved for layer thickness between 2000 and 5000 nm. However the increases of the layer thickness lower the optical transmittance of the layer from 85% (at 100 nm) down to 40% at 1000 nm.

Conducting polymers are used in many applications, as antistatic coating for cathode ray tubes (47), primers for electrostatic spray coating (48), hole injection layer on ITO substrates for organic electroluminsce devices (49), in sensors devices (50), and as transparent electrode for photovoltaic devices (51).

2.4 Transparent conducting oxides (TCO)

Transparent conducting oxides (TCO) are the most common used materials to produce transparent conducting films. They are essentially based on In_2O_3 , SnO_2 , ZnO , CdO , etc. These materials are usually insulators and have a wide band gap ($E_g > 3 \text{ eV}$), so that they show an excellent transparency in the visible region. To get them conducting nonstoichiometry and/or appropriate dopants, like Sn for In_2O_3 , Sb, F for SnO_2 , Al, Ga for ZnO , etc., should be introduced in order to create an electron degeneracy in the wide band gap (52).

The number of products and technologies that used these materials on a variety of substrates (glass, plastic, ceramic, metal, etc.) is growing tremendously. TCO thin films can now widely utilized for optoelectronic devices, such as flat panel displays, thin film transistors, electroluminescent devices, heat reflectors, gas sensors, organic light emitting diodes, solar cells and variety of other significant applications in demisting and deicing glass for automotive, train and aircraft (52-59).

2.4.1 Transparent semiconducting materials

a) Tin oxide

Tin oxide (SnO_2) is the first transparent conductor to have received significant attraction and commercialization. It is an n-type, wide band gap semiconductor ($E_g = 3.97 \text{ eV}$) with a transmittance cut off at 330 nm, a refractive index in the visible spectral range of about 2.0 and it is chemically stable (60, 61). It is largely used as a transparent conductive layer for ovens and electrodes (58, 62), in the fabrication of gas sensor devices (63), white pigmented conductive paint coatings (64), and as active catalyst for the partial oxidation and the amino oxidation of olefins (65).

Tin oxide has a tetragonal (rutile) structure (66, 67). Each tin atom is at the center of six oxygen atoms placed approximately at the corners of a regular octahedron and every oxygen atom is surrounded by three tin atoms located approximately at the centers of an equilateral triangle.

SnO_2 is an insulator or at most an ionic conductor, when it is stoichiometric. The formation of oxygen vacancies in the lattice, e.g. by heating the material in a reducing atmosphere leads to a nonstoichiometric state and gives rise to free electrons and make this material conductive; however this nonstoichiometry is metastable. Stable conductivity of the SnO_2 thin films is generally obtained by doping the coating with fluorine ions (68, 69), antimony (70, 71), or boron (72). This doping is done by controlling the valence mechanism, whereas the dopant should be either a higher valency cation (e.g Sb^{5+}) or a lower valency anion (e.g F^-) than tin providing additional electrons to the semiconducting material.

Fluorine doped tin oxide (FTO) is the most effective dopant due to its smaller ionic radius compared with that of oxygen. Fluorine doped tin oxide material has the rutile structure with no changes in the lattice parameters. FTO layers have generally a higher mobility than pure

tin oxide materials (73). The lowest electrical resistivity of doped tin oxide thin film is in the range of $10^{-3} \Omega \cdot \text{cm}$ and the transparency is in the range of 80-90 %.

Many deposition techniques were used to get tin oxide film: spray pyrolysis (68, 69, 74), CVD (9), sputtering (75), evaporation (76) and also sol gel deposition methods (77-82).

b) Indium oxide

Indium oxide (In_2O_3) is the most widely used material for transparent conductive materials in technical applications due to its superior electrical properties, combined with high transparency and high infrared reflectivity. In_2O_3 exists in a modified cubic crystallographic phase (space group Ia3) called the bixbyite structure (also called c-type rare earth oxide structure) with two non-equivalent In sites (Fig. 4), 16 molecules (80 atoms) per unit cell and a lattice constant of 1.012 nm (58, 83).

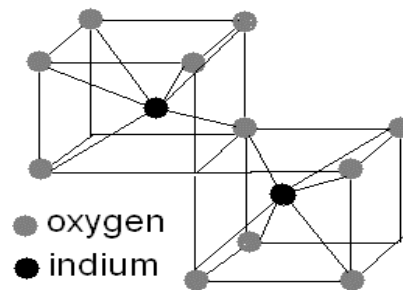


Fig. 4: Crystal structure of In_2O_3 .

The band structure of In_2O_3 is highly complicated. To explain the conductivity mechanism Hamberg and Granqvist (84) have assumed a simple parabolic band structure characterized by an effective mass m_c^* for the conduction band and m_v^* for the valence band with a direct band gap of 3.75 eV.

In_2O_3 is a poor conductive material when it is stoichiometric. The conductivity is enhanced strongly by a reducing treatment or by doping the lattice by an appropriate dopant such as Sn. The reducing process of indium oxide material creates oxygen vacancies, each one leaving two extra electrons in the lattice. The donor state lies just below the conduction band. High electron concentration (10^{17} - 10^{20} cm^{-3}) can be achieved with an oxygen deficiency (e.g., $\text{In}_2\text{O}_{3-x}$) or an excess metal atoms (e.g. $\text{In}_{2+y}\text{O}_3$).

The doping process leads to controlled valence semiconductors. The replacement of indium by higher valence cations such as aluminum, titanium, zinc, zirconium, germanium(85-88) and tin increases the n-type conductivity, however the last compound being the most popular.

In Tin doped indium oxide (ITO) Sn replaces the In^{3+} atom in the cubic bixbyite structure (substitutional doping). An Sn atom forms an interstitial bond with oxygen and exists either as SnO (valence +2) or SnO_2 , (valence +4). The valence state has a decisive effect on the ultimate conductivity of ITO. The low valence state, Sn^{+2} , acts as a trap for the charge carriers and therefore reduces the electrical conductivity (lower concentration of free electrons). On

the other hand Sn^{4+} act as a n-type donor releasing one free electron to the conduction band. Actually both substitutional Sn^{4+} and oxygen vacancies contribute to the high conductivity and the chemical formula of the material can be represented as $\text{In}_{2-x}\text{Sn}_x\text{O}_{3-2x}$. ITO films have a lattice parameter close to that of indium oxide and lies in the range of 1.012 to 1.0131 nm (83).

The high conductivity of ITO films is due to the high carrier concentration rather than to the high Hall mobility (52). The observed low mobility of ITO, compared to that of bulk In_2O_3 and its dependence on carrier concentration and deposition temperature has been explained in terms of scattering mechanisms due to ionized impurities or grain boundaries. The high crystallinity degree obtained by depositing the film at high temperature enhances the mobility of the films (89).

The high optical transmittance of ITO films is a direct consequence of the wide band gap of the semiconductor. The direct band gap ranges from 3.5 to 4.1 eV so that the fundamental absorption edge lies in the ultraviolet region. It shifts to shorter wavelengths with increasing the carrier concentrations, n due to the so-called Moss-Burstein shift (90). The transmittance of ITO films is also influenced by the surface roughness and optical inhomogeneity in the direction normal to the film surface.

ITO thin films have been obtained using many deposition techniques such as spray pyrolysis (20, 91), ion beam pulsed laser deposition (92-94), sol-gel deposition techniques (95-98) and sputtering. The latter technique being the most extensively used. Their structural, optical, electrical and mechanical properties have been discussed in many reports (99-102).

ITO coatings are used as transparent heating elements for aircraft and car windows, antistatic coatings over electronic instrument display panels, heat reflecting mirrors, antireflection coatings and even in high temperature gas sensors. Many electrooptic devices such as display devices, solar cells, light emitting and photo diodes, photo transistors and lasers use ITO coatings as electrodes. ITO is therefore becoming an integral part of modern electronic technology and the improvement of its properties remains the focus of many researches worldwide (52, 57, 58, 103-108).

c) Zinc Oxide

Zinc oxide (ZnO) is also an important material which is used in many field of applications. It is an n-type semiconductor with poor electrical conductivity in its pure state and has a direct band gap of about 3.2 eV. Doped zinc oxide films are extensively studied, since their high optical transmission and electrical conduction have great potential for application in photo-electronic devices such as solar cells and displays (109), and as low emissivity coatings in windows.

Zinc oxide is a tetrahedrally coordinated solid that crystallizes in the wurtzite structure. The electrical conductivity of intrinsic ZnO materials is mainly due to an excess of zinc at interstitial positions. The electrical properties of zinc oxide materials can be improved by thermal treatment in hydrogen, or by an appropriate doping process, by cationic substitution,

such as Al, Ga, Si, Ge, Ti, Zr or Hf (84, 110, 111), the last two elements being the best ones. This is attributed to the fact that the ion radius of Al^{3+} and Ga^{3+} is slightly smaller than that of Zn^{2+} , in comparison to other impurities.

ZnO films have been prepared by many techniques such as reactive evaporation (109), sputtering (112, 113), spray pyrolysis (114) and also by sol-gel methods (115).

d) Other transparent conductive materials

With the increase in demand for transparent electrodes for various optoelectronic devices, the need to develop new materials bearing these properties is becoming a very interesting and attractive issue for many researchers. Although $\text{In}_2\text{O}_3:\text{Sn}$ (ITO), $\text{SnO}_2:\text{F}$ (FTO) and $\text{ZnO}:\text{Al}$ (AZO) are the most commonly used materials at present, they often have limited applications due to their chemical instability, lack of corrosion resistance, poor adhesion under various environments. New transparent conducting materials have been already prepared, such as MgIn_2O_4 , $\text{In}_2\text{O}_3:\text{Mo}$, $\text{CdO}:\text{In}$, Cd_2SnO_4 , new ternary $\text{ZnO}-\text{V}_2\text{O}_5$ and p-type conductors (110, 116-122).

p-type semiconductors are interesting materials, which have been recently investigated. When compared to n-type semiconductors, they show a lower conductivity for the same transparency because of the smaller mobilities of the charge carriers. Several types of p-type semiconductors have been prepared recently in the CuAlO_2 and SrCu_2O_2 family (118). Tate et al (122) have prepared p-type oxides exhibiting conductivity and transparency high enough to turn them useful in the manufacture of transparent p-n junction diodes and other transparent devices.

2.4.2 Electrical properties

Transparent conducting oxides obey the Drude free electron theory (123). The basis of the conduction mechanisms of these materials is discussed in this section.

Electrical conductivity occurs through the moving of electrical charges (electron, holes and ions) due to an applied electric field. The electrical conductivity of an n-type material, σ , the reciprocal of the resistivity, ρ is defined as the product of the number of charge carriers, n , the electric charge, e , and the charge mobility, μ (124).

$$\sigma = \rho^{-1} = ne\mu \quad [8]$$

From the above equation it is clear that for obtaining a high conductivity, it is important to have simultaneously a high concentration of the electrons and a high mobility.

The electrical sheet resistance of the film R_{\square} , is a good index to evaluate the electrical properties of conductive films. The sheet resistance describes the resistance of a square layer area. It is usually carried out using the four point technique (see Appendix A.2.1). The relation between R_{\square} and ρ is calculated by knowing the thickness of the film as:

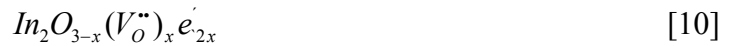
$$R_{\square} = \rho/t \quad [9]$$

For a given specific resistivity the sheet resistance R_{\square} decreases as the film thickness, t , increases. The experimental determination of ρ , R_{\square} , n and μ are discussed in Appendix A.3.2.

Charge carriers concentration

A high charge carrier concentration in these materials can be achieved by two ways:

a) Stoichiometry: A high electron concentration can be achieved by a stoichiometric deviation owing to oxygen deficiency, e.g. $\text{In}_2\text{O}_{3-x}$ or to an excess of metal atoms, e.g. $\text{In}_{2+y}\text{O}_3$. The oxygen deficiency can be achieved by removing the oxygen atoms during a reducing treatment leaving two electrons in the lattice, and the material can be described, using standard notation, as (58)



where x is normally less than 0.01. $\text{V}_\text{O}^{\bullet\bullet}$ denotes doubly charged oxygen vacancies and e' denotes electrons which are needed for charge neutrality on the macroscopic scale.

When the concentration of the positively charged oxygen vacancies is high, they become a site for electron trapping. This results in a reduction of the number of charge carriers and to a lower conductivity (84, 85).

Nonstoichiometry in SnO_2 can also be achieved by creating oxygen vacancies. A nonstoichiometric oxide $\text{Sn}_{1-x}^{4+}\text{Sn}_x^{2+}\text{O}_{2-x}^{2-}$ is formed by combining x moles of SnO with $1-x$ mole of SnO_2 . The material contains x mole of oxygen vacancies and x moles of Sn^{2+} free to donate $2x$ moles of electrons contributing to the conduction process (52).

b) Doping: Dopants are substitutive materials (cations or anions) which are added into the host lattice in order to create free charge carriers and enhance the electrical conductivity. There are several requirements (85) that should be taken into consideration when choosing an appropriate doping material:

- 1- The doping cation should possess a higher valence than that of the host metal, for example Sn^{4+} to substitute In^{3+} in the indium oxide lattice. The replacement of metal atom with higher valency releases a free electron which increases the n-type conductivity. When the dopant cations have a lower valence, then vacancies will be produced that act as an electric trap in the lattice and therefore the electrical conductivity decreases. On the other side a doping anion possessing a lower valence than oxygen such as fluorine (F^-) will contribute to increase the conductivity (e.g. $\text{SnO}_2 : \text{F}$).
- 2- The diameter of the doping ion should be smaller or equal to the diameter of the host ion it substitutes, otherwise it acts as a scattering site.
- 3- The doping oxide and the host oxide should not be able to form any compound or solid solutions with each other.

The dopant concentration can not exceed a critical value, which, where surpassed, decreases the electrical conductivity. The excess of dopants may occupy interstitial positions, may also form defects acting as carrier traps rather than electron donors and also be the concentration cause of phonon or impurity scattering centers and resulting in a decrease in charge carriers mobility and hence to a decrease in the electrical conductivity (52).

Charge carriers mobility

The mobility of the charge carriers is strongly influenced by the disorder in the crystal structure resulting from the modification of the crystalline periodicity as a result of doping. It is therefore strongly affected by the different scattering processes of free charge carriers.

Scattering mechanisms

a) Grain boundaries scattering: The grain boundaries in polycrystalline film play a very important role in the scattering mechanism. These boundaries contain fairly high densities of interface states which can trap free carriers from the bulk of the grain (58). The interface state results in a space charge region where potential barriers impede the charge transport. A model for the charge transport mechanism was proposed by Petritz (125) and modified by Seto (126) assuming thermoionic emission and a conduction through the grain boundary. It was found that:

$$\mu_g = el(2\pi m^* kT)^{-1/2} \exp\left(-\frac{e\phi_b}{kT}\right) \quad [11]$$

where l is the grain size, m^* is the effective mass of the charge carrier, and ϕ_b is the boundary potential barrier. A smaller grain boundary scattering is observed in films possessing larger grains which exhibit smaller grain boundary potential, ϕ_b . The grain size depends on the deposition process, the substrate temperature and was also found to increase with increasing the film thickness. The growth of the grain obtained by raising the annealing temperature results in lower value of the grain boundary and, consequently, to an increase of the mobility of charge carriers.(127).

b) Ionized impurity scattering : This kind of scattering is very effective for charge carriers, because of the electrostatic field of the charged impurities. As shown in some models of degenerate semiconductors, the contribution of the ionized impurity scattering is given by (128):

$$\mu_i = \frac{4e}{h} \left(\frac{\pi}{3}\right) n_i^{-2/3} \quad [12]$$

where n_i is the impurity concentration. The mobility therefore decreases with concentration of impurities.

c) Lattice scattering: The lattice vibration of the material is the cause of an electron phonon scattering due to the propagation of acoustical and optical waves through the lattice. The mobility due to this kind of scattering depends strongly on the temperature. The increase of the temperature increase the lattice vibration and hence decreases the mobility of the charge carriers. The mobility due to lattice scattering can be expressed as (20):

$$\mu_L = \frac{(8\pi)^{1/2} e\hbar^4 C}{3E_L m^{*5/2} (kT)^{3/2}} \quad [13]$$

where C is the elastic constant and E_L is the shift of the edge of the conduction band with temperature per unit dilation.

Electron-electron scattering: This scattering mechanism has a little effect on the mobility of the charge carriers, because the total momentum is not changed during electron collisions.

The total mobility, μ_T due to the different scattering sources can be written as the reciprocal sum of $\mu_g, \mu_i, \mu_L, \mu_{e-e}$, etc. (20):

$$\frac{1}{\mu_T} \approx \frac{1}{\mu_g} + \frac{1}{\mu_i} + \frac{1}{\mu_L} + \frac{1}{\mu_{e-e}} + \dots \quad [14]$$

The contribution of all the scattering processes to the mobility of the charge carriers depend mainly on the deposition method, the deposition rate and on the substrate temperature. For example, Chang et al (113) found that the ion impurity scattering is the dominant factor to explain the decrease of the conductivity of Al-doped zinc oxide thin films deposited by rf reactive magnetron sputtering. He found also that the scattering increases by increasing the deposition temperature of the film. Liu et al (129) found that the scattering due to the grain boundary is the dominant factor to explain the decrease of the electron mobility of ITO films deposited on glass substrate using the sol-gel dip coating method. An increase of the film thickness was found to increase the mobility of the charge carriers: a 10-layers dip coated ITO thin films shows a higher mobility than a 3-layer films (130).

2.4.3 Optical Properties

The optical properties of TCO materials, like the electrical ones, depend on the deposition methods, their microstructure, the impurity concentration, the annealing temperature and on their surface morphology. They are strongly correlated to the electrical properties and can be understood on the basis of the Drude's theory for free electron (123).

The interaction of free electrons with an electromagnetic field influences the relative permittivity, ε , of the material.

$$\varepsilon \equiv \varepsilon' - i\varepsilon'' = (n - ik)^2 \quad [15]$$

where n and k are the refractive index and the extinction coefficient of the material respectively. The permittivity is a frequency dependent function and can be written as (131):

$$\varepsilon(\omega) = \varepsilon_\infty - \frac{n e^2}{m^*} \frac{1}{(\omega^2 - i\omega\gamma)} \quad [16]$$

where m^* , e , n are the effective mass, charge and density of the electrons, respectively, $\omega = \frac{2\pi c}{\lambda}$ is the circular frequency, ε_∞ is the high frequency dielectric constant and γ is equal to $1/\tau$, where τ is a frequency independent relaxation time, i.e. the mean time between successive electron collision. Then ε' and ε'' can be written as:

$$\begin{aligned} \varepsilon' &= n^2 - k^2 = \varepsilon_\infty \left(1 - \frac{\omega_p^2}{\omega^2 + \gamma^2}\right) \\ \varepsilon'' &= 2nk = \frac{\gamma}{\omega} \frac{\varepsilon_\infty \omega_p^2}{\omega^2 + \gamma^2}, \end{aligned} \quad [17]$$

where ω_p is the plasma circular frequency given by:

$$\omega_p = (n e^2 / \varepsilon_0 \varepsilon_\infty m^*)^{\frac{1}{2}} \quad [18]$$

where $\varepsilon_0 = 8.854 \times 10^{-12}$ As/Vm is the permittivity of free space. Finally the equation [16] can be rewritten as:

$$\varepsilon(\omega) = (n - ik)^2 = \varepsilon_\infty \left[1 - \frac{\omega_p^2}{\omega^2 + \gamma^2} - i \frac{\omega_p^2 (\gamma / \omega)}{\omega^2 + \gamma^2}\right] \quad [19]$$

From the Maxwell equations the relative permittivity can be related to the complex resistivity $\tilde{\rho}$ by (132):

$$\varepsilon(\omega) = \varepsilon_\infty - \frac{i}{\varepsilon_0 \omega \tilde{\rho}(\omega)} \quad [20]$$

so that from equations 17 and 19, $\tilde{\rho}(\omega)$ can be derived as:

$$\tilde{\rho}(\omega) = \frac{\gamma + i\omega}{\varepsilon_0 \varepsilon_\infty \omega_p^2} \quad [21]$$

At zero frequency (long wavelength), the real part of the resistivity, ρ is defined as:

$$\rho = \frac{1}{ne\mu} = \frac{\gamma}{\varepsilon_0 \varepsilon_\infty \omega_p^2} \quad [22]$$

Therefore the relation between μ and γ is:

$$\gamma = \frac{e}{m^* \mu} \quad [23]$$

The mobility, μ , is the drift velocity of the conduction electrons in a material per unit of applied electric field and is therefore related to the average relaxation time $\langle \tau \rangle = \gamma^{-1}$.

The wavelength dependence of the optical properties of the material can be classified into three regions:

1) high frequency (short wavelength), with $\omega > \omega_p, \gamma$ (transparent region).

Using this approximation, equation [19] can be written as:

$$\varepsilon(\omega) \approx \varepsilon_\infty \left[1 - \frac{\omega_p^2}{\omega^2} - i \frac{\gamma \omega_p^2}{\omega^3} \right] \quad [24]$$

In this limit the refractive index and the extinction coefficient take the following forms:

$$n(\omega) \approx \varepsilon_\infty^{1/2} \left[1 - \frac{\omega_p^2}{\omega^2} \right]^{1/2} \quad \text{and} \quad k(\omega) \approx \varepsilon_\infty^{1/2} \left[\frac{\omega_p^2 \gamma}{2\omega^3} \right] \quad [25]$$

The behavior of the material is therefore that of a dielectric, where $k \rightarrow 0$ and the refractive index approaches $\varepsilon_\infty^{1/2}$.

2) Low frequency (long wavelength), with $\omega < \omega_p, \gamma$ (reflecting region).

In this region equation [19] can be approximated as:

$$\varepsilon(\omega) = \varepsilon_\infty \left[1 - \frac{\omega_p^2}{\gamma^2} - i \frac{\omega_p^2}{\gamma \omega} \right] \quad [26]$$

Taking the square root of $\varepsilon(\omega)$ and using the identity $\sqrt{i} = e^{\frac{\pi}{4}i} = \frac{1+i}{\sqrt{2}}$, we see that:

$$n(\omega) \approx k(\omega) \approx \omega_p \sqrt{\frac{\varepsilon_\infty}{2\omega\gamma}} \quad [27]$$

The normal reflectance can be written as (133):

$$R(\omega) = \frac{(n-1)^2 + k^2}{(n+1)^2 + k^2} \quad [28]$$

In the low frequency limit, equation [28] can be approximated by:

$$R(\omega) \approx 1 - \frac{2}{k(\omega)} \approx 1 - 2(2\rho\omega\varepsilon_0)^{1/2} \quad [29]$$

This equation shows that the material behaves like a perfect reflector for $\omega \rightarrow 0$.

At low frequency, the optical properties of TCO materials exhibit a metal-like behavior, while at high frequency they are like those of insulators. The plasma frequency, ω_p , is therefore the characteristic frequency at which the material changes from a metallic to a dielectric response and it depends on the concentration of free electrons as shown in equation [18].

3) Intermediate region $\omega_p > \omega > \gamma$ (reflecting region)

In this region, equation [19] can be written as:

$$\varepsilon(\omega) = \varepsilon_\infty \left[1 - \frac{\omega_p^2}{\omega^2} - i \frac{\omega_p^2 \gamma}{\omega^3} \right] \quad [30]$$

so that

$$n \simeq \frac{\omega_p \varepsilon_\infty^{1/2} \gamma}{2\omega^2} \quad \text{and} \quad k \simeq \frac{\omega_p}{\omega} \varepsilon_\infty^{1/2} \quad [31]$$

The refractive index reaches a minimum at $\omega = \omega_p$ and the extinction coefficient decreases rapidly for $\omega > \omega_p$. In this region equation [28] can be approximated to:

$$R = 1 - \frac{2\gamma}{\omega_p \varepsilon_\infty^{1/2}} \quad [32]$$

This equation indicates that the higher the plasma frequency is (shorter plasma wavelength), the highest reflectance of the material is.

Fig. 5 shows a typical T,R curve for commercial sputtered ITO layer on glass substrates. The reflection decreases and the transmission is high at high frequency and the coating behaves like a dielectric. In the intermediate region the free carrier absorption becomes important and the reflection starts to increase rapidly. A high reflection is observed for $\omega < \omega_p$. The plasma frequency has been defined as the cut-off frequency (transmittance = reflectance) (134), and some where else as the frequency at the minimum resistivity (58) (see Fig. 5).

Hamberg and Granqvist have studied a quantitative model to determine the dielectric function of ITO films from the spectrophotometric data (T, R) by combining the Drude free electron model with the effect of valence electrons and phonons. Brewer et al (135) also have used the reflectance data of ITO films to determine the plasma frequency using the the Drude free electron model, the dielectric function of ITO and the two- and three-phase Frensel equations for reflectance.

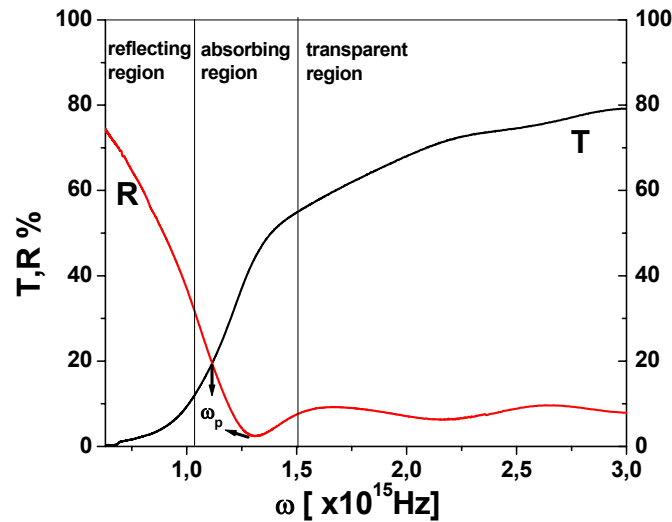


Fig. 5: Typical transmission and reflection spectrum of a commercial sputtered ITO layer (TEC 8).

Optical properties near the band gap:

At short wavelengths, light is strongly absorbed due to the forbidden band. The absorption coefficient, α , can be determined from the expression (136):

$$\frac{1-R}{T} = \exp(\alpha h) \quad [33]$$

where T , R and h are the transmittance, reflectance and the thickness of the film, respectively. The variation of the absorption coefficient with the photon energy for different band to band transition is given by (137):

$$\alpha = A(h\nu - E_g)^x \quad [34]$$

where $h\nu$ is the photon energy, E_g is the band gap energy (the difference between the conduction band and the valence band), A is a constant and the value of x is $\frac{1}{2}$ for allowed transition and $\frac{3}{2}$ for the forbidden transition. The energy gap for allowed transition can be determined from the plot of α^2 versus the photon energy by extrapolation the linear portion of the curve to zero absorption.

The value of the direct band gap shifts to higher value, when the charge carrier concentration increases, according to the Burstein-Moss (BM) theory (138). However, in a more complete theory one also has to include a band gap narrowing due to the electron-electron and electron-impurity scattering (84).

2.4.4 Application of transparent conducting oxides

The application areas of transparent conducting oxides are widespread. Different values of sheet resistance are needed to match each application. Table 1 shows some examples:

Table 2: Application of TCO materials and their electric requirements

Application	Required sheet resistance
Optoelectronics	very low to medium: $< 10^2 \Omega_{\square}$
Shielding	low: $10^0 - 10^1 \Omega_{\square}$
Electrostatic coating	medium to high: $10^2 - 10^4 \Omega_{\square}$
Antistatic	high: $10^6 - 10^9 \Omega_{\square}$

There is therefore no unique material which matches all the industrial demands. Moreover other criteria (139) also influence the choice of the transparent conducting materials to be used. Among them it can be mentioned the transparency, the value of the plasma frequency, the work function, the thermal stability, the mechanical and chemical durability, the etching capability, the deposition temperature, the toxicity and also the cost of the material. Some of the most important applications are discussed in the next section.

a) Low-emissivity and Heat Mirror Coatings

Low emissivity coatings, as well as heat mirror coatings, reduce the heat transfer through windows. They reflect the external heat in the summer months and retains the internal heat during winter months. These features can be achieved using low resistivity TC materials which transmit the visible spectrum and reflect the long wave thermal radiation. This application needs highly conductive coatings (105). In hot environment a short plasma wavelength ($\lambda_p \leq 1\mu m$) is required, but in cold environment fairly long plasma wavelength $\lambda_p \geq 2\mu m$ is sufficient. There is also an increasing interest for this kind of coatings in the fields of solar cells, fire protection glass, glazing car windows for avoiding dew and frost formation, to save the energy required to heat the filament of incandescent lamps and reducing the unwanted heat radiation (52, 62, 103). Very thin layer of silver and FTO layers are to be used broadly for heat insulated glasses (103).

b) Electromagnetic radiation shielding

Electromagnetic (EM) radiation in the frequency range from a few GHz to hundreds of MHz is emitted from many sources and may cause many kinds of damage. Conductive coatings aim to attenuate these radiations and are required e.g. for medical equipments, computer screens and for high frequency operated equipments. The shielding efficiency (SE) is measured in decibels as:

$$SE = 10 \log \frac{\text{incident intensity}}{\text{transmitted intensity}} (dB) \quad [35]$$

It depends on the sheet resistance of the coating, the type of the source of the radiation and its distance to the shielding layer. For far field ($d > \lambda/2\pi$) it is estimated as (103):

$$SE = 20 \log \frac{z_0}{2.R_{\square}} \quad [36]$$

where z_0 is the wave resistance of the vacuum ($z_0 = 377\Omega$) and R_{\square} is the sheet resistance of the coating. The above equation shows that the lower the sheet resistance is, the higher is the shielding efficiency. ITO coatings are the most widely used material to achieve this purpose (140).

c) Transparent electrodes

Transparent conducting layers are used as transparent hole injection electrodes in many devices. Typical applications are: liquid crystal displays (LCD), plasma displays panel (PDP), window panes with controllable transmittance based on the use of liquid crystals, photovoltaic modules, electrochromic cells and light emitting diodes, etc. Etching is a very important factor to obtain patterned electrodes (5, 57, 106, 107, 141-144).

ITO, FTO and AZO are the most widely used materials for transparent electrodes, but recently, silver-based layer systems have also been used. Modern display electrodes need a high transparency (> 90 %) and sheet resistance smaller than $5 \Omega_{\square}$ (145), which is difficult to be obtained using TCO materials. The low chemical and mechanical resistance of silver based layers restrict their use.

d) Touch panel controls

Touch panels or touch screens are optoelectronic devices in which an electrical contact (switch) is established by bringing together mechanically two conducting panes. Transparent switches are used as electronic keyboards to operate electrical and electronic devices and machines in air traffic and railway control terminals, in automatic ticket-vending machines and in household appliances (103). Coatings deposited on thin glass foils with sheet resistance smaller than $1 \text{ k}\Omega_{\square}$ and transmittance greater than 80 % are required for these applications. Low cost transparent conducting materials with high mechanical durability and easily etched are good choices for these applications.

e) Electrostatic and antistatic coatings

Glasses and plastics are electric insulators and their surface can be easily electrically charged by rubbing and when exposed to high-energy radiation. When these surfaces are touched by hand, high frequency voltage peaks of several kilovolts can be produced which may cause damage to high-cost electronic components or even fire and explosions leading to potentially serious accidents. In addition, the accumulation of dusts from the atmosphere on insulating surfaces is particularly undesirable in rooms subject to high hygienic standards.

Electrically conducting coatings can easily remove the electric charges from a surface and prevent also the accumulation of dust. Sheet resistance in the range of $\text{M}\Omega_{\square}$ is enough to prevent the dust accumulation on the surfaces. However a sheet resistance $R_{\square} \leq 10 \text{ k}\Omega_{\square}$ is usually required to remove electric charges (103). Chemical and mechanical stability are also

important factors to be taken into consideration. The antistatic coatings can be combined with antireflection and antiglare properties. Antistatic coatings are used in cathode ray tubes, in television tubes, computer displays, to coat food and drug containers and the walls and floors of clean rooms, to shield plastic displays windows and other plastic components that are suspected to lint and particulates build up and to coat plastic components of equipment used to handle microchips and other static sensitive devices (64).

f) Gas sensors

The changes in the conductivity of transparent conducting materials when exposed to certain gases make them interesting devices to detect hazardous gases (gas-sensing devices). ZnO and SnO₂ are widely used as sensing materials (146, 147). The sensitivity is related to the conduction mechanism of these materials, which is on the other hand correlated with the intrinsic defects structure. The major problems related to these materials are the inherently poor selectivity, the decrease in sensitivity and the degradation of their performance over a long period of operation (146).

2.5 Coatings deposited at low temperatures

The substrate temperature used during the deposition process and the post annealing treatments have a significant effect on the surface structure, morphology, microstructure, optical, electrical, and mechanical properties of the coatings. A high deposition or sintering temperature is usually necessary to crystallize many inorganic thin films. Wet chemical deposition methods usually require either hot substrates ($T > 400^{\circ}\text{C}$ - spray pyrolysis) or substrates which can be heated to high temperature after the deposition (sol-gel methods). These processes are therefore only adequate to coat substrates thermally stable at high temperatures such as ceramics and glasses (8).

There is however today a great interest to coat materials and devices which do not withstand high temperature such as preformed glasses or plastic substrates and also to lower the cost of energy required to heat the substrates in conventional deposition methods. The deposition of inorganic coatings onto these kind of substrates using sols adequate for high temperature process results usually in either a non-adherent layer or a soft surface that is easily scratched, so that new concepts are required.

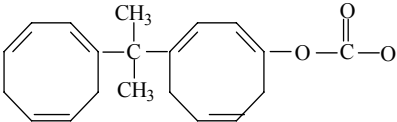
Coatings on Polymeric substrates

Plastic materials are today very common and used for containers, packaging, building materials, cloths, contact lenses, medical implants, etc. Their importance is growing due to benefits in forming and processing. They are also promising to substitute glass in many fields, because they are durable, cheap, safe (unbreakable), have a high flexibility, light weight and have little or no corrosion problems. Despite of their positive properties they have also several disadvantages which limit their application such as poor temperature stability, poor abrasion and scratch resistance, high sensitivity to UV radiation, high permeability for water vapor and oxygen and high fatigue when stressed.

Improvement of these properties by depositing a functional coating on their surface is the aim of many researches, especially for outdoor application where the abrasion resistance and the UV stability play an important role. Because of their poor thermal stability, the deposition techniques available to coat plastic substrates are therefore limited.

The surface properties of polymers are determined by their chemical composition and the differences between them are more significant than those of inorganic glasses and moreover they vary with the preparation conditions and aging. The most common plastics are made of long chains carbon atoms. Some of the most significant plastics and their structures are listed in Table 3 (11).

Table 3: Structure of some plastic materials

Material	Structure
Polystyrene (PS)	$\begin{array}{c} \text{H} \quad \text{H} \\ \quad \\ -\text{C} - \text{C}- \\ \quad \\ \text{H} \quad \\ \quad \quad \text{C}_6\text{H}_5 \end{array}$
Polyethylene (PE)	$\begin{array}{c} \text{H} \quad \text{H} \\ \quad \\ -\text{C} - \text{C}- \\ \quad \\ \text{H} \quad \text{H} \end{array}$
Polycarbonate (PC)	
Polymethyl methacrylate (PMMA)	$\begin{array}{c} \text{CH}_3 \\ \\ -\text{C} - \text{C}- \\ \quad \\ \text{H} \quad \text{H} \\ \quad \quad \\ \quad \quad \text{C} \\ \quad \quad // \quad \backslash \\ \quad \quad \text{O} \quad \quad \text{O} - \text{CH}_3 \end{array}$
Polyvinyl chloride (PVC)	$\begin{array}{c} \text{H} \quad \text{H} \\ \quad \\ -\text{C} - \text{C}- \\ \quad \\ \text{H} \quad \text{Cl} \end{array}$

Cleaning the plastic substrates before coating is a difficult task because of their poor mechanical stability. In most cases, special surface pretreatments should be done to increase the free surface energy to obtain a good coating adhesion and mechanical durability. Such process include flame, plasma, corona, chemical, UV-irradiation or the deposition of an adhesion promoting primer. These processes generally roughen the surface of plastics and remove part of a weakly bound layer present on the top surface which alter the surface chemistry of the surface. The surface pretreatment processes to be applied depend significantly on the type of the substrates, the type of the coating material to be deposited and also on the deposition method. For example, PMMA can be modified by a DC cathode sputtering and water-reactive gas mixture to restructure the surface polymer to ease the

deposition of thin films by evaporating technique. However, in the case of PC substrate, a light argon-ion treatment using a plasma source is sufficient to activate the surface of the substrate (148).

For many application the plastic substrates need to be coated to obtain the required properties, e.g. antistatic, abrasion resistance, antireflection etc.. Processes like magnetron activated deposition, hollow cathode activated deposition and pulsed magnetron sputter deposition process (149) have been developed to coat such substrates with hard optical coatings. The introduction of reactive gas into the chamber or the production of a plasma close to the substrate enhance the layers properties. Low temperature arc vapor deposition (LTAVD) method (150) has been developed to coat plastic substrates with thick conducting and semiconducting materials with enhanced adhesion by generating a large flux of energetic ions even at 25 °C.

The most used materials required to modify the surface characteristics are inorganic-organic materials based on the processing of metal alkoxide and organosiloxanes by the sol-gel method (28, 151), and can be cured thermally at low temperatures (152, 153) or by UV-irradiation (19, 154). These materials form a cross-linked Me-O-Me inorganic backbone providing high abrasion resistance and the polymerization of the organic network offers better adhesion and impact toughness. When other inorganic compounds are added to the sol, additional functions such as nonlinear optical properties (155), antifogging, low energy coating materials (156), antistatic - antiglare (18, 157, 158) can be obtained.

2.6 Nanostructured Materials Technology

2.6.1 Introduction

Nanometer sized particles have unusual mechanical, optical, magnetic and electrical properties that make them of interest for novel applications. There is no universally agreed definition of a nanoparticle, However most research groups consider that particles with at least one dimension smaller than 100 nm are nanoparticles and those with dimension in the range $100 \text{ nm} < d < \sim 10 \text{ }\mu\text{m}$ are called microparticles. The physical properties of the nanoparticles can vary significantly as the particle size changes (159). The specific properties of nanoparticles include (160, 161): dispersability in an immiscible phase, uniformity and fine grain size, extremely high specific surface area, control of the scattering of light, enhanced chemical activity of atoms and molecules at the interface, absorptive capabilities, microstructure control, transport properties of small domains and in pores, controlled electronic states of atoms etc.

Due to these properties, nanoparticles have numerous commercial and technological applications (162-167). For instance, because of their very small size (20 times smaller than the wavelength of the visible light), they do not scatter light providing new perspectives for optical coatings (168). Their large specific area make them attractive to realize chemical or physical sensors for detecting the state of chemical reactions (169). Also these nanoparticles

demonstrate quantum effect resulting in material innovations in communication, data storage, non-linear optic or with special magnetic properties (170, 171).

Many of these applications deal with dispersions or coatings with enhanced specific features. Much of the demand comes from the cosmetic and pharmaceutical industries (160, 172), where they show incredible commercial potential as for example to shield the skin from particularly damaging ultraviolet irradiation (173). In the field of medicine, magnetic nanoparticles found application particularly for the precise delivery of drugs to the exact target tissue by application of external magnetic fields (174).

Various methods were used for synthesizing nanoparticles. The first development was made by Gleiter and Siegel (175, 176) by evaporation and condensation (nucleation and growth) in a subatmospheric inert-gas environment. This method, called gas phase synthesis, is similar to the physical vapour deposition (PVD), but instead of using a substrate, liquid nitrogen is used to condense the vaporized material. The disadvantages of this method are the high temperature processing, the difficulty to control the particle size and distribution and the low production rate. Various aerosol processing techniques have been then reported to improve the production yield of nanoparticles (177). These include synthesis by combustion flame, plasma, laser ablation, chemical vapor condensation, and plasma spray (178-182).

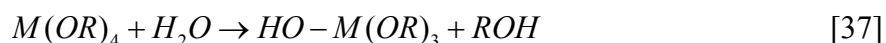
The chemical synthesis of nanoparticles is a promising technique to produce nanomaterials via low temperature processes. The sol-gel process (discussed in the next section) can form nanoparticles starting with precursors of different composition and structure. The institute of new materials (INM) in Saarbruecken is one of the few research centers which succeeded to produce a broad range of nanoparticles like TiO_2 , Al_2O_3 , BaTiO_3 , ITO, ATO, etc through this process. The new materials built with these nanoparticles have already found many industrial applications (183-189).

2.6.2 Synthesis of nanomaterials via Sol-Gel technology

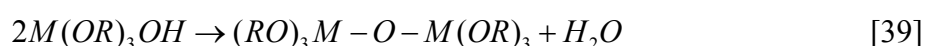
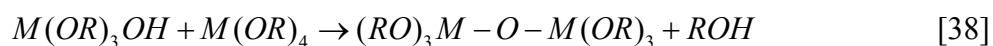
The sol-gel process is a versatile solution process for making ceramic and glass materials. It involves the transition of a system from a colloidal suspension, called sol, into a solid "gel" phase. The precursors used in the preparation of the "sols" are usually inorganic metal salts or metal organic compounds such as metal alkoxides which are subjected to hydrolysis and polymeration reactions to form a colloidal suspension. By further processing (drying, heat treatment), ceramics or glass materials in a wide variety of forms can be obtained: ultra-fine powders, thin film coatings, ceramic fibers, microporous inorganic membranes, monolithic ceramics and glasses, or extremely porous aerogel materials (28, 190). This low-temperature process for synthesizing materials can be totally inorganic in nature or involve inorganic and organic parts and due to a reduction of the loss of volatile components it is a more environmental friendly process.

The most commonly used precursors for sol-gel film formation are metal alkoxide ($\text{M}(\text{OR})_z$), where R stands for an alkyl group ($\text{C}_x\text{H}_{2x+1}$) and M for a metal. Normally, the alkoxides are

dissolved in alcohol and hydrolyzed by the addition of water under acidic or basic conditions, as in the following simplified example:



The chemical reactivity of metal alkoxides is related to the R groups; the larger the R is, the slower is the hydrolysis. Condensation reactions involving the hydroxyl ligands produce polymeric species composed of M-O-M bonds, and in most cases, water or alcoholic by-products as shown below:



Drying and / or heating lead eventually to the formation of metal oxides.

The sol-gel process is also a versatile technique for the preparation of crystalline nanopowders. The synthesis chemistry is very complex and controlled by a large number of parameters which were studied extensively (24, 70, 191-201). Among the advantages of this technique is the possibility to obtain raw materials with better sintering activities, more homogeneous powders in multicomponent systems and to tailor grain sizes and distribution (191).

The emulsion and the precipitation routes are the main nanoparticles sol-gel routes. In the former case, a sol-gel reaction is carried out in “mini” reactors containing a dispersed liquid phase in another one, such as an emulsion of water-in-oil (w/o) or oil-in-water (o/w). The stability of the emulsions are controlled by adjusting the interfacial tension of the two systems by using surface active additives (emulsifiers) (202).

The chemical precipitation is a well established method for producing a large variety of nanoparticles. The process is a controlled growth technique, initiated by a nucleation step followed by the growth of the particles. Nucleation is the least understood step. Three main types occur in chemical precipitation (161): homogeneous, heterogeneous and secondary nucleation. The first one occurs in the absence of solid interface, the second one in the presence of foreign seed surfaces and the last one in the presence of solute particle’s interface. The dominance of each nucleation type varies with the precipitation conditions. After the nucleation process, the particles growth takes place and the kinetic of this process determines the structure and particle size distribution, a very important task.

Normally crystals do not occur as discrete units but usually form clusters. The agglomeration of the particles during their growth can be avoided by controlling the thermodynamics of the interfaces either by restricting the reaction volume in the case of the microemulsion techniques or by controlling the surface energy of the particles by in-situ surface modification in the case of the controlled growth reaction, which provides steric repulsive forces between the particles.

2.6.3 Colloidal Suspension

A colloidal suspension, as defined by Ostwald (203), is a system consisting of two phases, i.e. a continuous phase in which the other phase, containing entities having at least on the 1 to 1000 nm length scale, is dispersed. The particles in the suspension undergo a Brownian motion and collide with each other. When they come close enough to each other, they stuck due to the Van der Waals attraction and aggregates are formed leading to phase separation. The aggregation of particles can be prevented or reduced by different mechanisms.

Steric stabilization: The steric force is a repulsive force used to prevent the particle to come close to each other by attaching physically or chemically a surfactant or polymers to the surface of the particle. When two particles with their envelopes of organic chains approach each other, the chains in the gap between the particles lose its conformational entropy and resist a further approach as shown in Fig. 6 (204). This dispersion (or stabilization) repulsive force is a function of the surfactant coverage, the type of bond formed at the surface and the type of the solvent(205).

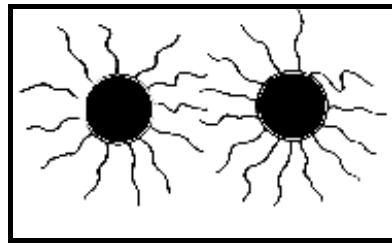


Fig. 6: Nanoparticles dispersion via steric stabilization.

Electrostatic Stabilization (double layer): The electric charging of the particle can arise from different mechanisms and can be manipulated and controlled by adjusting the suspension pH and by using suitable dispersants. This is done by measuring the so-called zeta potential. The particles charge is balanced by equal and opposite amount of charges carried by the ions in the surrounding liquid. These counter ions tend to cluster in diffuse clouds around the particles forming a so-called an electrical double layer (Fig. 7). The electrical potential drops off exponentially with the distance from the particle and reaches a uniform value in the solvent outside the diffuse double layer. The zeta potential is the voltage difference between a plane at short distance from the particle surface and the solvent beyond the double layer (206).

When two particles come close together so that their double layers overlap, they repel each other. The strength of the electrostatic force depends on the zeta potential. If it is too small (typically less than about 25 mV), the repulsive force is not strong enough to overcome the Van der Waals attraction between the particles and they start to agglomerate. A high zeta potential prevents the particle-particle agglomeration and keeps the dispersion uniform and free flowing. Therefore, the goal in most formulations is to maximize the zeta potential. This is particularly important to produce high strength ceramic materials (207).

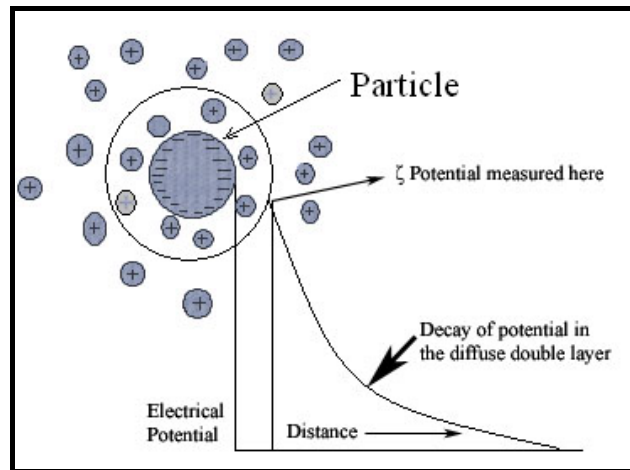


Fig. 7: The electrical double layer and the zeta potential (208).

A well electrostatically stabilized sol can be used for ceramic processing or the deposition of coatings using the conventional sol-gel methods. However the transformation of sols to gels is the crucial point in the nanoprocessing (209). The removal of the electric charge from the stabilized sol leads to a very fast gelation process which is difficult to control and which result in a high concentration of defects and a broad size pores distribution. These pores could be eliminated by sintering the coatings at very high temperatures.

Chapter 3

TCO coatings: state of the art

This chapter presents an overview of the state of the art of TCO coatings deposited on both glass and polymeric substrates. The industry demand for TCO materials is continuously growing as such coatings are today essential components in numerous applications. The choice of TCO materials depends mainly on the specific requirements and for many of them a low resistivity and, simultaneously, a high transparency is mandatory.

3.1 Transparent conducting coatings on glass substrates

Glass is one of the most important industrial materials. Their properties can be changed by depositing specific coatings on their surface leading to new chemical, surface, mechanical, electrical and optical properties. Making glasses electrically conductive by depositing on their surface a TCO material and letting them at the same time retain their optical quality has opened many avenues for their application. Electrical resistivity, optical transmission, IR reflection, environmental and life time stability, structural and morphological properties of the surface, chemical resistance and etchability of the layers are among the most important required properties.

Transparent conductive coatings have been deposited on glass substrates by vapor and wet chemical deposition methods. Each of these methods has its own advantages and disadvantages. The properties of such coatings have been studied extensively as a function of the deposition parameters for a variety of TCO materials such as oxides of cadmium, tin, indium, zinc and complex ternary and quaternary oxide compounds.

3.1.1 Vapor deposition of TCO coatings on glass

Sputtering

It is the most extensively used method for obtaining high quality transparent conducting coatings. The deposition temperature of the substrate ranges from 30°C to 600°C and high quality films are obtained if the deposition rate is low. The TCO films obtained by this method require usually a post deposition heat treatment under protective atmosphere in order to enhance their electrical conductivity.

The properties of sputtered TCO films are controlled by many parameters. Bhagwat et al. (210) have studied the effect of the deposition time, oxygen flow rate, argon partial pressure, etc. on the electrical, optical and mechanical properties of indium tin oxide coatings deposited by d.c. magnetron sputtering. Resistivity of $10^{-3} \Omega\text{cm}$ and visible transmission of about 85% have been obtained at room temperature. By annealing the films in argon atmosphere at 200°C, the conductivity was improved by 20 to 40% and only little variation of the transmission was observed. The same technique was also used to produce transparent conductive ZnO and Al doped ZnO (AZO) films on silicon and quartz substrates (211). The

resistivity of ZnO:Al film was found seven order of magnitude smaller than that of pure ZnO. AZO film with a resistivity of $3.3 \times 10^{-2} \Omega\text{cm}$ was obtained at a substrate temperature of 350°C . Increasing the substrate temperature to 560°C decreased the resistivity to $9.3 \times 10^{-3} \Omega\text{cm}$. Chang et al (113) have observed an enhancement of the crystallinity and of the grain growth of AZO films by raising the substrate temperature. The lowest obtained resistivity was $4.1 \times 10^{-4} \Omega\text{cm}$ for a substrate temperature of 250°C .

The properties of TCO sputtered thin films were also found to depend on the sputtering atmosphere. The presence of hydrogen gas during the process enhances the smoothness and the number of charge carriers of ITO films deposited at low temperature (212). The electrical conductivity of rf sputtered TCO films can also be enhanced by further post annealing in nonoxidising atmosphere at higher temperature ($300\text{--}400^\circ\text{C}$). For example it was found by Nanto et al (213) that heating rf sputtered ITO films in air deteriorates the electrical conductivity; however, heating in vacuum or nitrogen atmosphere decreases the resistivity, as the number of charge carriers increases. By these post-deposition heat treatment, resistivity as low as $2 \times 10^{-4} \Omega\text{cm}$ was obtained. The influence of the post annealing treatment was also investigated for rf sputtered AZO films (214). A resistivity as low as $6.2 \times 10^{-4} \Omega\text{cm}$ and a transparency greater than 80 % were obtained when the films were post annealed in vacuum at 400°C for 20 min.

El Akkad et al (101) reported a detailed study of the properties of ITO films deposited under various preparation conditions using the rf sputtering technique. The influence of the thickness was examined and the electrical resistivity of the film was found to decrease from 1.07×10^{-3} to $3.14 \times 10^{-4} \Omega\text{cm}$ when the thickness increased from 90 to 850 nm, respectively.

Evaporation

This method was also used to deposit transparent conductive indium oxide thin films (83, 89, 215, 216). The substrate temperature has a significant effect on the surface structure, composition and morphology of the coatings. Changes in the morphology of ITO thin films are reported in (89) and (217). An increase of the deposition temperature helps the substitution of Sn^{4+} at the In^{3+} site and increases the mobility of the charge carriers. George et al (218) has reported a significant decrease of the resistivity of electron beam evaporated ITO films from $3 \times 10^{-2} \Omega\text{cm}$ to $3 \times 10^{-4} \Omega\text{cm}$ when the substrate temperature was increased from 50 to 350°C . High quality ITO films with resistivity as low as $2.2 \times 10^{-4} \Omega\text{cm}$ and average transmission of 88 % were reported by Nath and Bunshah (83) using activated reactive evaporation with a substrate temperature of 350°C . By producing a dense plasma at the same temperature, a resistivity of $7.5 \times 10^{-5} \Omega\text{cm}$ and average transmission of 85 % was reported for ATO films (219).

Pulsed laser deposition (PLD)

This method was used successfully to deposit high conductive transparent films on many type of substrates (53, 220-222). Their electrical and optical properties are influenced significantly by the substrate temperature and the oxygen pressure during the deposition. ITO thin films

were deposited by PLD on glass substrates using a KrF excimer laser ($\lambda = 248$ nm) (223). Their electrical conductivity was increased significantly by raising the substrate temperature from 25 to 300 °C due to the growth of the grain size. In another work, Suzuki et al (94) have deposited ITO films on glass and quartz substrate using an ArF excimer laser coupled to a magnetic field perpendicular to the plume. A very low resistivity of $7.2 \times 10^{-5} \Omega\text{cm}$ and a high optical transmittance of more than 90 % in the visible range were obtained for a 30 nm thick films deposited on a substrate at a temperature of 300 °C. The high conductivity was due to the high carrier concentration of $2.5 \times 10^{21} \text{ cm}^{-3}$. Similar result was obtained by Adurodija et al (220). For a substrate temperature of 300 °C, a resistivity as low as $8.5 \times 10^{-5} \Omega\text{cm}$, a high carrier concentration of $1.2 \times 10^{21} \text{ cm}^{-3}$ and a high Hall mobility, 40-57 $\text{cm}^2/\text{V.s.}$, were achieved.

High quality indium-zinc oxide thin films were deposited on glass substrate at a substrate temperature of 500 °C and oxygen pressure of 10^{-3} mbar (224). The lowest resistivity, $\rho = 6.5 \times 10^{-4} \Omega\text{.cm}$, was obtained for the $\text{Zn}_2\text{In}_2\text{O}_5$ composition with a band gap of about 3.5 eV and a 90 % transmission in the visible region. PLD methods have been also used to deposit transparent conducting mixed oxides of ZnO and ZrO_2 at $T = 200$ °C (222). A resistivity of $5.4 \times 10^{-4} \Omega\text{cm}$ and a transparency of more than 80 % in the visible range were obtained.

Chemical vapor deposition (CVD, MOCVD)

This method is simple and inexpensive, but it needs usually high deposition temperature. Yadava et al (225) have used a CVD technique in order to produce highly transparent conducting tin oxide films on glass from the reactive thermal evaporation of SnCl_2 . The best results concerning the structural, optical and electrical properties were obtained at a substrate temperature in the range of 500-550 °C. Highly transparent conducting FTO coatings with resistivity of $5 \times 10^{-4} \Omega\text{cm}$, carrier concentration of $7 \times 10^{20} \text{ cm}^{-3}$ and carrier mobility of 20.1 $\text{cm}^2/\text{V.s}$ were prepared by atmospheric pressure CVD (APCVD) (226). Low pressure CVD of fluorine doped indium oxide films was performed by Miinea et al (87) using an alkoxide complex. The films were polycrystalline, with a transparency of more than 85 % in the visible region and a resistivity of ca. $1.4 \times 10^{-3} \Omega\text{cm}$ after annealing in Argon atmosphere at 500 °C.

Zhao et al (227) have prepared tin doped CdO films deposited on glass substrate at temperature in the range of 200-300 °C by atmospheric metalorganic chemical vapor deposition (MOCVD). The film showed a strong adherence to the substrate and its resistivity showed a minimum of $2.1 \times 10^{-4} \Omega\text{cm}$ at 250 °C. The value was further improved by post annealing under He or H_2 atmosphere and the state of the art value is $1.4 - 1.6 \times 10^{-4} \Omega\text{cm}$.

Conclusion

Vapor deposition methods allows to deposit TCO films with low specific resistivity on glass substrates. Typical values are in the range of 10^{-3} to 10^{-4} Ωcm , however resistivity of the order of 10^{-5} Ωcm has been reported for films deposited by PLD and ARE techniques. Deposition and post annealing temperature, which lead to higher electron mobility and carrier density, are decisive in enhancing the conductivity of the coatings. These films show high transmittance ($> 80\%$) in the visible range.

3.1.2 Wet chemical deposition of TCO on glass (high temperature process)

As shown in section 2.2.2, spray pyrolysis, pyrosol and sol-gel (spin or dip coating) are adequate processes to deposit high quality TCO coatings on glass with sintering at high temperatures.

Spray pyrolysis

This method was used extensively to deposit indium oxide (In_2O_3), tin oxide (SnO_2) and zinc oxide (ZnO) (20, 68, 72, 114, 228, 229). The substrate temperature was found to affect strongly the structural, electrical and optical properties of spray deposited films. The resistivity of Boron doped tin oxide deposited on glass decreases from 5.4×10^{-3} to 7.0×10^{-4} Ωcm when the deposition temperature was raised from 425°C to 500°C (72). The low resistivity was achieved because of the higher degree of crystallinity of the films. Bisht et al (230) studied the deposition of FTO, ATO and ITO coatings on hot borosilicate glass substrates. A low resistivity of $2\text{-}3 \times 10^{-4}$ Ωcm was obtained for ITO layers after reducing the samples in forming gas at 400°C , a higher value of 1×10^{-3} Ωcm was obtained for ATO layers and a value of 5×10^{-4} Ωcm was obtained for FTO layers. Therefore sheet resistance less than $10 \Omega_{\square}$, i.e. comparable to those obtained by sputtering, can be achieved for 200 nm thick ITO coatings or 500 nm FTO coatings. ATO coatings showed a lower transmittance in the visible region (70-75 %) compared to that of ITO and FTO coatings ($> 80\%$).

Shanthi et al (231) reported a similar resistivity (5.5×10^{-4} Ωcm) for FTO films with high optical transmission ($> 80\%$) with a substrate temperature of 400°C . Both the concentration and the mobility of free carriers was found to increase with the substrate temperature, the change in the mobility being however larger than that of the carrier concentration.

Pyrosol

It is a CVD method where the precursor of the material to be deposited is dissolved in a solvent. Smith (74) has reported the deposition of ZnO and SnO_2 based films. The relation between the solution chemistry, growth rate and the morphology of the film was studied. This method was also used to prepare undoped and Al-doped zinc oxide thin films on heated Corning 7059 glass substrates with transparency of 80 % and a resistivity of 3.5×10^{-3} Ωcm (232). Similar result was obtained for IZO films deposited on the same substrate at $425\text{--}475^\circ\text{C}$ (233). The pyrosol method was also used to deposit FTO thin films on large-area soda-lime glass substrates. Resistivity of 5×10^{-4} Ωcm and optical transmittance in the visible

region of more than 80 % for 300 nm thick films were obtained by Dutta et al (27). High conducting ITO thin films with resistivity of $1.7 \times 10^{-4} \Omega \cdot \text{cm}$ and transparency of ca. 94 % were prepared on glass substrates at a deposition temperature of 480 °C (234).

Sol-gel processes

Sol-gel transparent conductive films have been frequently studied. It has been reported by Arfsten (105) that ITO thin films with electrical and optical properties comparable to those obtained by PVD methods could be processed on glass substrates by controlling the process parameters.

Heat and post annealing treatment: Sol-gel films are strongly affected by either heat treatment and post annealing treatment, because a high thermal energy is needed to densify and enhance the crystallinity of the layers. Nishio et al (235) have prepared ITO thin films on quartz glass substrates by dip coating process. The resistivity of the coatings decreased from 1.5×10^{-2} down to $1.5 \times 10^{-3} \Omega \cdot \text{cm}$ by increasing the heat treatment temperature from 400 to 800 °C. Takahashi et al (97) have also observed a decrease of the resistivity of dip coated ITO films by one order of magnitude by increasing the firing temperature from 400 to 700 °C. This decrease was due to the remarkable increase of the carrier mobility from $1.3 \text{ cm}^2/\text{V} \cdot \text{s}$ at 400 °C to $14 \text{ cm}^2/\text{V} \cdot \text{s}$ at 700 °C. After annealing the films at 650 °C in Nitrogen a resistivity of $4 \times 10^{-4} \Omega \cdot \text{cm}$ was obtained. Tahar et al (236) have prepared cadmium stannate films by a dip coating technique with resistivity of $3.3 \times 10^{-4} \Omega \cdot \text{cm}$ after annealing at 680 °C in Nitrogen, similar to ITO films prepared at 650 °C by the same technique (237).

The fabrication of indium tin oxide films on a Corning glass by multi-dip coating process using ethanolic solution of chlorides and surfactants was reported in (238). The coatings were sintered at 600 °C in air for 30 min and then post annealed in forming gas ($\text{N}_2/\text{H}_2 = 90/10$) at 600 °C for 1 h. The resistivity of the ITO layers decreased drastically from $2 \times 10^{-3} \Omega \cdot \text{cm}$ down to $2.5 \times 10^{-4} \Omega \cdot \text{cm}$. The post annealing in nonoxidizing atmosphere was found to increase remarkably the carrier concentration from $2.5 \times 10^{20} \text{ cm}^{-3}$ to $9.1 \times 10^{20} \text{ cm}^{-3}$ and the mobility from $20 \text{ cm}^2/\text{V} \cdot \text{s}$ to $30 \text{ cm}^2/\text{V} \cdot \text{s}$. Similar annealing effect was also reported by Shiegeno et al (239). The resistivity of a 200 nm thick film obtained by the dip coating method decreases from $1.9 \times 10^{-3} \Omega \cdot \text{cm}$ down to $3.1 \times 10^{-4} \Omega \cdot \text{cm}$ when annealed at 600 °C for 1 h in a N_2 -0.1% H_2 atmosphere.

Effect of other annealing treatments: Wakagi et al (240) reported that spin coated ITO films post treated using an electron plasma exhibited lower resistivity compared to thermally annealed ones. The explanation given is that such plasma annealing leads to a higher density and a lower amount of organic impurities. Kololuoma et al (241) have studied the effect of argon plasma post treatment on the electrical conductivity of spin coated ATO thin films. The sheet resistance decreased from $600 \Omega_{\square}$ to about $200 \Omega_{\square}$ after about 20 to 75 min. This improvement was attributed to the porous nature of the sol-gel films. The depletion layers between the particles was effectively removed by the process and more oxygen vacancies

were created in the bulk of the film. No measurements of the carrier concentration and the carrier mobility were carried out to investigate the plasma treatment.

Multi-layer deposition: The influence of multilayer dip coating deposition of tin oxide film on the thickness, microstructure and the electrical properties was investigated by Park et al (242). The resistivity was reduced by a factor 10 by increasing the number of the layers from 1 to 10, while the porosity of the coatings was found to decrease significantly from 60 % down to 12 %. Takahashi et al (97) observed that multilayer deposition of ITO films develop a columnar structure with resistivity of $4 \times 10^{-4} \Omega \cdot \text{cm}$, while single layers are composed of particles of spherically shape with resistivity of $6.4 \times 10^{-3} \Omega \cdot \text{cm}$. Aegerter et al (82) have studied the influence of multiple deposition of ATO coatings produced by the dip coating method. It was also observed that the resistivity decreases with the number of layers and that the coatings become denser.

Single thick layer: It is difficult to produce single layer with reasonable thickness using sol-gel methods. Therefore multiple coating processes are required in most cases to produce thick films, a process which is inadequate for practical application. Nevertheless Furusaki et al (22) succeeded to dip coat ITO films with a thickness up to $2 \mu\text{m}$ using a single dipping-firing procedure (550°C for 30 min). The resistivity was $0.1 \Omega \cdot \text{cm}$ and the transparency in the visible region was greater than 90 %. On the other hand Gallagher et al (243) prepared single dip coating ITO films sintered at 518°C with a thickness of 273 nm, a specific resistivity of $1 \times 10^{-3} \Omega \cdot \text{cm}$ and a transparency of 95 %.

Wet deposition using conducting nanoparticles

The use of conducting nanoparticles to produce transparent conducting films via wet chemical deposition is an interesting issue which has not been extensively studied. Solutions made of dispersed particles allow to deposit a thick layer in a single step. Aikens et al (244) have prepared crystalline ITO nanopowder by the gas phase condensation method. Aqueous dispersion of such particles could effectively be deposited on glass substrates by the spin coating method but the films had however a high sheet resistance, $R_{\square} = 10^6 \Omega_{\square}$. After a thermal treatment in air at 350°C , the sheet resistance decreased down to $10^4 \Omega_{\square}$. With a further heat treatment under forming gas at 350°C for 30 min, a reduction of the sheet resistance down to $10^3 \Omega_{\square}$ was obtained. The thickness of the layers was not reported.

Ederth et al (245) also studied the electrical and the optical properties of films prepared by spin coating a dispersion of nano-sized ITO particles. The films had a resistivity of $30 \Omega \cdot \text{cm}$. After annealing in vacuum at $200\text{--}400^\circ\text{C}$ for 2 hours, and subsequently in air at 500°C for 2 hours, the resistivity decreased down to $1 \times 10^{-3} \Omega \cdot \text{cm}$. The layers had a transmittance of 90 % in the visible range.

ATO particles prepared by a co-precipitation method followed by a hydrothermal processing step was used to produce thick transparent conductive layers (200 – 700 nm thickness) on glass substrate (70). An aqueous ATO sol was spinned and then fired at different temperature

up to 700 °C. The films dried at low temperature (50 °C) showed a resistivity of 7.5 Ω.cm and by increasing the sintering temperature up to 700 °C the resistivity decreased significantly down to 7.5×10^{-3} Ω.cm. It was reported that the sintering at higher temperature was accompanied by a decrease in the specific BET surface of the particles, resulting in a better contact between them and a lower grain scattering.

Burgard et al (246) have deposited transparent conductive ATO coatings on glass substrates using aqueous solution of fully dispersed nanocrystalline particles, made by the controlled growth reaction method. The deposited layers were conducting after thermal densification at $T > 400$ °C and showed a minimum resistivity of 2.5×10^{-2} Ω.cm and a transparency of 90 % in the visible range. In another work, Goebert et al (247) prepared crystalline ITO and ATO nanoparticles using the same method. Suspensions of these particles were used to prepare transparent conductive coatings on glass substrates using wet chemical deposition methods. For ATO coatings, the lowest resistivity, $\rho = 1.7 \times 10^{-2}$ Ω.cm was obtained after sintering at 550 °C. In the case of ITO layers, the lowest resistivity, $\rho = 3.4 \times 10^{-3}$ Ω.cm was obtained after sintering temperature at 900 °C and a post annealing at 300 °C in nitrogen atmosphere. The optical transmission of both coatings was excellent in the visible range (> 90 %). Kawata et al (248) have claimed that transparent conductive films can be formed using a transparent electroconducting ink made of dispersed ITO nanoparticles and a binder. The specific resistivity of films backed at temperatures of 400 °C or higher ranged from 0.5 to 0.01 Ω.cm.

Conclusion

TCO films deposited on glass substrates by wet chemical deposition methods showed low resistivity down to about 10^{-4} Ω.cm like those obtained by vapor deposition methods. The need of high temperature sintering is essential to bring the crystallite grains into contact together easing the transfer of the charge carriers across the layer. Post annealing treatment under reducing atmosphere increases the carrier density of ITO films which exhibit the lowest resistivity among the TCO family. Low sheet resistance can however only be obtained by multilayer deposition.

The production of thick films in a single step is still a challenge. The use of sols made of dispersed conducting nanoparticles allows to obtain thick films with high transparency in a single step; however a very high thermal energy is needed to sinter the particles. The lowest resistivity obtained from such coatings was in the range of 10^{-3} Ω.cm.

3.2 Transparent conductive coatings on plastic substrates (low temperature)

There is a growing interest in replacing glass substrates by polymeric ones in many applications. Therefore the need to coat such heat sensitive substrates and also preformed glasses which can not withstand high temperature sintering treatments have considerably increased. The challenge is to find suitable conducting materials which can be deposited at low temperature and to find a method allowing to crystallize the materials at low temperature

without affecting the film optical quality. As shown above the conductivity of TCO materials is proportional to the product of the carrier concentration and mobility. The obtention of a high carrier mobility needed to achieve both low resistivity and high transparency is the major problem for coatings deposited at low deposition temperature because the mobility was found to strongly increase with the deposition temperature (249, 250). A low value will always limit the electrical conductivity unless non-thermal techniques are developed to improve the coating microstructure (251) without damaging the heat sensitive substrates.

3.2.1 Physical deposition

ITO is a material which crystallizes at relatively low temperature, about 150 °C. The deposition of films on unheated substrate via a low energy process may therefore result in the formation of an amorphous layer. Paine et al (252) have monitored the crystallization process starting from an amorphous ITO film. They have found that under annealing, amorphous films undergo a structural relaxation occurring via local ordering that increases the carrier density and a crystallization process occurring via the classical nucleation and growth mechanisms which enhances the carrier mobility. The crystallization of reactive evaporated ITO films was achieved at temperature lower than 150 °C by increasing the film thickness as observed by Muranaka (253).

New low temperature deposition techniques have been also developed. Akagi et al (254) prepared high quality ITO films using synchrotron radiation ablation at room temperature. A resistivity as low as $1.3 \times 10^{-4} \Omega \cdot \text{cm}$ and a transparency of 85 % at 550 nm were obtained. Using a dual ion beam sputtering system, polycrystalline ITO films were obtained on glass substrates at room temperature (255). By increasing the assisted ion beam voltage, they observed an increase of the transmittance from 80 % to 90 % and unfortunately an increase of the resistivity from $1.3 \times 10^{-3} \Omega \cdot \text{cm}$ to $3 \times 10^{-3} \Omega \cdot \text{cm}$ due to the decrease of the grain size of the crystals. Reactive evaporation method was also used by Ma et al (256) to deposit ITO thin films with resistivity of $7 \times 10^{-4} \Omega \cdot \text{cm}$ on different polymeric substrates such as PET, PI and polyester substrates at temperatures between 80 and 240 °C. A new method called dc arc-discharge ion plating was reported recently to produce low resistivity ITO thin films on SiO_2 coated polycarbonate substrates at temperature less than 100 °C (257). The films were polycrystalline with [111] preferred orientation and exhibit a resistivity of $2.45 \times 10^{-4} \Omega \cdot \text{cm}$ and a transmission of 80 % in the visible spectrum without any deformation of the substrate.

Pulsed laser deposition method is also a quite effective method to deposit transparent conducting films at low temperatures (258, 259). The crystallization state and consequently the resistivity of ITO films are affected by the substrate temperature. On glass substrates amorphous films with resistivity of $4.5 \times 10^{-4} \Omega \cdot \text{cm}$ have been obtained at room temperature while polycrystalline layers with lower resistivity of $1.6 - 1.8 \times 10^{-4} \Omega \cdot \text{cm}$ have been obtained at 200 °C (260-262).

This technique has been used to deposit ITO films on different polymeric substrates. Resistivity value of $7 \times 10^{-4} \Omega \cdot \text{cm}$ and $4.1 \times 10^{-4} \Omega \cdot \text{cm}$ were obtained for ITO films deposited on

PET substrates at 25 and 100 °C, respectively (263). For PC substrates a CeO₂ thin film was first deposited to prevent the coloring of the substrate (264). The deposition of an Al₂O₃ layer between the PC substrate and the CeO₂ layer resulted in a marked decrease of the resistivity of ITO layer.

dc magnetron sputtering techniques have also been used to deposit TCO on polymer web at low temperature (265). Minami et al (266) produced ITO films on PET substrate with a resistivity of $1 \times 10^{-3} \Omega \cdot \text{cm}$ by annealing the film at 150 °C for 100 h. ITO coatings have been deposited on curved polymer substrates (267) at low temperature by controlling the sputter deposition uniformity across the complex shapes. Low resistivity of $6.2 \times 10^{-4} \Omega \cdot \text{cm}$, carrier concentration of $3.6 \times 10^{20} \text{ cm}^{-3}$ and mobility of $28 \text{ cm}^2 \text{ V}^{-1} \text{ s}^{-1}$ were obtained on unheated polymer substrates. A kinetic energy controlled sputter-deposition technique (268) was found to decrease the resistivity of ITO films down to $3.5 \times 10^{-4} \Omega \cdot \text{cm}$ even at temperature below 50 °C.

Ando and Haacke have claimed (269) that cadmium stannate thin films can be deposited on polymeric substrates (PC, PMMA) using dc magnetron sputtering method. The pre-coating of the plastic substrates with a metal oxide, such as SiO₂ or TiO₂, improves the adherence of the films onto the substrate. The average optical transmission was 80 %, the sheet resistance was $26 \Omega_{\square}$ and the films passed the tape adhesion test.

rf sputtering method allows to deposit thin films onto substrates without requiring substrate heating during the film preparation or any additional post annealing treatments. Kulkarni et al (270) have obtained a resistivity of $1.2 \times 10^{-3} \Omega \cdot \text{cm}$ for ITO film on PET, polycarbonate and glass substrates. rf sputtering was used successfully to prepare zero stress ITO films on polyester substrates near room temperature (271) with a low resistivity of $3 \times 10^{-4} \Omega \cdot \text{cm}$ and a high transparency (> 80 %).

Rf magnetron sputtering method was used by Wu et al (102, 272) to deposit transparent conductive ITO films on acrylic and PC substrates. To prevent the deformation of the acrylic substrate, the temperature of the substrate was maintained at 80 °C and a low rf power was used. For PC substrates higher values could be used. A low resistivity of $6 \times 10^{-4} \Omega \cdot \text{cm}$ was obtained for ITO films on both substrates and that deposited on PC substrate showed higher visible transparency (~ 90 %) and IR reflection than that on acrylic substrate (~ 74 %).

Nanto et al (213) have prepared highly conducting (resistivity ~ $2 \times 10^{-4} \Omega \cdot \text{cm}$) ITO thin films with high transparency (85 %) in the visible region on low temperature ($T < 140 \text{ }^{\circ}\text{C}$) substrates with a relatively high deposition rate by rf magnetron sputtering technique using Ar and O₂ gas mixture under plasma focused by magnetic field. In another work Maniv et al (273) have deposited transparent conducting zinc oxide and indium tin oxide films on plastic substrates using a modified reactive planar sputtering. The best zinc oxide film was achieved by a radio-frequency discharge close to the substrate to increase the oxidation rate. The films were polycrystalline with transmittance of 80 % and electrical resistivity of $3 \times 10^{-2} \Omega \cdot \text{cm}$ but their chemical stability was poor. In the case of ITO films a transmittance of 79 % and

resistivity of $1 \times 10^{-4} \Omega \cdot \text{cm}$ were obtained by coupling an rf power of 105 mW with a substrate self-bias voltage of less than 5 V. These films were amorphous and chemically stable. Transparent conducting Al-doped zinc oxide was deposited by rf magnetron sputtering (274) on different polymeric substrates, such as polypropylene (PPA), polyisocyanate (PI) and polyester substrates exhibiting a good adhesion, low resistivity ($\sim 5.8 \times 10^{-4} \Omega \cdot \text{cm}$) and high transmittance ($\sim 80\%$).

Conclusion

Transparent conductive oxide coatings can be produced at low deposition temperature using conventional physical and new developed deposition methods on glass as well as on polymeric substrates with resistivity ranging between 10^{-2} and $10^{-4} \Omega \cdot \text{cm}$ and transparency higher than 80%. ITO is the most preferred material to realize this task because of its low crystallization temperature.

3.2.2 Wet chemical deposition of TC coatings on plastics

The use of the conventional sol-gel techniques to deposit transparent conducting coating on polymeric substrates face a real challenge because a heat treatment of the coatings at high temperature can't be avoided to get good electrical, optical and mechanical properties. There are therefore not much works reported for the preparation of sol-gel made transparent conducting coatings on such substrates.

Foot (275) has claimed a sol-gel route to deposit TCO films on glass, PC and PMMA using spin, spray, dip and brush techniques. For instance sheet resistance of $380 \text{ k}\Omega_{\square}$ and visible transmittance of 90% were obtained with pre-treated PC substrate exposed to UV/ozone for two hours after drying the coatings under vacuum during more than 8 hours at 20 to 30 °C and followed by a short period of illumination with near infrared radiation. No information was reported about the adhesion of the coatings on the substrate. In another patent, Murouchi et al (276) have claimed the production of transparent conductive films on glass and plastic substrates with thickness in the range 0.5 to 5 μm with a sheet resistance of the order of $10^2 - 10^5 \Omega_{\square}$, a transmittance of at least 80% in the visible range and a haze not greater than 6%. The films were formed from a composition of ITO powder dispersed in a binder solution and cured by an actinic radiation (UV-light, 0.1 – 5 J/cm^2) or an electron beam ($\sim 200 \mu\text{C}/\text{cm}^2$).

Imai et al (277) have reported the deposition of sol-gel ITO films which have been crystallized by exposing the coatings to a low fluence UV-irradiation of an ArF laser (193 nm, 10 – 20 mJ/cm^2). Resistivity of $6.6 \times 10^{-2} \Omega \cdot \text{cm}$ was obtained for coatings applied on polyimide, PET and glass substrates; however the process failed for PC and polyethyl-ethylketone substrates because of the degradation of the substrate by the UV-irradiation. The mechanical properties of such coatings were not mentioned.

Conducting polymers

Conducting polymers are another group of very interesting materials which have been developed over the past two decades. These materials are mainly based on polyaniline,

polypyrrole, polythiophene, polyacetylene, polyphenylvinylene, etc. (44, 45, 278). Depending on the conducting polymer the doped and the undoped state can be either transparent or intensely coloured. Most of the known conducting polymers are coloured and a very thin layer is required for obtaining high transparency. The electrical and the chemical properties of these conducting polymers change strongly during storage in environmental atmosphere. The electrical resistivity changes by the reaction with various redox agent or because of their instability to moisture (279). This makes them very useful as sensors.

The stability of the mechanical and the electrical properties of polypyrrole films were investigated as a function of the dopant concentration and the oxidative aging (280). The films were prepared by the galvanostatic electrochemical synthesis method with p-toluene sulphonate doping concentration of 0.005, 0.01 and 0.05 M yielding an initial resistivity of 66.6, 2.5 and 0.03 $\Omega\cdot\text{cm}$, respectively. The rate of loss of the conductivity was higher in the case of low dopant concentration.

Lee et al (281) have reported a novel transparent electrically conductive polymer composite prepared by blending a conductive poly(3,4-ethylenedioxythiophene) (PEDOT) and an inorganic silica network. The PEDOT polymer act as the conducting material and the silica network enhances the mechanical properties of the coatings. The films were spin coated and then processed at 130 °C in air for 1 hour. An increase in the content of PEDOT increases the conductivity but decreases the optical transparency. Films with a resistivity of $5 \times 10^{-3} \Omega\cdot\text{cm}$, more than 80 % transparency and 9 H pencil hardness have been obtained for a weight ratio PEDOT/silica of 0.6.

Conducting polymers are used extensively in organic light emitting diodes (OLED) devices. Gustaffson et al (282) have reported that polyaniline coated glass or plastic substrates are effective anode for these devices. They increase the work function of the anode and this results to a lower device operating voltage and a higher quantum efficiency due to the enhanced injection of holes into the highest occupied molecular orbital of the emitting organic layer. Cao et al (283) have prepared optical quality transparent conducting films of polyaniline and of conducting blends of polyaniline with amorphous bulk polymers by casting from a solution. The films are clear and combine low surface resistance with excellent transparency. By varying the thickness of the film and / or the volume fraction of polyaniline, the sheet resistance of the film can be controlled over very broad range ($10^2 \Omega_{\square} < R_{\square} < 10^6 \Omega_{\square}$).

Conclusion

Producing transparent conducting coatings on polymeric substrates via wet deposition methods is a difficult task. The lowest reported resistivity of TCO layers is of the order of $10^{-2} \Omega\cdot\text{cm}$. Transparent conducting polymers are good candidates to produce films with lower resistivity, however the degradation of their electrical, optical, chemical and mechanical properties by aging is still a real challenge.

Chapter 4

Experimental Methodology and Procedure

Introduction

The synthesis method of redispersable nanocrystalline $\text{In}_2\text{O}_3:\text{Sn}$ (ITO) powders, used in this work, is based on the so called in-situ surface modification of the particles performed during the precipitation and the growth process in a liquid phase. By the control of their free surface energy, their growth and the crystallite size can be adjusted and the aggregation process can be prevented. This chapter describes the synthesis of the redispersable ITO conducting nanopowder, the preparation of transparent conductive layers on glass and polymeric substrates and the patterning of the coatings at low temperature. All chemicals used are listed in appendix B.

4.1 Preparation of conducting ITO nanopowders

The preparation of the nanoparticles follow a recipe given in (91, 189, 246). A mixture of indium chloride (InCl_3), tin chloride pentahydrate ($\text{SnCl}_4 \cdot 5\text{H}_2\text{O}$) and C-caprolactam are dissolved using bidistilled water in a three neck round flask. The molar ratio indium chloride: tin chloride pentahydrate: C-caprolactam: water was 1: 0.012: 0.075 :114. This mixture is stirred continuously until a clear solution is obtained. Then the solution is heated up to 50°C in an oil bath. When the temperature of the solution is 50°C , an aqueous solution of ammonium hydroxide (25 wt.%) is slowly added dropwise to the solution under vigorous stirring. A white suspension is formed and left under stirring for 24 h at the same temperature (50°C). The pH of the solution is then adjusted between 11 and 14, by adding further amount of ammonia for complete precipitation. The solution is then cooled down to RT and centrifuged at 4000 rpm for 30 minutes to separate the solid phase from the liquid phase. The obtained powder is then washed with bidistilled water and again centrifuged at 4000 rpm for 30 min several times. Then the resulted white powder is dried at 150°C for 24 hr.

The dried material is grinded using a hammer mill to reduce the size of the agglomerates until a fine powder is obtained (size < 0.2 mm). It is then post annealed at different temperatures ($250\text{-}600^\circ\text{C}$) under forming gas (N_2, H_2) atmosphere using a GERO furnace. It is first evacuated and then N_2 gas is supplied at a flow rate of 100 l/h during the heating process at a rate of $250^\circ\text{C}/\text{h}$. When the desired temperature was achieved, the furnace is left for 60 min. under the flow of forming gas ($\text{N}_2/\text{H}_2: 92/8$) at a flow rate of 75 l/h and then cooled down to RT under a flow of N_2 with a flow rate of 50 l/h. The cooling rate is $1500^\circ\text{C}/\text{h}$. The so-obtained post annealed powder shows a green-blue colour. The powder is then characterized to determine the phase structure and the crystallite size using XRD technique. The density and the specific (BET) surface area were also determined. Detailed description of the methods of characterization of the prepared powders is found in appendix A.1.

4.2 Preparation of ITO coating solution

The post annealed ITO powders were used to prepare coating solutions by dispersing the powders in solvents like water or organic compounds, (e.g. ethanol). Two kinds of sols were used in this work: called a “pure ITO sol” and a “modified ITO sol”:

4.2.1 Pure ITO sol

The ITO powder is wetted in a small amount of EG/DBG (1 : 1 in weight) and a dispersion agent like TDOS. The concentration of the dispersing agent to the ITO powder ranges between 3 to 7 wt.%, which gives a pH value between 3 and 5. The concentration of ITO powders in the ranges between 75 – 80 wt.%. The wetted ITO powder is dispersed mechanically using a three roll mill (Exact) during 10 to 15 min. The process breaks up the agglomerated powder and insures that the particles are evenly wetted and dispersed down to the primary size. A thick and highly viscous dark blue ITO paste is obtained. This paste is the raw material for the coating solution, and it can be easily dissolved in water or ethanol.

Typically, to obtain a sol with a 25 wt. % ITO particles (~ 14 vol. %), 35 g of ITO paste is dissolved in 65 g of ethanol and then stirred for 30 min at RT. The blue suspension is centrifuged at 4500 rpm for 10 min to remove the large remaining agglomerates and then it is filtered using a 0.45 μm filter.

These sols were used to coat glass and polymeric substrates using the dip and spin coating methods. They were found stable for more than one year.

4.2.2 Modified ITO sols

A modification of the ITO sol was done to allow the curing of the coatings at low temperature ($T < 150\text{ }^{\circ}\text{C}$) or by applying UV-irradiation or a combination of these different low temperature treatments. Organic and inorganic-organic hybrid materials were used as coupling agents in order to bind the particles together and which can be polymerised at low temperature. A small amount of prehydrolysed TEOS, GPTS, MPTS etc. (see the list of chemicals in appendix B) are added to the pure ITO sol and mixed in an ultrasonic bath for 5 min. The concentration of the coupling agent referred to the pure ITO coating solution ranges from 0 to 20 wt. %. A UV curing agent, such as Irgacur 184, was also incorporated into the formulation in order to promote the polymerization and the hardening of the coatings.

The modified sols were used to coat glass and polymeric substrates by dip or spin coating methods followed either by a thermal or a UV curing process. These sols are stable for more than 6 months depending on the concentration of the additives.

The hydrolysis of some functionalised silanes used as a modifier are described below:

Hydrolysis of MPTS

100 g of MPTS were put in a two necks round glass flask. 10.9 g of 0.1 M HCl was added slowly to the MPTS under stirring with reflux. The molar ratio MPTS:H₂O was 1:1.5. When a clear solution obtained, the sol was heated to 40°C in an oil bath and stirred vigorously for

24 h. Thereafter the sol was cooled to RT and then the methanol, resulting from the reaction, was extracted using a rotary evaporator at 40°C, 80 mbar for 30 min.

Hydrolysis of GPTS

123 g of GPTS were put in a two necks round glass flask. 13.5 g of 0.1 M HCl was added slowly to the GPTS under stirring with reflux. The molar ratio GPTS:H₂O was 1:1.5. When a clear solution is obtained, the sol was heated to 40°C in an oil bath and stirred vigorously for 16 h. Thereafter the sol was cooled to RT and then the methanol resulting from the reaction was extracted using a rotary evaporator at 40°C, 80 mbar for 30 min.

Hydrolysis of TEOS

Two solutions were prepared: for the first one, 49.44 g of TEOS was mixed with 31.92 g ethanol and stirred together in a two necks round glass flask. For the second one, 31.92 g of ethanol was mixed with 36.94 g of 0.1M HCl under stirring. The second solution was added to the first solution. The resultant sol was stirred at RT for 2h.

4.3 Deposition methods

The conventional sol-gel methods (spin and dip coating) were used to deposit transparent conductive thin films on glass and polymeric substrates at room temperature. Before deposition, all coating sols were carefully filtered using a 0.45 µm filter. All prepared coating sols were suitable to be deposited using these coating processes, but the first method was preferred as it uses less material. The description of these methods is found in Appendix A.2.2. The spinning and withdrawal speed were varied to obtain films with different thicknesses and optimized to obtain crack free thin films with good optical quality.

4.3.1 Coatings on glass

Different sizes and shapes of float glass, borosilicate glass and fused quartz substrates were coated. Before the coating processes all substrates were cleaned carefully (see Appendix A.2.1). The deposited layers were then dried and densified using different hardening and sintering treatments. Coated fused quartz substrates have been heat treated up to 1000 °C, borosilicate glasses were treated at lower temperatures (400 < T < 550 °C) and soda lime glasses (float glass) have been heated till 500 °C because of their poor thermal stability and to avoid the Na diffusion into the coating, which strongly affect the electrical properties of TCO layers. The modified ITO coating sols were deposited on glass substrates and hardened at low temperatures (< 130 °C) or by UV-irradiation curing.

4.3.2 Coatings on polymeric substrates

Different kinds of polymeric substrates, such as PC, PMMA, PVC, PE, PET and PC foils have been coated using the modified ITO sols. Because of the low thermal stability of the substrates, the coatings were heated at low temperature (T < 150 °C) for several hours or cured by using an UV-irradiation source (Beltron, GmbH). Some polymeric substrates were pretreated using a plasma source to examine the adhesion of the film material on the substrate.

4.4 Post-treatment of the coatings

The deposited layers were dried and cured using different methods.

4.4.1 Heat treatment

The films deposited on fused quartz substrates were heat treated from 80-1000°C either in ambient atmosphere or in a reducing atmosphere. The films were introduced in a furnace previously heated to the desired temperature and then left for different periods of times. The films were then post annealed in a flux of forming gas ($N_2/H_2 : 92/8$) using a Gero furnace. The furnace was first evacuated to remove the ambient air from the furnace and N_2 gas is then introduced during the heating up to the desired temperature at a constant rate. The samples were then kept under a flux of the forming gas for a period ranging from 30 to 120 min. Finally the furnace was cooled down to 20°C under a flux of N_2 with a fixed cooling rate of 1500°C/h.

4.4.2 UV-Irradiation

UV-curing was carried out to densify the deposited films using a UV-system with emission ranging from 200 to 600 nm (UV / IR dryer, TYP 20 / III with strong emission lines at 365, 405, 435, 550 and 580 nm, Beltron GmbH, Germany). The samples were moved by a conveyor at different speeds+ ranging from 0.2 to 6 m/min. The average UV-energy received by the coating during one run depends on the speed of the conveyor. Fig. 8 shows the relationship between the total average energy density, the temperature measured at the surface of a substrate and the conveyor speed of the Beltron system. As the process also heats the substrate (strong emission bands in the visible and near infrared range), a conveyor speed of 0.4 m/min was used for glass substrates, of 0.8 m/min for PC substrates, of 2 m/min for PMMA and PE, of 5 m/min for PVC substrates and of 6 m/min for PC and PET foils.

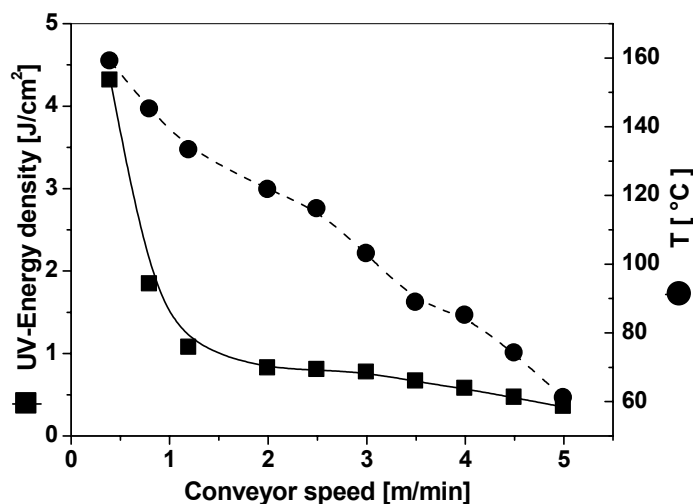


Fig. 8: Relationship between the total energy density and the temperature measured at the surface of a substrate and the conveyor speed of the Beltron system during one run.

4.4.3 Plasma treatments

Argon plasma treatment were also applied to ITO coatings as a post treatment. The plasma was consisting of high energetic argon ions at room temperature. The treatment was carried out in a previously high evacuated chamber at a plasma power of 400 watt (Plasma Electronic, Buck Technology).

4.4.4 Combination of treatments

A combination of UV-irradiation and heat treatment was also performed. The samples were irradiated with UV-irradiation and then heated under ambient atmosphere or forming gas or vice versa. The electrical properties were then measured to determine the best combination to obtain the best electrical and optical properties.

4.5 Shelf life under different atmospheres

The ITO coatings were characterized for their electrical, optical, mechanical and surface properties. The time evolution of these properties was examined during the storage of the prepared samples under different atmospheres, such as ambient atmosphere, vacuum, nitrogen, argon and oxygen.

4.6 Patterning of ITO coatings

The patterning of ITO coatings was carried out by irradiating the wet deposited modified ITO films with UV-irradiation through a various structured masks. The masks were fitted on the top of the layers and illuminated during 2 to 3 min with UV irradiation. The substrate was then washed in an ultrasonic ethanolic bath for 2 min. The unexposed parts of the film are removed and the exposed parts remain on the substrate. The morphology of the patterned structure was determined using a WLI equipment (see Appendix A.3.4). Fig. 9 shows schematically the patterning process.

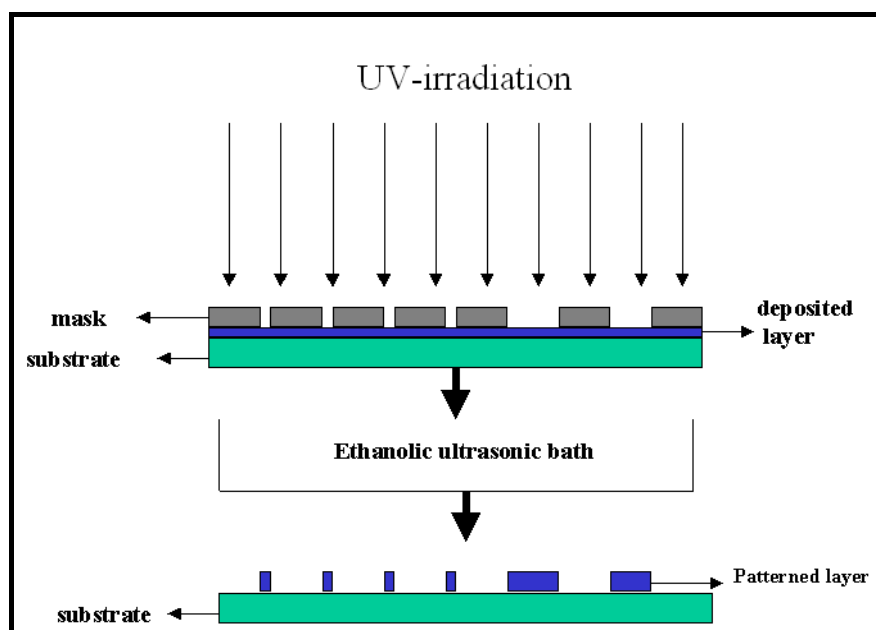


Fig. 9: Schematic digram of the patterning process.

4.7 Conclusion

The structural, morphological, optical, mechanical and surface properties of the ITO layers deposited on glass and polymeric substrates were done using different techniques. The description of these techniques is given in appendix A.3.

Finally, Fig. 10 illustrates the different stages of the experimental steps used to produce and characterize transparent conducting ITO nanoparticles films on polymeric and glass substrates via the sol-gel technology.

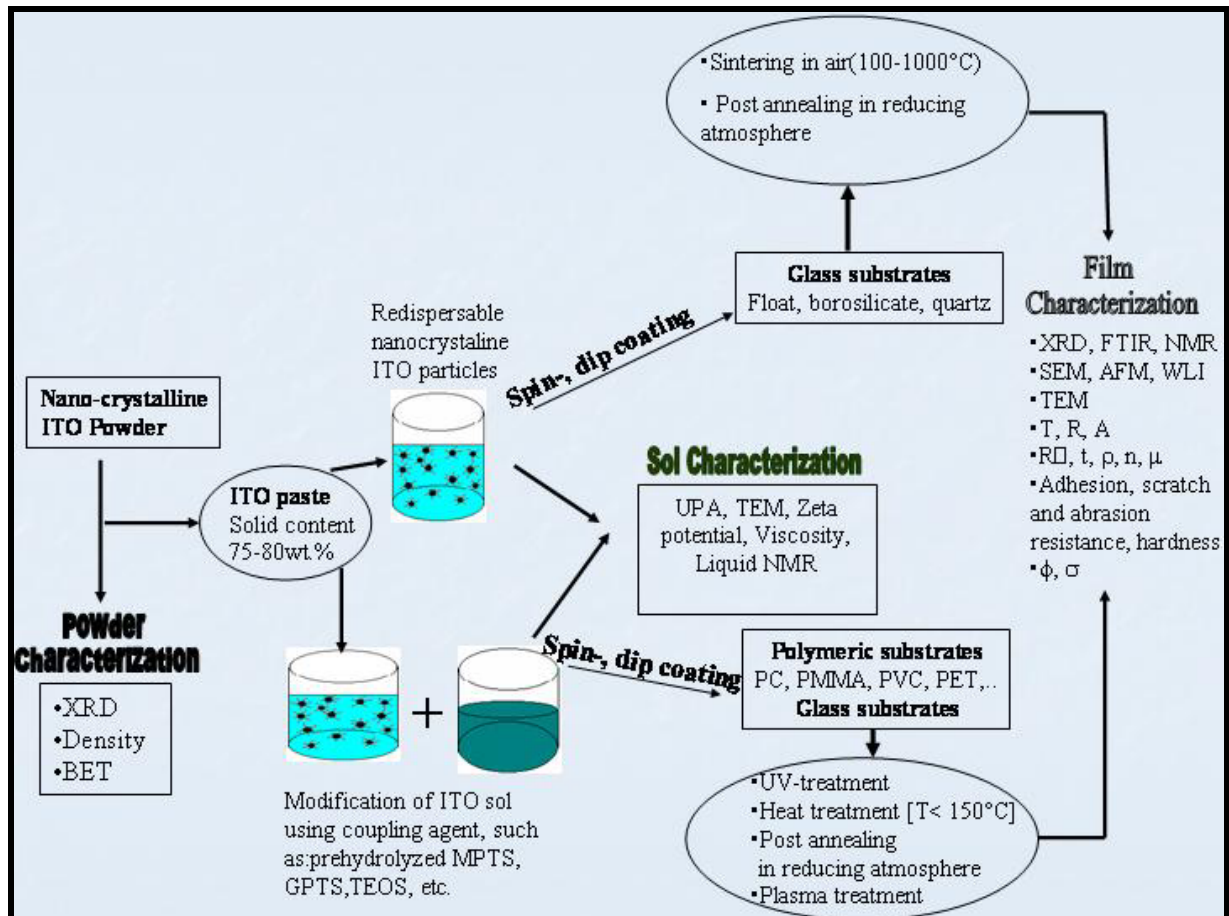


Fig. 10: Schematic diagram illustrating the different stages to produce and characterize transparent conducting ITO nanoparticle layers on glass and polymeric substrates.

Chapter 5

Results and Discussions

5.1 Structural and physical properties of ITO powders

Indium tin oxide powders with Sn / In mol ratio up to 12 at. % are white in colour after drying and turn to a blue colour after post annealing treatment between 250 and 550°C under forming gas (N₂:H₂ = 92:8) for 1 h. The powders were denoted ITO250, ITO300, ITO350, ITO400, ITO550 respectively. This section reports on their phase structure, density and BET specific surface area.

5.1.1 Phase structure (XRD)

The XRD patterns of ITO300 powders with Sn / In mol ratio 0, 3, 6, 8, 12 at. % are shown in Fig. 11. The patterns of all powders are independent of the Sn concentration and show clearly that the particles are already crystalline with the In₂O₃ cubic bixbyite crystal structure (JCPDS card no. 06-416) without the existence of any SnO_x phases. The ITO crystallites are not oriented. There is a slight shift of the peaks toward small angles by increasing the Sn concentration indicating an expansion of the unit cell caused by the substitution of In atoms by Sn atoms (25).

The crystallite size (inset in Fig. 11) calculated using the Scherrer equation from the broadening of the [222] peak decreases continuously with the increase of Sn concentration. The value is 39 nm for 0 at% Sn, 21 nm for 6 at % Sn and 18 nm for 12 at %. This is a consequence of the substitution of Sn⁴⁺ ion for In³⁺ ion in the In₂O₃ host lattice because of the smaller ionic radius of Sn⁴⁺ (0.71 Å) in comparison to In³⁺ ion (0.81 Å). Yanagisawa et al (284) reported for hydrothermal treated ITO powders that a high solubility of Sn⁴⁺ ions decreases the volume of the ITO unit cell. Above 6 wt.% Sn concentration only a slight decrease of the crystallite size is observed indicating a lower solubility of Sn⁴⁺ ion in the host lattice. Frank and Köstlin (285) observed the formation of bound complexes of Sn⁴⁺ ions at doping concentration above 5 at.% Sn according to the ionisable and non-ionizable tin-oxygen defects. Yamada et al (286) studied the mechanism of the Sn doping in In₂O₃ host lattice using XRD and Mössbauer spectroscopy and found that the Sn-based defects depends on the Sn concentration. They begin to appear at 4-5 at.% Sn and their amount increases above 5 at.% Sn.

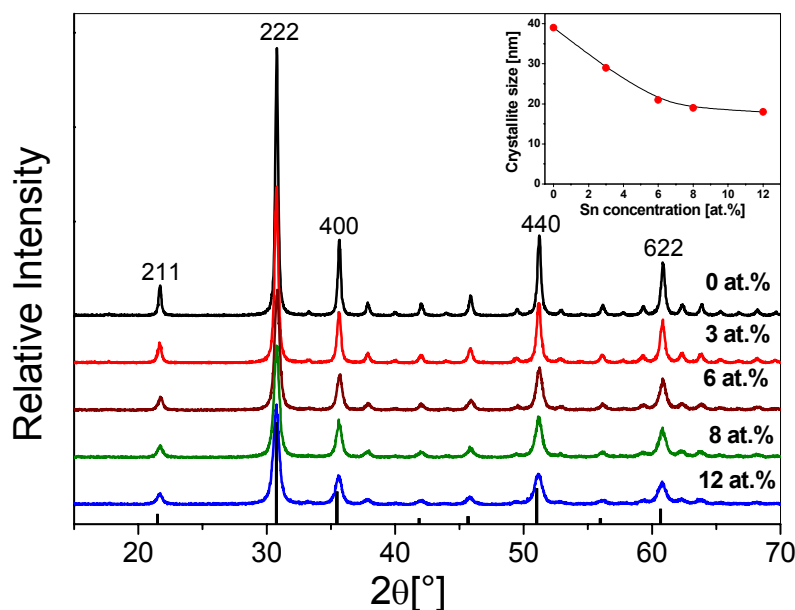


Fig. 11: XRD patterns of dried and post annealed ($T = 300^{\circ}\text{C}$) $\text{In}_2\text{O}_3:\text{Sn}$ powder with different Sn concentrations. The vertical lines refer to the JCPDS database (06-416). The inset shows the crystallite size as a function of the Sn concentration calculated from the (222) peak.

Fig. 12 shows the XRD pattern of $\text{In}_2\text{O}_3:\text{Sn}$ (8 at. %) powders annealed at different temperatures up to 550°C . All spectra are typical of polycrystalline ITO particles having the same cubic In_2O_3 phase. No evidence was found for the existence of an SnO_x phase structure. The material can be described as $\text{In}_{2-y}\text{Sn}_y\text{O}_3$ (unreduced system) or $\text{In}_{2-y}\text{Sn}_y\text{O}_{3-2x}$ (reduced system). The particles are already crystalline at 250°C with crystallite size of 17 nm. A calcination at higher temperature increases the crystallite size up to 38 nm at 550°C (see inset of Fig. 12). The intensity of the diffraction peaks increases with the calcination temperature and, in all spectra, the intensity of the (222) peak is always greater than the intensity of the (400) peak. However the ratio $I(222)/I(400)$ decreases gradually by increasing the post annealing temperature from 3.52 at $T = 250^{\circ}\text{C}$ (practically the value determined from the JCPDS database) down to 1.7 at $T = 550^{\circ}\text{C}$. This behaviour is not understandable; however it shows that the crystallites have a tendency to grow along the (400) crystallographic plane as the calcination temperature increases.

The shift of the diffraction peaks toward higher angles observed at 550°C may be a result of a distortion in the bixbyite structure due to the increase of the thermal microstrains in the lattice, particularly observed for high index surfaces (287).

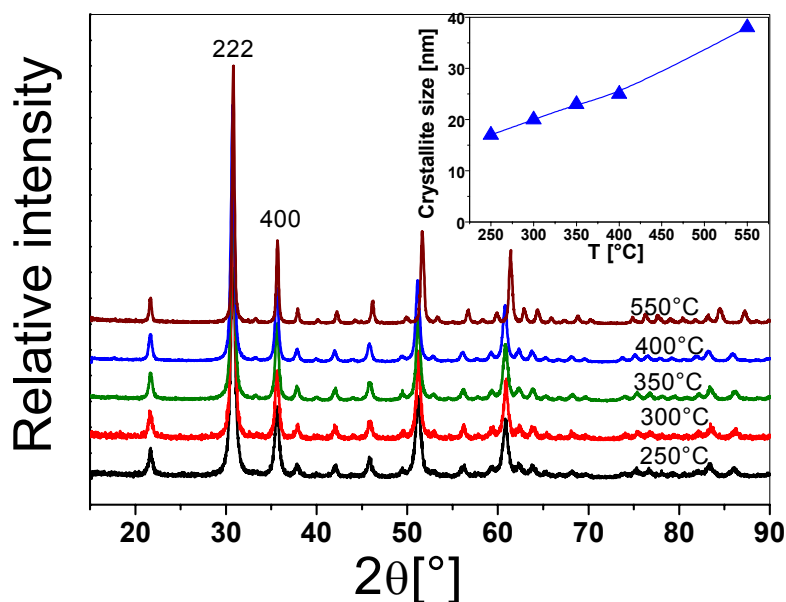


Fig. 12: XRD patterns of ITO(Sn: 8 at. %) powder calcined at different temperatures. The inset shows the crystallite size growth with the temperature of calcination.

5.1.2 Particle density and specific BET surface area

The density of ITO particles calcined at $T = 350^\circ\text{C}$ as a function of the Sn-doping concentration and that of particles doped with 8 at. % Sn as a function of the calcination temperature are shown in Fig. 13. Pure indium oxide particles heat treated at 350°C are quite dense, $\rho \sim 6.93\text{ g/cm}^3$, about 96.5 % of the theoretical value (7.18 g/cm^3) but their density decreases gradually with the increase of the Sn concentration down to 6.6 g/cm^3 (12 at. % Sn) (Fig. 13 a). This means that the tin doping leads to a lower packing within the particles (larger porosity).

For a given doping concentration, the ITO particles become denser as a function of the sintering temperature (Fig. 13 b). This means that the pores inside the particles are gradually removed and that the grains building the particles become more tightly packed.

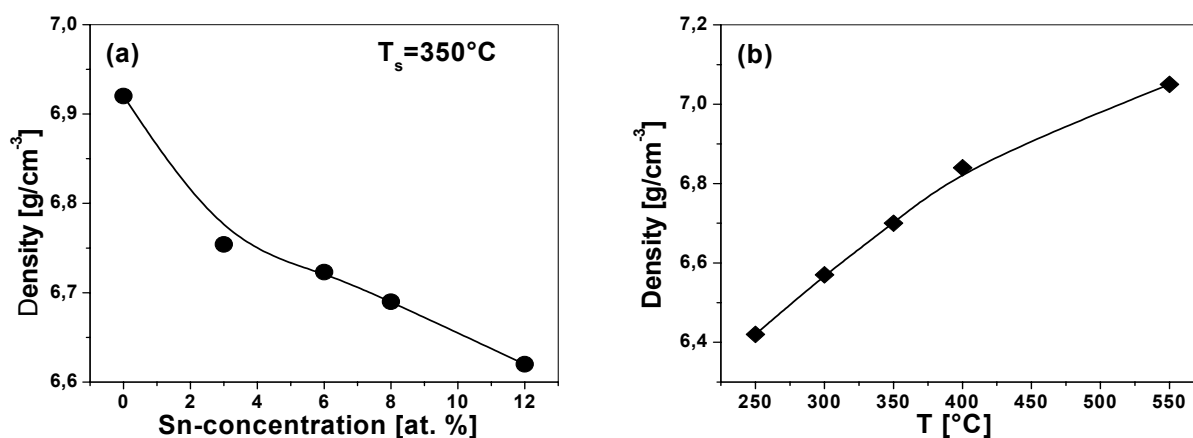


Fig. 13: Density of ITO particles (a) as a function of the Sn-doping concentration for particles calcined at 350°C and (b) as a function of the calcination temperatures for 8 at. % Sn.

Fig. 14 shows that the specific surface area (BET) of the powders decreases gradually by increasing the calcination temperature from $64 \text{ m}^2/\text{g}$ at $250 \text{ }^\circ\text{C}$ down to $21 \text{ m}^2/\text{g}$ at $550 \text{ }^\circ\text{C}$. This result is due to the thermal growth of the crystallites as shown by the XRD measurements (Fig. 12). Higher temperatures also result in the formation of larger and denser aggregates of primary particles with more contact points between the particles resulting in a lower specific surface area. Song et al. found a sharp decrease in the BET surface area of tin oxide particles as the calcination temperature is increased (63). This reduction was also explained by a better contact between the grains building the particles due to the elimination of ammonia and the physically and chemically adsorbed water in the precursor powder.

The average size of the particles was calculated from the BET values and the density of the particles, assuming that their shape is spheric (see appendix A1.2). The particle size increases from 15 nm at $T = 250 \text{ }^\circ\text{C}$ up to 47 nm at $T = 550 \text{ }^\circ\text{C}$ (Fig. 14).

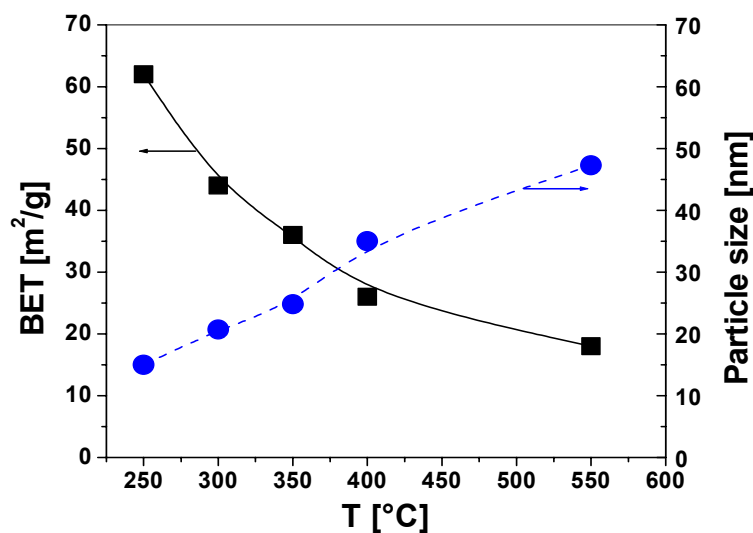


Fig. 14: Specific (BET) surface area of crystalline ITO nanopowder and calculated particle size as a function of the calcination temperature.

The crystallite size measured from the XRD (222) peak broadening and the particle size calculated from the BET surface area and the particle density, ρ (from Fig. 14) are listed in Table 4. Both values increase with the calcination temperature and follow the same trend. It is interesting to observe that the average size of the particles is almost equal to the average crystallite size up to about $350 \text{ }^\circ\text{C}$. This indicates that each particle consists practically of a single crystal. At higher temperature the size of the particles increases more than the crystallite size, an indication that they are made of more than one crystallite.

Table 4: Crystallite and particle size of nanocrystalline ITO powders.

powder	crystallite size(nm) (from XRD)	Particle size (nm) (from BET and ρ)
ITO250	16	15
ITO300	19	20
ITO350	22	25
ITO400	26	35
ITO550	37	48

5.1.3 Conclusion

Crystalline indium tin oxide (ITO) nanoparticles exhibit the indium oxide cubic structure and no other phases were detected. At a given calcination temperature the substitution of the Sn^{4+} ion in the indium oxide host lattice leads to a decrease of the crystallite size. The prepared conducting particles are highly dense and their density increases with the calcination temperature. The specific BET surface area decreases with increasing the sintering temperature while the size of the particles grows gradually. Comparing the particle and crystallite size, it was concluded that the particles calcined up to 350 °C are in average built with a single crystallite, while those calcined at higher temperature begin to contain several crystallites.

5.2 Characterization of the coatings sols

The coatings sols consist of surface modified ITO nanoparticles redispersed in ethanol as a solvent. The powders annealed at temperature up to 350°C have been successfully redispersed and stable coating solutions were obtained. It is difficult to redisperse powders prepared at $T > 400$ °C and the resulting sols prepared from these powders are only stable for a few hours. The resulting suspensions were also modified by the addition of functional coupling agents, like TEOS, GPTS, MPTS and other organic materials.

This section reports on the characterization of the coatings sols.

5.2.1 Zeta Potential

The pH value has an enormous effect on the stability of the colloidal suspensions. The measurements of the Zeta potential is a good index of the magnitude of the interaction between the colloidal particles and is used to assess the stability of a colloidal system as a function of the pH.

Fig. 15 shows the measurements over a pH range $2 < \text{pH} < 12$ for suspensions obtained with ITO nanoparticles calcined at $T = 250, 300, 350$ and 550 °C and dispersed mechanically in TDOS (dispersion agent). The isoelectric point of the suspensions pH_{iep} lies between 7.5 and 8 and therefore it is necessary to use a $\text{pH} < 6$ in order to obtain stable suspensions.

The suspension made with the ITO550 powder has a weak zeta potential (< 20 mV), meaning that the repulsive force between the particles does not overcome the Van der Waal forces. The suspension is not stable because large aggregates are formed (precipitation). Further work should be done to find a suitable dispersion agent or a better process to redisperse such particles. On the other hand the ITO250, ITO300 and ITO350 sols have a higher zeta potential. The dispersed particles with positive potential higher than $+30$ mV ($\text{pH} < 6$) form a stable suspension and no aggregation was observed during their storage at room temperature for more than one year. The sols used for the deposition of the coatings had a pH of about 3 to 4.

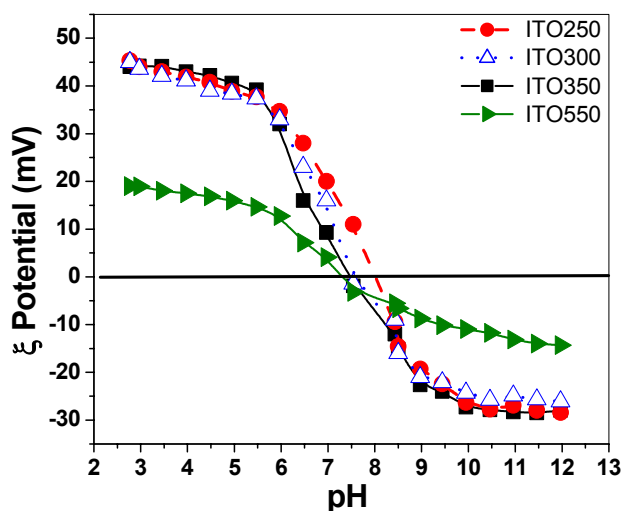


Fig. 15: Zeta potential of ITO suspension as a function of pH.

5.2.2 Sol morphology (TEM)

The coating sols prepared from the dispersion of ITO250, ITO300 and ITO350 nanoparticles were investigated using TEM microscopy (Fig. 16 a,b,c). The images show clearly that the suspensions consist of almost monodispersed nanoparticles, with size in the range from 15-40 nm. As expected the ITO250 suspension has a finer and smaller particles distribution than the others.

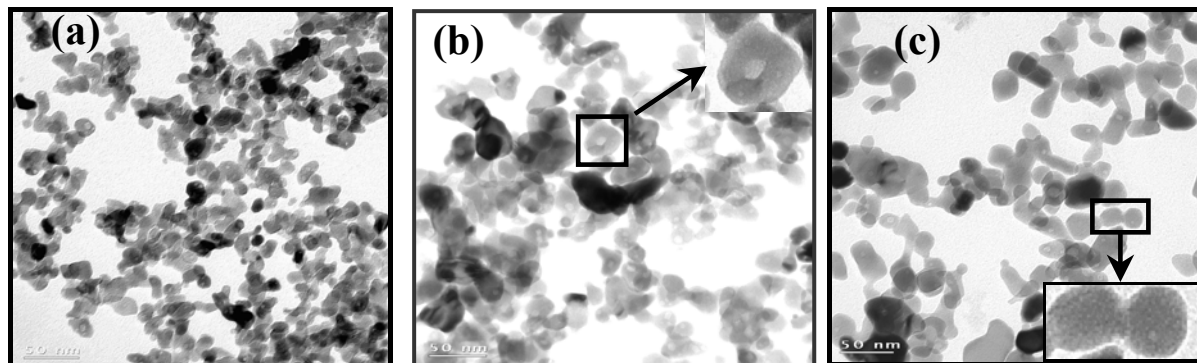


Fig. 16: TEM images of the crystalline nanopowders redispersed in ethanol.
(a) ITO250, (b) ITO300, (c) ITO350 (size of the bar is 50 nm)

Many particles show crystallites with a regular “etch pit” at their surface (as shown in the inset of Fig. 16 b and c). These pits were formed during the particle growth and are typical manifestations observed during the crystal growth on low indexed surfaces, like the cubic ones (288). Gleiter (289) reported that the formation of this core structure is a result of the constraining forces acting between the atoms of the surrounding crystal lattices and the atoms in the core region.

The crystallinity of the particles can be also clearly identified from the structure imaging of the particles by the presence of lattice fringes as shown in Fig. 17. The In_2O_3 cubic phase is identified when comparing these diffractions with the JCPDS references 06-416 and 44-1087.

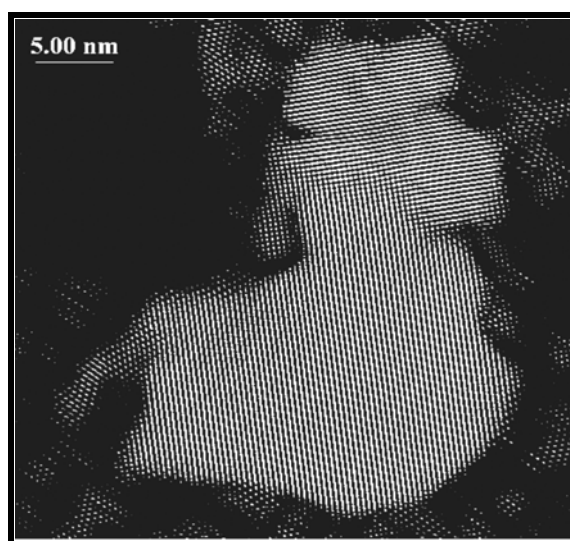


Fig. 17: Structure imaging showing the diffraction pattern of a polycrystalline ITO250 nanoparticle.

The composition of ITO powders was determined by Energy Dispersive X-ray (EDX) technique. The energy of the K-lines of In and Sn, referred to the different L-spectrum were resolved quantitatively. Fig. 18 shows that the atomic ratio of In / Sn in the particle is about 10.52 / 1 which is, within the precision of the technique ($\pm 20\%$), comparable to that of the sol preparation (8 at. % Sn, In / Sn = 11.5 / 1).

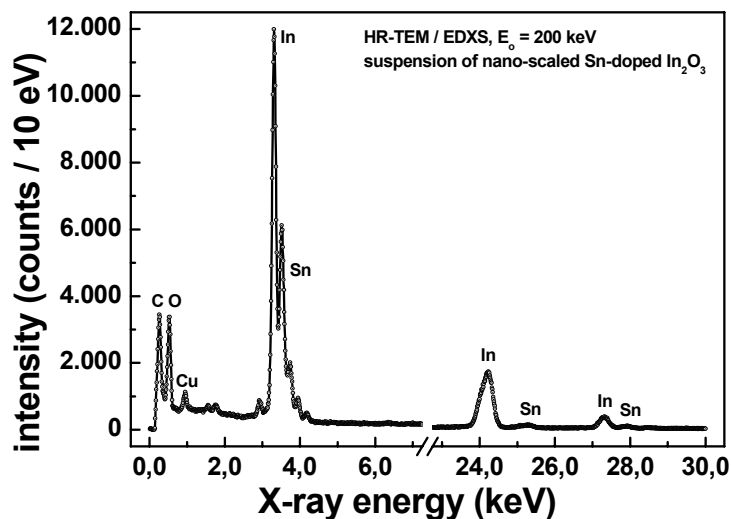


Fig. 18: EDX spectrum of an ITO350 sol (8 at. % Sn).

5.2.3 Particle size distribution (UPA)

The hydrodynamic particle size distribution of pure and MPTS modified ITO colloidal suspensions were determined using an Ultrafine Particle Analyzer (UPA) as shown in Fig. 19.

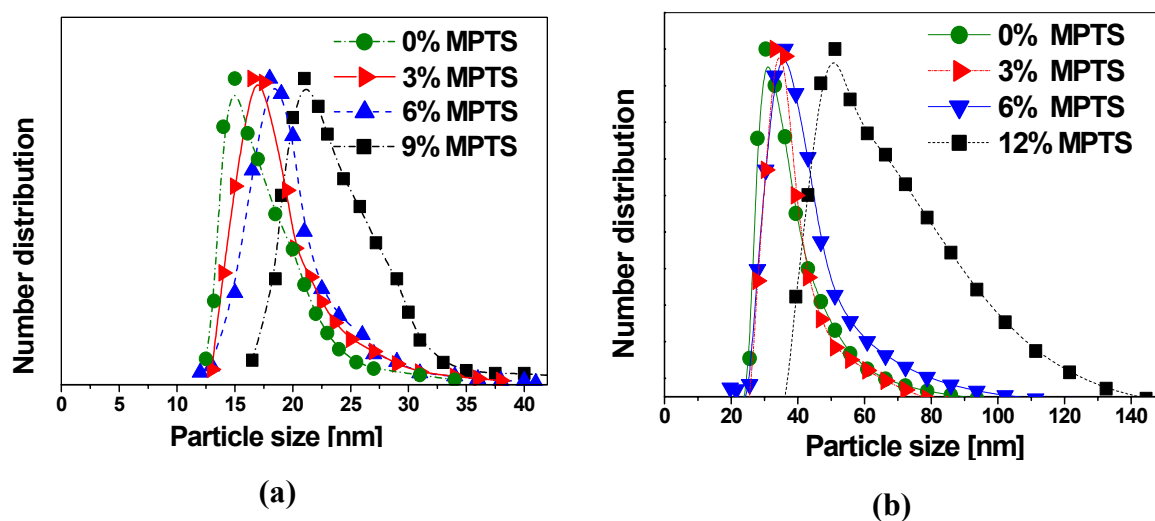


Fig. 19: Particle size distribution of (a) ITO250 and (b) ITO350 powders dispersed in ethanolic solution without and with different amount of MPTS (modifier).

All distributions are monomodal. The one for pure ITO250 particles has a size ranging between 15 to 20 nm and the previous results obtained from XRD, BET (see Table 1) and HRTEM (Fig. 16-a) are confirmed. The size distribution of the particles modified by the addition of up to 6 wt.% MPTS is almost in the same range (17-23 nm) although a slight shift towards larger size is observed. For higher MPTS concentration larger particles are observed due to the aggregation of the primary ITO particles. This may be due to a decrease of the ζ potential of the surface of the particles forcing the particles to aggregate and form larger clusters.

On the other hand the colloidal pure ITO350 particles are distributed in the range 20 to 40 nm, a value somewhat larger than the primary particle size; each particle appears therefore to be formed by two or three primary particles (see Fig. 16 c). When different concentration of MPTS are added, the size distribution follows the same behaviour observed for the ITO250 particles suspension. For a concentration of 12 wt.%, a broader size distribution and large clusters are formed with a range of 40 to 120 nm.

5.2.4 Rheology

The rheology of the sols is an important property to be determined as the viscosity controls the thickness of spin or dip coated layers and as a Newtonian behaviour of the sol is preferable for these coating processes (see equation 1).

Table 5 summarizes the values of the kinematics viscosity of the four different sols a function of the solid content (wt. %). Up to 30 wt. % the viscosity increases only slightly and the sols behave practically as a Newtonian fluid (Fig. 20). The sols made with ITO350 particles have

always a slightly higher viscosity than those made with ITO250 particles. The addition of 6 wt. % MPTS also slightly increases the sol viscosity.

The behaviour of the paste (72 wt. % of ITO particles) is however different. The values of the viscosity is much higher and a clear shear thinning behaviour is observed. Such property is quite promising for web-coating process.

Table 5: Kinematic viscosity of the four coating solutions as a function of the solid content concentration.

solid content (wt.%) \ Viscosity (mm ² /s)	ITO250	ITO250+6%MPTS	ITO350	ITO350+6%MPTS
5	1.85	1.92	1.96	2.16
10	1.93	2.09	2.14	2.26
15	2.07	2.21	2.2	2.37
20	2.16	2.35	2.25	2.5
25	2.37	2.54	2.45	2.66
30	2.56	2.71	2.75	2.8

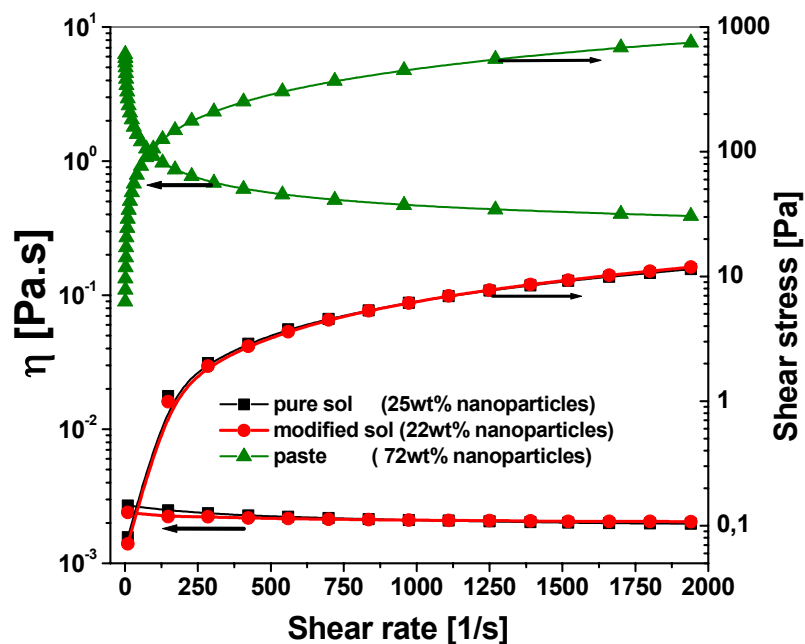


Fig. 20: Dynamic viscosity and shear stress of the ITO paste, the pure and MPTS modified ITO sols as a function of the shear rate.

5.2.5 Thermal analysis (DTA/TG)

The thermal behaviour of both pure and MPTS modified coating sols made with redispersed ITO250 and ITO350 particles and dried at 130 °C under UV-irradiation (Beltron, 5 min.) are

shown in Fig. 21 a, b. All DTA/TG investigations were carried out in air under the same conditions.

The thermogram of Fig. 21 a, b shows that no endothermic peak is observed for $T < 130\text{ }^{\circ}\text{C}$ for both pure and MPTS modified ITO particles indicating that the ethanol was evaporated during the UV drying pretreatment. An exothermic peak is seen in Fig. 21 a for the ITO250 sample at $235\text{ }^{\circ}\text{C}$ with a shoulder at $286\text{ }^{\circ}\text{C}$ corresponding to a weight loss of 6 %. For the ITO350 sample the exothermic peak and its shoulder are slightly shifted to $259\text{ }^{\circ}\text{C}$ and $315\text{ }^{\circ}\text{C}$, respectively and correspond to a weight loss of 4.5 %. The source of these exothermic peaks are probably due to the thermal degradation of the organic groups used to disperse the particles.

Larger weight losses are observed for the MPTS modified samples (Fig. 21 b). This is clearly due to the presence of MPTS in the sol leading to more decomposition and combustion of organic species. The first exothermic peaks observed between 250 and $300\text{ }^{\circ}\text{C}$ are certainly related to the same peaks observed for the pure ITO samples. The exothermic peaks at 390 and $490\text{ }^{\circ}\text{C}$ are therefore related to the decomposition of the different organic bonds of MPTS and the formation of the Si–O–Si network. The slight shift of the peaks to higher temperature for the ITO350 particles with respect to those for the ITO250 particles is probably related to the particle size, as ITO250 particles have larger surface area ($64\text{ m}^2/\text{g}$) than the ITO350 ones ($35\text{ m}^2/\text{g}$) which means better thermal conductivity.

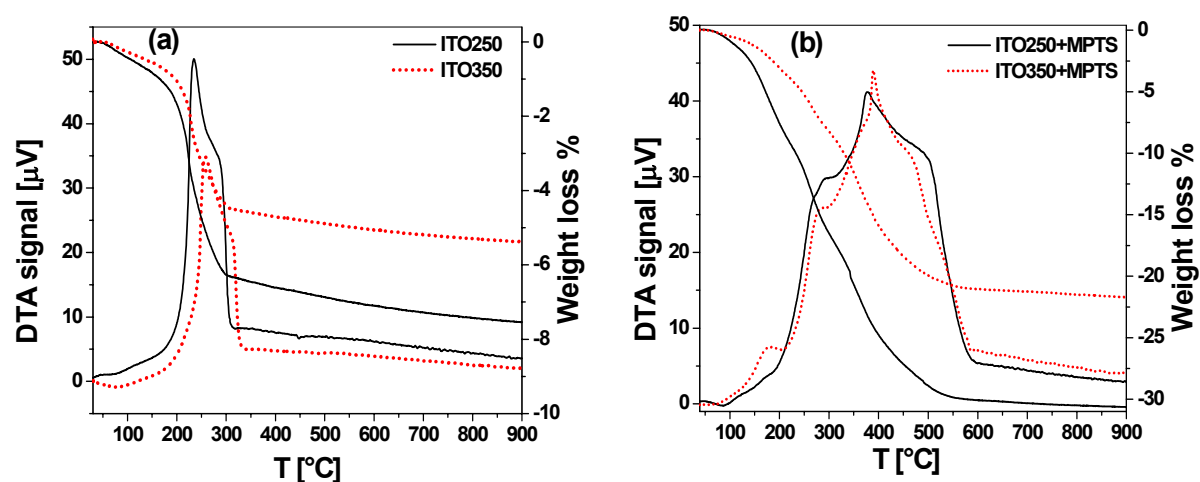


Fig. 21: DTA/TG curves for colloidal particles (a) ITO250 and (b) ITO350 after drying the samples at $130\text{ }^{\circ}\text{C}$ during UV-irradiation.

5.2.6 Stability of the coating sols (Liquid-NMR-spectroscopy)

The colloidal stability of all the sols was visually observed by letting them in a closed vessel at room temperature until a precipitation was observed and it is reported in Table 6. The ITO250 systems are more stable than the ITO350 ones and when unmodified they retain their original properties for more than 1 year. The addition of MPTS reduces the stability.

Table 6: Storage time without observable precipitation for the colloidal systems ITO250 and ITO350 as a function of the concentration of MPTS.

MPTS-concentration (wt.%)	ITO250	ITO350
0	~2 years	~ 1 year
3	~ 1 year	~ 6 months
6	~ 1 year	~ 6 months
9	~ 2 months	~ 2 weeks
12	~ 1 week	~ 2 days

In order to get a better insight in the evolution of the condensation and polymerisation degree of a pure prehydrolysed MPTS sol, a study was performed by means of liquid ^{29}Si and ^{13}C NMR spectroscopy, respectively. ^{29}Si -NMR measurements were carried out with solutions stored at 5 °C within a period of one to 240 days after the hydrolysis of MPTS. The degree of the condensation of the $\text{RSi}(\text{O}_{0.5})_3$ -units, i.e. the percentage of built Si-O-Si was calculated by integrating the different signal intensities. Fig. 22 shows the NMR spectra.

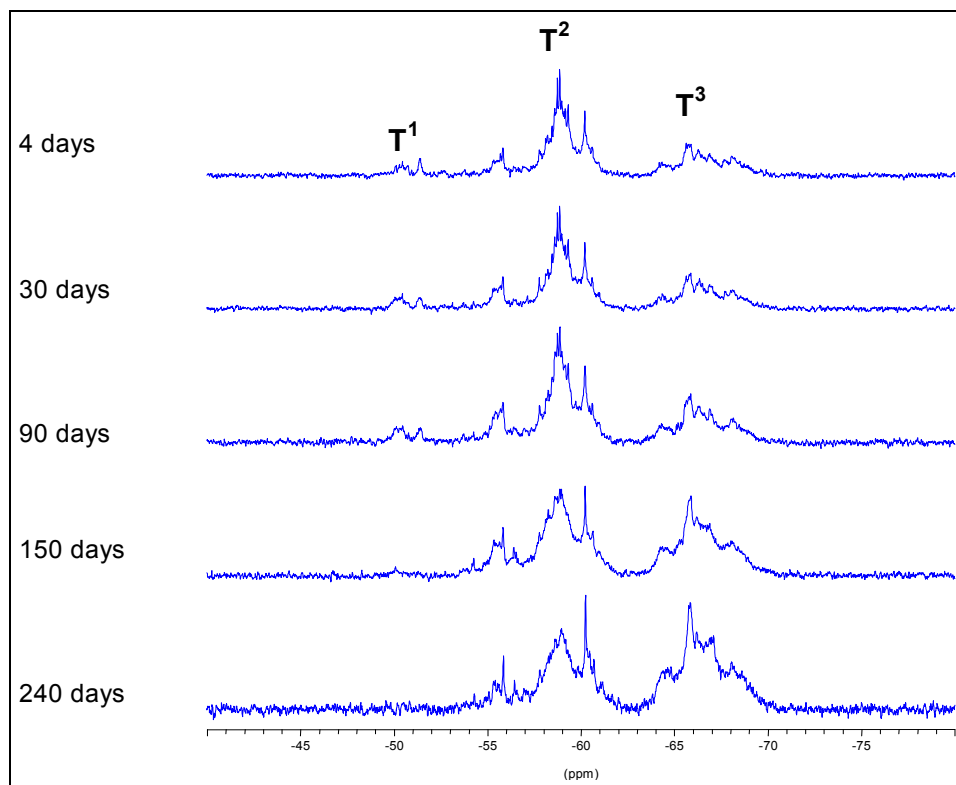


Fig. 22: ^{29}Si -liquid NMR spectra of prehydrolysed MPTS sol after storage at 5°C for different times.

The percentage changes of the T-groups are listed in Table 7. During the first 3 months no changes are observed for T^1 , T^2 and T^3 . T^1 then decreases and totally disappears after 8 months. T^2 decreases from 62 to 55 % after 5 months and further decreases to 47 % after 8 months. The amount of T^3 increases significantly from 33 to 53 %, when the sample was stored for 8 months. The degree of condensation calculated according to the formula given in appendix A.1.8 remains constant up to 90 days, about 76%, but then increases to reach 84 % after 8 months.

Table 7: Percentage of the T-groups, degree of condensation and viscosity of prehydrolyzed MPTS sols as a function of the storage time.

Storage time	T ⁰ (%)	T ¹ (%)	T ² (%)	T ³ (%)	Degree of condensation (%)	Viscosity η (Pa.s)
4 days	0	5	62	33	76	0.41
30 days	0	5	63	32	76	0.43
90 days	0	5	62	33	76	0.45
150 days	0	1	55	44	81	0.86
240 days	0	0	47	53	84	1.06

The viscosity of the prehydrolysed MPTS sol increases after the extraction of methanol from 8 mPa.s to 0.41 Pa.s. The time evolution of the viscosity of the prehydrolysed MPTS sol stored at 5°C is also shown in Table 7. There is a very slight increase during the first three months, but a significant increase is observed after 150 days (0.86 Pa.s) and 240 days (1.06 Pa.s). These results are in agreement with the time evolution of the condensation degree of the prehydrolysed MPTS sol and show that the prehydrolyzed MPTS sol retains its original properties (stable) up to three months when stored at 5 °C.

The corresponding ¹³C-NMR-spectrum which allows to characterize the polymerisation of the methacryloxy groups was measured for an 8 months old MPTS sol. Fig. 23-A shows the signals of the C = C and C = O bonds (135 ppm, 167 ppm) of the methacryl groups but no signals characteristics of the polymerization products expected at approx. 45 ppm and 177 ppm were found (labelled as 5* and 4* in Fig. 24). This means that the reactive double-bonds are still present in the MPTS sol after the condensation reaction of the Si-OH units and that the methacryl groups can be polymerized.

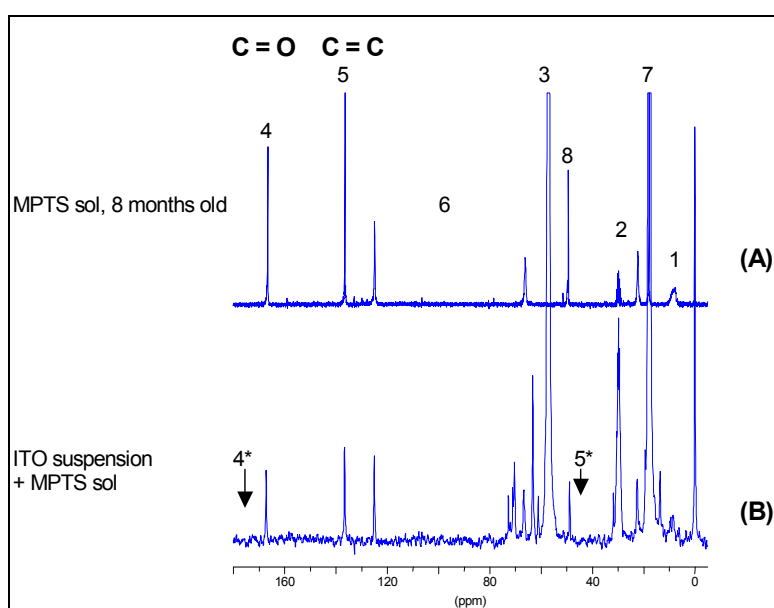


Fig. 23: ¹³C-NMR spectroscopy of (A) prehydrolysed MPTS sol, 8 months old and (B) ITO/MPTS sol (20 h old)

^{13}C -NMR-spectrum was also determined to examine the effect of ITO particles on the stability of the double bonds. Fig. 23-B shows the spectrum of a mixture of prehydrolysed MPTS sol and ITO suspension measured after storage at RT during 20 h. No polymerisation of the methacryl groups (4* and 5* in Fig. 24) is found, so that the MPTS / ITO sol can be polymerized.

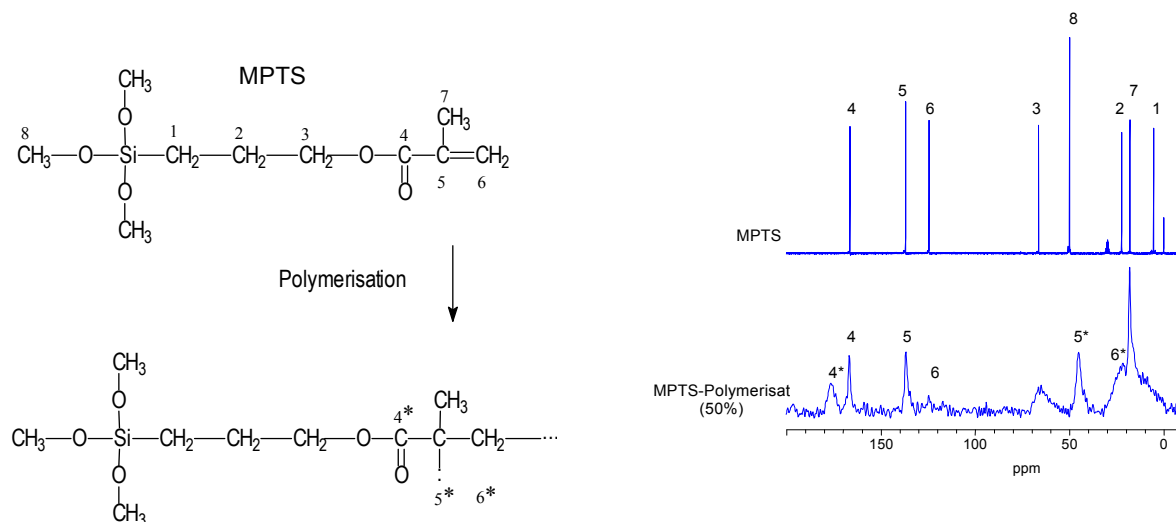


Fig. 24: ^{13}C -NMR spectroscopy of MPTS product and 50 % polymerized MPTS (right), and the corresponding scheme of MPTS (left) (290).

5.2.7 Conclusion: Sol Characterization

Nanocrystalline ITO powders calcined at temperature lower than 350 °C were successfully redispersed in water or organic solvents, such as ethanol (zeta potential > 30 mV). The best pH value to obtain a stable sol with a shelf life of more than 1 year is between 3 and 4. However those calcined at higher temperature are difficult to redisperse as they show a large aggregation and a zeta potential smaller than 20 mV.

TEM and UPA investigations of ITO colloids have confirmed that the nanocrystalline particles are well dispersed with a size in the range of 15 – 40 nm. The structural phase of the particles corresponds to the In_2O_3 cubic phase. The addition of small amount of MPTS (up to 6 wt. %) to the ITO colloidal suspensions shifts slightly the size distribution towards larger value; this shift increases by increasing the concentration of MPTS. The addition of MPTS reduces the stability of the sol.

Sols with solid content lower than 30 wt. % have a kinematics viscosity ranging between 1.85 and 2.7 mm^2/s and behave as a Newtonian fluids.

^{29}Si -NMR spectroscopy showed that the prehydrolyzed MPTS sol is stable if stored in a closed vessel at 5 °C during 90 days. An increase of the viscosity and the condensation degree was observed for large storage time. ^{13}C -NMR spectroscopy showed that the MPTS sol can be polymerized even after long time storage (8 months) and that the presence of ITO particles

do not affect the stability of the C = O and C = C double bonds (at least during a 20 h storage time).

5.3 Coating thickness

The coating sols containing ITO nanoparticles dispersed in ethanol with solid contents of 5 to 30 wt.% were deposited on borosilicate, quartz and float glasses and polymeric substrates (PC, PMMA, PET, PVC, etc.) using the spin and dip coating techniques. The sols made with nanocrystalline ITO particles annealed at 250 and 350 °C are called “ITO250” and “ITO350” sols, respectively. These sols were also modified by adding a suitable coupling agent like MPTS, TEOS, GPTS to produce conducting coatings cured at low temperature and are called thereafter “modified ITO250” and “modified ITO350” sols, respectively.

The thickness of the deposited thin films was measured as a function of the deposition parameters, the composition and the concentration of the sols.

5.3.1 Dip coated ITO films

Fig. 25 shows the thickness variation of pure ITO single layer deposited by the dip coating technique at a withdrawal speed of 4 mm/s on borosilicate glass substrates as a function of the solid content of the sol. The films were sintered at 550°C in air during 30 min.

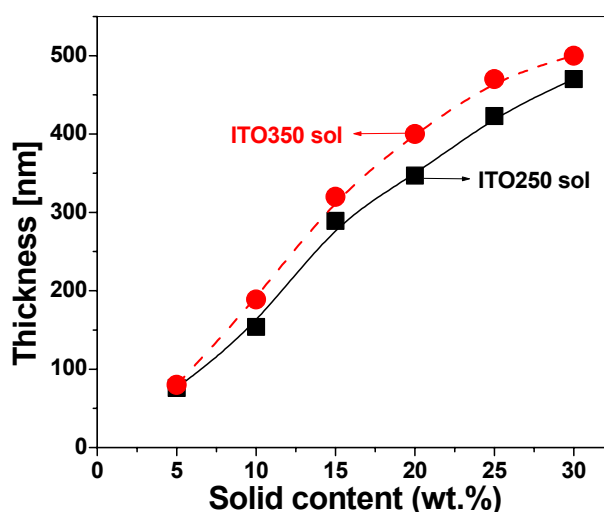


Fig. 25: Thickness of dip coated ITO250 and ITO350 films deposited on a borosilicate glass substrate heat treated at $T = 550^{\circ}\text{C}$ during 30 min as a function of the solid content concentration.

Both ITO250 and ITO350 sols lead to the same behaviour: the thickness increases with the solid content concentration from 90 nm for a solid content of 5 wt% up to 500 nm for a concentration of 30 wt.%. This is due to the increase of the sol viscosity with the solid content given (see Table 5). As the ITO350 sols were always found slightly more viscous than the ITO250 sols, it is understandable that the thickness of the ITO350 film is always higher than that of ITO250 film for a same concentration.

The effect of the withdrawal speed on the thickness of a single layer deposited with the ITO250 sol having a solid content of 25 wt% is shown in Fig. 26. The behaviour is in good agreement with the $v^{2/3}$ dependence of Landau-Levich equation (equation 1).

Although crack free single layers have been obtained up to a withdrawal speed of 8 mm/s, a value of 4 mm/s was usually used in all the work to assure an optimum film quality.

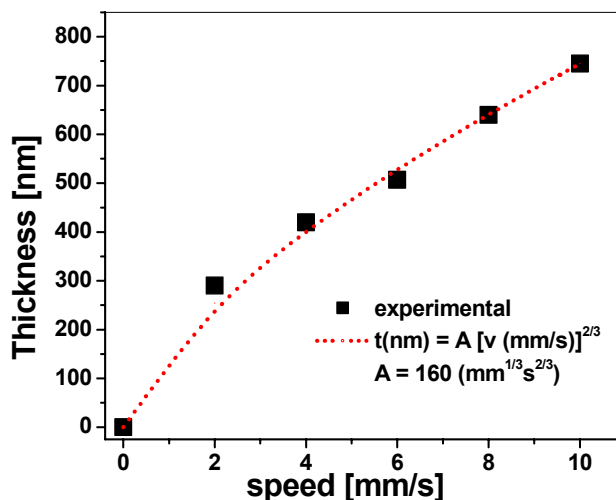


Fig. 26: Single layer thickness of pure ITO250 films deposited on glass substrates and heated at 550 ° for 30 min versus the withdrawal speed. The dashed line represents a fit with the Landau-Levich equation.

Fig. 27 shows the thickness variation of single layers withdrawn at a speed of 4 mm/s and hardened using UV-irradiation (Beltron, 5 min) as a function of the amount of the additives, such as MPTS, GPTS and TEOS. As the viscosity increases with the addition of the coupling agents, the thickness of the film consequently increases.

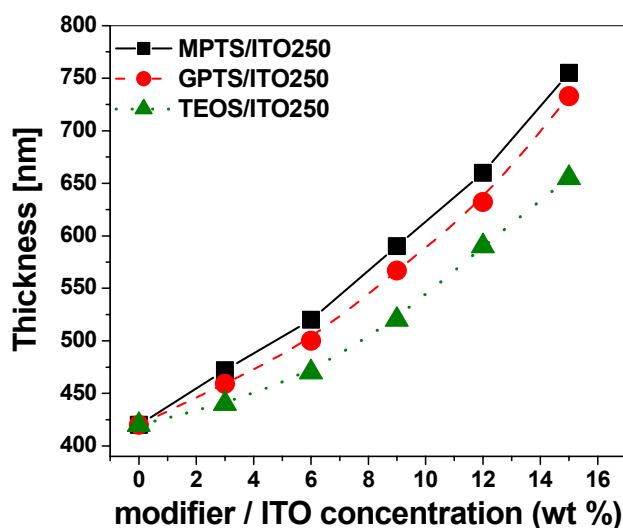


Fig. 27: Effect of the modifier (MPTS, GPTS, TEOS) concentration on the thickness of the dip coated film (withdrawal speed of 4 mm/s).

5.3.2 Spin coated ITO films

Spin coating is also a successful method to produce good quality transparent conducting coatings. This method was preferred in our work in order to reduce the amount and cost of the solution used for the deposition. The coatings were obtained using a spinning speed between 500- 3000 rpm and spinning time of about 10-15 s. The variation of the thickness of single layers made with the MPTS modified ITO350 sol (solid content of 25 wt%) with the spinning speed is shown in Fig. 28. It decreases with increasing spinning speed or by diluting the sol (lower viscosity). The films were then hardened using UV-irradiation (Beltron, 5 min.). Crack free coatings with thickness of 630 nm were typically obtained at a spinning speed of 1000 rpm.

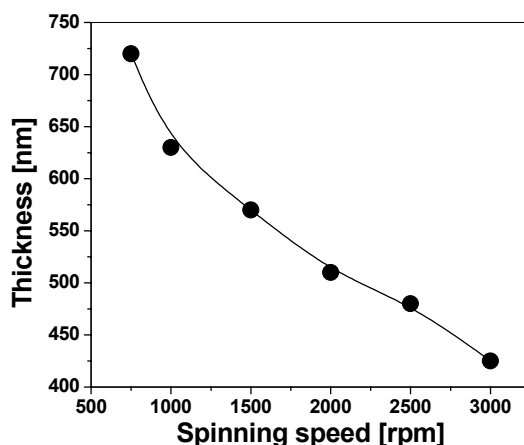


Fig. 28: Variation of the thickness of spin coated film on glass substrate made with the MPTS modified ITO350 sol (solid content 25 wt%) with the spinning speed (UV hardening)

Multilayers coating can also be deposited in order to obtain thicker coatings by repeating the coating process (spinning, drying, densification). The thickness of the layers increases practically linearly, however the process leads to a slight reduction of the optical quality. Fig. 29 shows the variation of the thickness and the optical transmittance at $\lambda = 550$ nm of multilayers MPTS/ITO350 films deposited on glass substrate and cured by UV-irradiation.

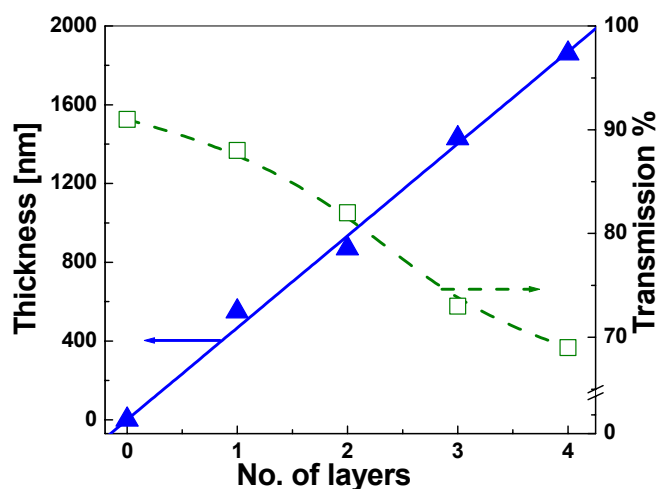


Fig. 29: Variation of thickness and optical transmission ($\lambda = 550$ nm) of multilayer spin coated ITO/MPTS films on glass substrate (UV-treated).

5.3.3 Conclusion

The coating sols used in this work consisted of redispersable ITO nanoparticles post annealed in forming gas at 250 °C or 350 °C. Dip and spin coating methods produce transparent conducting films. The thickness of the films were examined as a function of the solid content concentration, the sol viscosity, the spinning and withdrawal speed.

The thickness of the film increases significantly by increasing the concentration of ITO particles in the sol, as a result of the increase of the viscosity. Single good optical quality layers with thickness between 400 and 500 nm were obtained for a solid content of 25 wt.%. The addition of a modifier like TEOS, GPTS or MPTS to the coating sol increases its viscosity and consequently the thickness of the film.

Multilayers can be obtained to produce thicker films by repeating the deposition and the hardening steps; however the optical transmission of the resulting coatings decreased with the number of layers.

5.4 Transparent conducting coatings deposited on glass substrates

Films were deposited on different glass substrates (float, borosilicate and fused quartz) and heat treated at different temperatures up to 1000°C. This section reports on the characterization of their structural, morphological, electrical, optical and mechanical properties.

5.4.1 Structural and morphological properties

Phase structure (XRD)

XRD measurements were carried out in order to investigate the structural properties of pure ITO coatings made of redispersable indium tin oxide nanopowders. Fig. 30 shows typical XRD patterns made with the the ITO350 sol and spin coated on fused quartz substrates and then heat treated in air at 130, 550, and 1000°C. The layer heated at low temperature 130°C was deposited on borosilicate glass.

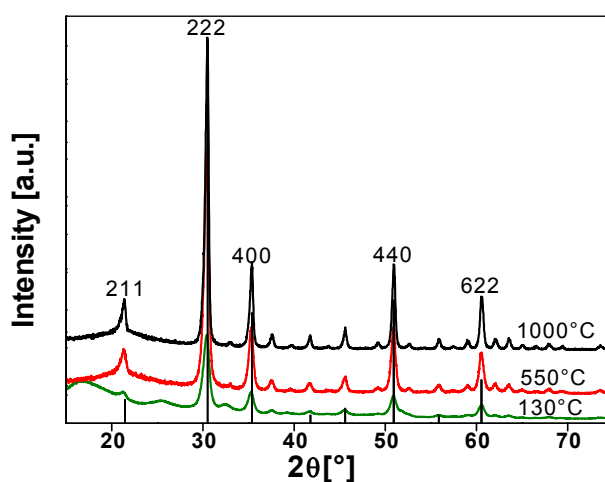


Fig. 30: XRD patterns of spin coated ITO layers on borosilicate and quartz glass heated at 130°C, 550°C and 1000°C. The vertical lines refers to the JCPDS database (06-416).

As expected all the films are polycrystalline. They show the same cubic bixbyite In_2O_3 phase crystal structure (JCPDS of indium oxide, card number 06-416) independent of the sintering temperatures up to 1000 °C. No phases of Sn oxides or hydroxide were found.

There is however a slight difference between the 2θ -peaks positions and those of the JCPDS of pure Indium oxide. This can be explained by the substitution of In ions by Sn ions which leads to a slight lattice expansion because of the size differences of the atoms. Another possibility for this deviation may be due to a strain effect due to the thermal expansion coefficient mismatch between the film and the substrate. Similar results have been observed by Shigesato et al (291) who studied the doping mechanisms of ITO films deposited by highly dense plasma assisted electron beam evaporation. They reported that the slight shift of the XRD peaks observed by doping the In_2O_3 lattice with tin oxide was due to the presence of crystallographic faults.

The intensity of the diffraction peaks increased significantly when the layers are sintered at higher temperatures indicating the better crystallization. The crystallite size also increases from 20 nm at 130 °C, 25 nm at 550 °C then 35 nm at 1000 °C. It is also found that the ratio $I(222)/I(400)$ decreases from 3.62 at 130 °C to 3.56 at 550 °C then to 2.43 at 1000 °C, indicating a gradual growth of the crystallite with an orientation normal to the (400) crystallographic plane. A similar behaviour was already observed for the powders (see section 5.1.1). ITO films grown with a (400) crystallographic orientation were found to have larger grain size than the (222) textured ones(292, 293).

Surface morphology (SEM)

The surface morphology of the coatings sintered at different temperatures and post annealed in a reducing atmosphere is shown in Fig. 31. As expected, all films consist of nano-crystalline particles, which have approximately a regular granular shape. The growth of the particles with the sintering temperature is clearly observable. The grain size of the film sintered at 550°C ranges between 35-45 nm, that of films sintered at 750°C between 50-60 nm and that sintered at 1000°C is larger and ranges between 75-90 nm. It is also seen that the edge texture of the particles become sharper and the grain boundaries become clearer by increasing the sintering temperature. The obtention of large grain size is important for transparent conducting thin films. This leads to smaller electron scattering and therefore the higher is the charge mobility and the electrical conductivity (see section 5.4.2).

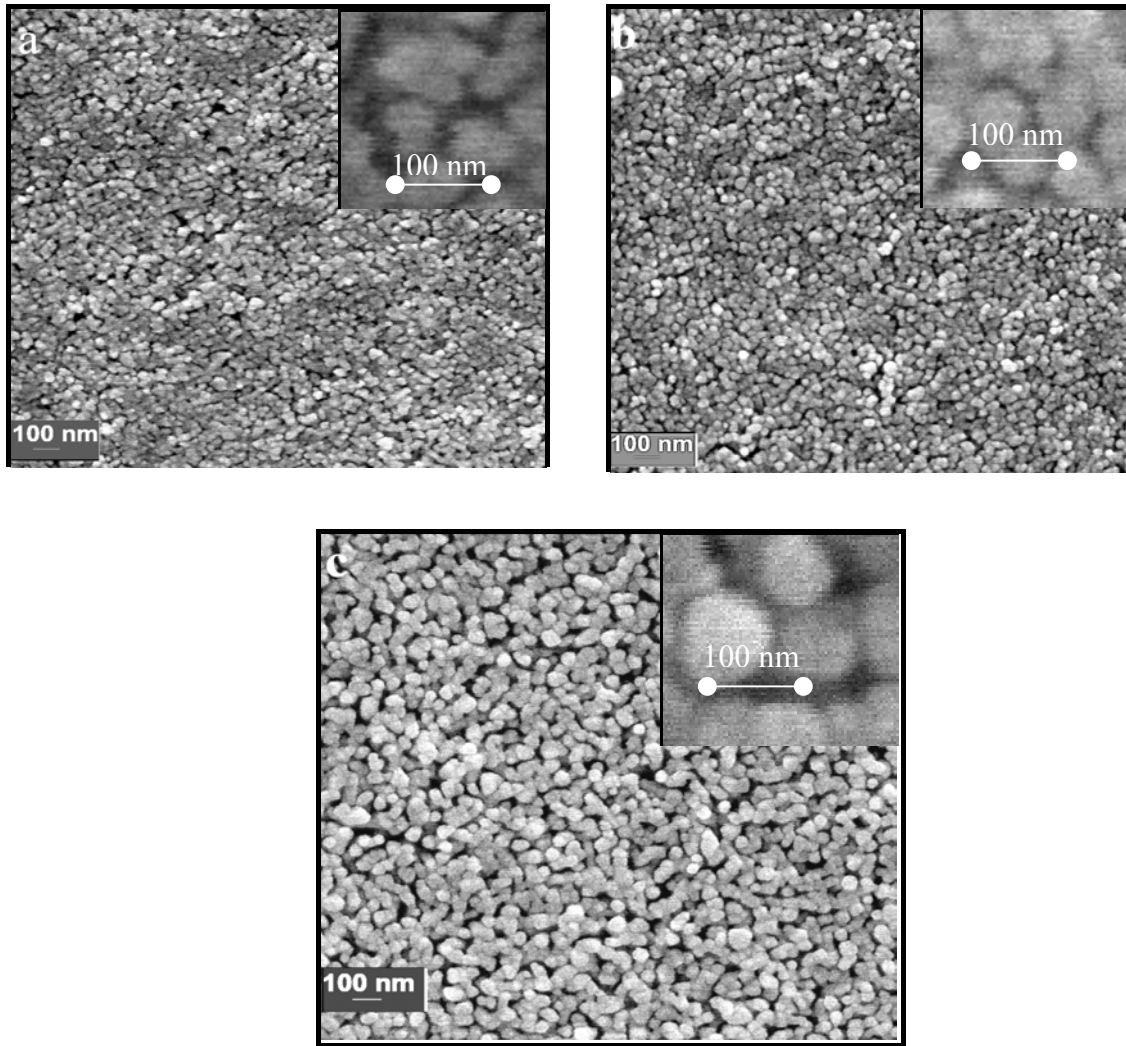


Fig. 31: SEM images of the surface morphology of spin coated ITO layers on quartz substrates sintered at a) 550°C, b) 750°C and c) at 1000°C. The insets are an enlargement of a part of the figures.

5.4.2 Electrical Properties

The electrical properties of indium tin oxide coatings were characterised as a function of the doping concentration (Fig. 32), the heat treatment (Fig. 34, Fig. 35) and the type of the coating sol (Fig. 32). As shown in Fig. 32, the specific resistivity of spin coated ITO layer sintered in air at $T = 550\text{ }^{\circ}\text{C}$ first decreases with increasing Sn concentration, passes by a minimum at around 6 to 8 mol % and then increases. The ITO layers made of ITO350 particles show a minimum of the resistivity at a slightly lower Sn/In ratio than those made of ITO250 particles. Undoped indium oxide layer with thickness between 400 to 460 nm has a resistivity $\rho \sim 1\ \Omega\cdot\text{cm}$ ($R_{\square} > 20\ \text{k}\Omega_{\square}$). The minimum resistivity is about $7.5 \times 10^{-2}\ \Omega\cdot\text{cm}$ ($R_{\square} = 1.7\ \text{k}\Omega_{\square}$) at Sn concentration of 8 wt.% (ITO250) sol and to $4.6 \times 10^{-2}\ \Omega\cdot\text{cm}$ ($R_{\square} = 0.9\ \text{k}\Omega_{\square}$) at Sn concentration of 6 wt.% (ITO350 sol). The resistivity of the film is $0.32\ \Omega\cdot\text{cm}$ at 12 wt.% Sn concentration.

The slightly different behaviour between the two type of particles is probably due to the temperature at which the particles have been prepared. ITO 350 particles were heat treated at

higher temperature, and therefore the diffusion of Sn ions into the indium oxide matrix was more effective than in the case of the particles sintered at lower temperature. In addition the ITO350 particles were found to have larger crystallite size than the ITO250 ones, so that the electron scattering at grain boundaries is smaller.

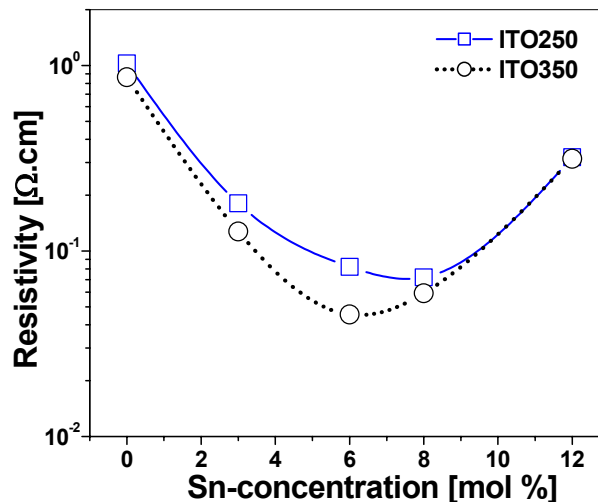


Fig. 32: Variation of the resistivity of ITO250 and ITO350 films deposited on borosilicate substrate by spin coating and sintered at 550°C in air as a function of Sn concentration in the coating sol.

The specific resistivity, carrier density and mobility of ITO350 layers as a function of the doping concentration is shown in Fig. 33. It is seen that the carrier mobility is low and continuously decreases with increasing Sn doping and, as expected, that the carrier concentration increases, passes by a maximum at 6 wt. % and then decreases. This shows that the decrease of the resistivity of the films with the Sn concentration is essentially due to the increase of the electron density. The substitution of Sn^{4+} ion for In^{3+} ion releases one electron in the lattice contributing to the conductivity. When the Sn concentration increases, the crystallite size decreases (Fig. 1) and this results in more grain boundaries, which behave as barriers for the electron mobility and this explain the behaviour of μ . An excess of tin concentration in the film may also form defects such as Sn_2O , Sn_2O_4 , and SnO , which behave as electron traps rather than effective donors (58). The variation of the specific resistivity of indium oxide thin films with the doping concentration of Sn was studied intensively in many papers (258, 294-299) and follows the same tendency.

Frank and Köstlin (285) reported that for a concentration of above 5 at. % Sn, the ITO film become less conductive, where the excess of Sn doping results in a formation of impurity scattering centers and do not donate free electrons. Omata et al (295) reported that the increase of Sn concentration in ITO layers results in an increase of the interstitial oxygen ions which behave as a trap of the mobile electrons.

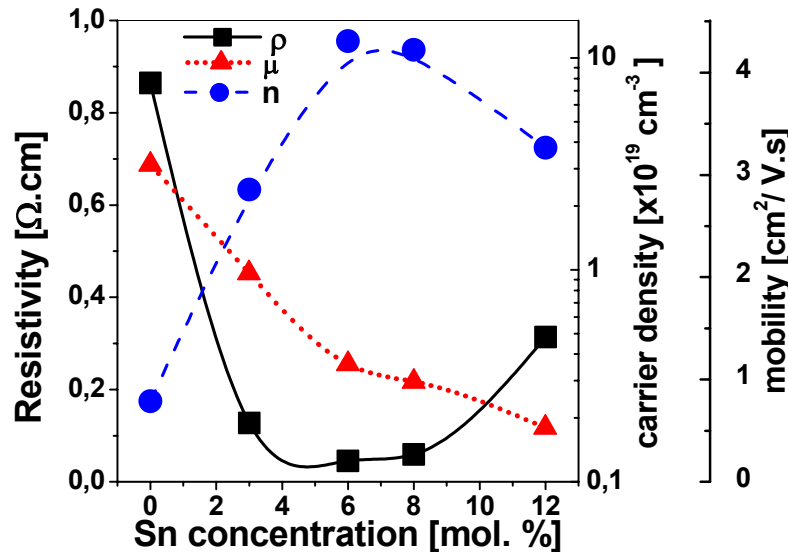


Fig. 33: Specific resistivity, carrier concentration and mobility of ITO350 layers deposited on borosilicate substrate and sintered at 550 °C in air for 30 min.

The effect of the sintering time on the specific resistivity was tested at 550 °C for spin coated ITO250 layers (Fig. 34). The specific resistivity first decreases, passes by a minimum value for a firing time of about 30 min and then slightly increases. This period of time is sufficient to sinter the particles and to bring them close together. The increase of the resistivity at longer time may be attributed to the oxidation of the film due to a slow oxygen surface chemisorption effect, which removes the oxygen vacancies and reduces the concentration of charge carriers.

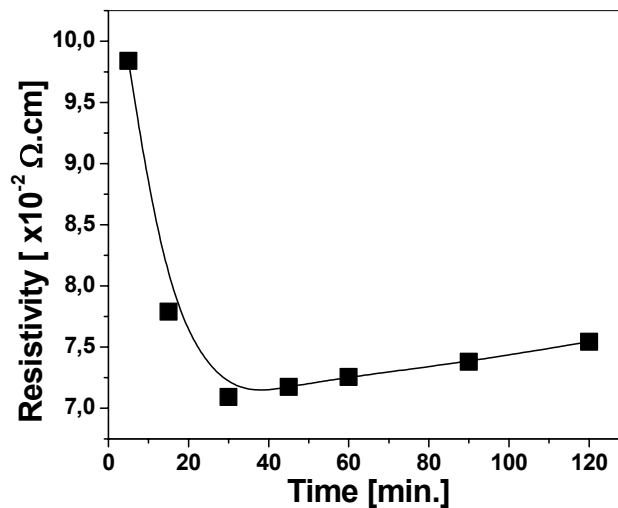


Fig. 34: Variation of specific resistivity of ITO coating as a function of the duration of the heat treatment in air at 550°C.

The sintering of the layers was also tested up to 1000 °C with films deposited by spin coating on fused quartz substrates. Fig. 35 shows the variation of the specific resistivity, ρ , and the sheet resistance, R_{\square} , of single ITO350 layer fired in air at different temperatures during 30 min and also further post annealed in forming gas (N_2/H_2 : 92/8) at 350°C during 30 min. The Sn concentration of the coatings was 7 mol%. The resistivity of the film fired in air at

550°C is $4.8 \times 10^{-2} \Omega\text{cm}$ and decreases gradually by increasing the firing temperature down to $1.2 \times 10^{-2} \Omega\text{cm}$ at $T = 1000^\circ\text{C}$.

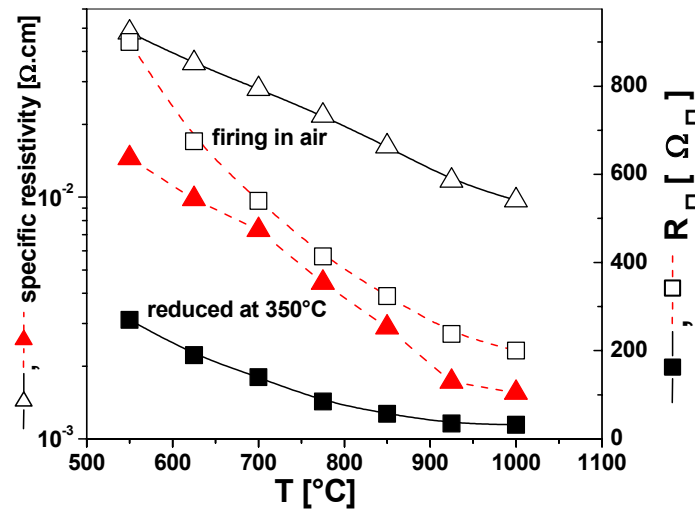


Fig. 35: Sheet resistance, R_{\square} , and specific resistivity, ρ , of a 500 nm thick nano-ITO coating deposited on quartz substrate as a function of the sintering temperature in air during 30 min. and also further annealed under reducing gas (350°C, 30 min.)

This behaviour is related to a better sintering and to the growth of the particles which improve remarkably the carrier mobility which varies from $1.08 \text{ cm}^2 / \text{V.s}$ at 550°C to $4.25 \text{ cm}^2 / \text{V.s}$ at 1000°C as shown in Fig. 36. Increasing the sintering temperature also leads to a slight increase of the carrier concentration from $1.19 \times 10^{20} \text{ cm}^{-3}$ at 550°C to $1.55 \times 10^{20} \text{ cm}^{-3}$ at 1000°C . These results are in agreement with the growth of the crystallite size calculated from the XRD pattern (section 5.4.1) which increases from 25 nm at 550°C to 33 nm at 1000°C and with the SEM observations of the surface morphology of the coatings where the growth of the particles and a denser structured layer with larger and sharper grain size is clearly observed by increasing the firing temperature (Fig. 31).

The mobility of the charge carriers in polycrystalline ITO thin films is affected by two main scattering mechanism: ionised-impurity scattering and grain boundary scattering. As the firing temperature is raised, the growth of the grain size results in smaller grain boundary and smaller grain boundary potential (see equation 11, chapter 2), and consequently to a smaller grain boundary scattering. This leads to a better transport of the electrons and consequently higher conductivity.

The same trend was found by Takahashi et al (97), who found that the main parameter affecting the resistivity of dip coated ITO films sintered at different temperatures is the mobility of the carriers rather than the carrier concentration. A few nanometer increase of the crystallite size assists the growth of the ITO particles and increases the conductivity of the formed films. Seki et al (300) observed that the mobility of dip coated ITO films was affected mainly by grain boundary scattering rather than by scattering inside the grains. The effect of heat treatment in air on the electrical properties of sol-gel ATO coatings made of redispersed nanocrystalline ATO particles was investigated in ref. (70). It was found that the specific

resistivity of these ATO layers decreased with increasing the firing temperature (up to 750 °C) and that a high firing temperature results in a large contact surface between the particles leading to smaller grain boundary scattering. It was also believed that the increase of the charge mobility was the dominant factor.

The slight increase of the carrier concentration will be discussed later.

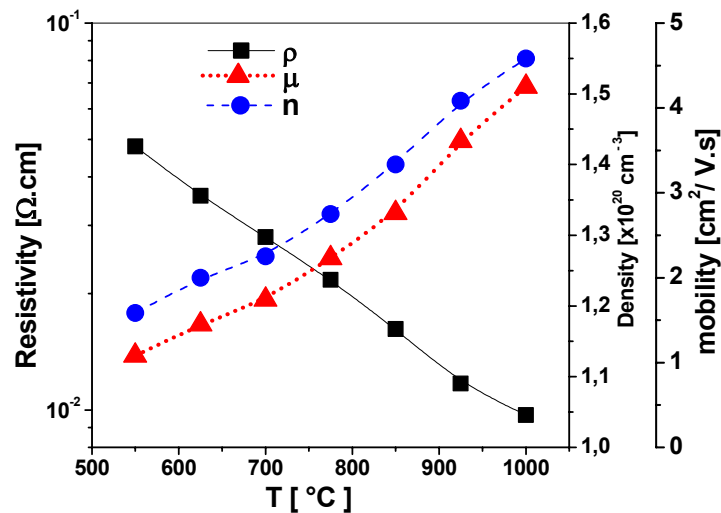


Fig. 36: Variation of ρ , n and μ of ITO350 layers sintered in air at different temperatures.

Fig. 35 also shows that the conductivity of the coatings is improved remarkably by post annealing treatment in a forming gas at 350°C during 30 min. For instance the specific resistivity of the coatings fired in air at 550 °C and 1000°C which is 4.8×10^{-2} and 9.7×10^{-3} Ωcm , respectively decreases down to 1.45×10^{-2} and 1.55×10^{-3} Ωcm , respectively after the reducing process.

The treatment in non oxidizing atmosphere leads to a slight increase (typically 11 %) of the charge mobility but to a significant increase of the carrier concentration as shown in Fig. 37. The mobility and the carrier density for the film sintered at 550 °C in air are $1.08 \text{ cm}^2 / \text{V} \cdot \text{s}$ and $1.2 \times 10^{20} \text{ cm}^{-3}$, respectively (Fig. 36) and increases after post annealing to $1.2 \text{ cm}^2 / \text{V} \cdot \text{s}$ and $3.32 \times 10^{20} \text{ cm}^{-3}$ respectively (Fig. 37). The carrier mobility and concentration increase gradually with the sintering temperature up to $5.32 \text{ cm}^2 / \text{V} \cdot \text{s}$ and $7.63 \times 10^{20} \text{ cm}^{-3}$ at 1000 °C. The improvement of ρ by the reducing treatment is more effective for layers sintered at higher temperature.

The remarkable increase of the carriers concentration after post annealing is due to the increase in oxygen vacancies which ideally produce two free electrons (see equation 10, chapter 2). The oxygen concentration in ITO films were investigated by Hunda et al (301) and Mizuna et al (302) before and after post annealing of the films in vacuum. It was found that the oxygen concentration decreased upon post annealing.

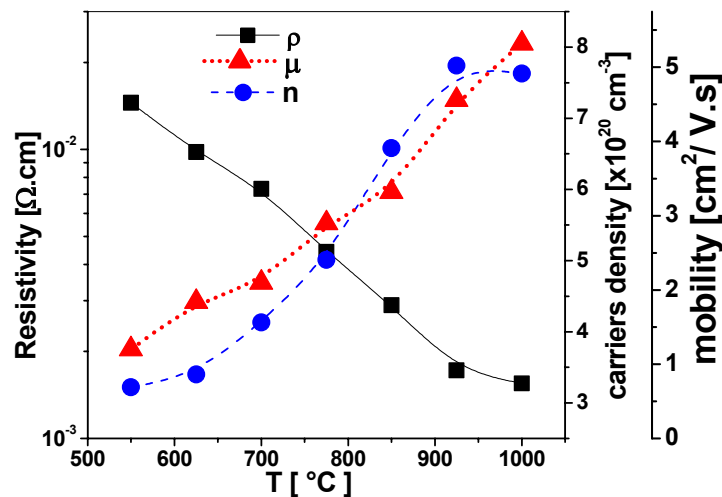


Fig. 37: Variation of ρ , n and μ of ITO350 layers sintered in air at different temperatures and further post annealed at 350 °C in forming gas for 30 min.

It was also observed that the post annealing temperature affect the electrical and optical properties of the coatings. A post treatment performed at temperature higher than 350 °C leads to a slight decrease of the specific resistivity and the optical quality of the films deteriorates. All the films reduced at $T > 400^\circ\text{C}$ have a smoky-brown appearance, typical of metal-rich ITO.

The values shown in Fig. 35, 36 were measured at least one week after the production of the coatings and correspond to stable values. Interestingly it was observed that the specific resistivity and the sheet resistance of the post annealed coatings measured immediately after the process was lower and unfortunately increases with time until reaching a stable value. Fig. 38 shows the sheet resistance of the ITO coatings measured at three different stages: before annealing, immediately after annealing and after storage in air during one week (20 °C, 40 % RH). The time evolution of the sheet resistance of the post annealed layers varies significantly and depends on the temperature at which the layer was sintered in air before the reducing process. For instance a layer sintered in air at 550 °C shows a sheet resistance of $70 \Omega_{\square}$ immediately after the reducing process and then increases by about 285 % until reaching a stable value. By increasing the sintering temperature to 775 °C or 1000 °C, the variation is smaller, 96 and 28 %, respectively. The layers sintered at higher temperature show a higher degree of stability after the reducing process.

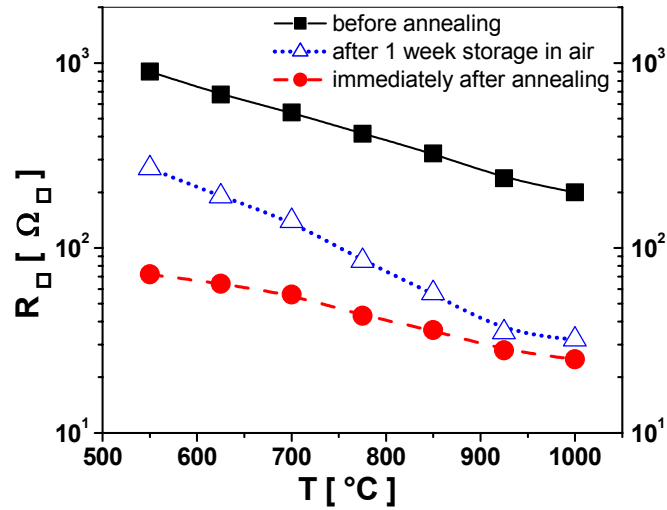


Fig. 38: Sheet resistance of ITO coatings deposited on fused quartz glass measured before annealing in reducing atmosphere, directly after the annealing and after one week storage in air (stable values)

These results indicate that the improvement of the electrical conductivity after post annealing the samples which essentially originate from the creation of oxygen vacancies, is not stable and that back reactions with oxygen species occur within the coating. It is believed that these species are chemisorbed at the surface of the ITO particles and capture free electrons decreasing therefore the charge carrier concentration. Coatings fired at high temperatures ($T > 750$ °C) are denser so that the diffusion of oxygen species in or out the coatings become more difficult and the specific surface area of the particles become smaller so that the surface chemisorption reactions are reduced. This explains the slighter changes of the sheet resistance of the samples fired at 1000 °C comparing to that fired at lower temperatures. This also explain the small variation shown for the carrier density in Fig. 36, where smaller surface results in less interaction with the adsorbed oxygen species.

To get a better insight on this phenomena, the porosity of the films was estimated by measuring the refractive index of the coatings using the following relation (22, 242):

$$P(\%) = \left[1 - \frac{n_p^2 - 1}{n_s^2 - 1} \right] \times 100 \quad [40]$$

where P and n_p are the porosity (in %) and the refractive index of the porous material, respectively and n_s is the theoretical refractive index of the dense material ($n = 1.9$ at $\lambda = 550$ nm (259)).

The refractive index of the coatings was measured by the VASRA method (see appendix A3.3). Fig. 39 shows the θ_B shifts to higher value when the firing temperature raises. The refractive index of the coating at $\lambda = 550$ nm increases from 1.52 to 1.62 when the firing temperature raises from 550 to 1000 °C respectively.

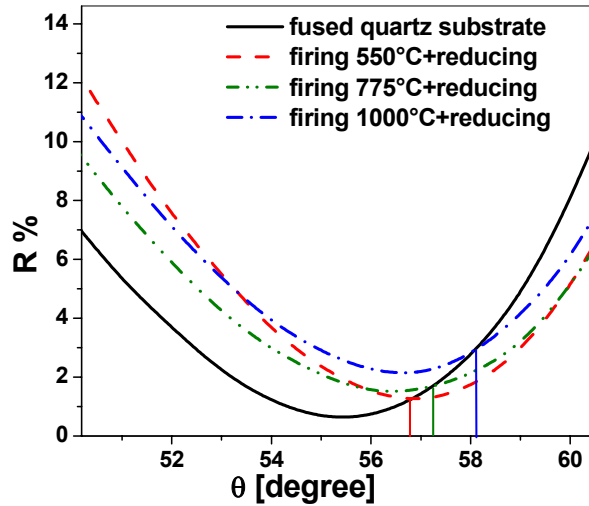


Fig. 39: Reflection determined according to the VASRA method (at $\lambda = 550$ nm) for coatings deposited on fused quartz glass and fired at different temperatures.

The measurements of the refractive index using the ellipsometry method shows the same trend. All the results are listed in Table 8.

The porosity of the films decreases from 51% to 37% by increasing the firing temperature from 550°C to 1000°C. The densification of the coatings results in a filling of the open pores, and the coatings sintered at higher temperatures, although still porous, become denser and the distances between the ITO grains become smaller. It is worth to note that films made by sol-gel methods remain too porous even after a high temperature sintering. Choi et al (303) reported that the film density influences the electrical properties of sputtered ITO thin films and in particular that the carrier mobility increases with the film density. This confirms that the grain boundary scattering is the main factor influencing the carrier mobility. ITO coatings made of conducting nanoparticles have a higher resistivity than those made by physical methods indicating that point defects, pores and voids in the films are probable the major scattering source for the charge carriers. The maximum mobility obtained for the ITO layer sintered at 1000 °C is about $5 \text{ cm}^2 / \text{V.s}$, a very small value compared to those obtained by sputtering ($40 - 50 \text{ cm}^2 / \text{V.s}$) (293, 304) or conventional sol-gel deposition methods ($10-30 \text{ cm}^2 / \text{V.s}$) (97, 300, 305).

Table 8: Measured refractive index at 550 nm and estimated porosity of ITO coatings on fused quartz substrates fired at different temperatures.

Firing Temperature °C	Refractive index (550 nm, VASRA)	Refractive index (550 nm, ellipsometry)	Porosity (%)
550	1.52	1.52	51
775	1.55	1.53	46
1000	1.61	1.62	37

5.4.3 Optical Properties

The optical properties of pure ITO350 coatings deposited on fused quartz substrate and submitted to different thermal treatments were characterized by measuring the transmission, absorption and reflection spectrum from UV to IR range.

Far infrared range

In this region practically only the reflection property of ITO coatings can be measured because of the high absorption of the substrate. Fig. 40 shows some representative data of ITO coatings sintered in air at different temperature and further heat treated in a forming gas atmosphere at 350 °C during 30 min.

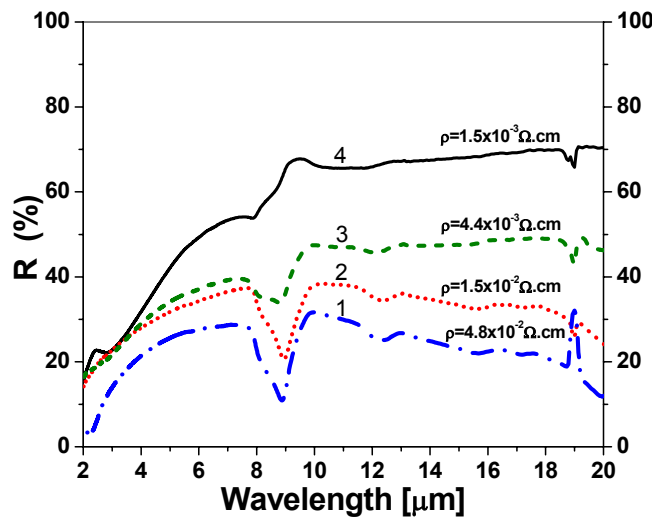


Fig. 40: IR optical reflection of ITO films fired at different sintering temperatures T_s and annealed in forming gas at 350 °C: 1. $T_s = 550$ °C fired in air, 2. $T_s = 550$ °C and annealed, 3. $T_s = 775$ °C and annealed, 4. $T_s = 1000$ °C and annealed.

The far IR reflectance of the coatings depends on the dc resistivity and increases when ρ decreases. However the results are only in partial agreement with the Drude theory (see section 2.4.3). In the IR range the Hagen-Rubens relation states that for a given frequency $1 - R \propto \rho^{1/2}$. This expression is however only valid when $\omega \ll \gamma$, $\gamma = e/m^* \mu$ being the inverse of the average electron relaxation time assumed to be independent of the frequency.

Fig. 41 shows a plot of the IR reflection of all studied samples measured at $\lambda = 22 \mu m$. The Hagen-Rubens relation hold well only for the low resistivity coatings (reduced samples sintered at $T \geq 775$ °C). This probably indicate that the condition $\omega \ll \gamma$ is not satisfied for the coatings having a high dc resistivity.

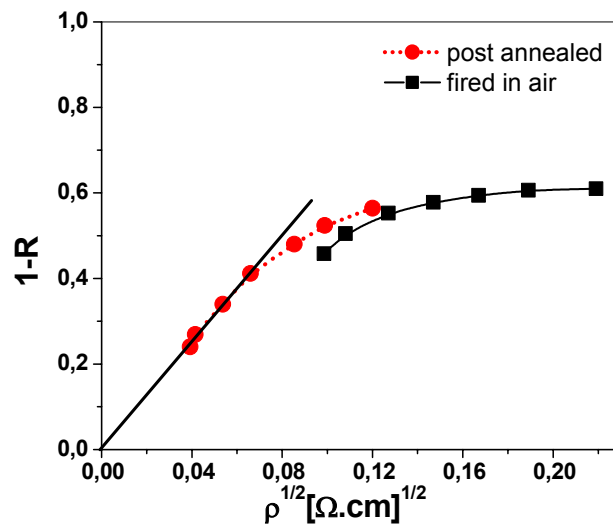


Fig. 41: $1-R$ vs $\rho^{1/2}$ for reflection data taken at $\lambda = 22 \mu\text{m}$.

Vis- near IR range

Fig. 42 shows the transmission T , reflection R and absorption A (calculated as $1-(T+R)$) for a 550 nm thick pure ITO350 coatings sintered at 550 °C in air ($\rho = 4.8 \times 10^{-2} \Omega\cdot\text{cm}$) and then further reduced in forming gas at 350 °C for 30 min ($\rho = 1.5 \times 10^{-2} \Omega\cdot\text{cm}$).

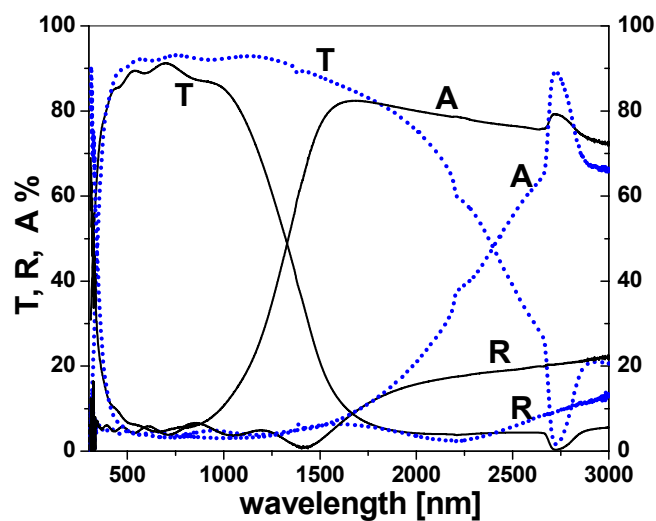


Fig. 42: T , R and A for coatings sintered in air at 550 °C (.....) and then reduced in forming gas (—).

Both films exhibit a high transmission in the visible range, that for the reduced ones being however somewhat smaller. The coating sintered in air shows a large transmission window extending from the UV up to $\lambda = 2.3 \mu\text{m}$ ($T = 50\%$). This window is however sharply reduced in the near IR range for the reduced coating ($\lambda = 1.25 \mu\text{m}$, $T = 50\%$).

For a very thin dense ITO coating obtained for instance with a sputtering process, a sharp decrease of the transmission around $\lambda = 1.25 \mu\text{m}$ would have indicated a coating exhibiting a very low sheet resistance with resistivity of the order of a few $10^{-4} \Omega\cdot\text{cm}$ (high n and μ). It

would also have been accompanied by an almost anticorrelated sharp rise of the reflection up to value close to 80 % for $\lambda = 2.5 \mu\text{m}$. This is not the case here. The reflectance curve shifts towards shorter wavelength (shift of the plasma wavelength from about $2.7 \mu\text{m}$ to $1.7 \mu\text{m}$), indicative of a large increase of the carrier concentration but the values of the reflectance remain very low (about 20 % at $\lambda = 2.0 \mu\text{m}$). Therefore its contribution to the decrease of the transmission is small. The main effect comes from the presence of a high broad and asymmetric absorption peaking at about $1.7 \mu\text{m}$ related to the free carriers. This photon loss is given by (298):

$$A = C \frac{nt}{\mu} \quad [41]$$

where C is a constant and t is the thickness of the coating. As t and n are high and μ is small, the value of A is particularly high for this reduced coating.

The optical behaviour can not be fitted with a simple Drude model (306). The asymmetric shape of the curve is also an indication that this model is not adequate to describe the optical behaviour in this frequency range. This is due to the different morphology of the coatings (aggregation of dense particles, most of them made of a single crystallite and probably highly conducting, see section 5.1.2). The photons in this frequency range begin to probe the behaviour of electrons within the particles so that the values of the resistivity and mobility are not the low values which have been determined by dc electrical methods (corresponding to those obtained optically in the far infrared, $\omega \ll \gamma$) which are limited by grain boundary scattering but those corresponding to the inside of the particles for which ρ should be lower and μ should be higher as they will be limited only by ion impurity scattering.

Another information which corroborates the above discussion is the optical behaviour of the coatings sintered at different temperatures and further annealed in forming gas. Fig. 43 and Fig. 44 show some representative T and A curves for coatings sintered between 550°C and 1000°C .

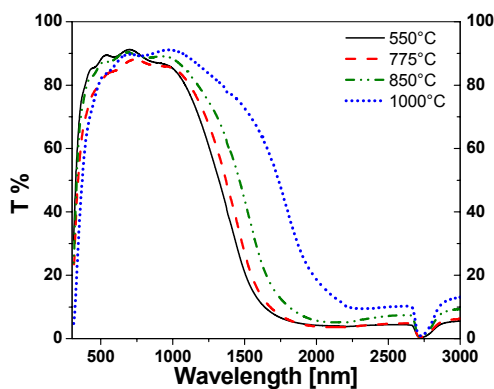


Fig. 43: Transmission of 550 nm thick coatings sintered in air at different temperature and then further annealed in forming gas at 350°C for 30 min.

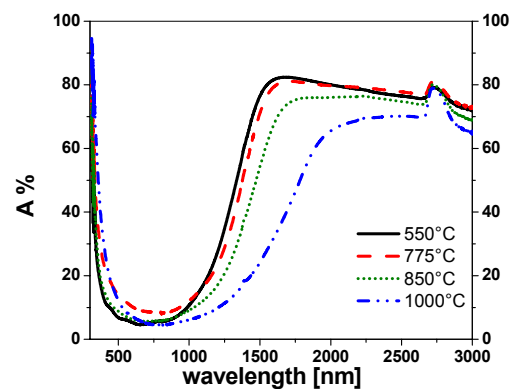


Fig. 44: Corresponding absorption of the coatings shown in Fig. 43.

As the electrical resistivity strongly decreases with the increase of the sintering temperature (see Fig. 35), a shift of the near IR transmission edge toward lower wavelength was expected, but the contrary is observed. This behaviour is due to the shift of the large IR absorption edge toward longer wavelength (Fig. 44). Equation [41] and the variation of the ratio n/μ obtained from the dc electrical data (see Fig. 37) indicate that such a behaviour should be observed, but the values independent of the frequency can not explain the results. Similar observation was found by Bommel et al (70) for layers made of redispersable ATO particles, however no explanation for the shift toward longer wavelength was given.

Therefore the theoretical model to be used for describing the visible- near IR range optical behaviour is much more complicated and can only be made using a computer fitting program. From a theoretical point of view the layer should also not be treated as a homogeneous one but probably as an effective medium as proposed by Bruggeman (307) involving highly conducting ITO particles connected in a percolating network surrounded by a dielectric background (e.g air). Similar consideration have been reached by Ederth (308) for ITO coatings made with 20 nm size ITO particles, although heat treatments and consequently the results were different from ours.

UV range

The band gap energy can be estimated from the transmission and reflection spectra in the UV region according to equation [34]. Fig. 45 shows how the direct energy gap of the same coatings mentioned previously has been estimated by extrapolating the linear part of α^2 vs. photon energy with the abscissa. Some representative curves for coating sintered in air at 550, 775 and 1000 °C are shown in Fig. 45. A large shift of the absorption band toward lower energy (longer wavelength) is observed for increasing sintering temperature. A value of 3.77 eV is obtained for the coating sintered at 1000 °C in agreement with published values but the data for the two other coatings are not good enough to ascertain a value. The value of the energy gap E_g is proportional to $n^{2/3}$ (138), therefore the data indicate that $n_{1000} < n_{775} < n_{550}^{\circ\text{C}}$ which is contrary to the results given by the dc electrical measurement which shows that n slightly increases. Such behaviour was also reported without explanation by Bommel et al (70) for ATO coatings made of redispersable nanoparticles, where no shift of the optical band gap was observed although the resistivity of the coatings decreased by 3 order of magnitude.

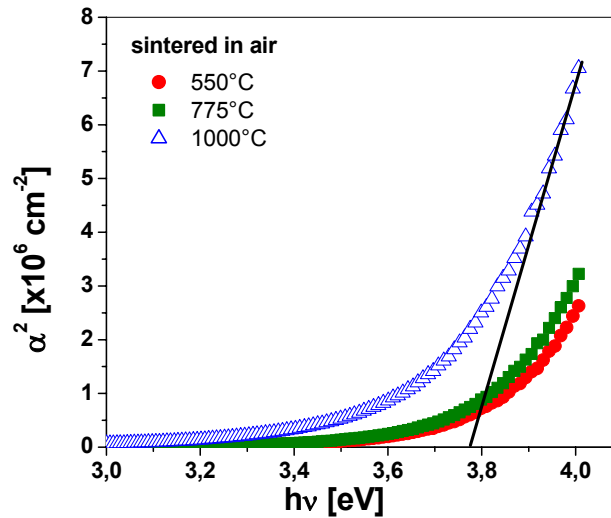


Fig. 45: α^2 vs. $h\nu$ for ITO coatings deposited on quartz substrate fired in air at 550, 775 and 1000 °C.

A similar behaviour has been observed for coatings sintered at the same temperature and then reduced in forming gas at 350 °C for 30 min, although in this case a much larger variation of n with the temperature has been observed (Fig. 37).

A comparison of the data for both type of coatings (Fig. 46) shows nevertheless that the reduced coatings have a larger optical band gap for all sintering temperatures which is in agreement with the data of n and confirm the Moss-Burstein shift when coatings sintered at the same temperature are compared.

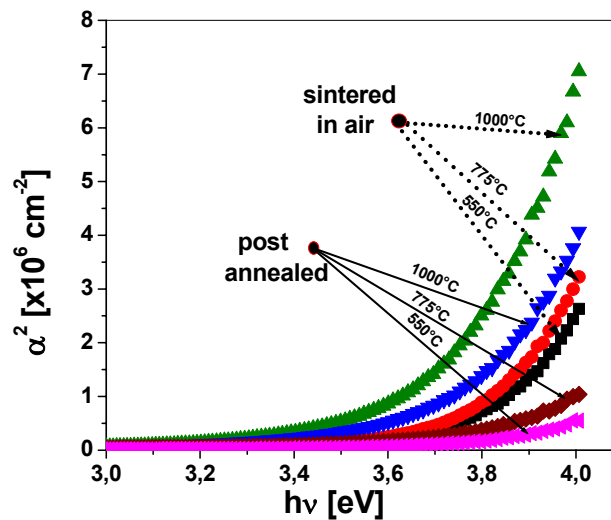


Fig. 46: Comparison of α^2 vs. $h\nu$ for ITO coatings deposited on quartz substrate sintered only in air and also further post annealed in forming gas at 350 °C for 30 min.

Figure of Merit

The figure of merit, ϕ is a measure of the quality of the films and it is estimated by the following relation (108):

$$\phi = T^{10} / R_{\square} \quad [42]$$

where T is the average transmission in the visible range and R_{\square} is the sheet resistance.

The calculated figure of merit of the coatings deposited on quartz substrate after different kind of treatments are shown in Table 9. The figure of merit is enhanced with increasing the firing temperature and is improved drastically by post annealing the films under forming gas. The values are nevertheless smaller than those obtained for rf sputtered ITO films (108) which range between 14×10^{-3} and $40 \times 10^{-3} \Omega^{-1}$.

Table 9: Figure of merit calculated from the electrical and optical properties of ITO films on quartz substrates

Substrate temperature (°C)	Φ (Without reducing) $\times 10^{-3} \Omega^{-1}$	Φ (With reducing) $\times 10^{-3} \Omega^{-1}$
550	0.5	1,2
625	0,7	1
775	1	2.1
850	1.3	4.6
925	1.7	6.9
1000	1.85	6.8

5.4.4 Mechanical properties

The mechanical properties (adhesion, abrasion resistance, hardness) of transparent conductive thin films have a significant meaning for industrial application. They are listed in Table 10. They become better as the firing temperature is increased but are not very good in view of some demands of industrial application. The abrasion test with a rubber under a load of 9.8 N is a severe test for such coatings and the films are totally removed after rubbing the surface of the coating during 10 cycles.

Table 10: Mechanical properties (adhesion, abrasion resistance) of ITO films sintered at different temperatures.

T (° C)	Tape test DIN 58196-K2	Cloth test DIN 5896-H25	Rubber test DIN 58196-G10
120	Totally removed	Class 5	Class 5
550	Partially removed	Class 3	Class 5
775	Ok	Class 2	Class 4
1000	Ok	Class 2	Class 3

The addition of a small amount of prehydrolysed organosilane, such as TEOS, GPTS in the coating sol, improves the adhesion and the abrasion resistance (see 5.5.9). However the sheet resistance of the silane modified coatings is higher than those sintered without binder at temperature higher than 300 °C. Fig. 47 shows the variation of the sheet resistance of ITO coatings deposited on borosilicate glass made with the ITO350 sol and the GPTS modified ITO350 sol as a function of the heat treatment. At low temperature the GPTS modified

coatings have a lower sheet resistance than the pure ones; however at higher temperature ($T > 300^{\circ}\text{C}$) the opposite is found. This can be interpreted as a result of the transformation of GPTS into silica in form of a very thin SiO_2 layer surrounding the conducting particles. This was confirmed from FTIR spectrum where the formation of a Si – O - Si network is clearly seen (Appendix E).

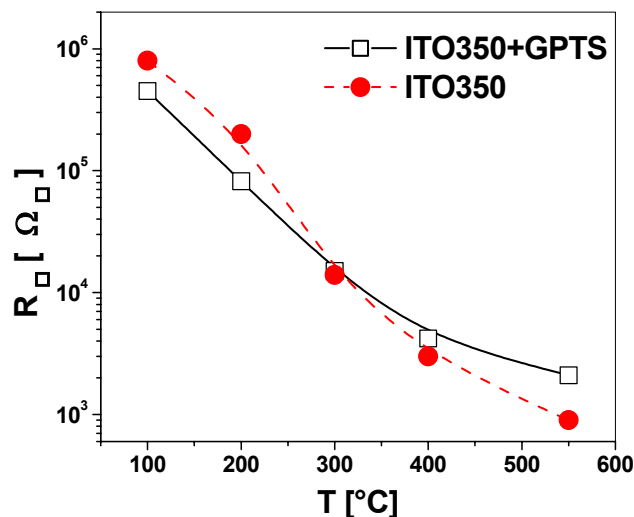


Fig. 47: Sheet resistance variation of ITO350 and GPTS modified ITO350 coating with heat treatment.

5.4.5 Conclusion

Transparent conductive films were deposited on glass substrates using the spin and dip coating method using sols made of nanocrystalline ITO particles dispersed in ethanol. The thickness of the deposited films is determined by the concentration and the viscosity of the sol and follows the Landau-Levich relation. The wet films were sintered in air at different temperatures up to 1000°C and with further post annealing in a nonoxidising atmosphere.

The lowest film resistivity was achieved for a doping concentration between 6-8 wt. %, and was found to decrease by increasing the firing temperature, an effect essentially related to the increase of the charge carriers mobility. Further improvement of the electrical resistivity was obtained by a further post annealing of the coatings at 350°C for 30 min in forming gas atmosphere. This effect was related to the increase of the number of charge carriers due to the creation of oxygen vacancies. The minimum resistivity for a 500 nm single ITO layer was $1.55 \times 10^{-3} \Omega \cdot \text{cm}$ for samples fired at 1000°C and further annealed at 350°C in a forming gas. By increasing the firing temperature the porosity of the film decreased, the surface morphology becomes denser and the particle size increases.

All the films exhibit a transparency greater than 85% in the visible range. A shift of the plasma wavelength toward shorter wavelength was observed in the NIR region and related to the change of the carriers density. The films behave as heat mirrors in the IR region, where the reflection increases up to 70% at $\lambda > 10 \mu\text{m}$. The band gap energy measured optically ranged between 3.7 and 3.9 eV. The widening of the energy gap observed by the reducing

treatment was related to the Moss-Burstein shift. The produced films have a figure of merit in the range of 1 to $7 \times 10^{-3} \Omega^{-1}$.

5.5 Transparent conducting coating cured at low temperature

This section presents the characterization of transparent conducting ITO coatings cured using low temperature processes ($T < 130^\circ\text{C}$). The coatings have been obtained by using modified ITO coating sols deposited by spin or dip coating methods mainly on polycarbonate (PC) substrate but also on other polymeric substrates and glasses which don't withstand thermal treatment at high temperature. The films have been hardened using either UV-irradiation (Beltron), by heating in air at $T < 130^\circ\text{C}$ or by a combination of both processes. Their structural, electrical, optical, and mechanical properties are described below.

5.5.1 Microstructure of the coatings (XRD)

Fig. 48 shows the XRD patterns of spin coated MPTS modified ITO thin films deposited on PC substrates. Both films are made of redispersible ITO250 and ITO350 particles and cured using UV-irradiation (Beltron). They consist of polycrystalline particles and have the same cubic bixbyite In_2O_3 phase structure as those made with pure ITO particles; as before no other phases were detected. The broad peak observed at 17° corresponds to the substrate.

The films made of ITO350 particles have stronger peak intensities than that those made with the smaller ITO250 particles. From the calculation of the line broadening of the major (222) peaks, the crystallite size of MPTS/ITO250 and MPTS/ITO350 films are 14 and 20 nm, respectively.

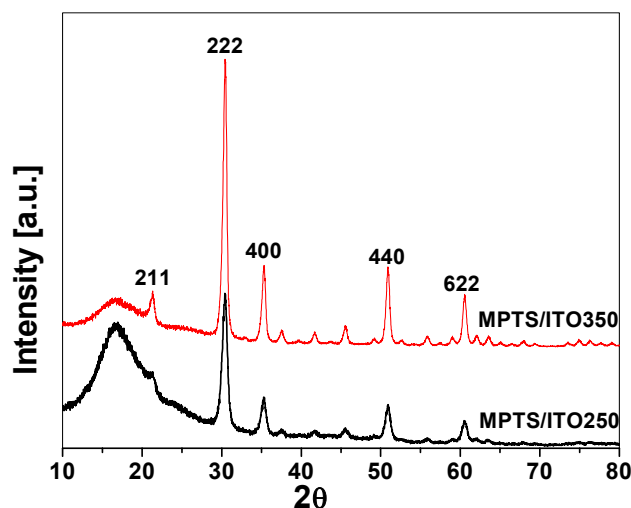


Fig. 48: XRD patterns of spin coated MPTS modified ITO250 and ITO350 layers on PC substrates after UV-treatment.

5.5.2 Electrical properties

Several organic or organic - inorganic coupling agents all polymerizable at low temperature or by UV-irradiation, have been used to link the particles together. The coatings were densified by irradiating the wet deposited films by UV-irradiation and by further heat treatment at

130°C for several hours as described in section 4.4. The sheet resistance, thickness, the optical quality (eye inspection) and the adhesion to a PC substrate are summarized in Table 11. The concentration of the additives given in Table 11 referred to the whole solution, and is that for which a minimum sheet resistance was obtained. The thickness of the ITO film without additives was 470 nm and it slightly increases by using the modified coating sols.

Table 11: Electrical, optical and mechanical properties of modified ITO350 coating treated with UV-irradiation (Beltron, 5 min) and further heat treatment at 130 °C for 10 h.

Additive	Additive concentration (wt. %)	Sheet Resistance R_{\square} ($k\Omega_{\square}$)	Thickness (nm)	Optical quality	Adhesion Tape test DIN 58196-K2
Without additive	0	640	470	transparent	failed
Dbasic Ester	7	100	513	transparent	Ok
Disobutyladipat	6	87	577	hazy	Ok
Butyldiglycolacetat	6	200	519	transparent	Ok
MPTS	6	8	570	transparent	Ok
GPTS	7	18	547	transparent	Ok
TEOS	8	63	510	transparent	Ok
APTS	4	70	550	hazy	Ok
MTEOS	5	80	549	transparent	Ok

The sheet resistance of a single pure ITO350 layer irradiated with UV ($105 \text{ mW} / \text{cm}^2$, 5 min) and further heated for 10 h. at 130°C is high, $640 \text{ k}\Omega_{\square}$, and the layer does not adhere well on the substrate. The modification of the coating sols enhances clearly the electrical conductivity and the adhesion of the ITO coatings to the substrate. The optical quality of the films is almost the same except for those made with APTS and disobutyladipate which were hazy. It is believed that these additives act as coupling agents binding the conducting particles together without the need to sinter them at high temperature.

TEOS, GPTS and MPTS are known as silane coupling agents and are predominantly used as mediators and binding organic to inorganic materials. Many reports (198, 309-312) have shown that these material can be used to improve the adhesion of coatings and paints on several substrates. They are also used as a thickening agent for sol-gel coating as can be seen in Fig. 27. They can be hydrolysed and polymerized to form chains and act as network former. These coupling agents were found the most promising materials for ITO particles as they produce a minimum sheet resistance of 65, 18 and $8 \text{ k}\Omega_{\square}$, respectively.

The effect of TEOS, GPTS, MPTS concentration on the sheet resistance of ITO350 thin films is shown in Fig. 49 a, b, c. The coatings were deposited by spin coating and hardened at low temperature either by heating the wet films at $T = 130 \text{ }^{\circ}\text{C}$ in air for 10 h, by UV irradiation

using a Beltron equipment (110 mW/cm^2 , 5 min.), by a combination of UV and heat treatment or by heating at $T = 130 \text{ }^\circ\text{C}$ in the presence of forming gas for 2 h.

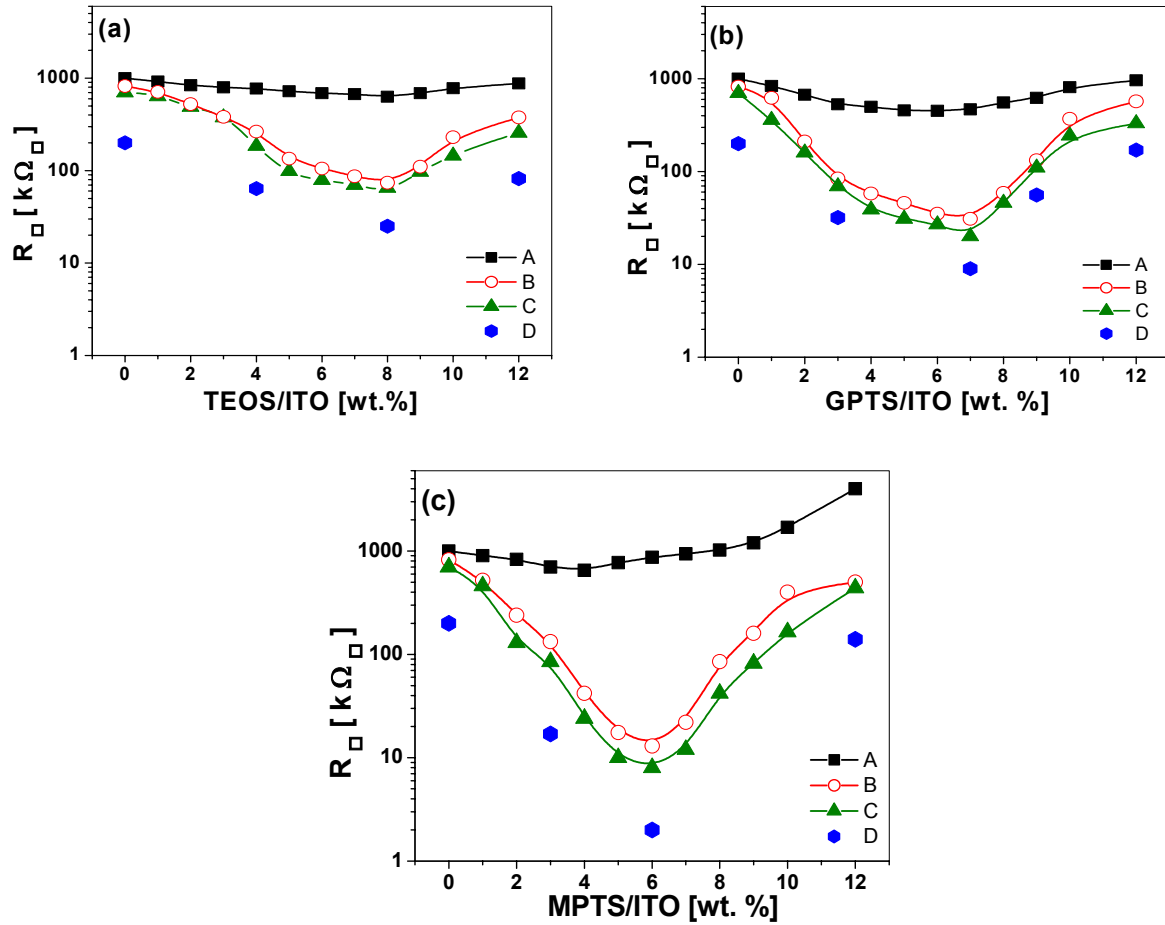


Fig. 49: Sheet resistance of ITO350 thin films on PC substrates hardened with different treatment as a function of (a) TEOS, (b) GPTS and (MPTS) concentration. A: heating at $130 \text{ }^\circ\text{C}$ for 10 h, B: UV-irradiation (Beltron, 5 min.), C: B+A, D: C+ heating in forming gas for 2 h.

In all cases the sheet resistance of the layers was found to decrease by increasing the concentration of the modifier in the coating sol up to a value of 8 wt. % (TEOS), 7 wt. % (GPTS) and 6 wt. % (MPTS). The lowest sheet resistance, $2 \text{ k}\Omega_{\square}$ was obtained by using MPTS modified ITO coating after reducing the UV treated MPTS/ITO layer in forming gas at $130 \text{ }^\circ\text{C}$ for 2 h. After the same treatment TEOS/ITO coatings showed a sheet resistance of $25 \text{ k}\Omega_{\square}$ and the GPTS/ITO coatings showed a sheet resistance of $9 \text{ k}\Omega_{\square}$. The results indicate a clearly observable effect of the modifier on the improvement of the electrical conductivity of such coatings.

A short time UV treatment (process B) is much more effective to decrease the sheet resistance of the coatings than the heat treatment at low temperature for several hours (process A). After 10 hours of heat treatment in air at $T = 130 \text{ }^\circ\text{C}$, the sheet resistance of TEOS/ITO, GPTS/ITO and MPTS/ITO coating were 630, 466 and $870 \text{ k}\Omega_{\square}$, respectively. However after 5 min of UV irradiation, the sheet resistance of the coatings decreased down to 74, 31 and $13 \text{ k}\Omega_{\square}$.

respectively. By further heating the UV-treated samples at 130 °C (process C), the sheet resistance of the coatings further slightly decreases down to 65, 20 and 8 $k\Omega_{\square}$, respectively.

Fig. 50 shows the time evolution of the sheet resistance of a spin coated MPTS / ITO layer under UV-irradiation. It decreases from $10^3 k\Omega_{\square}$ down to 13 $k\Omega_{\square}$ in almost 5 min. A longer irradiation time does not improve the conductivity. There is also a slight variation in the thickness of the deposited film with increasing the time of irradiation, but this variation is within the standard error of the profilometer.

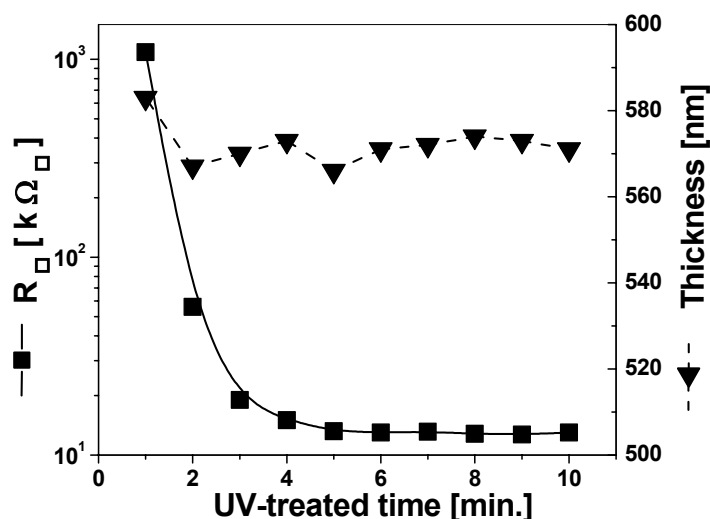


Fig. 50: Effect of UV-treatment time on the sheet resistance and the thickness of spin coated ITO/MPTS thin film deposited on PC substrate. 1 min correspond to a UV energy of 1.8 J/cm².

The same behavior was found in the case of GPTS and TEOS modified ITO coatings. It will be shown that the UV-treatment allows to polymerize the coupling agent (see section 5.5.7) enhancing the cross linking between the conducting particles and fill the pores of the layer that act as electron scattering centers. However at the same time it acts as a reducing process in which oxygen species are removed from the surface of the ITO particles. This results in an increase of the number of the oxygen vacancies and the charge carrier concentration leading to a drastic decrease in the sheet resistance.

The effect of UV-irradiation on the electrical properties of transparent conducting coatings were also studied by other authors. Kololuoma et al (313) have used suitable organic ligands to modify antimony doped tin oxide solution for patterning sol-gel ATO coatings by UV-irradiation. The authors believed however that the increase of the film conductivity by UV-irradiation results mainly from an increase of the crystallite size. It was nevertheless also observed from the analysis of the chemical composition of the surface that the concentration of oxygen species on the surface of the film decreased after the exposure to UV-irradiation.

In another study (314), it was observed that the electrical conductivity of tin oxide thin films grown by a sol-gel dip coating technique was improved by photodesorption of the films using UV-irradiation source. The conductivity was found to raise by 4 orders of magnitude by UV-irradiation followed by an annealing under vacuum. Imai et al (315) reported that a UV-laser

irradiation allows to effectively crystallize sol-gel derived indium oxide thin films and to decrease the sheet resistance. This decrease was explained as a result of the increase of the charge carrier concentration due to the formed oxygen deficiency. Petritz (125) studied theoretically the photoconductivity in semiconductor thin films and reports that the change in the conductivity observed under the irradiation can result from a change in the density of the charge carriers and from the reduction of the intercrystalline potential barriers.

Fig. 51 shows the variation of the sheet resistance of MPTS/ITO layer as a function of the conveyor speed of the Beltron equipment, after the coatings have been irradiated during 5 runs. It is worth to remember that the temperature reached by the coated substrates also depends on the conveyor speed (see Fig.8).

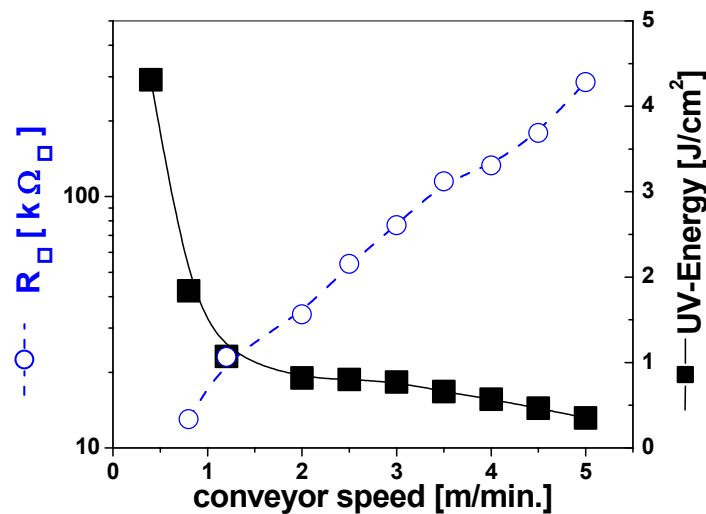


Fig. 51: Dependence of the sheet resistance of MPTS/ITO layer on the conveyor speed of the Beltron equipment, after the layers have been irradiated during 5 runs. The right axis represents the corresponding amount of UV energy emitted by the lamp during 1 run.

The right axis in Fig. 51 represents the amount of the UV-energy received by the samples during each run. It is obvious that an increase of UV energy decreased the sheet resistance. The sheet resistance of samples treated with the higher energy (speed = 0.8 m/min, 5 runs, about $9.5 J/cm^2$) was $13 k\Omega_{\square}$ and is much lower than that obtained for samples treated with lower UV-energy, $280 k\Omega_{\square}$ (speed = 5 m/min, 5 runs, about $2 J/cm^2$).

Fig. 52 shows the variation of the sheet resistance of UV irradiated (5 runs at 0.8 m/min.) GPTS/ITO and MPTS/ITO layers as a function of the duration of a heat treatment at $130^{\circ}C$ in air. The value of both layers further decrease slightly with the subsequent heat treatment from $33 k\Omega_{\square}$ down to less than $20 k\Omega_{\square}$ for GPTS/ITO layers after 40 h and from $13 k\Omega_{\square}$ down to $8 k\Omega_{\square}$ for MPTS/ITO layers after about 20 h.

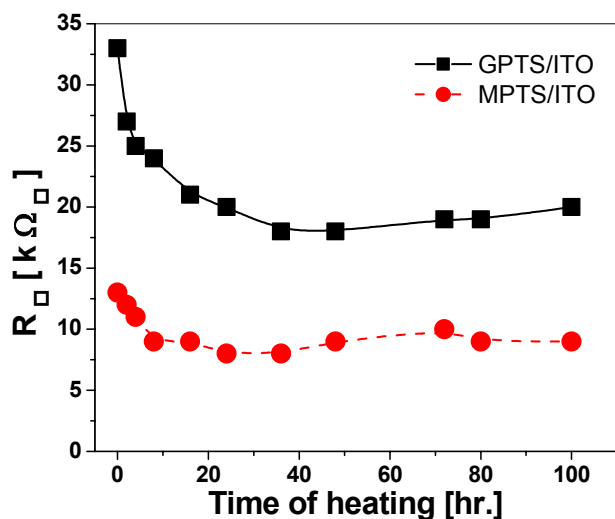


Fig. 52: Time variation of the sheet resistance of UV-irradiated GPTS and MPTS modified ITO coatings during heating at 130°C in air.

A heat treatment in a reducing atmosphere (N_2/H_2 : 92/8) at 130 °C has however a more drastic improvement on the sheet resistance of the layers which is decreased from about 8 $k\Omega_{\square}$ down to 2 $k\Omega_{\square}$ after a two hours treatment (Fig. 53). An increase of the time slightly degrades the sheet resistance by about 5 %.

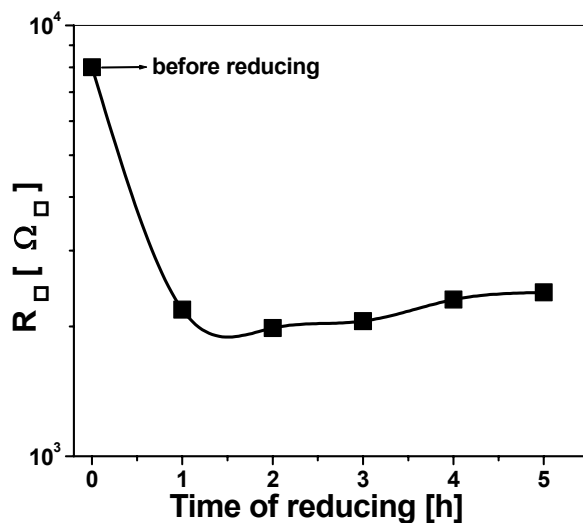


Fig. 53: Dependence of the sheet resistance of MPTS/ITO layers on the time of reducing in the presence of forming gas.

5.5.3 Coatings on other polymeric substrates

The same modified coating sols were deposited on other polymeric substrates. The deposited layers with thickness between 550 and 600 nm were also UV-irradiated several times using Beltron's conveyor speeds which maintain the substrate temperature below a value for which no deformation is observed. The substrates were allowed to cool down to room temperature after each run.

Table 12 show the electrical sheet resistance of a single MPTS/ITO layer deposited on different polymeric substrates. The values for all coatings lay between 13 and 30 $k\Omega_{\square}$, the lowest one being that of coated PC substrate, 13 $k\Omega_{\square}$.

Table 12: Sheet resistance of MPTS/ITO coatings deposited on different polymeric substrates treated with UV-irradiation.

Substrate	Thickness of substrate (mm)	Conveyor-speed (m/min.)	No. of UV-runs / total UV energy (J/cm^2)	R_{\square} ($k\Omega_{\square}$)
PC	3	0.8	4-5 / 9.2	13
PVC	1	5	17 / 6	17
PC-foil	0.05	6	25 / 5.3	30
PMMA	2	2	8 / 6.6	15
PET-foil	0.1	5	20 / 7	15
PE	2-3	2	7 / 5.8	20

Fig. 54 shows the evolution of the sheet resistance of MPTS/ITO coatings on PVC and PMMA substrates as a function of the number of runs (a) under UV-irradiation (Beltron) and the corresponding UV energy (b). Similar to the behavior shown in Fig. 50 the sheet resistance decreases by increasing the amount of the UV energy and reaches its minimum, 15 $k\Omega_{\square}$, after 9 runs ($7.3 J/cm^2$) for PMMA substrate and 17 $k\Omega_{\square}$, after 18 runs ($6.4 J/cm^2$) for PVC substrate. Fig. 54 b shows also clearly that the parameter to reduce the sheet resistance is the total UV energy density received by the sample. The sheet resistance was further slightly reduced to 15 and 12 $k\Omega_{\square}$, respectively, after further heating them in air at 80 °C for several hours.

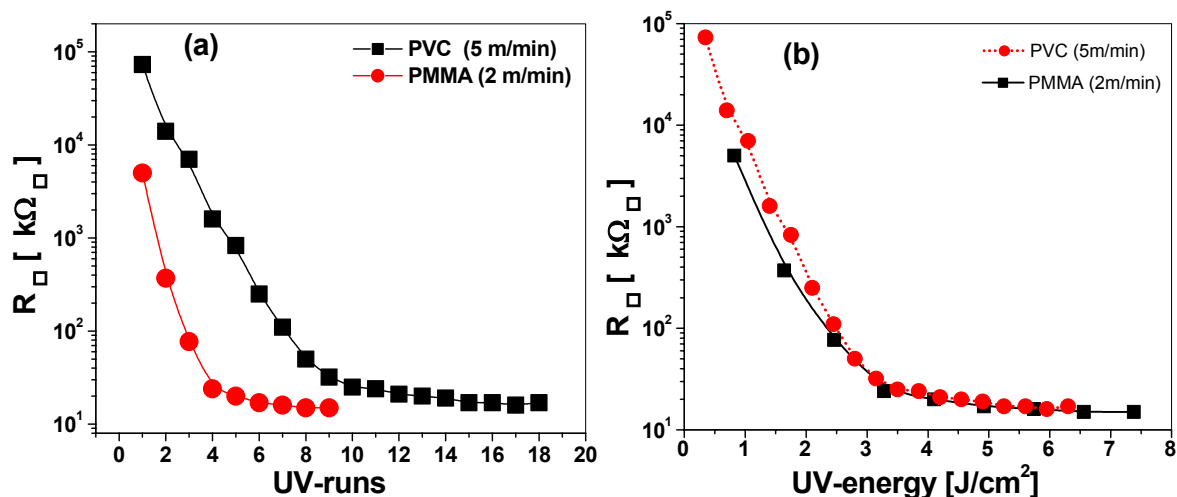


Fig. 54: Sheet resistance of MPTS/ITO single layer deposited on PVC and PMMA substrates as a function of the number of UV-runs (a) and the UV-energy (b) through the Beltron equipment.

5.5.4 Time evolution of the electrical properties

The values of the sheet resistance given in the last section are stable values measured after storing the films in ambient atmosphere (20°C, 40 RH) during many days. However the effect of the UV and reducing treatments is more effective than that presented. Fig. 55 a, b shows the time evolution of the sheet resistance of a 530 nm thick GPTS/ITO (a) and 570 nm thick MPTS/ITO (b) coatings on PC substrates after UV-irradiation for layers kept under different atmospheres, such as vacuum, air (20 °C, 40 % RH) and water (20 °C). In this example a sheet resistance of 7 k Ω_{\square} and 3.7 k Ω_{\square} for GPTS/ITO and MPTS/ITO respectively were measured directly after 5 runs of UV-irradiation. The value remains constant for long time (> 200 h) when the UV treated samples are stored under vacuum or nitrogen atmosphere. When the samples are stored in ambient atmosphere, the sheet resistance increases gradually with time by a factor of about 4.5 for GPTS/ITO and 3.3 for MPTS/ITO coatings to reach a stable value of 30 k Ω_{\square} and 12.5 k Ω_{\square} , respectively after 200 h. The sheet resistance change of a sample stored in water increases to even higher value, 80 k Ω_{\square} , (a factor of about 10) after a period of 200 h.

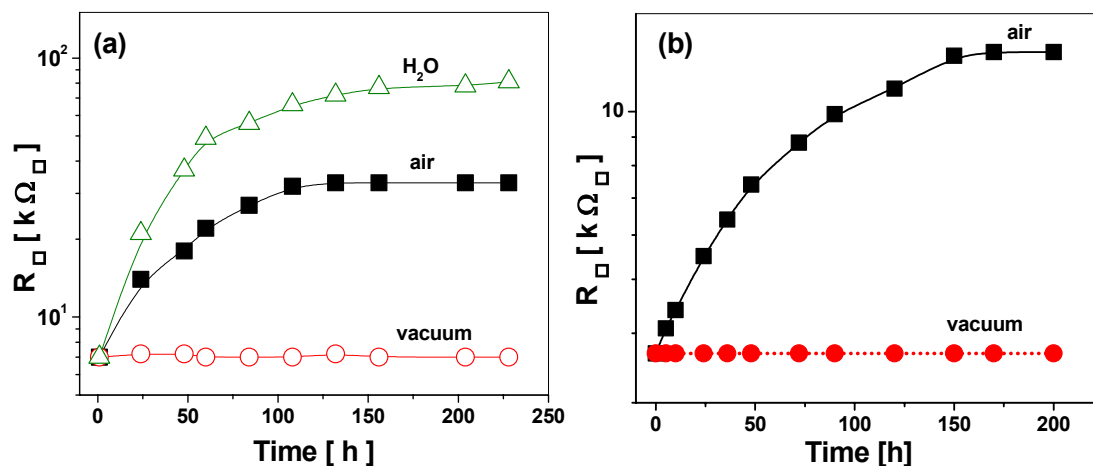


Fig. 55: Time evolution of the sheet resistance of coatings deposited on PC substrate and stored in different atmospheres, vacuum, air and water. a) GPTS/ITO, b) MPTS/ITO

It is believed that the effect of the storage atmosphere on the stability of the sheet resistance is related to the chemisorption of oxygen and OH species on the ITO particle surface. A confirmation was obtained by analyzing the evolution of the mobility and carrier concentration in air under the same conditions (Fig. 56). The increase of the electrical sheet resistance during storage in an oxidizing atmosphere (Fig. 55) is accompanied with an observable decrease of the carrier concentration from $8.2 \times 10^{19} \text{ cm}^{-3}$ measured immediately after the UV treatment down to $3.2 \times 10^{19} \text{ cm}^{-3}$ after 200 h and also a slight decrease of the mobility (Fig. 56). This can be referred to the reduction of the amount of oxygen vacancies (created during the UV-irradiation), by the diffusion of the oxygen species into the layer. The catalytic action of water (Fig. 55 a) may activate and accelerate the diffusion of oxygen species into the layer and the oxidation process (316).

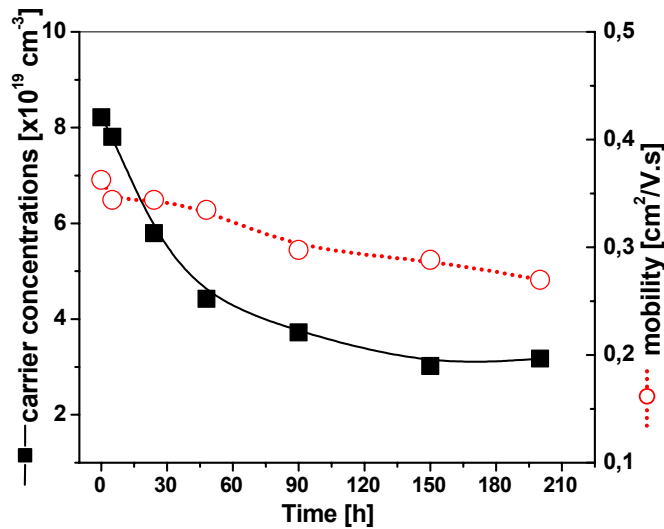


Fig. 56: Evolution of carrier concentration and mobility of UV irradiated 570 nm MPTS/ITO layer during storage in air.

The time evolution of the sheet resistance was also determined after heating the sample in a reducing atmosphere. Fig. 57 shows the results of a 570 nm thick MPTS/ITO layer (Fig. 49 c) post annealed at 130 °C in forming gas for 2 h (process C) and then stored either in ambient atmosphere (20 °C, 40 % RH), under vacuum or under a protective gas (N₂, Ar). The sheet resistance measured just after the reducing treatment is 800 Ω_□, i.e. a factor 10 lower than before the reducing treatment. It does not change when the sample is stored in vacuum or under a protective gas. However it increases from 800 Ω_□ to 1650 Ω_□ (a factor of about 2) when the film is left in air for 200 h.

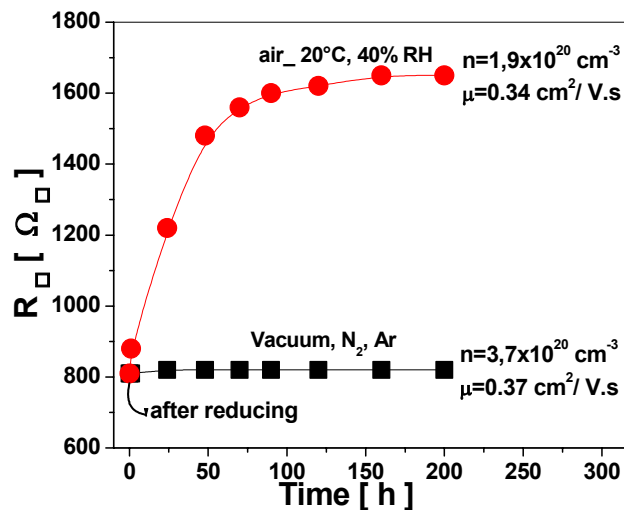


Fig. 57: Time evolution of the sheet resistance of 570 nm thick MPTS/ITO coating on PC, after reducing the coating at 130 °C in forming gas.

This behavior is clearly linked to the decrease of the carrier concentration from $3.7 \times 10^{20} \text{ cm}^{-3}$ to $1.9 \times 10^{20} \text{ cm}^{-3}$ and the slight decrease of the mobility. It is interesting to note that this behavior is fully reversible and the lowest value of the sheet resistance can be reproduced by repeating the reducing process. The UV irradiation and the reducing process result in a

metastable state of the electrical properties. When the samples are exposed to air, oxygen species diffuse back into the layer decreasing the number of the created oxygen vacancies and consequently of the carrier concentration. The high porosity of the layers is certainly responsible for the diffusion rate. It is therefore remarkable that the change of the sheet resistance comes mainly from the change of the carrier concentration, where the oxygen vacancies concentration play an important role.

The mobility of the charge carriers of the MPTS/ITO350 coatings is however very low value, about $0.5 \text{ cm}^2/\text{V.s}$ and remains practically constant during the different treatments. Similar measurements made with MPTS/ITO250 coatings (smaller particle size) leads to even smaller mobility, $\mu = 0.1 \text{ cm}^2 / \text{V.s}$. These values are far lower than those measured for films prepared by physical or chemical vapor deposition ($30 < \mu < 100 \text{ cm}^2 / \text{V.s}$) and from those obtained by conventional sol-gel methods ($10 < \mu < 30 \text{ cm}^2 / \text{V.s}$) (52, 317). This indicates that in our coating the free charges suffer a high scattering process during their drift. The size of the particles play an important role. The smaller the particles are, the larger is the grain boundary scattering. The low charge mobility is therefore a result of the scattering at particles and cluster grain boundaries. The slight decrease in the mobility of the charge carriers, about 8 %, (Fig. 56, Fig. 57) is probably also related to the oxygen diffusion mechanism at the grain boundaries as reported by Lopes et al (318), who claimed that oxygen species act as traps for the free charge carriers and increase the potential barrier between the grains (higher grain boundary scattering).

The reversible change of the optical and the electrical properties of indium oxide thin films by photoreduction and oxidation have been investigated by Fritzsche et al (319). The authors also observed that the resistivity of the films decreased by exposing the films to UV-light. By reoxidizing the films under ozone or oxygen plasma treatments, an increase of the resistivity was observed. The value of the optical band energy gap was also found to increase by exposure to UV-light, which is another confirmation of the increase of the charge carriers through the UV-irradiation. The change of the electrical properties of ITO films reduced in N_2 / H_2 atmosphere was studied in a recent work by Hultaker et al (320) who reported a decreasing in the conductivity due to water up-take by the ITO particles film when exposed to air. Barlow et al (321) have also observed a degradation of the electrical properties of ITO films consisting of fine particles when exposed to air.

The stability of the sheet resistance of our coatings was also investigated as a function of the thickness of the film. MPTS/ITO layers with different thicknesses were deposited on PC substrates using different sol concentrations and then cured under UV-irradiation. The sheet resistance was measured directly after the treatment ($R_{\square} (t = 0)$) and then after storage in air during 7 days ($R_{\square} (t = 7 \text{ days})$). The stability factor, defined as the ratio $R_{\square} (7 \text{ days}) / R_{\square} (t = 0)$, decreases from 12 down to 2 with the increase of the film thickness from 80 to 1000 nm, respectively as shown in Fig. 58. The increase of the thickness may result in a denser layer limiting the diffusion of the oxygen species back into the film.

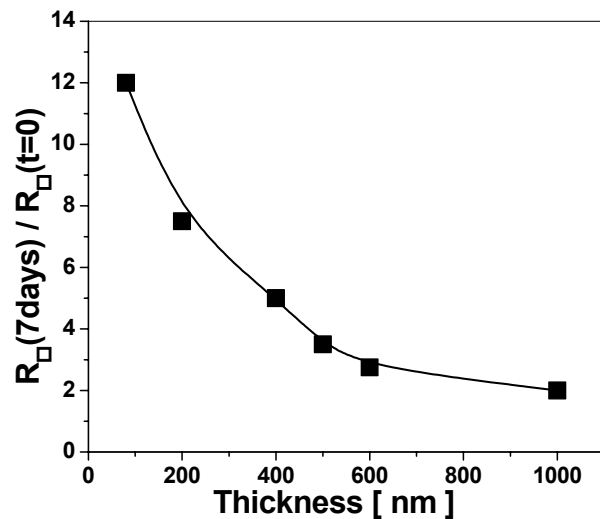


Fig. 58: Stability factor ($R_{\square}(7\text{days}) / R_{\square}(t=0)$) of UV cured MPTS/ITO layers as a function of the film thickness.

Fig. 59 (a) shows the effect of Ar-Plasma treatment on the sheet resistance of 570 nm UV-irradiated MPTS/ITO layer deposited on PC substrate as a function of the treatment time. It is observed that such process also enhances the conductivity of the coatings. After a 10 min treatment the sheet resistance of the film decreases from $13 \text{ k}\Omega_{\square}$ down to $6.5 \text{ k}\Omega_{\square}$. This plasma treatment therefore also acts as a reducing process for such coatings; however, as before, the sheet resistance of the treated film returns to its original value when the layer is left in air during 120 h (Fig. 59 b).

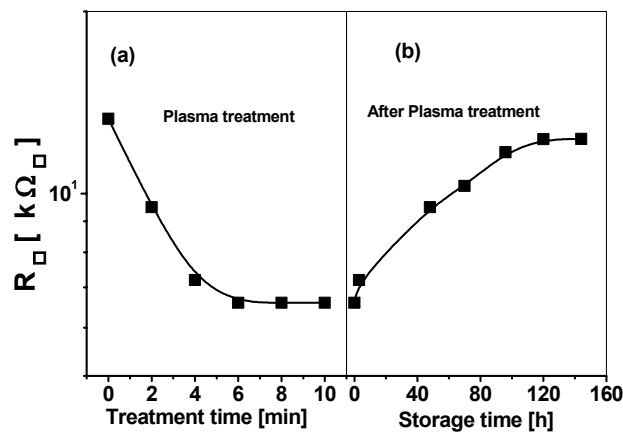


Fig. 59: Sheet resistance of 570 nm UV treated MPTS/ITO layer a) as a function of the Ar plasma treatment time, b) during storage in ambient atmosphere.

Fig. 60 represents the behavior of the sheet resistance of MPTS/ITO layer treated by heating in forming gas and submitted subsequently to an Ar plasma. It is interesting to note that the Ar-plasma treatment of a UV cured film further reduced in forming gas does not induce any change in the value of the sheet resistance (stage b). However, as before, during the storage in air the sheet resistance increases (stage c). A subsequent Ar-plasma treatment reduces the values but it is not as effective as the forming gas treatment because process can not reach the whole bulk of the layer, as does the reducing treatment in forming gas.

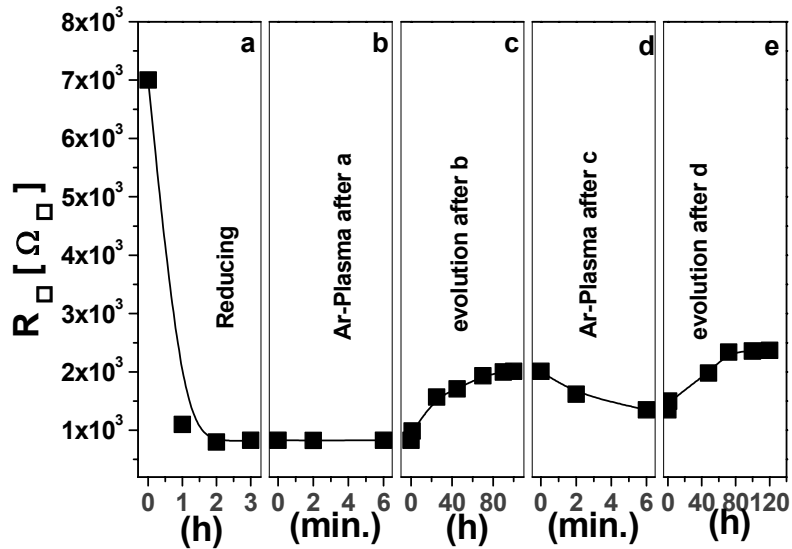


Fig. 60: Behavior of R_{\square} of MPTS/ITO layer as a function of several processes:

- a) Reducing (130 °C, forming gas), b) Ar-plasma treatment directly after a, c) evolution of R_{\square} after b, d) repeating Ar-plasma after c, e) evolution of R_{\square} after d.

5.5.5 Optical Properties

The optical properties (transmission, reflection) of the coatings were measured in the UV-VIS-NIR region (0.3- 3 μm) and the IR reflection in the IR region (3- 20 μm). The transmission of a UV-treated pure ITO350 layer on PC substrate and that of a 3 mm thick PC substrate are shown in Fig. 61. The average transmission in the visible region is about 87%. The coatings exhibit a high near IR absorption band starting at a wavelength of $\sim 1.0 \mu\text{m}$ and an increase of the reflection beginning at about $1.75 \mu\text{m}$ both due to the presence of the free charge carriers. The layer shows a strong absorption in the UV region, which is due to the excitation across the fundamental band gap similar to that observed in section 5.4.3. The sharp feature observed in all spectra are due to the PC substrate.

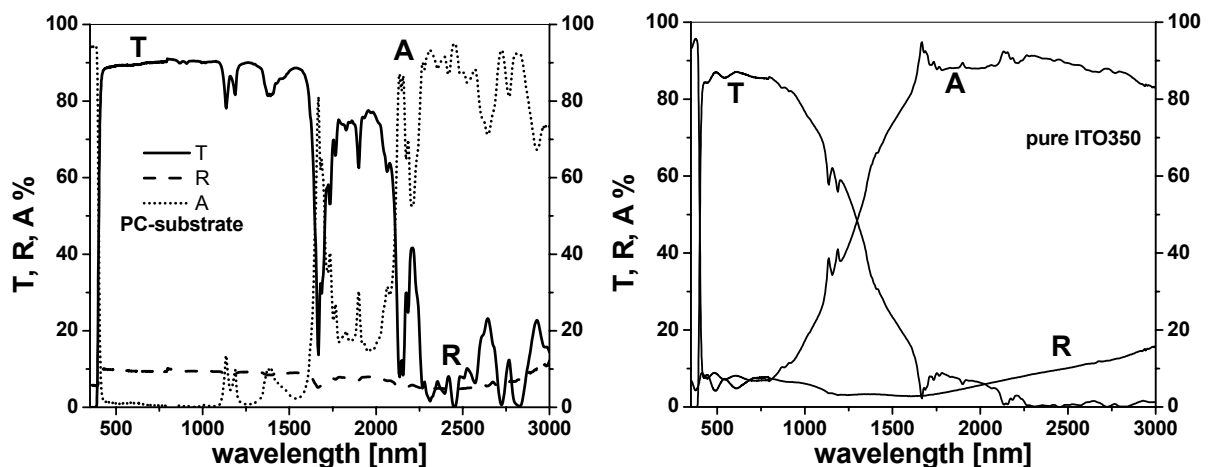


Fig. 61: Optical transmission, reflection and absorption in UV-VIS-NIR region of a 3 mm thick PC substrate (left) and that of a UV treated pure ITO 350 coating deposited on PC substrate.

Fig. 62 shows the transmission of a 570 nm thick 6 wt. % MPTS modified ITO layers deposited on PC substrates and treated during UV-irradiation. The layer exhibits also a high

transmission $> 87\%$ in the visible range like the pure ITO layer, a sharp decrease in the transmittance (strong absorption) at wavelength below 400 nm, a high absorption edge due to the free carrier absorption at $\lambda > 1.0\ \mu\text{m}$ and an increase of the reflectance for $\lambda > 1.6\ \mu\text{m}$ which reach about 20 % at $\lambda = 3\ \mu\text{m}$.

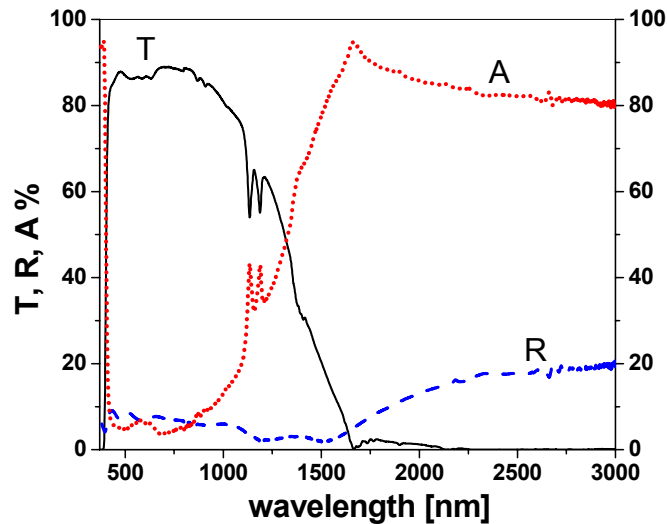


Fig. 62: Optical transmission spectra of MPTS / ITO layer on PC-substrate in UV-VIS-NIR region

The transmission spectra of MPTS/ITO coatings on different polymeric and glass substrate are shown in Fig. 63.

The following spectra show that all MPTS/ITO coated substrates have a transparency greater than 85 % between 400 and 800 nm whatever is the thickness of the substrate. All the spectra show a high absorption band beginning at $\lambda > 1.0\ \mu\text{m}$. These coatings act as IR-shielding coatings for $\lambda > 1.7\ \mu\text{m}$ as the transmission of the system is less than 1 %. At the same time the coatings have a strong absorption in the UV-region for wavelength smaller than 400 nm and therefore act also as a protective layer against the degradation of the polymeric substrates when exposed to UV-irradiation. For example PC substrates are found to change to a yellow-brown colour when exposed to UV-irradiation; however they remain clear with a transparency greater than 85 % in the visible range (400-800 nm) when coated with an ITO layer.

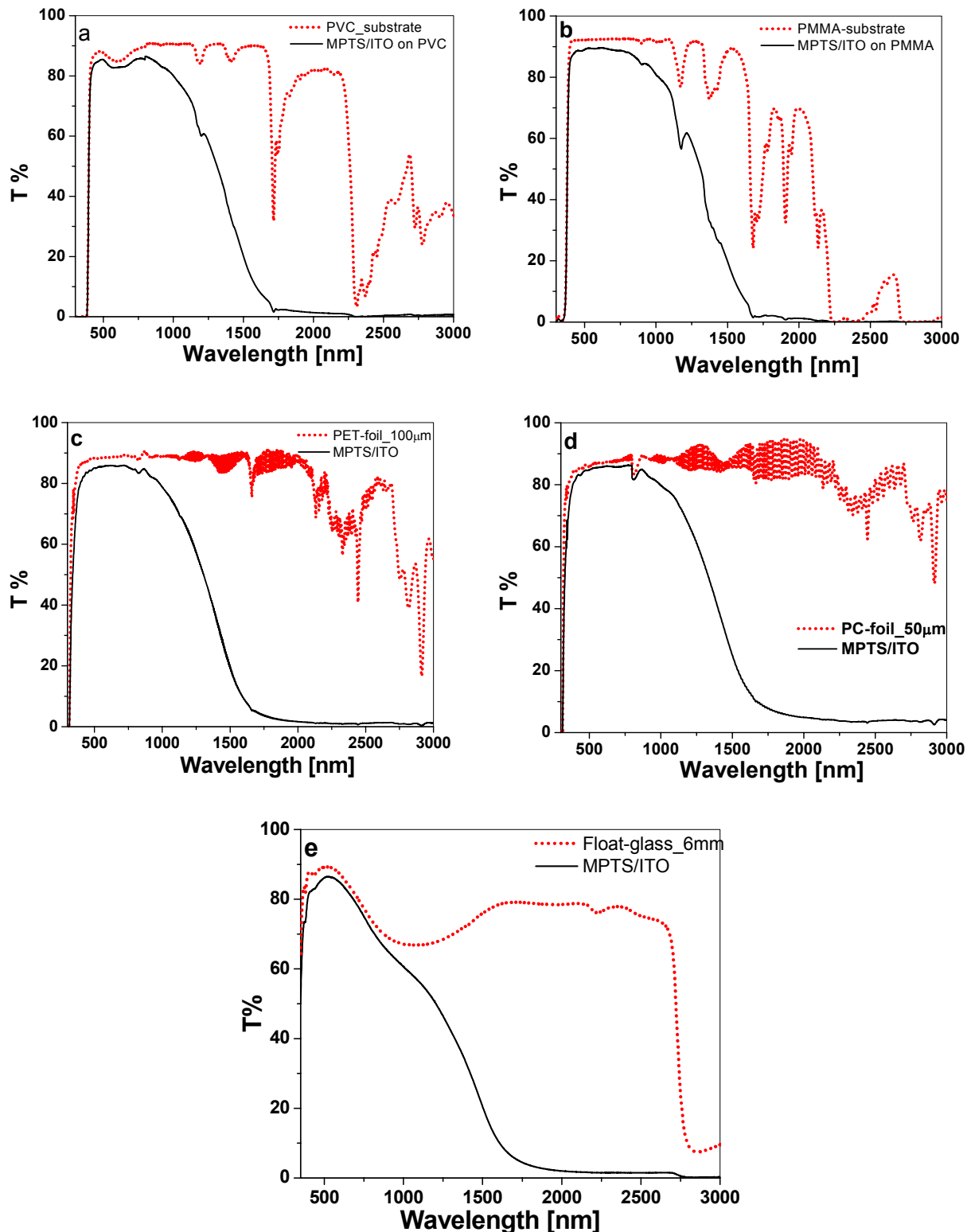


Fig. 63: Transmission spectra in the UV-VIS-NIR region of spin coated MPTS/ITO layers cured using UV-irradiation on a) PVC_1 mm, b) PMMA_2mm, c) PET_100 μm, d) PC_50 μm and e) Float glass_6 mm

The optical transmission and reflection spectra of a 570 nm thick MPTS/ITO layers coated on 3 mm thick PC substrate are shown in Fig. 64. The layers have been treated according to the process C and D in Fig. 49 c. The influence of the free charge carriers is clearly observed by the strong absorption occurring in the NIR and the increase of the reflection for $\lambda > 1.5 \mu\text{m}$.

The reduced sample exhibit a higher NIR reflection than that of the unreduced one because of the higher carrier concentration ($n = 1.6 \times 10^{20} \text{ cm}^{-3}$).

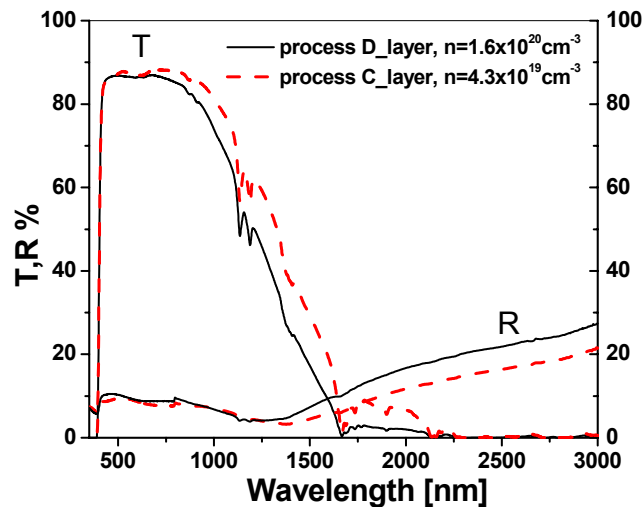


Fig. 64: UV-VIS-NIR transmission (T) and reflection (R) of 570 nm thick MPTS/ITO layer on 3 mm thick PC substrate for UV-treated and UV+ reduced (130 °C, forming gas) sample.

The far IR reflection spectra of a 3 mm uncoated thick PC substrate and a coated substrate with a 570 nm MPTS/ITO layer treated according to the process C and D and that of a commercial sputtered ITO layer on PC substrate are shown in Fig. 65. Because of its high conductivity, the sputtered ITO coating exhibits a higher reflection (about 80 %) than that of our coatings which only reflect 30 to 40 %.

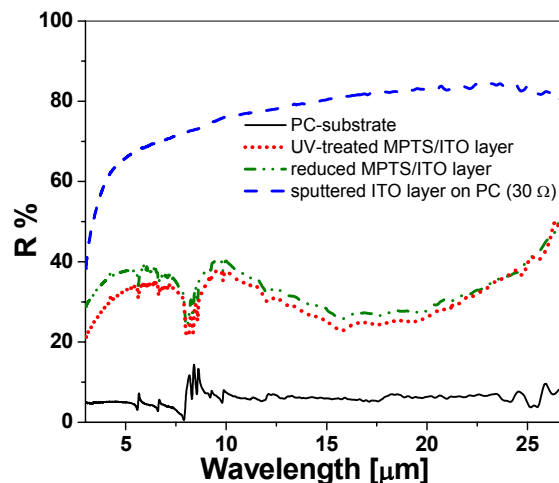


Fig. 65: IR-reflection of spin coated 570 nm thick MPTS/ITO coatings on 3 mm thick PC substrate and a commercial sputtered ITO on PC-substrate ($30 \Omega_{\square}$).

5.5.6 FTIR spectroscopy

The UV-irradiation treatment of GPTS, TEOS and MPTS/ITO coatings lead to high conductive coatings compared with the heat treatment at 130 °C in air for several hours. The UV-irradiation increases the number of oxygen vacancies into the film and affect as well the structural and the chemical composition of the layer. To better understand these effects a

FTIR spectroscopy study is presented in this section. MPTS was used as a photopolymerizable component in the modified ITO sol-gel coatings.

Fig. 66 shows the FTIR spectrum of untreated (as deposited), thermally cured (heating at 130 °C, 10 h) and UV treated (110 mW/cm², 5 min) coatings made of prehydrolyzed MPTS sol on Si-wafer substrate. The broad band at 3440 cm⁻¹ encompasses the overlapping O-H bands of hydrogen bonded molecular water and hydrogen bonded silanol. The band at 2954 cm⁻¹ and the well formed shoulders represent the vibration of the aliphatic CH stretching modes of methyl and methylene groups. The shape and the intensity of the OH and CH stretching modes depend on the annealing processes.

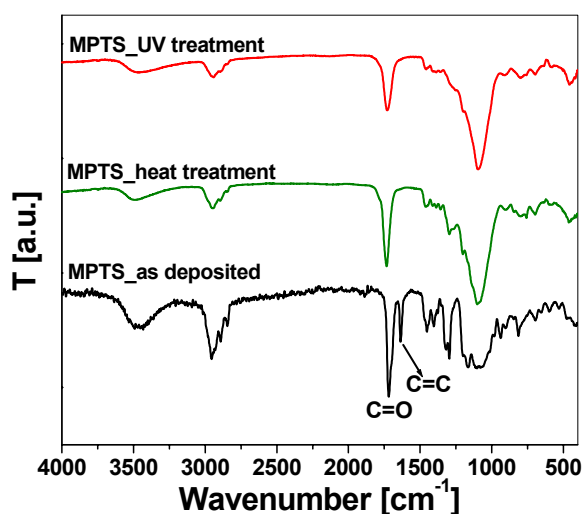


Fig. 66: FTIR spectroscopy of MPTS coating on Si-wafer: as deposited, with heat treatment (130°C,10h) and with UV irradiation (110 mW/cm²).

The bands at 1720 cm⁻¹ and at 1638 cm⁻¹ represent the carbonyl group C = O stretching mode and the vinyl group C = C stretching mode, respectively. As shown in the figure the C = C stretching mode disappeared after heating the film or after UV light exposure, indicating a polymerization of MPTS. The intensity of the C = O stretching mode decreases by heat and UV treatments and the band shifts to higher wavenumber, also indicative of a polymerization process in which the carboxyl group does not conjugate with carbon double bond any more (322). The C = O stretching mode of UV treated film decreases significantly compared with the thermally cured sample, indicating that the irradiation accelerates and promotes the polymerization of MPTS.

The bands between 1200 and 1400 cm⁻¹ represent the vibration of several organic groups, such as the methyl or methylene bending ν (CH₂, CH₃), the alkoxy groups δ (SiOCH₃), and the methacrylate group ν (O – CH₂ – C). Their intensity decreases after the heat treatment process and are totally eliminated by the UV illumination. It is therefore obvious that the UV irradiation reacts with the residual organics groups in the film producing volatile materials.

The band at 1166 cm⁻¹ observed in the as deposited sample corresponds to the methacrylate group and it is eliminated by the heating and UV treatments. The corresponding asymmetric alkoxy silane band of MPTS ν (Si - O - C) is found at the broad band at 1080 cm⁻¹. By heating

and UV-irradiation this band is transformed into the well defined Si–O–Si mode band at 1100 cm^{-1} which becomes sharper and distinct by the UV treatment. This means that the UV treatment results in the formation of a silicate network by further polymerization and condensation.

Fig. 67 shows the FTIR spectra of MPTS/ITO coatings deposited by spin coating method on Si-wafer and treated either thermally at $130\text{ }^{\circ}\text{C}$ for several hours, or UV irradiated or sintered at $550\text{ }^{\circ}\text{C}$. The decrease and the complete disappearance of the organic groups and the condensation of the silicate network are clearly observed for the film annealed at $550\text{ }^{\circ}\text{C}$. The broad band at 3440 cm^{-1} corresponding to the O-H group is eliminated in the as deposited MPTS/ITO layer and CH stretching mode band at 2954 cm^{-1} decreases significantly.

The figure also shows that the C = C band at 1630 cm^{-1} is completely eliminated by the UV treatment, but it is not eliminated in the case of the thermally cured sample. The C = O band at 1716 cm^{-1} is strongly reduced by the UV treatment. These results indicate that the UV treatment is highly efficient and fundamental to promote the coating photopolymerization, i.e. the reduction of the carbon double bonds which represents the degree of polymerization. This leads consequently to a well defined Si-O-Si network (band at 1080 cm^{-1}) which links the conducting particles together.

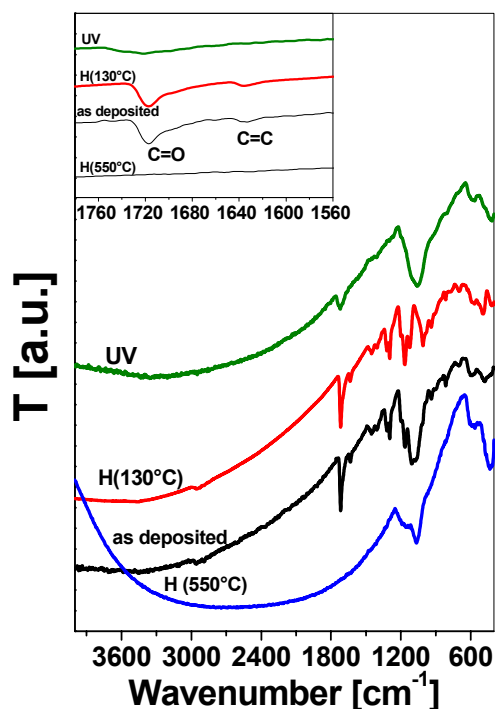


Fig. 67: FTIR spectra of MPTS/ITO layer on Si-wafer for untreated layer (as deposited) and for layers heated at $130\text{ }^{\circ}\text{C}$ for several hours, UV-treated or sintered at $550\text{ }^{\circ}\text{C}$.

The main Si–O–Si peak for thermally cured coatings ($130\text{ }^{\circ}\text{C}$) is shifted to higher wavenumber at 1166 cm^{-1} with two shoulders at 1124 and 1197 cm^{-1} , which correspond to the Si–O–C vibration. Some small peaks between 600 and 1000 cm^{-1} are observed in the spectra of thermally cured sample and are attributed to non bridging oxygen atoms of the Si–

OH vibrations. These peaks disappear after the UV treatment and are transformed into the Si – O – Si network.

The previous results give an explanation why the UV treatment of the MPTS/ITO coating system induces a far better conductivity compared with those only heat treated, even for several hours. The thermal curing alone is not effective for the polymerization and the condensation process of the coatings. On the opposite, the UV treatment eliminates the C = C band, strongly reduces the C = O band and forms a well defined Si-O-Si network linking homogeneously the particles together.

5.5.7 NMR spectroscopy

The determination of the polymerization and the condensation degree of the MPTS composite were carried out using solid state NMR spectroscopy. The polymerization degree of the methacryl group of MPTS was determined using ^{13}C -NMR spectroscopy by comparing the C-signal intensity of the double bonds (C = C, peak 5 at 136.9 ppm and 5* at 45.5 ppm in Fig. 24) and that of the carboxy group (C = O, peak 4 at 166.9 ppm and 4* at 137 ppm in Fig. 24) with the original intensity of the corresponding C atom of MPTS at 45.4 ppm and 177.0 ppm, respectively.

Fig. 68 shows the ^{13}C -solid state NMR spectra of a MPTS/ITO composite thermally cured at 130 °C for 15 h (a) and UV cured (b). The degree of polymerization of the UV cured sample (process a) is 74 % and much higher than that of thermally cured sample, 22 %. Remembering that the polymerization degree of a thermally cured pure MPTS system is 64 %, this shows therefore that the presence of the ITO nanoparticles impedes the thermal polymerization. The significant difference between the two processes corroborate the effectiveness of the photopolymerization process in enhancing the electrical conductivity of the films.

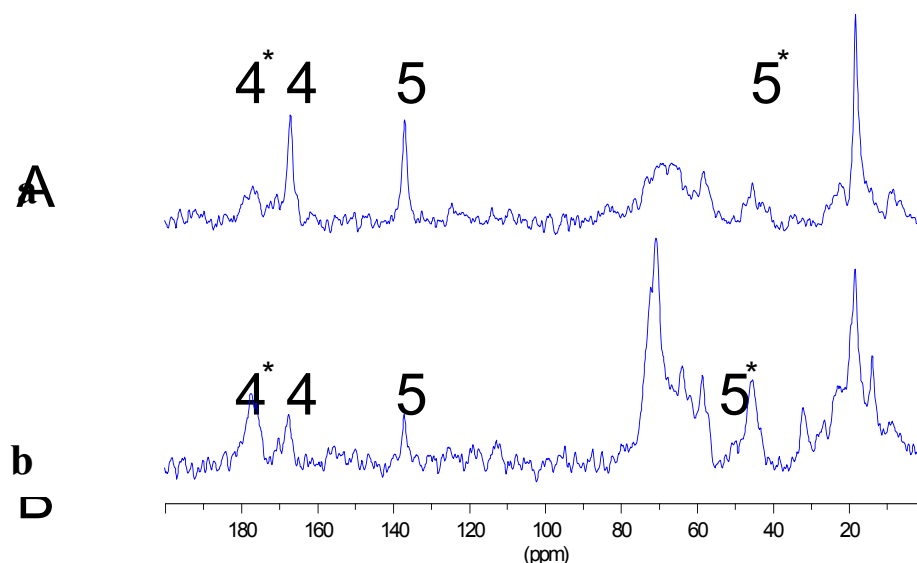


Fig. 68: ^{13}C -solid state-NMR spectroscopy of MPTS/ITO composite as thermal cured sample (a), and for UV cured sample (b).

Fig. 69 shows the ^{29}Si solid state NMR spectra for MPTS/ITO film material after heat and UV-treatments. The condensation degree of the Si – O Si network, i.e. the percentage of built Si-O-Si bonds, was calculated for both treatment according to the formula given in appendix A.1.8. The results show that both composites have the same condensation degree, about 78 %. The T^0 unit is not present and the amount of T^1 , T^2 and T^3 units are 4, 55 and 41 %, respectively. This means that the condensation degree contrary to the polymerization degree does not depend on the treatment process.

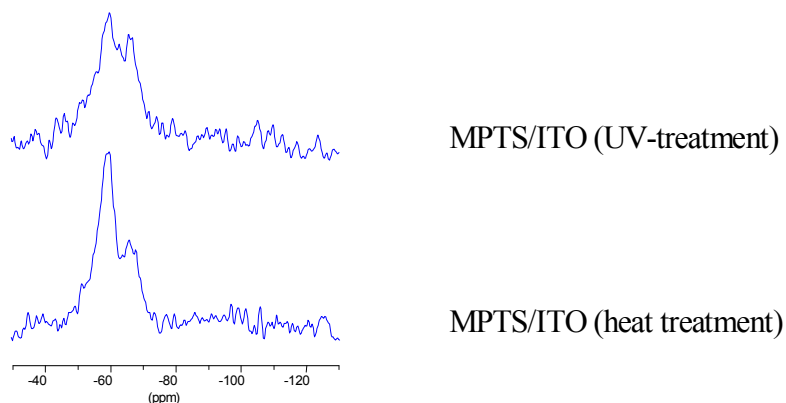


Fig. 69: ^{29}Si -solid state NMR spectroscopy of MPTS/ITO layer

5.5.8 Structural and morphological properties

a) SEM and TEM observations

The morphological and structural features of coatings deposited on PC substrates were also investigated using SEM and TEM methods. Fig. 70 a depicts SEM picture of the surface of a pure ITO layer treated using UV-irradiation and further cured thermally at 130 °C for 10 h. The film consists of very loosely packed globular highly porous grains with size ranging from 20 to 40 nm formed by the aggregation of two or three primary particles.

The surface morphology of a GPTS/ITO layer (Fig. 70 b) is different. The particles aggregate together to form large clusters with sharp grains with size ranging from 60 to 80 nm. The layer is highly porous.

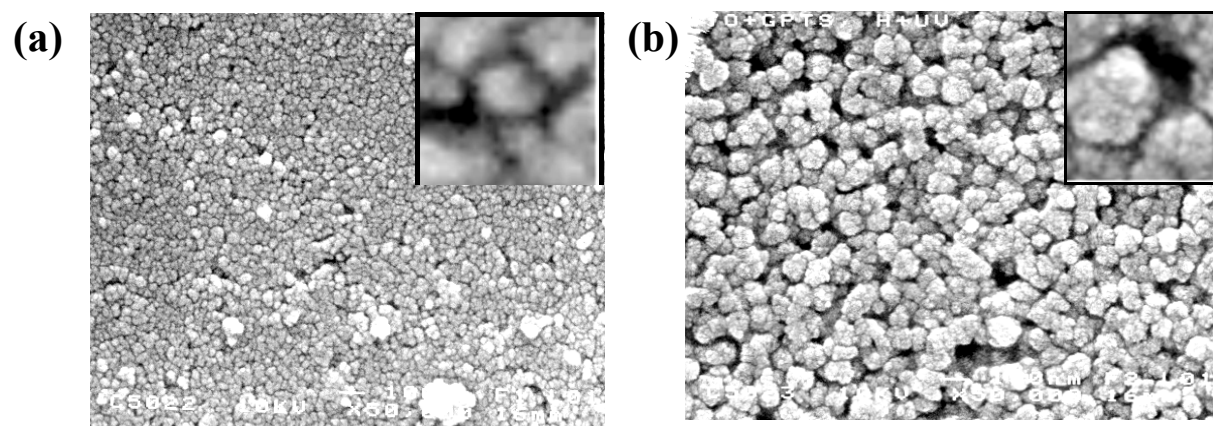


Fig. 70: SEM micrograph of the surface of a) pure ITO layer and b) GPTS/ITO layer deposited on PC substrate after UV-irradiation and further thermal treatment (130 °C, 10 h)

The surface of an MPTS/ITO layer showed in Fig. 71 a has another morphology. It consists of ITO nanoparticles linked together by a small strip of polymerized MPTS (dark regions) forming raspberry like globular grains, about 80 - 100 nm in size. The microstructure is uniform and denser without any cracks but some nanoscale porosity is still present. The UV polymerization of MPTS brings the ITO nanoparticles in denser contact and stick them together to form large clusters, enhancing the transport of the free charge carriers between them and consequently the conductivity. A SEM cross section of a MPTS/ITO layer polymerized with UV-irradiation and further heat treated is shown in Fig. 72. The bonding between the conducting clusters increases the density of the film and reduce the porosity.

The thermally cured MPTS/ITO layer shown in Fig. 71 b has a different morphology than the UV-cured one. The micrograph shows spherical particles dispersed and well separated from each other in the MPTS matrix. It is clear that the polymerization of the MPTS is not complete. This result explains also the big difference of the conductivity between the thermally and UV cured samples.

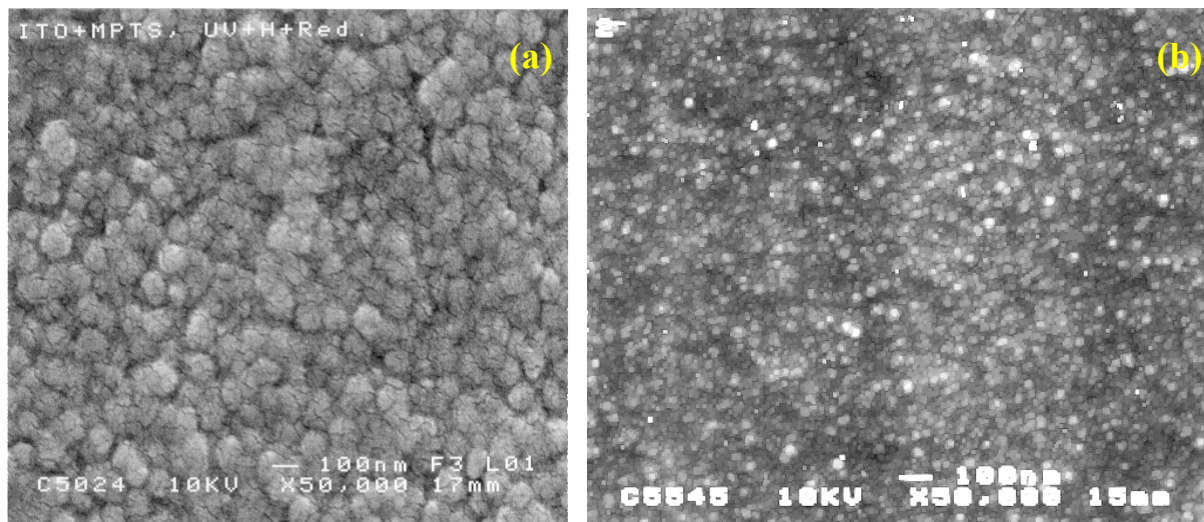


Fig. 71: SEM micrograph of the surface of a spin coated MPTS/ITO layer on PC-substrate a) UV cured and b) heat treated.

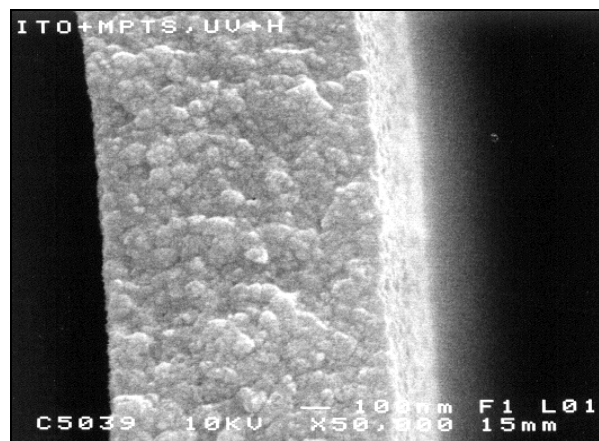


Fig. 72: SEM-cross sectional view of MPTS/ITO layer deposited on PC-substrate and treated using UV-irradiation and further heat treatment at 130 C for 10 h.

To better investigate the structure of MPTS/ITO coatings on polymeric substrate, TEM spectroscopy was carried out. The preparation of thin cross sections using the conventional ion-milling technique is very difficult because of the ion damage of the polymeric substrates, thus ultramicrotomy was used instead.

Fig. 73 shows TEM images of a 550 nm thick of MPTS/ITO films deposited on PC substrate cured by UV-irradiation (a and c) or only heat treated at 130 °C for several hours (b). The TEM images reveal a dense packing of 20 – 50 nm size crystalline ITO particles in the case of UV-cured MPTS/ITO layer (Fig. 73 a) and a very loose packing ITO particles in the case of thermally cured sample (Fig. 73 b).

Fig. 73 c shows an enlarged TEM picture of the UV-cured MPTS/ITO layer fragment indicating the presence of MPTS surrounding the ITO particles. The thickness of the MPTS strips are typically 3 to 6 nm. The particles appear strongly bonded together by the polymerized matrix. The above result is a direct explanation why UV cured MPTS/ITO layers have a higher conductivity than the thermally cured ones. However the UV-cured samples are still porous, and this explains the changes of the electrical properties due to the back diffusion of oxygen species into the layer. Further images of SEM and TEM images of the coatings on polymeric substrates are found in appendix (G).

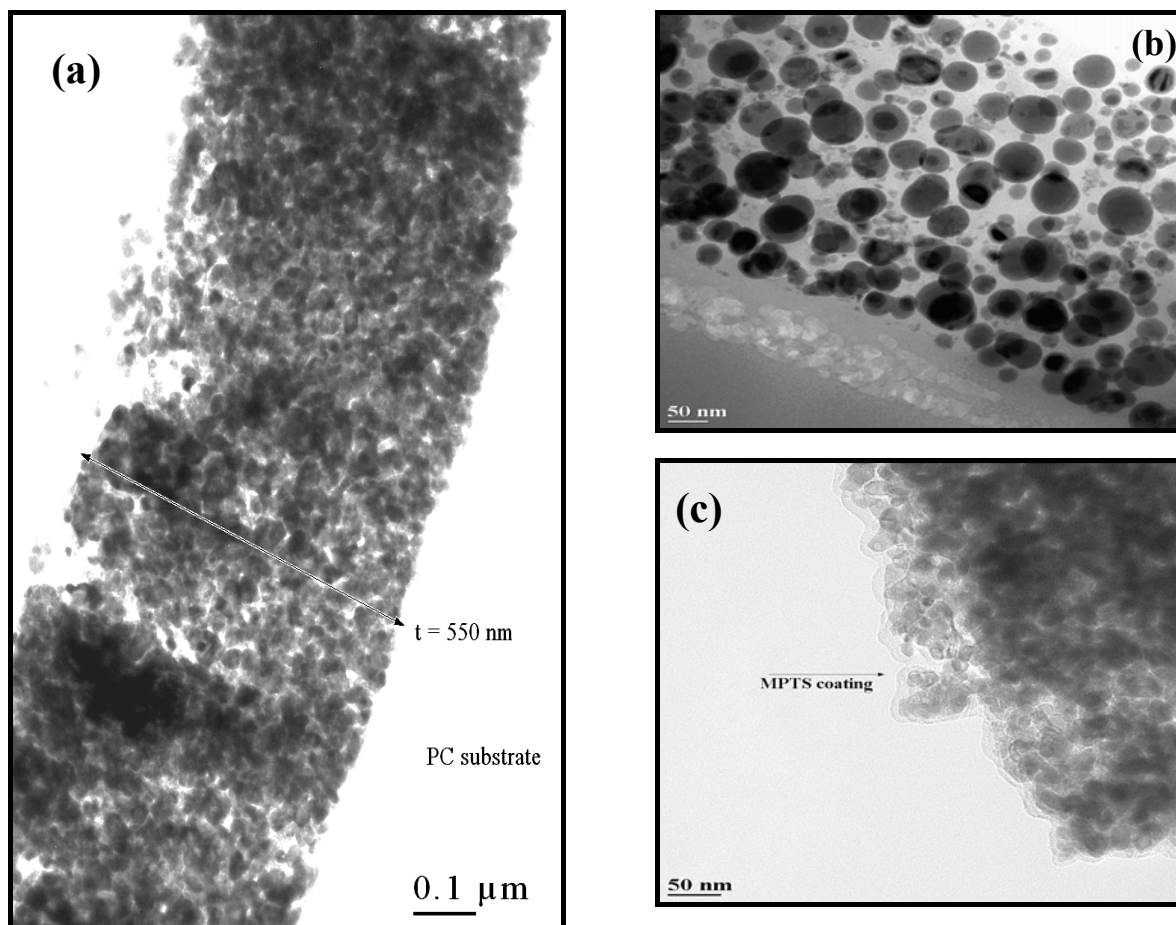


Fig. 73: TEM micrograph of cross section of MPTS/ITO thin film for UV-cured sample (a), thermal cured sample and (c) represents a layer fragment of the sample in (a).

b) WLI and AFM observations

Investigation of the surface of MPTS/ITO layer using white light interferometry allows to characterize the topography of the surface (Fig. 74 a). The coating roughness of a $53 \times 70 \mu\text{m}^2$ area with a lateral resolution of 600 nm determined without electronic filtering is $R_a = 0.8 \text{ nm}$, ($R_{\text{rms}} = 1 \text{ nm}$) and a peak-to-valley maximum value of $R_{\text{PV}} = 15 \text{ nm}$. No large defects were found on the coatings and the surface appears smooth on this length scale. The corresponding profile (Fig. 74 b) was obtained across the center of the tested area showing a peak-to-valley variation smaller than 15 nm. The high peak shown in the center of the profile is originated from a dust particle formed during the preparation of the coatings.

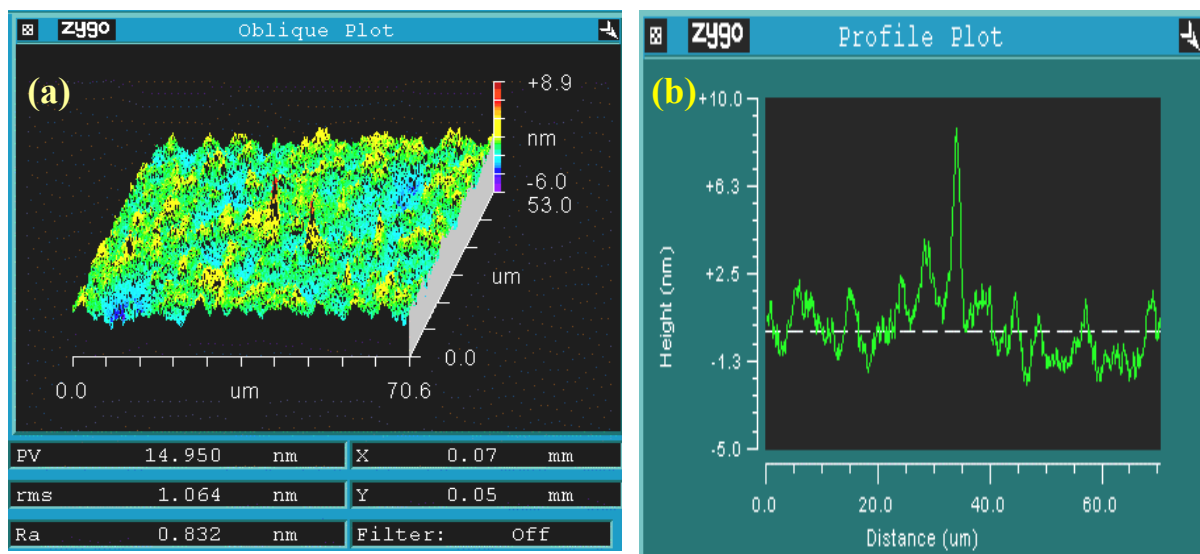


Fig. 74: Surface morphology of 570 nm thick MPTS/ITO coating observed with WLI on a $53 \times 70 \mu\text{m}^2$ area (a), and the corresponding surface profile taken within the center of the tested area (b).

Atomic force microscopy was also used to investigate the surface topography and to determine the average roughness of the coatings on a smaller region and at a smaller scale. Fig. 75 shows the surface of a 570 nm thick MPTS/ITO film deposited on PC substrate with a $53 \times 70 \mu\text{m}^2$ area. The surface consists of aggregated ITO nanoparticles with average size of 50 – 100 nm confirming the SEM investigation. The average roughness of this coating is 6 nm.

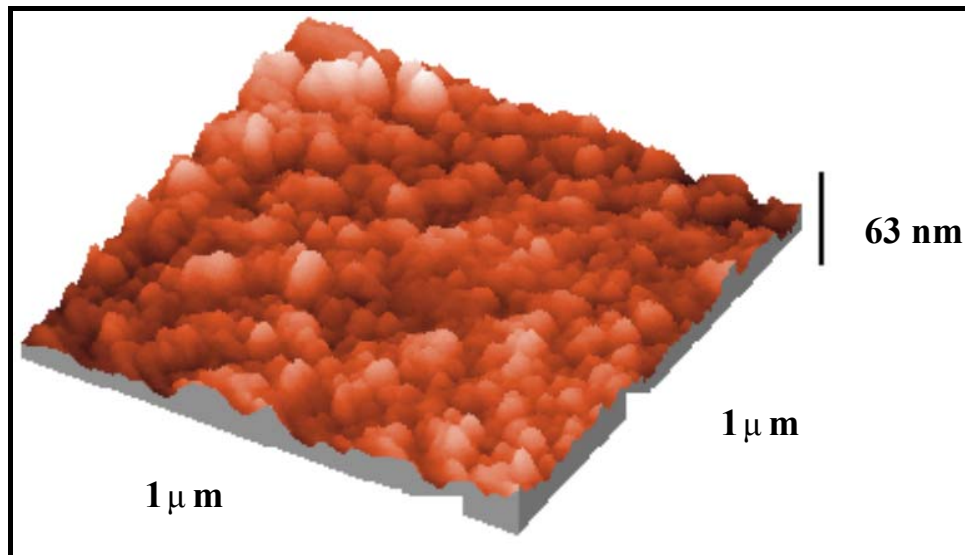


Fig. 75: Atomic force microscopy (AFM) of the surface of 570 nm thick MPTS/ITO coatings on PC substrate on a 1 x 1 μm² area

5.5.9 Mechanical properties

This section presents the mechanical properties (adhesion, abrasion and scratch resistance, and hardness) of the films deposited on polymeric substrate. They are summarized in Table 13.

The mechanical properties of pure ITO thin films are very poor as the layers are removed or partially destroyed after each test.

Those of ITO coatings made by adding different silane modifiers (MPTS; TEOS, GPTS) to the coatings sols were improved drastically. All coatings showed an excellent adhesion on the substrate in agreement with the Tape test procedure (DIN 58196-K2) and the result of the lattice cut test (ASTMD 3359, DIN 53151) was Gt 0, i.e. the cutting edges are completely smooth. No scratch (class 1) was observed for MPTS or GPTS modified ITO coatings after 10 rubbing cycles with an eraser under a load of 10 N (DIN 58196-G10) and only slight scratches (class 2) are observed for TEOS/ITO coatings. The milder rubbing test with a cotton cloth, 25 rubbing cycles under a load of 10 N (DIN 58196-H25) is also class 1 (no scratch) for all types of modified ITO coatings.

The hardness measured using the Pencil test ASTM D 3363-92a is 1H for MPTS/ITO coatings, F for GPTS/ITO coatings and HB for TEOS/ITO coatings. The amount of TEOS, GPTS and MPTS in the coating sols were 6 to 8 wt. %. It is particularly noteworthy to notice that only a relatively small amount of these coupling agents is sufficient to enhance the mechanical properties of the ITO films. Better mechanical properties are obtained when the amount of silane is increased, but such coatings present also a higher value of the sheet resistance.

Table 13: Mechanical properties of transparent conducting ITO coatings and modified ITO coatings deposited on a 3 mm thick PC substrate.

Test method	ITO	MPTS/ITO	GPTS/ITO	TEOS/ITO
Tape test DIN 58196-K2	fail	pass	pass	pass
Lattice cut test ASTM D 3359, DIN 53151	Gt5	Gt0	Gt0	Gt0
Cotton test DIN 5896-H25	Class 4	class 1	class 1	class 1
Rubber test DIN 58196-G10	class 5	class 1	class 1	class 2
Pencil test ASTM D3363-92a	6B	1H	F	HB

The enhancement of the mechanical properties of the coatings on polymeric substrates is already obtained by a short UV curing time. This is therefore attributed to the building of a silica network (Si – O – Si) during the photopolymerization and the condensation of the functionalized silanes. It is possible that the functional groups on the substrate surface also react with the silanol functional groups (i.e., SiOH). It was observed that the MPTS modified ITO coatings have the best adhesion and abrasive resistance among all of the used modifier. This may be attributed to the homogeneity of the polymerization and the high degree of condensation, which enable the functional groups to form a denser inorganic network with a higher adhesive and abrasive resistance.

The changes of the electrical sheet resistance and the optical transmission at 550 nm of MPTS/ITO coatings on different polymeric substrates after applying different mechanical tests are listed in Table 14. The values remain practically identical except for those of the sheet resistance determined after storing the layer in a 95 % RH humidity during 100 h which decreases by about 20 to 30 % and those of the transmission which decreases by 3 to 7 %. As shown in Table 14 the coatings deposited on a PC substrate was the most durable coating. This is probably due to the fact that the adherence of the coating to this surface is higher than the other polymeric substrates. Lee et al (323) also found that the adhesion and the abrasion resistance of the coatings on a PC substrate is better than on a PMMA substrate. The authors argued that this was due to the less water adsorption on PC (0.4 %) as compared with that on PMMA (2.2 %).

Table 14: Changes of the electrical sheet resistance and transmission at 550 nm of MPTS/ITO coatings deposited on polymeric substrates after abrasion, adhesion and humidity tests.

	Abrasion resistance DIN 58196-G10 (rubber test)				Adhesion resistance DIN 58196-K2 (tape test)				Humidity resistance 95 % RH, 60 °C, 100 h			
	PC	PMMA	PVC	PET	PC	PMMA	PVC	PET	PC	PMMA	PVC	PET
Increase in sheet resistance (%)	6	7	10	10	< 1	< 1	< 1	< 1	20	26	29	30
decrease in transmission (%)	< 1	2	2	3	< 1	< 1	< 1	< 1	3	5	5	7

The evolution of the sheet resistance of MPTS/ITO coatings on PC and PE substrates investigated during the eraser rubbing test is shown in Fig. 76. For PC substrate the value remains constant up to 10 cycles and then increase continuously, reflecting a decrease of the thickness of the coatings. A similar behavior is observed for coatings deposited on PE substrates.

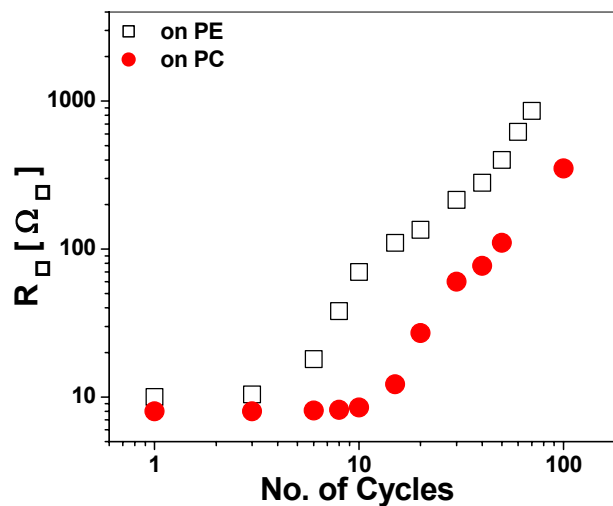


Fig. 76: Sheet resistance of MPTS/ITO coatings on PC and PE substrates vs. the number of rubbing cycles of an eraser under 10 N load.

Fig. 77 shows the evolution of the sheet resistance of MPTS/ITO and GPTS/ITO layer deposited on PC substrate after scratching an insulated area of the coatings with pencils of different hardness scales (6B – 9 H) and measured across the scratch (see appendix A.2). In the case of MPTS/ITO layer no cut or scratch is observed by using pencils softer than 1H and the sheet resistance remains constant. For GPTS/ITO layer the value was F. For both systems the layer is not completely cut when a scratch is made with the hardest pencil (9H). In the worst cases the sheet resistance of MPTS/ITO and GPTS/ITO coatings increased by a factor 10 and 50 respectively

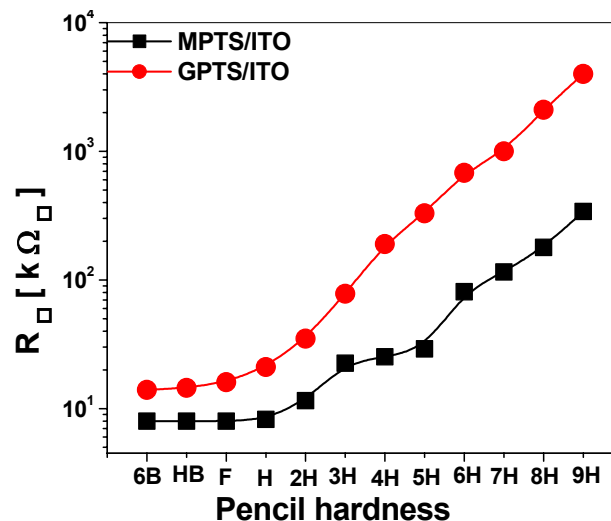


Fig. 77: Sheet resistance of MPTS/ITO and GPTS/ITO layers on PC-substrates versus different scales of pencil hardness

The mechanical properties of our modified ITO coatings deposited on PC substrates are quite similar to those obtained with a commercial conducting polymer such as Baytron® P [20] but better than commercial Japanese products (PCND MR680, TAKIRON CO., LTD., antistatic layer on PC substrates). Fig. 78 shows a photograph of the surface of our coating (left) and that of Takiron Co. Ltd after a 10 cycles rubbing with an eraser under 10 N load (DIN 58196-G10). The MPTS/ITO coatings withstands the test (class 1, no scratch) but a reasonable scattering is observed for the Japanese product (class 3).

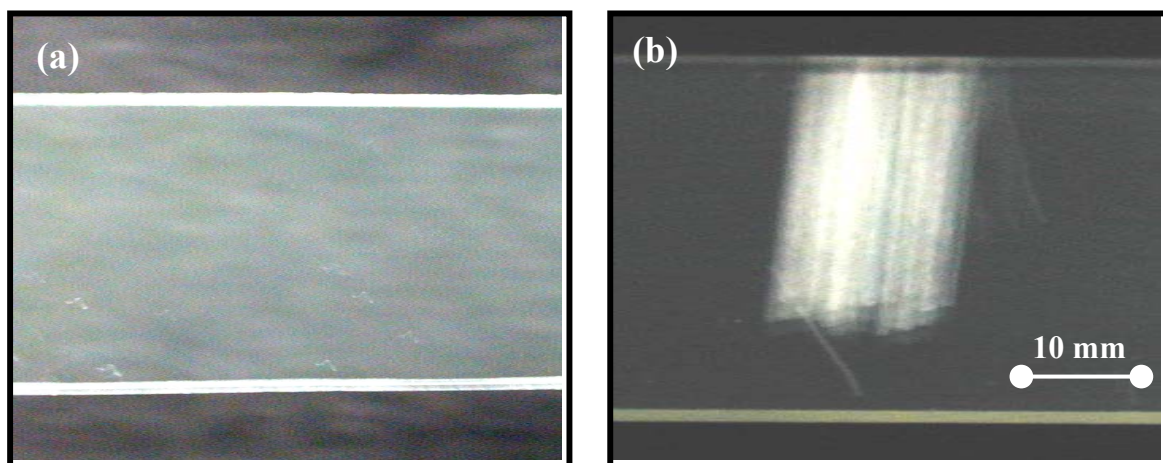


Fig. 78: The surface of a MPTS/ITO coating on PC substrate (a) and of a commercial antistatic Japanese product (b) after rubbing each surface with an eraser 10 cycles under 1 kg load.

Taber test (DIN 52347/CS10F/5.4 N) performed on 570 nm thick MPTS/ITO coating deposited on PC substrate leads to a 15 % haze after 50 cycles and 42 % after 1000 cycles. The coatings are not hard enough to protect the surface of the polymeric substrates from hard mechanical influences. Nevertheless, comparing the values obtained after 1000 cycles Taber test with an uncoated substrate (haze = 60 %), the MPTS modified ITO coating brings some

protection, but does not achieve the properties of specially designed hard coatings derived from organic-inorganic nanocomposites (Nanomer) on plastics (154).

5.5.10 Conclusion

The modification of the ITO nanoparticle ethanolic sols by adding a small amount of a UV polymerizable binder such as a hydrolysed silane (TEOS, GPTS, MPTS) allows the deposition of transparent conducting and antistatic coatings fully processable at low temperature ($T < 130^{\circ}\text{C}$). Single layers with thickness up to 600 nm have been obtained by spin or dip coating processes on different plastic (PMMA, PC, PE, PVC, PET,..) and glass substrates.

The MPTS modified ITO coatings exhibit the best results compared to the other modifiers used to bind the conducting particles. The best curing process involves a UV irradiation (105 mW/cm^2 , 5 min) followed by a heat treatment at $T = 130^{\circ}\text{C}$ during several hours followed by a reducing treatment in forming gas for 2 h. The sheet resistance of the coatings measured directly after the UV-irradiation or after a reducing treatment is only stable in vacuum or a protective gas atmosphere. When the samples are kept in air the values unfortunately increase slowly with time to a stable value, and the variation depending on the thickness of the film. This was explained as a result of a decrease of the charge carrier concentration due to the diffusion of oxygen species into the layers. A stable sheet resistance as low as $1.7 \text{ k}\Omega_{\square}$ (resistivity $\rho = 9.4 \times 10^{-2} \text{ }\Omega\text{cm}$) was achieved for a single 570 nm thick MPTS/ITO layer deposited on PC substrates cured by UV-irradiation, followed by a heat treatment at $T = 130^{\circ}\text{C}$ during several hours and then a reducing treatment in forming gas at 130°C for 2 h.

A short period of UV irradiation is much more effective than a very long time heat treatment. FTIR and NMR spectroscopy of the coatings revealed that the UV treatment resulted in a better polymerization and condensation of the binder leading to a more homogeneous particle bonding of the material. These results were confirmed by visualizing the morphological structure of the coatings by SEM and TEM investigations. The average roughness of the coatings measured by WLI on a $53 \times 70 \text{ }\mu\text{m}^2$ area is 0.8 nm while that determined in a smaller region ($1 \times 1 \text{ }\mu\text{m}^2$) measured by AFM is 6 nm.

The transparency of coatings on plastic substrates was higher than 85 % in the visible region and the transmission decreased sharply for $\lambda > 1.2 \text{ }\mu\text{m}$ due to the presence of a strong absorption band. The reflection of the coatings increases for $\lambda > 1.5 \text{ }\mu\text{m}$ and reflect 40 % of the spectrum at $\lambda \geq 10 \text{ }\mu\text{m}$.

The modification of the ITO particle layers enhanced very significantly the mechanical properties of the coatings. The abrasion resistance is in agreement with DIN 58196-G10 class 1, the adhesion passes the tape test DIN 58196-K2 and the lattice cut test ASTM D 3359 or DIN 53151 and the pencil hardness according to ASTM D 3363-92c is 1 H.

5.6 Patterning ITO coatings with a low temperature process

The modified ITO transparent conductive coating can be easily patterned using a one step short time UV-irradiation without using a complicated photoresist based photolithography process. A metallic mask with different opening has been used. The unexposed part of the wet coating remained in the original state, i.e. the as deposited state and can be easily removed by washing the film in alcohol in an ultrasonic bath. The exposed parts hardened by UV light, become insoluble. The thickness of the resulted patterned structure is almost the same as the thickness of chemically etched UV exposed film.

Fig. 79 a shows a pattern obtained by irradiating a $1.8 \times 1.35 \text{ mm}^2$ MPTS/ITO film with UV light and (b) shows the surface profile plot measured on the center of the tested area. The surface morphology of a $70 \times 50 \text{ }\mu\text{m}^2$ exposed area is shown in (c). The edges of the pattern are sharp and indicate that the patterning process is highly effective. The roughness of the UV-exposed area is 0.7 nm and is almost the same as that obtained in Fig. 74.

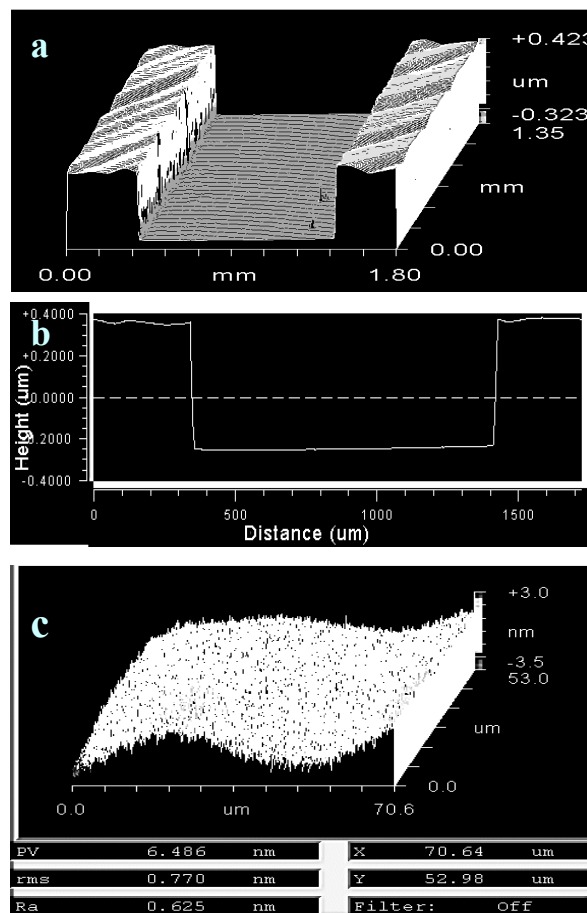


Fig. 79: WLI photograph of a 600 nm thick $1.8 \times 1.35 \text{ mm}^2$ MPTS/ITO patterned structure (a). Surface profile plot through the center of the tested area (b). Surface morphology of the exposed part of the pattern observed with WLI on a $53 \times 70 \text{ }\mu\text{m}^2$ area (c).

The UV-irradiation approach allows therefore to fine pattern such nanocomposite coatings. MPTS nanocomposite system were already used by Krug et al (324) to produce fine patterns

of thin sol-gel films by embossing the wet films with a stamper followed by a UV-irradiation and by a further thermal treatment at 130 °C. It was reported that the build-up of the inorganic backbones takes place during the sol-gel synthesis, while the final polymerization takes place during the UV-irradiation. Tadanaga et al (325) have prepared fine patterns, 3 to 50 μm in width, of transparent conducting SnO_2 thin films by UV-irradiation. They reported that the UV-irradiation led to a change of the solubility of the films in alkaline solution. The unexposed part was removed by leaching in alkaline solution.

The use of finer grids allows to pattern the coating with even smaller features (Fig. 80). The edges wall are almost straight and very sharp. Other patterned structure of MPTS/ITO coatings are shown in appendix H.

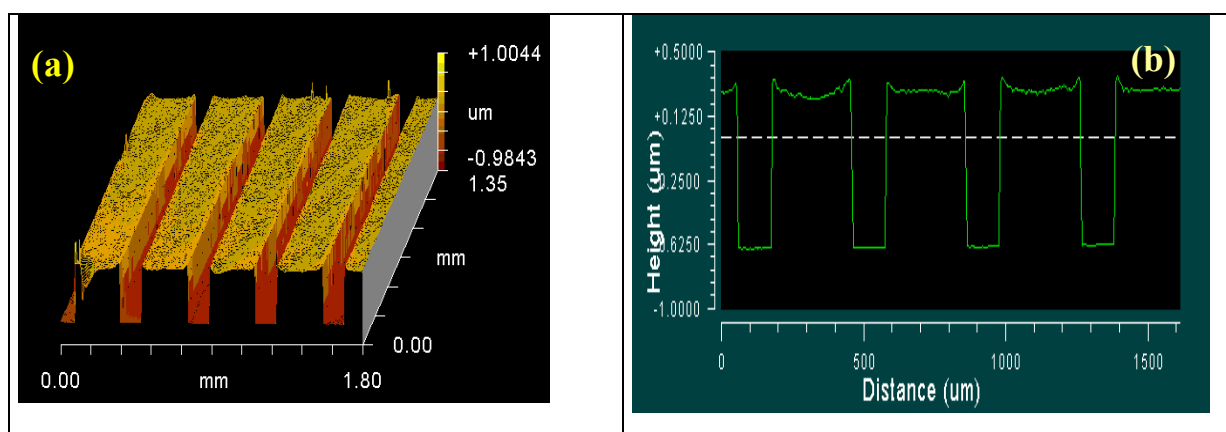


Fig. 80: WLI photograph of (a) MPTS/ITO patterned structure and (b) shows the profile of the pattern.

5.7 Surface properties

The surface properties such as surface energy and work function of transparent conducting thin films have been seldom studied. They change significantly when the coatings are exposed to certain surface treatments (41, 326-330), or when they are exposed to different atmospheres and the variations have been usually attributed to adsorption and desorption processes. Because of the high degree of porosity of the sol-gel films, these processes will not only occur at the surface but also in the bulk of these films and their knowledge is of a great importance for obtaining stable properties.

The previous observations (see sections 5.4 & 5.5), have shown that the time evolution of the sheet resistance of ITO coatings was strongly dependent on the UV irradiation, the reducing treatment and the storage conditions. These variations were essentially attributed to reaction occurring in the bulk of the coatings. In this section we discuss the changes of the surface properties (work function, surface energy) of ITO nanoparticles coatings observed during the UV treatment and their storage.

5.7.1 Work function

The work function is defined as the amount of energy required to bring the most loosely bound electrons from the Fermi energy level to the vacuum energy level. Fig. 81 shows its variation for GPTS/ITO and MPTS/ITO films deposited on PC substrates as a function of the

UV-treatment duration. Both layers were prepared one month before and were deposited using the spin coating method, hardened by UV-irradiation and subsequently heat treated at 130 °C for 10 hrs. The work function of both layers decreased during the UV illumination from 5.37 down to 4.97 eV for the GPTS/ITO layer and from 5.29 down to 4.92 eV for the MPTS/ITO layer. The work function of GPTS/ITO films was always found slightly higher than that of MPTS/ITO films. This perhaps refers to the cluster size formed by the aggregation of the ITO particles during the polymerisation. It was reported in ref. (161) that the work function of metal thin films increases by decreasing the cluster size.

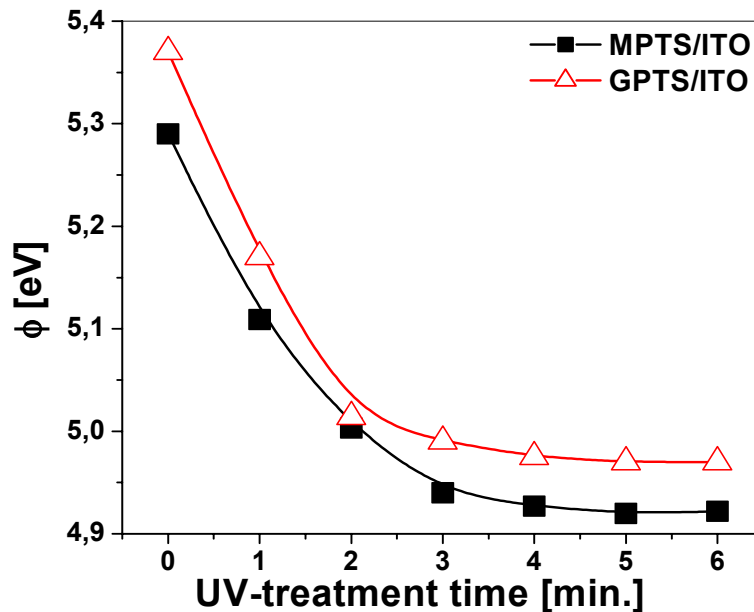


Fig. 81: Work function (ϕ) of GPTS/ITO and MPTS/ITO layers as a function of the duration of the UV-treatment (105 mW/cm²).

It is worth to note that the main decrease of the work function during the UV-treatment occurs during the first 3 min and then the value remains practically constant. These variations indicate changes of the surface compositions. It was reported (331) that the work function of ITO films was depending of three factors: I) the O / In ratio, II) the carbon contamination at the surface and III) the In / Sn ratio (in decreasing order of importance). Mazon et al (332) reported that the work function of ITO film is largely determined by the surface oxygen concentration. From the data shown in section 5.5.4, it was found that the concentration of the charge carriers, n , of UV-treated MPTS/ITO layer increases during the UV treatment or in other words the oxygen concentration in the films is reduced. This results in an upward shift of the Fermi energy level, since the Fermi energy (ϵ_f) is proportional to $n^{2/3}$ (333). This shift results in a reduction of the work function. Fan et al (334) also reported that oxygen vacancies form donor states which cause an upward shift to the Fermi energy of ITO and a decrease in the work function. Similar consideration have been reported by Minami et al (335) for transparent conducting multicomponent oxide films and by Ishida et al (336) for electron beam evaporated ITO films. On the other hand Kim et al (337) have measured the work function and the Hall constants of indium tin oxide surfaces submitted to various surface

treatments such as oxygen plasma, aquaregia or a combination of both processes. All the processes led to an increase of the work function consistent with a large number of defect states (neutral or ionised) created just below the edge of the conduction band pushing the Fermi level to lower values.

The work function appears therefore as a sensitive indicator of the state of the surface and for the monitoring of reactions occurring with the environment atmosphere. The adsorption species may induce substantial variation of the energy required to remove electrons from the Fermi level (338). Fig. 82 shows the time evolution of the work function of UV-treated MPTS/ITO film (see Fig. 81) as a function of the storage time in two different atmospheres. A slight increase is observed when the layer is stored in a low vacuum but a larger increase occurs if the UV-treated layer is exposed to air, an effect certainly related to the adsorption of oxygen species and organic contamination onto the layer as reported in (328, 330). The same low value of the work function can be obtained by switching again the UV-treatment. A similar behaviour was observed by Kim et al (see figure 1 in (339)) for oxygen plasma treated ITO film.

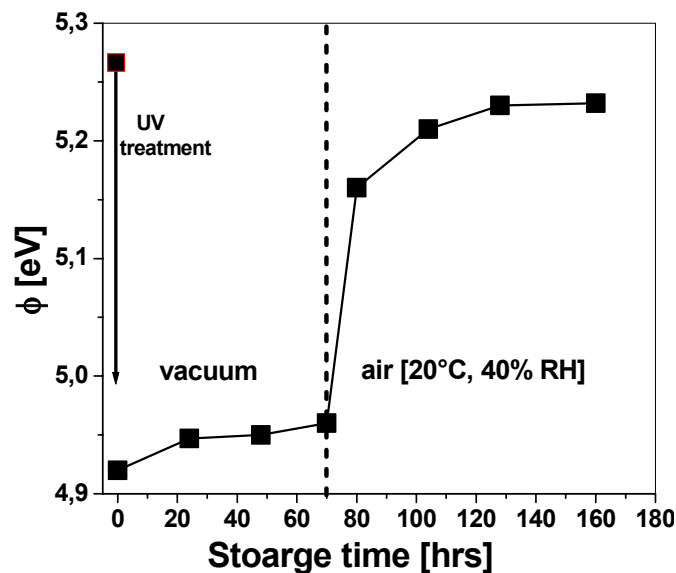


Fig. 82: Time evolution of the work function of UV-treated MPTS/ITO film during storage in vacuum and air atmosphere.

5.7.2 Contact angle and surface energy

The contact angle measurement is a practical technique to determine the free energy of a surface. Its determination is obtained by measuring the contact angle of drops of different solutions deposited on the surface and was modelled by several authors. The total surface energy σ_s consists of two components, a polar part σ_p resulting from the different intermolecular forces due to the permanent and induced dipoles and hydrogen bonding and a dispersion part σ_d (nonpolar) due to the instantaneous dipole moment (327).

Fig. 83 shows the time variation of the contact angle of water and the surface energy of MPTS/ITO film during the UV-treatment and determined using the model of Wu (340). The

contact angle of water decreases considerably from 54° down to a minimum of 11.4° and the surface becomes hydrophilic. The total surface energy of the layer increases from 32.3 mN/m to a maximum value of 74.7 mN/m . The variation occurs during the first 3 minutes of UV-irradiation and is essentially due to the polar component, σ_p , as the nonpolar component, σ_d remains almost constant ($\sim 14 \text{ mN/m}$). Consequently a UV-light irradiation increases the polarity of the surface energy of the film.

The changes of the contact angle and the surface energy observed after UV-irradiation are stable if the layers are stored in vacuum or in a protective gas atmosphere. When they are stored in ambient atmosphere, the surface energy decreases gradually until it reaches its original value (before the UV-treatment). The processes are fully reversible. These changes can be also interpreted as a result of the variation of the chemisorbed oxygen or water on the surface of the layer. Zhong et al (341) have studied recently the evolution of the surface energy of ITO films during an oxygen plasma treatment using the same technique. They also observed a similar behaviour. This was attained to re-contamination or to the re-arrangement on the ITO surfaces.

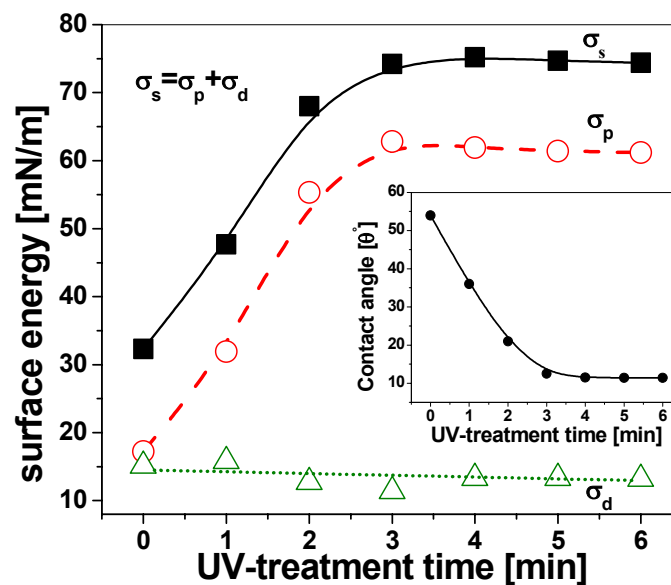


Fig. 83: Variation of the surface energy (dispersion and polar component) of MPTS/ITO surface as a function of the duration of UV-treatment

Fig. 84 summarizes the variation of the electrical sheet resistance and the surface properties (work function and surface energy) for MPTS/ITO layer UV irradiated, stored thereafter in vacuum and then exposed to ambient atmosphere (20°C , 40 % RH). It is clear that the UV-treatment has a significant effect on the electrical and the surface properties of the MPTS/ITO layer. The sheet resistance decreased from 8 to $2 \text{ k}\Omega_{\square}$, the work function decreased from 5.3 to 4.92 eV , and the surface energy increased from 32 to 74 mN/m .

Under vacuum storage conditions, the sheet resistance, work function and the surface energy remains almost constant. However by exposing the layer to air (oxidizing condition), the sheet

resistance, the surface energy and the work function returned to their initial values before the UV-treatment. The diffusion of oxygen into the layer results in a decrease of the number of the charge carriers (see section 4.5.4), and a downward shift of the Fermi energy level resulting in an increase of the work function. The rate of change of the surface properties is clearly faster than the rate of change of the electrical sheet resistance (bulk phenomena), as the oxygen species react first with the top surface layer and slowly with the bulk of the film.

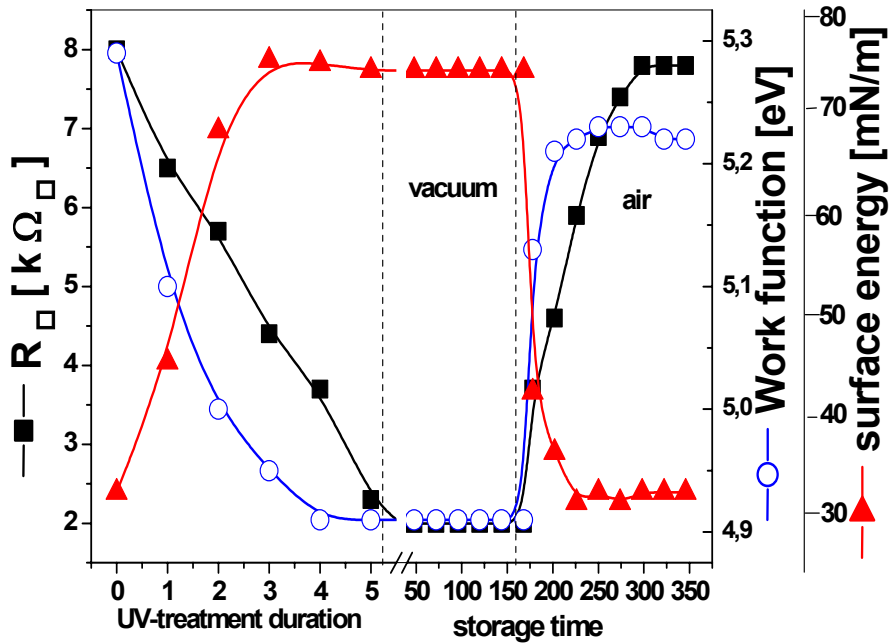


Fig. 84: Variation of the electrical sheet resistance and the surface properties of MPTS/ITO thin film as studied during the UV-treatment and storage in vacuum and then as exposed to ambient atmosphere.

Fig. 85 shows that there is a linear correlation between both surface properties but no correlation was found between the surface and the electrical properties except during the first 3 min of the UV-treatment (Fig. 86). To obtain a minimum of the sheet resistance a longer treatment time is needed since the change in the sheet resistance is due to a bulk effect.

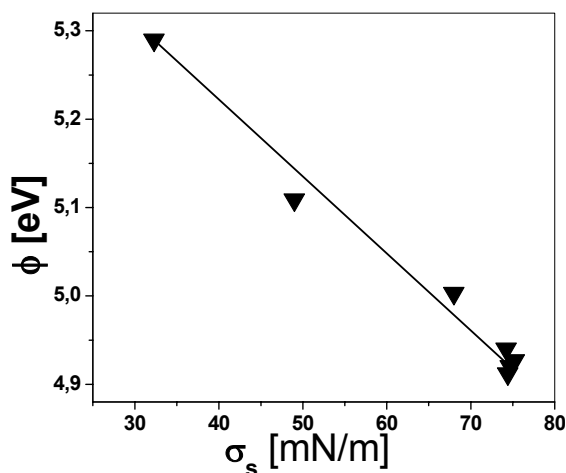


Fig. 85: Correlation between the surface energy and the work function of MPTS/ITO surface..

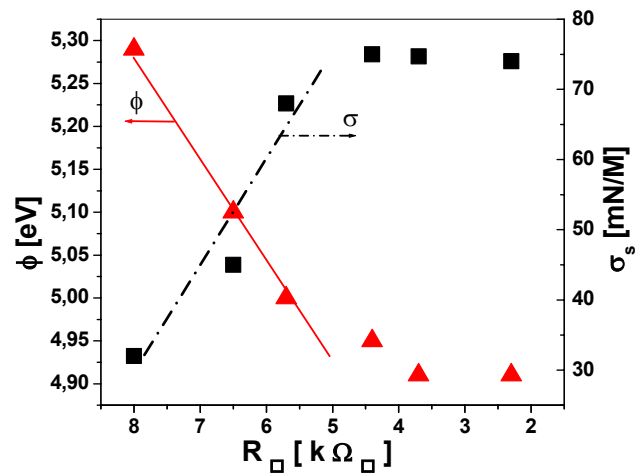


Fig. 86: Relation between the electrical sheet resistance and the surface properties (work function, surface energy) of MPTS/ITO film.

5.7.3 Conclusion

The evolution of the electrical properties of ITO particle layers and their surface properties (surface energy and work function) were examined during the UV-treatment and their storage in different conditions. The UV-treatment decreases the sheet resistance and the work function but increases the surface energy of the MPTS/ITO layer. The water contact angle decreases and the surface become highly hydrophilic. It is worth to note after UV-irradiation the coatings have a high surface energy 75.4 mN/m, dominated by a high polar component. (62.8 mN/m).

The evolution of the sheet resistance and the surface properties of UV-treated MPTS/ITO coating depend on the storage atmosphere. No change was observed when the coatings were stored under vacuum or inert gases but an increase of the sheet resistance, accompanied with an increase of the work function and a decrease of the surface energy was observed when the layers are left in air. These variations are believed to be due to the reaction of the layer with the surrounding atmosphere.

Chapter 6

Summary and conclusions

Tin doped indium oxide (Sn: In₂O₃) crystalline conducting nanoparticles were synthesised successfully using the so called controlled growth technique. The conducting nanoparticles are highly dense and their size grows with the calcination temperature. The average crystallite size ranges from 20 to 35 nm when the particles are calcined between 250 to 500 °C.

The powders calcined at temperature lower than 350 °C were successfully redispersed in water or organic solvents, such as ethanol (zeta potential > 30 mV) down to their primary particle size forming stable coating sols with a shelf life of more than 1 year. However, those calcined at higher temperature are difficult to redisperse and the suspensions form large aggregates and a zeta potential smaller than 20 mV. The particle size distribution of the coating sols is monomodal with a size in the range of 15 to 40 nm. The addition of a small amount of polymerizable inorganic-organic binder such as MPTS shifts slightly the distribution to larger value and up to 6 wt.% of MPTS the coating sols retain their stability.

The sols described above have been used to obtain transparent conducting coatings on glass and plastic substrates by spin and dip coating methods. The thickness of the film increases significantly by increasing the concentration of ITO particles in the sol, as a result of the increase of the viscosity. Single high optical quality layers with thickness between 400 and 500 nm were obtained for a solid content of 25 wt.%. The addition of a modifier like TEOS, GPTS or MPTS to the coating sol also increases the viscosity and consequently the thickness of the film.

Pure ITO suspensions were used to deposit coatings on glass substrates with a further processing at high temperature up to 1000 °C. The electrical resistivity of such layers was found to decrease by increasing the sintering temperature because of the better contact between the conducting particles, the decrease of the porosity of the layers (denser morphology) and increase of the particle size. All these effects lead to a significant increase of the charge carrier mobility.

Further post annealing of the layers in forming gas was found effective to further decrease the resistivity as observed by the increase of the charge carrier concentration produced by the creation of oxygen vacancies. The lowest stable resistivity for a 500 nm thick single ITO layer deposited on fused quartz substrate was $1.5 \times 10^{-3} \Omega \cdot \text{cm}$ (corresponding to a sheet resistance $R_{\square} \sim 30 \Omega_{\square}$) when the layer was sintered in air at 1000 °C for 30 min and further reduced in forming gas at 350 °C for 30 min.

All the films exhibit a transparency greater than 88% in the visible range. A shift of the plasma wavelength towards shorter values related to the increase of the carriers density was observed in the NIR region. In the IR region the reflection increases up to 70% at $\lambda > 10 \mu\text{m}$ and the films behave as heat mirrors. The measured optical band energy gap of the films

ranged between 3.7 and 3.9 eV. The films have a figure of merit in the range of 1 to $7 \times 10^3 \Omega^{-1}$.

The modification of the ITO suspensions by adding a small amount of a UV polymerizable binder such as a hydrolysed silanes (TEOS, GPTS, MPTS) allows the deposition of transparent conducting, and antistatic coatings on different plastic (PMMA, PC, PE, PVC, PET,..) and also on glass substrates fully processable at low temperature ($T < 130^\circ\text{C}$) using UV-light irradiation.

The MPTS modified ITO coatings exhibit the best results compared to the other modifiers used to bind the conducting particles. The sheet resistance of the coatings measured directly after the UV-irradiation or after a reducing treatment is only stable in vacuum or a protective gas atmosphere. When the samples are kept in air it unfortunately increases with time. The variation however decreases with the thickness of the film. This was explained as a result of a decrease of the charge carrier concentration due to the diffusion of oxygen species into the layers. A stable sheet resistance as low as $1.7 \text{ k}\Omega_{\square}$ (resistivity $\rho = 9.4 \times 10^{-2} \Omega\text{cm}$) was achieved for a single 570 nm thick MPTS/ITO layer deposited on PC substrates cured by UV-irradiation, followed by a heat treatment at $T = 130^\circ\text{C}$ during several hours and then a reducing treatment in forming gas at 130°C for 2 h.

A short period of UV irradiation is much more effective than very long time of the heat treatment. FTIR and NMR spectroscopy of the coatings revealed that the UV treatment resulted in a better polymerization and condensation of the binder leading to a more homogeneous particle bonding of the material. These results were confirmed by visualizing the morphological structure of the coatings by SEM and TEM investigations. The average roughness of the coatings measured by WLI on a $53 \times 70 \mu\text{m}^2$ area is 0.8 nm while that determined in a smaller region ($1 \times 1 \mu\text{m}^2$) measured by AFM is 6 nm.

The coatings on plastic substrates showed a transparency higher than 85 % in the visible region which decreases sharply for $\lambda > 1.2 \mu\text{m}$ due to the presence of a strong absorption band. The reflection of the coatings increases for $\lambda > 1.5 \mu\text{m}$ and achieves a value of 40 % at $\lambda = 10 \mu\text{m}$.

Pure ITO coatings processed at low temperature showed a bad adhesion to the substrate and also a weak abrasion resistance. On the contrary the silane modified ITO particle layers exhibit an excellent adhesion to the different substrates and pass the tape test DIN 58196-K2 and the lattice cut test ASTM D 3359 or DIN 53151. The abrasion resistance of these layers is in agreement with DIN 58196-G10 class 1 and the pencil hardness according to ASTM D 3363-92c is 1 H. The mechanical properties can be further enhanced by adding more binder to the ITO sol; however the sheet resistance of the layer increases.

The surface energy and work function of MPTS modified ITO layers deposited on PC substrates were examined as a function of the UV-treatment and the storage conditions. It was found that the UV irradiation produces a highly hydrophilic surface with a surface energy of 75.4 mN/m, dominated by a high polar component (62.8 mN/m). The increase of the surface

energy was correlated with a decrease of the work function. Similarly to the electrical properties these properties are also affected by the storage atmosphere due to the reaction of the layer with the surrounding atmosphere.

In conclusion:

- Sols made with redispersible nanoparticles allows to deposit thick coatings (up to 600 nm) in a single step process using conventional sol gel techniques.
- The conductivity of the ITO nanoparticles coatings increases by increasing the contact surface between the particles (higher sintering temperature leads to lower electron scattering and higher charge carrier mobility) and by creating oxygen vacancies to increase the charge carrier concentration.
- The obtention of denser conducting layers (lower porosity) is an important issue to prevent the chemisorption of oxygen species into the layer and consequently to get lower and stable sheet resistance.
- The presence of already conducting crystalline ITO nanoparticles in a sol containing a polymerizable inorganic-organic binder allows the wet deposition of transparent conductive coatings on several plastic or preformed glass substrates processed totally at low temperature using a UV-irradiation.
- The UV treatment is a fundamental process for such coatings to perform the polymerization of the binder and to bring together homogeneously the conducting particles and at the same time to increase the number of charge carrier concentration.
- The evolution of the electrical resistivity of such coatings in a normal atmosphere after the reducing treatment is still a problem to face the obtention of higher conductivity.
- The electrical, optical and mechanical properties of the so produced layers processed at low temperature are promising and find increasing demands for several industrial applications (antistatic, antistatic-antiglare, electrostatic and also EM shielding).

Appendices

A.Methods of Characterization

Several methods of characterization were used to analyze the prepared materials and coatings.

A.1 Powder and suspension

A.1.1 Crystalline phase and crystallite size

An x-ray powder diffractometer is primarily used for the identification of phases and the determination of the crystallite size of powders. An x-ray beam of known wavelength is focused on a powdered sample and x-ray diffraction peaks are measured using a germanium detector. The d-spacing of the observed diffraction peaks is calculated using Bragg's Law $n\lambda = 2d \sin \theta$ and the mean crystallite size (d) can be evaluated from the line broadening of the XRD peaks using the Scherrer's equation:

$$d = \frac{k\lambda}{\beta \cos \theta} \quad [43]$$

where d is the average diameter of the crystallite lying in the (hkl) lattice plane, K is a constant ~ 0.94 , λ is the X-ray $\text{CuK}\alpha$ wavelength ($\lambda = 1.5418 \text{ \AA}$), β is the full width at half maximum and θ is the diffraction angle.

All ITO powders obtained after the various treatments and with different tin concentrations were analyzed using a $\theta - 2\theta$ X-ray Powder Diffractometer, SIEMENS Type D500 employing a $\text{CuK}\alpha$ radiation ($\lambda = 1.5418 \text{ \AA}$) source and equipped with a 25 kV power. The data were taken in the range $10 < \theta < 90^\circ$ with the step-scan mode using 0.02° steps and scan speed of $3^\circ/\text{min}$. The evaluation of the phases and the different diffraction patterns were analysed using a SIEMENS Software and compared to the joint commission of power diffraction standard (JCPDS) data files.

A.1.2 Particles density and specific BET surface area measurements

The bulk density of the particles refers to the average mass per unit of particle volume. The volume of the particles is most commonly determined by a helium Pycnometer.

The density of the synthesized ITO powders obtained after various treatments and different tin concentration was determined using a helium AccuPyc1330, pycnometer from Micromeritics calibrated with steel spheres of known densities. The data obtained are the average value of five measurements with standard deviation of about $\pm 0.02 \text{ g/cm}^3$.

The Brunauer-Emmelt-Teller (BET) gas adsorption measurement technique was used to measure the specific surface areas of the powders. The measurement was conducted at the saturation vapour pressure of liquid nitrogen using an ASAP 2400, Micromeritics equipment. The powder samples were degassed in vacuum for 12 h at 130°C prior analysis. The particle

size, d_{BET} was evaluated by assuming that the powder was composed of spherical particles using the equation:

$$d_{\text{BET}}(\text{nm}) = \frac{6000}{S_{\text{BET}}(\text{cm}^2/\text{gm}) \cdot \text{density}(\text{g}/\text{cm}^3)} \quad [44]$$

A1.3 Hydrodynamic size distribution

The coating solutions were characterised by measuring the hydrodynamic particle size distribution using an Ultrafine Particle Analyzer (UPA 400, Grimm). The equipment determines the Doppler shift of the scattered light caused by the moving particles. Smaller particles cause a greater shift in the frequency than larger particles. The difference in the frequency of the scattered light is used to determine the size of the particles.

A1.4 Morphology of the ITO suspension

Transmission electron microscopy (TEM) is a good tool to determine the particle size and morphology of the colloidal suspensions down to a nanometer scale as well their crystalline structure. It is possible to study the local chemical composition of the suspension using energy dispersive X-ray (EDX) and to identify the crystal structure by analysing the electron diffraction patterns. The ITO suspensions were characterized using a high resolution transmission electron microscopy (HRTEM-CM200 FEG, Philips).

A1.5 Thermal analysis (DTA/TG)

Thermal analysis are methods by which the physical and chemical properties of a substance, a mixture and/or reaction mixtures are analyzed as a function of temperature or time, while the sample is subjected to a controlled temperature program. The program may involve heating or cooling (dynamic), or holding the temperature constant (isothermal), or any combination of these.

The thermal behaviour of the sols and the coated materials obtained after different post deposition treatments were examined simultaneously by differential thermal analysis (DTA) and thermogravimetry (TG) using a Bähr Gerätbau, STA501 equipment. For this purpose two types of samples were examined. First the coating sols were poured into Al_2O_3 crucibles and heated up to 1000°C at a heating rate of $10^\circ\text{C}/\text{min}$ under synthetic air atmosphere. The second type of samples were xerogels obtained by drying the sols and precured using UV irradiation. The samples were put in Al_2O_3 crucibles and fired up to 1000°C at a heating rate of $10^\circ\text{C}/\text{min}$ under synthetic air atmosphere.

A1.6 Zeta Potential measurements

The particles charge can be manipulated and controlled by adjusting the suspension pH and by using suitable dispersants. The optimization of the formulation of the sols requires a suitable method for measuring the particle's charge, known as the zeta potential. The zeta potential is positive for low pH values and negative for high pH values. The pH at which the

zeta potential of the particle is zero, is known as the isoelectric point (IEP) of the colloid and is a property of the particle surface.

The zeta potential of the coating solution was measured using an Acoustosizer II equipment, Colloidal Dynamics. It was determined by titrating the pH, starting from a value of 2 up to 12.

A.1.7 Viscosity

The dynamic viscosity (η) was measured according to DIN 53018 using a physical Rotational Viscometer ME2 using the disc ninepin accessory. About 12 ml solution was filled into the gap to obtain a contact with the bell-shaped rotor both on the inside and outside. The viscosity was calculated using a commercial software RS120. This technique was used for measuring solutions with viscosity higher than 50 mPas.s.

For solutions of lower viscosity, the kinematic viscosity (ν) was carried out with Schott Ubbelohde capillary viscosimeter according to DIN 51 562 at a constant temperature of 20 °C. The measurements were performed by measuring the time needed for a distinct volume of a liquid to flow in a capillary under laminar condition. The solutions were filtered before the measurements and 5 runs were carried out with each sample and the results were averaged.

By knowing the density of the liquid (ρ), the dynamic and the kinematic viscosity are related as:

$$\eta = \nu\rho \quad [45]$$

A.1.8 Liquid NMR-spectroscopy

Liquid ^{29}Si and ^{13}C NMR-spectroscopy were used to characterize the stability of the MPTS sols. The degree of condensation and polymerization were calculated out from the spectra. The degree of polymerization of a mixture of ITO sol and MPTS sol was also examined. A liquid-NMR-Spectrometer AC200 from Bruker was used to carry out these measurements. The evaluation of the polymerisation degree was carried out from the ^{13}C NMR spectra by comparison of the intensity of the methacrylate group with that of the methylene group signal used as reference.

The condensation degree was carried out from the ^{29}Si NMR spectra by comparing the integrated T^n signal of the Si-O-Si binding groups with that of the internal standard. The condensation degree was evaluated according to the formula (290):

$$C(\%) = 0.33T^1 + 0.67T^2 + 1.0T^3 \quad [46]$$

where T^n is the condensed silanol units indicating the conversion of silanol gel into silica network. T^1 , T^2 , T^3 are corresponding to dihydroxy-, monohydroxy- and nonhydroxy-substituted silica, respectively.

A.2 Coating procedure

The coating sols consisting of dispersed nanocrystalline conducting ITO particles were used to produce transparent conducting coatings on different kind of substrates using the spin or dip coating techniques. The pre-treatment of the substrate before coating and the methods to harden the wet film are affecting strongly the properties of the coatings.

A.2.1 Cleaning of the substrates

Before the coating process the substrates were cleaned by different methods. The used substrates and the cleaning processes are listed in Table 15.

Table 15: Cleaning methods performed to different substrates before coating.

Substrates	Cleaning
Fused quartz glass Borosilicate glass	All substrates were polished using CeO ₂ powder and washed in a professional IR 6001, MIELE Aqua Purificator dishwashing machine G7795/1 (program 17).
Si-wafer, p-doping	The substrates were etched in 3 wt.% HF solution, then washed with bidistilled water and dipped in a 2-propanol bath, and then dried in a flow box.
Polycarbonate (PC) Polymethyl methacrylate (PMMA) Polyvinyl chloride (PVC)	All these substrates were coated after removing the protective foil covering the substrates (as received). The substrates have been also pre-treated in an O ₂ -plasma (40W, 2 min.) to examine the adhesion of the coating on the substrates.
Polyethelene PC-foils PET-foils	These substrates were immersed in a 2-propanol bath and then dried in a flow box.

A2.2 Coatings methods

Single and multilayer Transparent conducting films have been obtained using the well known spin- or dip-coating processes on either polymeric and glass substrates.

Dip coating method: The dip coating process was carried out in flow box with relative humidity of 40 ± 2 % and a temperature of 20°C using homemade equipments. The substrates with size up to 10 x 10 cm were dipped into the coating sol and pulled out at a withdrawal speeds ranging between 2 and 10 mm/s. The whole process was controlled by a software controlling the step motor. The film was dried at 130°C for 5 min. or irradiated by UV-irradiation for 30 s. The whole cycle was repeated several times to obtain coating with higher thickness.

Spin coating method: The coating sols were deposited onto cleaned substrates using a spin coater model 1001 CPS II from CONVAC with spinning speed ranging between 500 and 2000 rpm for 15 s. The substrates were fixed on a vacuum chuck. The layers were then dried

at 130°C for 5 min. or irradiated by UV-irradiation for 30 s. The whole cycle was repeated several times to increase the desired film thickness.

A3. Coatings characterization

A.3.1 Film thickness

The measurement of the film thickness was carried out using a Tencor P-10 surface profiler. The surface of the sample was scanned by a diamond stylus through uncoated part obtained by etching the coating using a mixture of zinc powder and hydrolic acid. The stylus registers the vertical motion at the etched edges and thereby allow to determine the thickness of the coatings.

A.3.2 Electrical properties

The sheet resistance, resistivity, concentration of charge carriers, charge mobility of the films were measured using different methods. The time evolution of these properties was also examined during the storage of the samples in various atmospheres.

Sheet resistance (R_{\square}): The sheet resistance R_{\square} of the films was measured using the four-point probe technique. The probe consists of four equally spaced gold tips with finite radius. Each tip is supported by springs on the other end to minimize the sample damage during probing. A current is supplied through the outer two probes and a voltmeter measures the voltage across the two inner probes (Fig. 87).

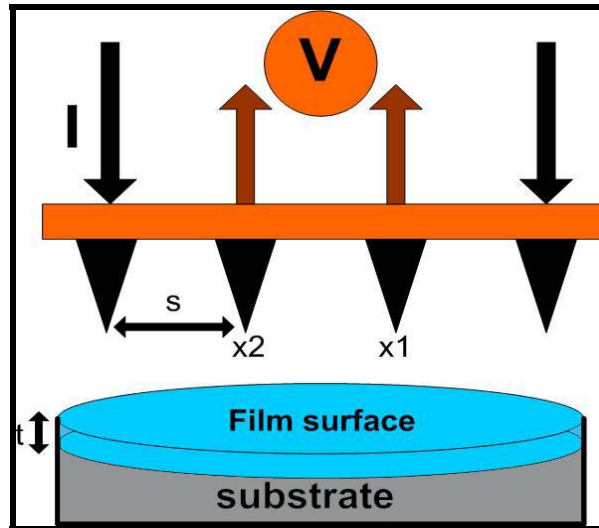


Fig. 87: Scheme of the four-point probe configuration

The measurements were carried out using a 34401-A Multimeter of Hewlett-Packard. For a thin layer (thickness $t \ll s$), assuming a current ring through the sheet and the expression of the area $A = 2 \pi xt$, the sheet resistance is derived as (342):

$$R = \int_{x_1}^{x_2} \rho \frac{dx}{2\pi xt} = \int_s^{2s} \rho \frac{dx}{2\pi xt} = \frac{\rho}{2\pi t} \ln(x) \Big|_s^{2s} = \frac{\rho}{2\pi t} \ln 2 \quad [47]$$

consequently, for $R = \frac{V}{2I}$, the specific resistivity for a thin sheet is given by:

$$\rho = \frac{\pi t}{\ln 2} \left(\frac{V}{I} \right) \quad [48]$$

The specific resistivity for a thin sheet can be written as $\rho = R_{\square} t$, so that the sheet resistance is given by:

$$R_{\square} = \frac{\pi}{\ln 2} R_0 = 4.53 R_0 \quad [49]$$

where $R_0 = V/I$ is the resistance in ohm measured by the multimeter. The results given are the average value of 5 measurements.

The sheet resistance was also measured using a contactless nondestructive system (LEHIGHTON Electronics, Inc.). The operating principle relies on the generation of eddy-currents. The tested sample was positioned into the gap of two circular ferrite cores. An oscillating magnetic field produces eddy-currents in the sample. The power absorbed in the layer is proportional to the conductivity of the sample. The device is calibrated using a Si wafer with known conductivity. The measured data are processed with a software giving the values of the sheet resistance in Ω_{\square} . The results given are the average value of 5 measurements.

Resistivity, mobility and carrier density: The density and mobility and sign of the charge carriers determines the specific conductivity of a conductor σ . The equation defining the specific conductivity is:

$$\sigma = en\mu \quad [50]$$

where e is the electronic charge (1.6×10^{-19} C), n is the carrier density in cm^{-3} and μ is the mobility of the charge carriers in $\text{V}/\text{cm}^2 \cdot \text{s}$. These parameters can be measured using the Van der Pauw- and Hall effect techniques.

The measuring system consists of a MPS-50 programmable power supply H-50, a Hall van der Pauw controller with a K-20 programmable temperature controller from MMR Technologies. The van der Pauw method allows to measure the resistivity, while measurements of the Hall coefficient allows to determine the mobility and the sign of the charge carriers, by placing the material into a magnetic field. The intensity of the magnetic field (B) was 1.3 T. The samples were cut into a size of $1 \times 1 \text{ cm}^2$ and 4 copper wires were glued to the sample using a silver conducting paste, (H20H part A, B from Polytec). These contacts were hardened in a dry oven at 130°C for 15 min. For each sample the validity of the Ohm's law was verified and 10 measurements were carried out and averaged at $T = 300 \text{ K}$.

A3.3 Optical Properties

UV-VIS-NIR Spectroscopy: The transmission, reflection, and absorption of the coatings were measured using a CARY 5E UV-VIS-NIR spectrophotometer from Varian. The measurements were carried out within the range 300 to 3000 nm. All measurements were done at room temperature. The transmission (T) was measured at normal incidence against air as reference. The reflection (R) was carried out using the VW-geometry with a near normal incidence of 7°. From the T and R results, the absorption (A) was calculated as $A = 1 - T - R$. The true absorption coefficient α was calculated using the transmission and reflectance data as:

$$T = (1 - R)e^{-\alpha t} \quad [51]$$

where t is the film thickness.

The absorption coefficient data were used to determine the values of the energy gap, E_g , using the relation (137) :

$$\alpha h\nu \approx (h\nu - E_g)^{1/2} \quad [52]$$

where $h\nu$ is the photon energy. By plotting α^2 versus $h\nu$, the value of the direct optical band gap, E_g , was determined by the extrapolation of the linear region of the plot to zero absorption.

IR-Reflection: The reflection of the coatings in the middle infra red range between 3 to 20 μm was measured using a FTIR-Spectrometer (Brucker IFS 66V). The samples were measured against a gold reference.

Refractive index: The refractive index of the films was measured using the Variable Angle Specular Reflectance Accessory (VASRA) of the Cary 5 E equipment. The measurements were carried out by measuring the reflection spectrum at a given wavelength, as the sample rotates around an axis parallel to the plane of incidence of a polarized light throughout an interval between 20° to 70°. The refractive index can be estimated using the relation (343):

$$n = \tan \theta_B \quad [53]$$

where θ_B is the Brewster's angle, i.e. the angle at which the reflection of the substrate is the same as that of the film. The accuracy of the measurements for isotropic and homogeneous transparent layers is within ± 0.002 .

A.3.4 Structural and morphological properties

XRD: The structural characterization of the deposited films was carried out using the X ray Diffractometer SIEMENS Type D 500. The identification of the phases and the determination of the crystallite size were done as mentioned in A.1.1.

FTIR-Spectroscopy: Fourier Transform Infrared (FTIR) spectroscopy was used to get information about the curing and the polymerisation of the coatings. The structure of the

molecules was measured using a Bruker (IFS 66V) FTIR spectrometer in the range of 400 to 4000 cm^{-1} with resolution of 4 cm^{-1} . The coatings were deposited on Si wafer substrates by the spin coating method and cured using different treatments.

Solid state NMR-spectroscopy: Nuclear magnetic resonance (NMR) spectroscopy was used to measure the polymerisation and condensation degrees of MPTS in the modified ITO coatings. All measurements were performed with a very small amount of a bulk material hardened using UV- or heat treatments at 130°C. The solid state ^{29}Si and ^{13}C spectra were recorded at room temperature using a Bruker MSL 200 spectrometer at 4.7 Tesla. The quantitative evaluation of the spectra was carried out by comparing the integrated signal intensity with that of the internal standard (see A.1.8)

Scanning Electron Microscopy (SEM): The scanning electron microscopy (SEM) is the most widely used equipment in the field of materials science (344) to get information about the surface of materials.

The surface of the coatings was imaged using a high-resolution scanning electron microscopy FR-SEM (JSM6400F, JEOL) using the secondary electron signal excited by a 10 keV primary beam. To get charge free surfaces, a very thin gold conducting layer was previously sputtered on the surfaces of the sample.

HR-Transmission Electron Microscopy (HR-TEM): High-resolution transmission electron microscopy gives information about the crystallinity, structure and the texture of coatings. TEM cross sections were prepared by thinning the specimens using Ar^+ ion-milling. Using the electron diffraction contrast (bright and dark field modes) the crystalline structures can be determined by Fourier analysis. Quantitative chemical compositions of the coatings were obtained using energy X-ray spectrophotometry.

The characterization were made using a HRTEM-CM200 FEG, Philips equipped with an energy dispersive X-ray spectrometer (DX-4 system, EDX). The investigation of the layer structure of the coatings deposited on polymeric substrates was difficult as the thinning of the specimen by ion-milling technique damages the polymeric substrates. Thus ultramicrotomy (345) was used to prepare thin cross sections.

Atomic Force Microscopy (AFM): The topography of the coatings can be measured using an atomic force microscope (AFM), where a sharp tip is scanned over a surface with a feedback mechanism that enables the piezo-electric scanner to maintain the tip under a constant force to obtain height information. AFM operates by measuring attractive forces (noncontact mode) or repulsive forces (contact mode) between the tip and the sample.

The measurements were carried out using the noncontact mode with a NewViewTM head from L.O.T. ORIEL attached to the white light interferometer (Zygo New View 5000).

White Light Interferometer (WLI): The surface morphology as well as the roughness of the coatings were characterized using a White Light Interferometer (WLI), Zygo New View 5000. It is a 3D surface profiler imaging a surface detail and providing accurate measurements

without contacting the surface. The measurements were carried out using a white light beam, divided within an optical objective. One portion is reflected from the tested part and the other from a high quality flat reference. Interference patterns are formed and all intensities are directed onto a solid state camera. A MetroPro software was used to convert the intensities into images. The time of measurements is very short and the surface topography with feature up to 5 mm height can be determined with a vertical resolution down to 0.1 nm. Surface characterization, such as forms, volumes, roughness, step height (film thickness) and waviness are available. This method was used to characterize the pattern structure of the coatings and the average roughness R_a of the layers is defined as:

$$R_a = \frac{y_1 + y_2 + y_3 \dots + y_N}{N} \quad [54]$$

where y is the absolute value of each point and N is the number of discrete elements.

A.3.5 Mechanical properties

The mechanical properties of the coatings, such as adhesion, abrasion resistance and hardness were examined following DIN-Norm and ASTM tests.

Adhesion: It is an important property, which is related with the durability of the coating. The adhesion of the coating was examined by the lattice cut test (Erishsen, ASTM D 3359, DIN 53151) and the tape test (DIN 58196-6-K2). The classification of the cut test ranges from $GT/TT = 0$ (excellent adhesion) to $GT/TT = 5$ (no adhesion). The tape test classification follows a visual observation after pulling off of a tape from the substrate. The layer is classified as either wholly removed, partially removed or left on the substrate.

Abrasion: The abrasion resistance is a mechanical test to determine how much physical damage the coating will take. This can be performed by rubbing a loaded cloth (DIN 58196-4) or a loaded eraser (DIN 58196-5). The tests were done by applying a 9.8 N force by rubbing the coating with a cloth during 25 cycles and during 10 cycles in the case of the rubber. The surface is examined by illuminating the tested surface with a lamp and the result is classified from no visible damage, class 1 to totally damaged layer, class 5. The abrasion resistance was also monitored by measuring the electrical sheet resistance of the tested part of the coatings.

The abrasion resistance of the coating was also examined using the Taber abrasion test (ASTM D1044, D3389). The test specimen is placed on the abrasion tester and a 1000 g load is placed on top of the abrader wheel which is allowed to spin for a specified number of revolutions. A haze measurement is taken before and after the process. Results are expressed by percent changes of the haze per number of cycles.

Hardness: Pencil leads of known hardness allows to evaluate the film hardness. The process is a traditional test for gauging the hardness and to determine the scratch resistance of coatings by simply scratching the surface with a pencil. The pencil is held against the film at a 45° angle and pushed away from the operator with a 6.5 mm stroke. The process is initiated

with the hardest pencil and continued down the scale of hardness of the pencil that will not cut the film. The classification of the drawing leads meets the following scale:

$$\frac{6B - 5B - 4B - 3B - 2B - B - HB - H - 2H \dots 6H}{\text{softer} \dots \dots \dots \text{harder}}$$

The electrical sheet resistance of the coatings was also measured using a multimeter between two points around the stroke of the pencil.

A.3.6 Surface Properties

The surface properties such as work function, contact angle and surface energy of the transparent conducting coatings were characterized.

Work function: This property was measured using a vibrating capacitor Kelvin Probe system from KP technology in ambient atmosphere. The Kelvin method determines the contact potential difference (CPD) of a sample with respect to a reference electrode (stainless steel tip, diameter 5 mm). The CPD values were referenced to a nominal gold work function of 5.1 eV.(346).

Surface Energy: The surface energy of the coatings can be determined by measuring the contact angle of different liquids with the surface of the films using the sessile drop method. The determination of the contact angle is a measure of the wetting of a solid by a liquid and is an indirect method to determine the changes in the surface energy of a thin film. This method is used to estimate the wetting properties of a localized region on a solid surface. The angle between the baseline of the drop and the tangent at the drop boundary is measured. The surface energy of a surface is calculated from the contact angle data of a series of three well characterised wetting liquids selected with different viscosities, polarities and surface tension, such as distilled water, glycerine and formamide. Different models are used to estimate the surface energy of the solid. The determination of the surface energy were done due to the Wu model (340) using a G2/DSA 10 contact angle measuring system from Krüss with a G 40 programme.

B. List of used chemicals:

Chemicals	Symbol	Supplier	Purity
2-(2-Butoxyethoxy) ethyl acetate	$\text{CH}_3\text{CO}_2(\text{CH}_2\text{CH}_2\text{O})_2(\text{CH}_2)_3\text{CH}_3$	Aldrich	99%
3,6,9- Trioxadecanoic acid (TDOS)	$\text{CH}_3\text{O}(\text{CH}_2\text{CH}_2\text{O})_2\text{CH}_2\text{CO}_2\text{H}$	Aldrich	
3-Aminopropyl-trimethoxysilane (APTS)	$\text{H}_2\text{N}(\text{CH}_2)_3\text{Si}(\text{OCH}_3)_3$	Fluka	97 %
3-Glycidoxypropyl-trimethoxysilane (GPTS)	$\text{C}_9\text{H}_{20}\text{O}_5\text{Si}$	ABCR	98 %
3-Methacryloxypropyl-trimethoxysilane (MPTS)	$\text{C}_{10}\text{H}_{20}\text{O}_5\text{Si}$	ABCR	98.5
6-Caprolactam	$\text{C}_6\text{H}_{11}\text{NO}$	Fluka	>98%
Ammonium hydroxide solution	$\text{NH}_3.\text{aq}$	Fluka	25%
Bidistilled water	H_2O	INM	
DBE dibasic ester	$\text{CH}_3\text{O}_2\text{C}(\text{CH}_2)_n\text{CO}_2\text{CH}_3$	Aldrich	98 %
Diethylendlycole-monbutylether (DBG)	$\text{CH}_3(\text{CH}_2)_3\text{OCH}_2\text{CH}_2\text{OCH}_2\text{CH}_2\text{OH}$	Fluka	>99%
Diisobutyl adipate	$[-\text{CH}_2\text{CH}_2\text{CO}_2\text{CH}_2\text{CH}(\text{CH}_3)_2]_2$	Aldrich	99 %
Ethylene Glycole (EG)	$\text{HOCH}_2\text{CH}_2\text{OH}$	Fluka	>99.5%
Hydrochloric acid	HCl	Fluka	37%
Indium (III) Chloride	InCl_3	Chempur	99.999
Irgacur 184	$\text{C}_6\text{H}_{10}\text{OHCOC}_6\text{H}_5$	Ciba	
Tetraethoxysilane (TEOS)	$(\text{C}_2\text{H}_5\text{O})_4\text{Si}$	ABCR	98 %
Tin (IV) Chloride pentahydrate	$\text{SnCl}_4.5\text{H}_2\text{O}$	Aldrich	98%

C. List of equipments

The equipments used in this research are listed in the following table:

Measurements	Equipment	Supplier
Adhesion	Lattice cut test (model 295)	Erichsen
Atomic Force Microscopy (AFM)	NanoView™ AFM (noncontact mode)	L.O.T. ORIEL
Centrifuge	Hermel Z 323	Jochen Thieme
Contact angle and Surface energy	G2 / DSA 10, G40 programme	KRÜSS
Dip Coater	homemade	INM
Dynamic Viscosity	Rotation Viskosimeter UM PHYSICA, (ME DIN 53018)	Rheolab MC20 Physica
Film Thickness	Profilometer, P10 surface Profiler	TENCOR
FTIR Spectroscopy	IFS 66V	BRUKER
Heat treatment up to 1000 °C	L3/R Oven	Nabertherm
Heat treatment up to 600 °C	Furnace K 750/1	Heraeus
High Resolution Transmission Electron Microscope (HRTEM)	CM200 FEG	Philips
Kinematic Viscosity	Ubbelohde Viscosimeter, AV 5410_Thermosta CT 1450	SCHOTT
Liquid-NMR Spectroscopy	AC200	BRUKER
Particle Size distribution	Ultrafine Particle Analyzer (UPA 400)	Grimm
Paste synthesis	Three roller grinding mill	Exact
Post heat treatment	Protective gas tube furnace (Gero furnace)	GERO GmbH
Powder density	Gas Pycnometer, AccuPyc 1330	MICROMERITICS
Resistivity, charge carrier density and mobility	Van der Pauw method	MMR Technology, Inc.

Scanning Electron Microscopy (SEM)	JSM 6400 F	JEOL
Sheet Resistance (4-point technique)	34401A Multimeter	HEWLETT PACKARD
Solid state-NMR Spectroscopy	MSL 200	BRUKER
Spin Coater	Modell 1001; CPS II control system	CONVAC
Substrate cleaning	Rinsing machine, professional IR 6001	Miele
Surface area and Porosity	ASAP 2400	MICROMERITICS
Taber abrasion resistance	S 130 Abraser	Taber industry
Thermal Analysis (DTA/TG)	STA 501	Bähr Gerätebau
Thermal drying system	Drying furnace	Heraeus
UV-curing system	UV/IR dryer, TYP 20/III	Beltron-GmbH
UV-VIS-NIR Spectroscopy	Cary 5E	VARIAN
White Light Interferometry	Zygo Newview 5000	Zygo
Work function	Scanning Kelvin Probe System	KP Technology
X-ray Diffraction	XRD D500	Siemens
Zeta Potential	Acoustosizer II	Colloidal Dynamics

D. XRD spectrum

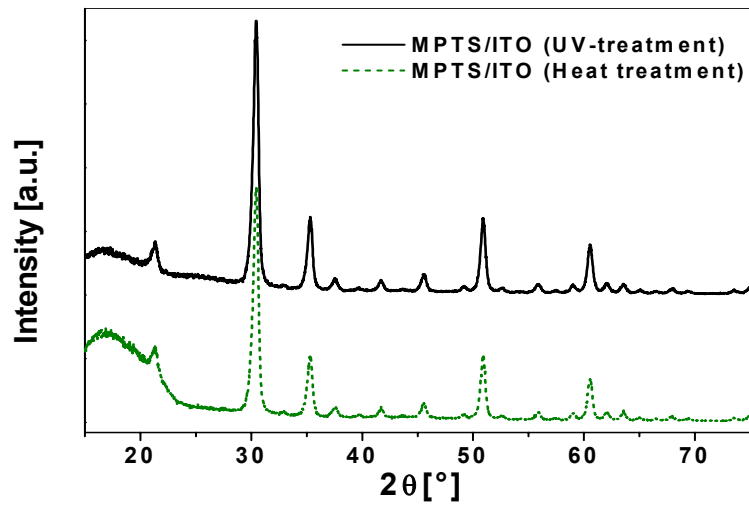


Fig. 88: XRD patterns of MPTS/ITO coatings on PC substrate. (—) as UV-treated film, (---) or thermally cured film at 130 °C for 10 h.

E. FTIR spectroscopy

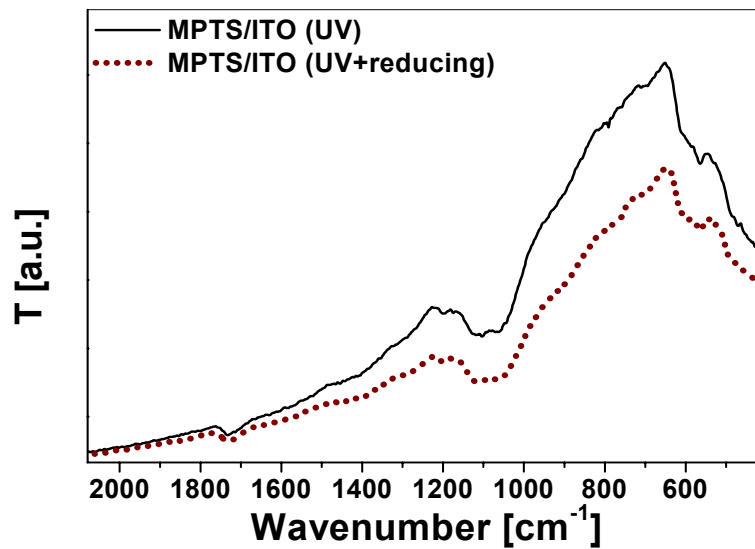


Fig. 89: FTIR spectrum of MPTS/ITO coatings deposited on Si-wafer with different curing treatment: UV and UV+reducing at 130 °C for 2 h in forming gas.

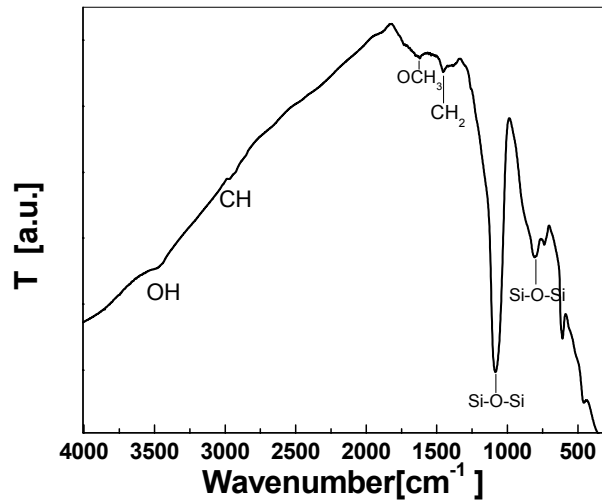


Fig. 90: FTIR spectrum of 470 nm thick GPTS/ITO layer deposited on Si-wafer substrate cured with UV-irradiation

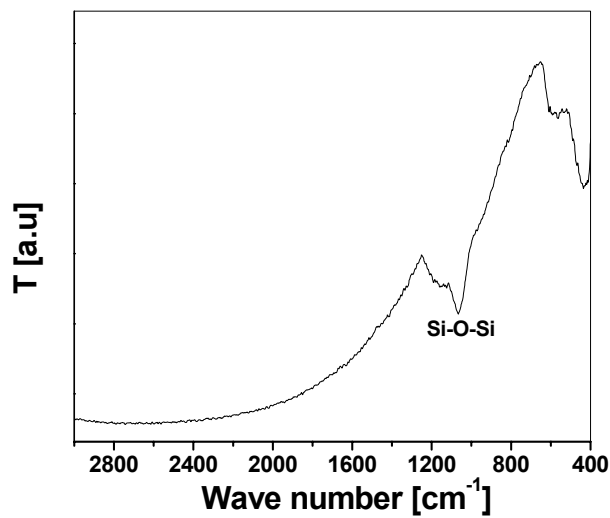


Fig. 91: FTIR spectrum of 520 nm thick GPTS/ITO layer deposited on Si-wafer substrate heated in air at 550 °C.

F. NMR spectroscopy

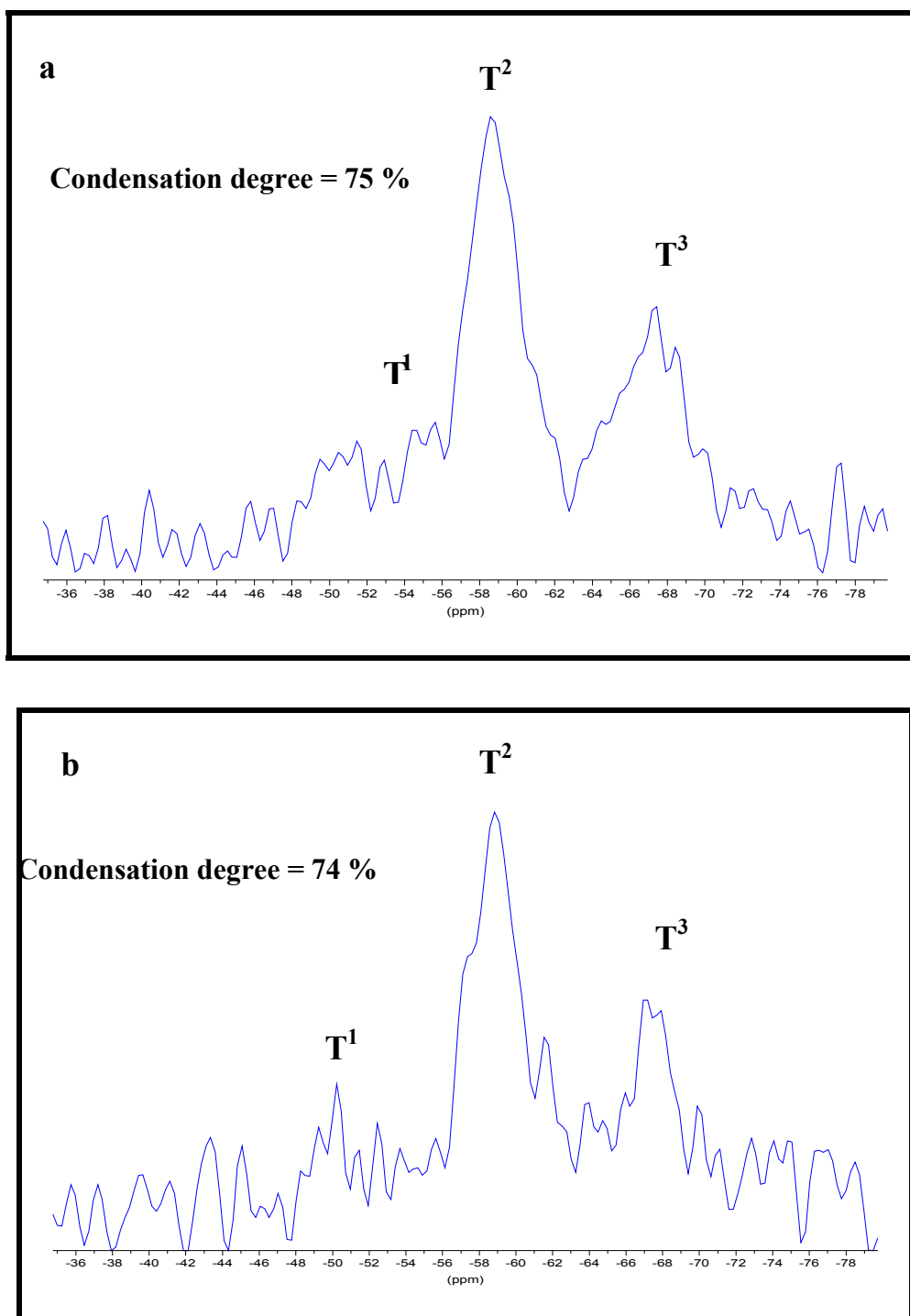


Fig. 92: ^{29}Si -NMR spectroscopy of GPTS/ITO coatings cured by
a) UV irradiation (5 min.), b) thermal treatment at 130 °C

G. Topography and morphology of the coatings

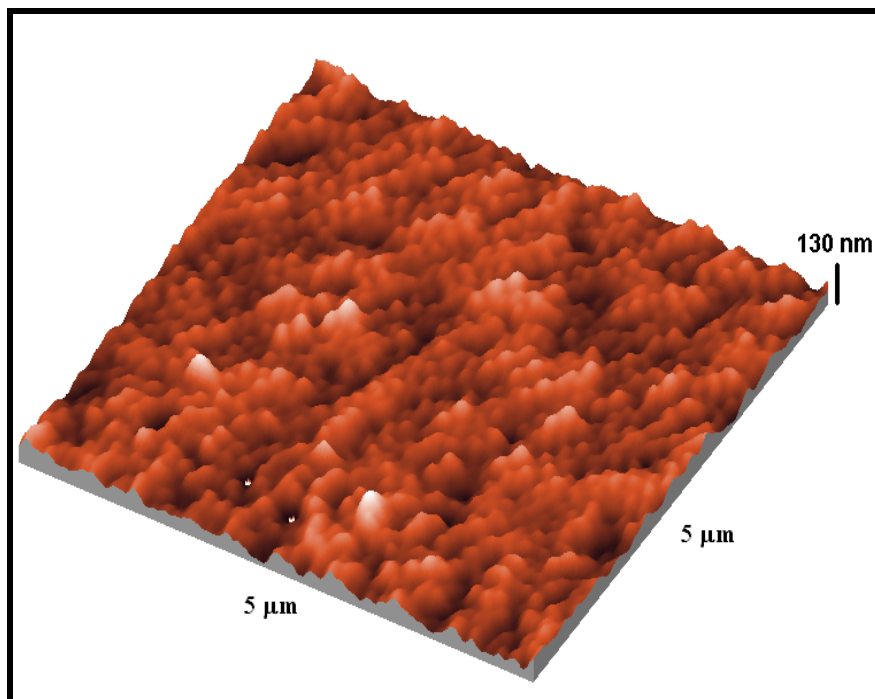


Fig. 93: AFM picture of spin coated ITO particle layer on borosilicate glass heated in air at 550 °C

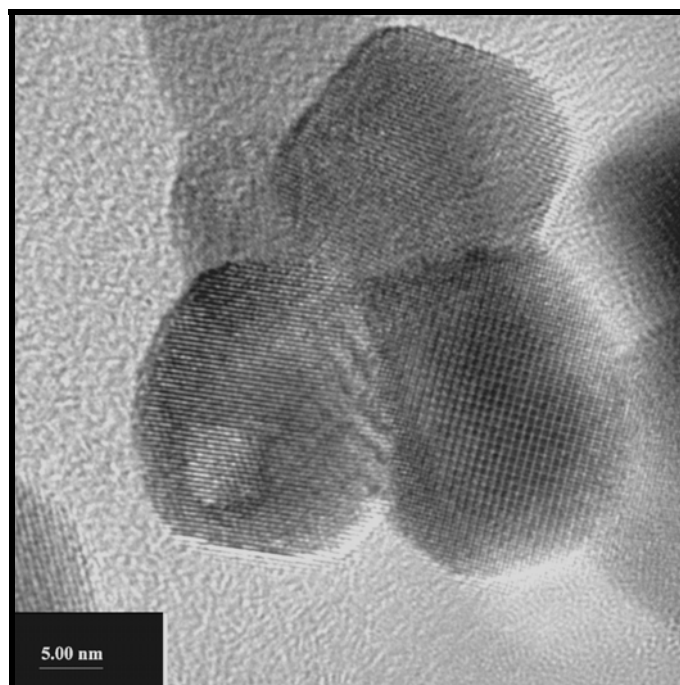


Fig. 94: TEM picture of ITO300 suspension showing the diffraction pattern of the ITO particles

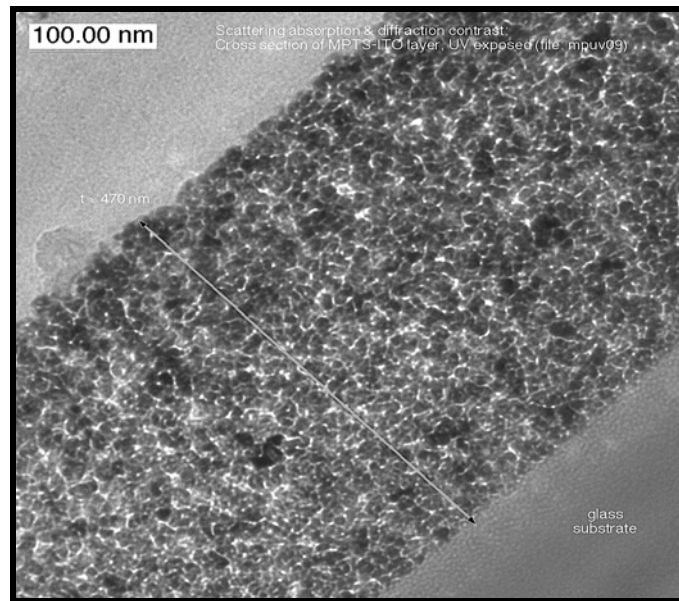


Fig. 95: TEM cross section of a 470 nm thick UV-treated MPTS/ITO250 layer deposited on a glass substrate.

H. Patterning of ITO coatings

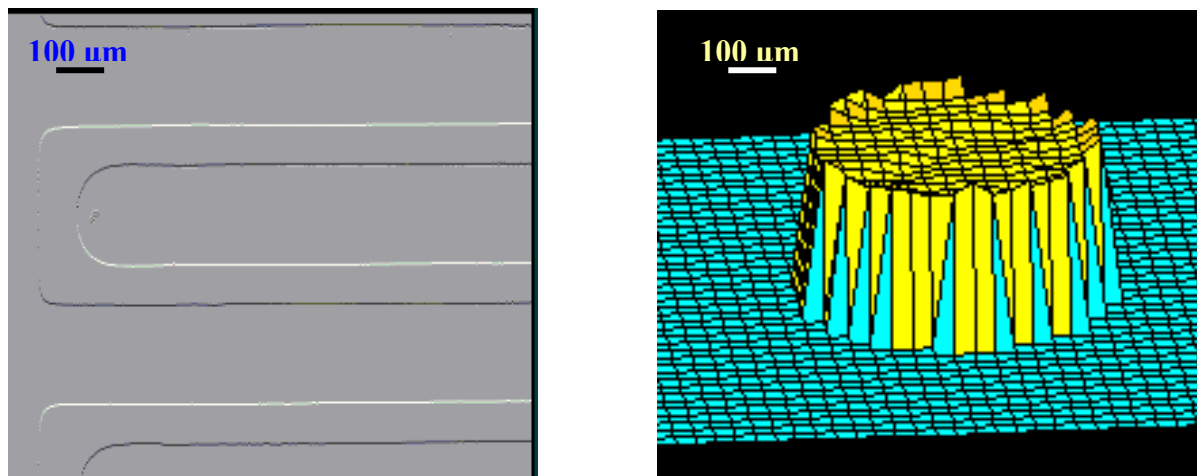


Fig. 96: WLI pictures of the topography of an ITO film patterned using UV-irradiation on PC-substrates.

References

- (1) A.Elshabini, F.Barlow, *Thin Film Technology Handbook*, McGraw-Hill, New York, 1998.
- (2) J.Anderson, M.Boudart, *Catalysis:Science and Technology*, 1, Springer-Verlag, Berlin, 1981.
- (3) D.Talbot, J.Talbot, *Corrosion Science and technology*, CRC Press, Boca Raton, 1998.
- (4) M.Madou, S.Morison, *Chemical Sensing with Solid State Devices*, Academic Press, Inc., Boston, 1989.
- (5) K.Chopra, I. Kaur, *Thin Film Device and Applications*, Plenum Press, New York, 1983.
- (6) K.Nitzsche, *Schichtmeßtechnik*, 1, Vogel Buchverlag, Würzburg, 1996.
- (7) M.Ohring, *The Material Science of Thin Films*, Academic Press, INC., San Diego, 1992.
- (8) H.Pulker, *Coatings on glass*, second revised edition. Elsevier Science, Amsterdam, 1984.
- (9) J.Szanyi, *Applied Surface Science* **185** (2002), 161.
- (10) H.Kozaka, M.Kajimur, T.Hirano, K.Katayama, *Journal of Sol-Gel Science and Technology* **19** (2000), 205.
- (11) W.Driver, *Plastics Chemistry and Technology*, Van Nostrand Reinhold Company, New York, 1979.
- (12) V.Moehl, *Metalloberfläche* **45** (1991), 205.
- (13) J.Affinito, S.Eufinger, M.Gross, G.Graff, P.Martin, *Annu. Tech. Conf. Proc. Soc. Vac. Coaters*, 40 (1997), 210.
- (14) D.Glocker, S.Shah, *Handbook of Thin Film Process Technology*, Institute of Physic Publishing, Bristol, 1995.
- (15) Thayer School of Engineering,
<http://thayer.dartmouth.edu/other/microeng/courses/es194/student/jiaying/sem/topic.html>, 2000.
- (16) T.Morimoto, Y.Sanada, H.Tomonaga, *Proc. of the 3rd-ICCG conference*, Maastricht (2000), 233.
- (17) T.Yoneda, T.Morimoto, *Thin solid films* **351** (1999), 279.
- (18) D. R.Uhlman, T.Surtwala, K.Davidson, J. M.Boulton, G.Teowee, *Journal of Non-Crystalline Solids* **218** (1997), 113.

- (19) S.SepEUR, N.Kunze, B.Werner, H.Schmidt, *Thin solid films* **351** (1999), 216.
- (20) K.Ramaiah, V.Raja, A.bhatnagar, R.Tomlinson, R.Pilkington, A.Hill, S.Chang, Y.Su, F.Juang, *Semicond. Sci. Technol.* **15** (2000), 676.
- (21) Y.Wang, C.Anderson, *Macromolecules* **32** (1999), 6172.
- (22) T.Furusaki, J.Takahashi, K.Kodira, *J. of the Ceramic Society of Japan, Int. Edition* **102** (1994), 202.
- (23) M.Atek, F.Luna, S.Messaddeq, M.Aegerter, *Journal of Sol-Gel Science and Technology* **8** (1997), 517.
- (24) C.Goebbert, M.Aegerter, D.Burgard, R.Nass, H.Schmidt, *J. Mater. Chem.* **9** (1999), 253.
- (25) P.Chandana, Y.Yanagisawa, *J. Am. Ceram. Soc.* **84** (2001), 251.
- (26) H.Schröder, *Physics of thin films*, Academic Press, New York, 1969.
- (27) J.Dutta, P.Roubeau, T.Emeraud, J.Laurenst, A.Smith, F.LebLanc, J.Perrin, *Thin solid films* **239** (1994), 150.
- (28) C.Brinker, C.Scherer, *The Physics and Chemistry of Sol-Gel Processing*, Academic Press, San Diego, 1990.
- (29) L.Landau, B.Levich, *Acta Physiochem* **17** (1942), 42.
- (30) C.Brinker, A.Hurd, P.Schunk, G.Frye, C.Ashley, *Journal of Noncrystalline Solids* **147&148** (1992), 424.
- (31) INM-information, Angle-Dependent Dip-Coating (ADDC) - A New Method for the Fabrication of Optical Interference Filters, Institut für Neue Materialien, Saarbruecken, (2000)
- (32) H.Schmidt, M.Mennig, <http://www.solgel.com/articles/Nov00/mennig.htm>, 2000.
- (33) P.Oliveira, Synthesis of NIR reflective coatings by ADDC, Institut für Neue Materialien, Saarbruecken, (1998), 9.
- (34) D.Birnie, <http://www.mse.arizona.edu/faculty/birnie/Coatings/KeyStages.htm>, 2000.
- (35) A.Emslie, F.Bonner, L.Peck, *J. Appl. Phys.* **29** (1958), 858.
- (36) D.Meyerhofer, *J. Appl. Phys.* **49** (1978), 3993.
- (37) R.Larson, T.Rehg, *Liquid Film Coating*, Chapman & Hall, London, 1997.
- (38) B.Yoldes, *SPIE-The International Society for Optical Engineering*, San Diego, California, 1328 (1990), 296.
- (39) A.Steckl, G.Mohammed, *J. Appl. Phys.* **51** (1980), 3890.
- (40) B.Choi, H.Yoon, H.Lee, *App. Phys. Lett.* **76** (2000), 412.

- (41) M.Utsumi, N.Matsukaza, A.Kumagai, Y.Shiraishi, Y.Kawamura, N.Furusho, *Thin solid films* **363** (2000), 13.
- (42) H.Liu, Y.Zhao, G.Ramanath, S.Murarka, G.Wang, *Thin solid films* **384** (2001), 151.
- (43) A.Epstein, *MRS Bulletin* **22** (1997), 16.
- (44) T.Skotheim, R.Elsenbaumer, J.Reynold, *Handbook of Conducting Polymers*, Marcel Dekker, New York, 1998.
- (45) J.Roncali, *J. Mater. Chem.* **9** (1999), 1875.
- (46) P.Tijssen, *Proc. of International Conference Conductive Coatings and Compounds*, Brussel (1999), 34.
- (47) J.Friedrich, W.Gerhard-Dieter, Bayer AG, EU 553671, 1993.
- (48) J.Friedrich, Bayer AG, DE 4229192, 1994.
- (49) J.S.Kim, M.Granström, R.Friend, N.Johansson, W.Salaneck, R.Daik, W.Feast, F.Cacialli, *J. Appl. Phys.* **84** (1998), 6859.
- (50) H.Pielartzik, H.Heuer, R.Wehrmann, *Kunststoffe* **89** (1999), 135.
- (51) A.Arias, M.Gransröm, D.Thomas, K.Petritsche, R.Friend, *Phys. Rev. B* **60** (1999), 1854.
- (52) K.Chopra, S.Major, D.Pandya, *thin solid films* **102** (1983).
- (53) H.Kim, C.M.Gilmore, *J. Appl. Phys.* **86** (1999), 6451.
- (54) S.Chappel, A.Zaban, *Solar Energy Materials and Solar Cells* **71** (2002), 141.
- (55) R.Hatton, S.Day, M.Chesters, M.Willis, *Thin solid films* **394** (2001), 292.
- (56) J.Lan, J.Kanicki, *Mat. Res. Soc. Symp. Proc.*, 424 (1997), 347.
- (57) Y.Akao, T.Haranoh, *Proc. of the 1st International Conference on Coatings on Glass*, Saarbrücken, Germany (1997).
- (58) H.Hartnagel, A.Dawar, A.Jain, C.Jagadish, *Semiconducting transparent thin films*, Institute of Physics Publishing, 1995.
- (59) W.Rees, *CVD of Nanometals*, VCH, Weinheim, 1996.
- (60) Z.Jarzebski, J.Morton, *J. Electrochem. Soc. Rev. News* **123** (1976), 199.
- (61) T.Arai, *J. Phys. Soc. Jpn.* **15** (1960), 916.
- (62) C.Lambert, *Solar Energy Mater.* **6** (1981), 1.
- (63) K.Song, Y.Kang, *Materials Letter* **42** (2000), 283.

- (64) M.Yoshizumi, K.Wakabayashi, *Proc. of the 17th Nat. SAMPE Technical Conference*, Azusa, 17 (1985), 410.
- (65) K.Wakabayashi, Y.Kamiya, N. Ohta, *Bull. Chem. Soc. Jpn* **40** (1967), 2127.
- (66) V.Casey, M.Stephenson, *J. Phys. D* **23** (1990), 1212.
- (67) F.Simonis, A.Faber, C.Hoogedorn, *Thin solid films* **105** (1987), 131.
- (68) D.Acosta, W.Estrada, R.Castanedo, A.Maldonado, M.Valenzuela, *Thin solid films* **375** (1998), 147.
- (69) S.Schanthi, C.Subramanian, P.Ramasamy, *Cryst. Res. Technol.* **34** (1999), 1037.
- (70) M.J.Van.Bommel, A.Groen W, H.A.M.Van Hall, W.C.Keur, T.N.M.Bernards, *Journal of materials science* **34** (1999), 4803.
- (71) C.Terrier, J.Chatelon, J.Roger, R.Berjoan, C.Dubois, *Journal of Sol-Gel Science and Technology* **10** (1997), 75.
- (72) S. Nasser, *Thin solid films* **342** (1999), 47.
- (73) Y.Matsui, Y.Yamamoto, S.Takeda, *Proc. of Mat. Res. Soc. Symb.*, San Francisco, 621 (2000), Q4.9.
- (74) A.Smith, *Thin solid films* **376** (2000), 47.
- (75) T.Karasawa, Y.Miyata, *Thin solid films* **223** (1993), 135.
- (76) D.Lane, T.Coath, H.Beldon, *Thin solid films* **221** (1992), 262.
- (77) C.Terrier, J.Chatelon, R.Berjona, J.Roger, *Thin solid films* **263** (1995), 37.
- (78) A.Maddalena, R.Maschio, S.Dire, A.Raccanelli, *Journal of Noncrystalline Solids* **121** (1990), 365.
- (79) S.Park, H.Zheng, J.Mackenzie, *Materials Letters* **22** (1995), 175.
- (80) A.Rizzato, L.Broussous, C.Santilli, S.Pulcinelli, A.Craievich, *J. Non-Crystalline Solids* **284** (2001), 61.
- (81) S.Park, J.Mackenzie, *Thin solid films* **258** (1995), 268.
- (82) M.A.Aegerter, A.Reich, D.Ganz, G.Gasparo, J.Puetz, T.K.Krajewski, *Journal of Non-Crystalline Solids* **218** (1997), 123.
- (83) P.Nath, R.Bunshah, *Thin solid films* **69** (1980), 63.
- (84) I.Hamberg, C.Granqvist, *J. Appl. Phys.* **60** (1986), R123.
- (85) I.Safi, R.Howson, *Thin solid films* **343-344** (1999), 115.
- (86) M.Mizuno, T.Miyamoto, *Jpn. J. Appl. Phys.* **39** (2000), 1849.

- (87) L.Miinea, D.Hoffman, *J. Mater. Chem.* **10** (2000), 2392.
- (88) H.Kim, G.Horwitz, G.Kushto, S.Qadri, Z.Kafafi, D.Chrisey, *App. Phys. Lett.* **78** (2001), 1050.
- (89) C.Carvalho, A.M.Rego, A.Amaral, P.Broqueira, G.Laverda, *Surface Coatings and Technology* **124** (2000), 70.
- (90) L.Gupta, A.Mansingh, P.Srivastava, *Thin solid films* **176** (1989), 33.
- (91) C.Goebbert, H.Bisht, N.Al-Dahoudi, R.Nonniger, M.aegerter, H.Schmidt, *J. Sol.-Gel - Sci. Tech.* **19** (2000), 201.
- (92) J.Bae, H.Kim, N.Lee, G.Yeom, *Vacuum* **56** (2000), 77.
- (93) H.Kim, J.Bae, J.Kim, K.Kim, Y.Jang, G.Yeom, N.Lee, *Surface and Coatings Technology* **131** (2000), 201.
- (94) A.Suzuki, T.Matsuhata, T.Aoki, Y.Yoneyama, M.Okuda, *Jpn. J. Appl. Phys.* **40** (2001), 401.
- (95) Seon-Soon.Kim, Se-Young Choi, Chan-Gyung Park, Hyeon-WOO Jin, *Thin solid films* **347** (1999), 155.
- (96) Radhouane Bel HadjTahar, Takayuki Ban, Yutaka Ohya, Yasutaka takahashi, *Journal of applied Physics* **82** (1997), 865.
- (97) Y.Takahashi, S:Okada, R.Tahar, K.Nakano, *Journal of Non-Crystalline Solids* **218** (1997), 129.
- (98) M.Alam, D.Cameron, *Thin solid films* **00** (2000), 455.
- (99) R.Mientus, K.Ellmer, *Surface and Coatings Technology* **142-144** (2001), 748.
- (100) D.Mergel, M.Schenkel, M.Ghebre, M.Sulkowski, *Thin solid films* **392** (2001), 91.
- (101) F.Elakad, A.Punnoose, G.Prabu, *Appl. Phys. A* **71** (2000).
- (102) W.Wu, B.Chiou, *Thin solid films* **298** (1997), 221.
- (103) H.Gläser, *Large Area Glass Coating*, 1st english edition. Von Ardenne Anlagentechnik GmbH, Dresden, 2000.
- (104) D.Manno, G.Micocci, A.Serra, M.Giulio, A.Tepore, *J. Appl. Phys.* **88** (2000), 6571.
- (105) N.Arfsen, *J. Non-crystalline solids* **63** (1984), 243.
- (106) P.Lemoine, D.Mariotti, J.McLaughlin, *Thin solid films* **401** (2001), 196.
- (107) F.Zhu, K.Zhang, E.Guenther, C.Jin, *Thin solid films* **363** (2000), 314.
- (108) F.Akkad, M.Marafi, A.Punnoose, G.Prabu, *Phys. stat. sol.(a)* **177** (2000), 445.
- (109) M.Jin, J.Feng, Z.De-hgeng, M.Hong-lei, L.Shu-ying, *Thin solid films* **357** (1999), 98.

- (110) T.Minami, T.Yamamoto, T.Miyata, *Thin solid films* **366** (2000), 63.
- (111) M.Chen, Z.Pei, X.Wang, C.Sun, L.Wen, *J. Mater. res.* **16** (2001), 2118.
- (112) T.Subramanyam, B.Srinivasulunaido, S.Uthanna, *Cryst. Res. Technol.* **34** (1999), 981.
- (113) J.Chang, M.Hon, *Thin solid films* **386** (2001), 79.
- (114) B.Lokhande, M.Uplane, *Applied Surface Science* **167** (2000), 243.
- (115) L.Armelao, M.Fabrizio, S.Gialanella, F.Zordan, *Thin solid films* **394** (2001), 90.
- (116) Y.Meng, X.Yang, H.Chen, J.Shen, Y.Jiang, Z.Zhang, Z.Hua, *Thin solid films* **394** (2001), 219.
- (117) S.Dali, M.Jayachandran, M.Chockalingam, *Journal of Materials science Letters* **18** (1999), 915.
- (118) J.Robertson, P.W.Peacock, M.Towler, R.Needs, *Thin solid films* **411** (2002), 96.
- (119) R.Asahi, A.Wang, J.Babcock, N.Edelman, A.Metz, M.Lane, V.Draavid, C.Kannewurf, A.Freeman, T.Marks, *Thin solid films* **411** (2002), 101.
- (120) T.Miyata, S.Suzuki, M.Ishii, T.Minami, *Thin solid films* **411** (2002), 76.
- (121) T.Mason, G.Gonzales, D.Kammler, N.Mansourian-Hadavi, B.Ingram, *Thin solid films* **411** (2002), 106.
- (122) J.Tate, M.Jayaraj, A.Draeseke, T.Ulbrich, A.Slight, K.Vanaja, R.Nagarajan, J.Wager, R.Hoffman, *Thin solid films* **411** (2002), 119.
- (123) P.Drude, *Ann. Phys.* **3** (1900), 369.
- (124) N.Ashcroft, N.Mermin, *Solid state Physics*, Saunders College, Philadelphia, 1976.
- (125) R.Petritz, *Phys. Rev.* **104** (1956), 1508.
- (126) J.Seto, *J. Appl. Phys.* **46** (1975), 5247.
- (127) W.Wu, B.Chiou, *Applied surface science* **68** (1993), 497.
- (128) V.Johnson, K.Lark-Horovitz, *Phys. Rev.* **71** (1947), 374.
- (129) J.Liu, E.Rädlein, G.Fischart, *Phys. chem. Glasses* **40** (1999), 277.
- (130) S.Seki, M.Ogawa, Y.Sawada, *Jpn. J. Appl. Phys.* **40** (2001), 1244.
- (131) H.Haitjema, *Spectrally selective tin oxide and indium oxide coatings*, PhD thesis, Technische Universitat Delft, 1989.
- (132) J.Jackson, *Electromagnetic theory*, Third. John Wiley and Sons, New York, 1998.
- (133) O.Heavens, *Optical properties of thin films*, Dover Publications, INC., New York, 1965.

- (134) H.Kim, A.Pique, J.Horwitz, H.Mutrata, Z.Kafafi, C.Gilmore, D.Chrisey, *Thin solid films* **377-378** (2000), 798.
- (135) S.Brewer, D.Brawn, S.Franzen, *Langmuir* **18** (2002), 6857.
- (136) H.Macleod, *Thin Film Optical Filters*, Hilger, Bristol, (1986)
- (137) J.Tauc, R.Grigorovoci, A.Vancu, *Phys. stat. sol.* **15** (1966), 627.
- (138) E.Burstein, *Phys. Rev.* **93** (1954), 632.
- (139) R.Gordon, *MRS Bulletin* **1** (2000).
- (140) M.Resso, J.Mayers, D.Evanicky,
http://www.oci.com/pdf_files/products/thin_film_cond_ar_coating.pdf, 1999.
- (141) J.Kim, E.Kim, Y.Han, K.Nam, D.Ihm, *Jpn. J. Appl. Phys.* **41** (2002), 237.
- (142) B.Lewis, D.Paine, *MRS Bulletin* **25** (2000), 22.
- (143) P.Nostell, A.Roos, B.Karlsson, *Thin solid films* **351** (1999), 170.
- (144) G.Kiriakidis, N.Katsarakis, M.Bender, E.Gagaoudakis, V.Cimalia, *Mater. Phys. Mech.* **1** (2000), 83.
- (145) Y.Aoshima, M.Miyazaki, K.Sato, Y.Akao, S.Takaki, K.Adachi, *Jpn. J. Appl. Phys.* **39** (2000), 4884.
- (146) S.Nicoletti, L.Dori, F.Corticelle, M.Leoni, P.Scardi, *J. Am. Ceram. Soc.* **82** (1999), 1201.
- (147) K.Efimenko, V.Rybak, V.Svorcik, V.Hnатовicz, *Appl. Phys. A* **68** (1999), 479.
- (148) U.Schulz, *Europhotronics*, vol. 6 (2001),39.
- (149) V.Kirchhof, N.Shiller, M.Neuman, H.Morgner, M.Fahland, K.Suzuki, Coating of plastic webs, Fraunhofer Institut Elektronenstrahl und Plasmatechnik, Dresden, (1999),21.
- (150) K.Narendrnati, <http://www.vaportech.com/brief/brf4.htm>, 1996.
- (151) G.Philipp, H.Schmidt, *J. Non Cryst. Solids* **63** (1984), 283.
- (152) B.Novak, *Adv. Mater.* **5** (1993), 422.
- (153) P.Judeinstein, C.Sanchez, *J. Mater. Chem.* **6** (1996), 511.
- (154) N.Mennig, P.Oliviera, A.Frantzen, H.Schmidt, *Thin solid films* **1999** (1999), 225.
- (155) M.Nogami, M.Watabe, K.Nagasaka, *Sol-Gel Optics*, San Diego, 1328 (1990), 119.
- (156) B.Lebeau, C.Sanchez, S.Brassellet, J.Zyss, G.Froc, M.Dumont, *New J. Chem.* **20** (1996), 13.

- (157) N.Al-Dahoudi, H.Bisht, C.Goebbert, T.Krajewski, M.A.Aegerter, *Proc. of 3rd ICCG Conference*, Maastricht (2000), 555.
- (158) N.Al-Dahoudi, H.Bisht, C.Göbbert, T.Krajewski, M.Aegerter, *Thin solid films* **392** (2001), 299.
- (159) M.Hines, P.Guyot-Sionnest, *J. Phys. Chem.* **100** (1996), 468.
- (160) R.Siegel, E.Hu, M.Roco, Nanostructured science and technology, National science and technology council, Maryland, (1999)
- (161) T.Turkki, *Studies of preparation and Properties of Nanophase metal Oxides.*, Royal Institute of Technology, 1999.
- (162) H.Weller, *Angew. Chem., Int. Ed. Engl.* **32** (1993), 41.
- (163) G.Bond, *Surf. Sci.* **156** (1985), 966.
- (164) G.Schmidt, *Chem. Rev.* **92** (1992), 1709.
- (165) L. Lewis, *Chem. Rev.* **93** (1993), 2693.
- (166) X.Jing, W.Zhao, L.Lan, *Journal of Materials science Letters* **19** (2000), 377.
- (167) U.Erb, *Nanostructured Materials* **6** (1995), 533.
- (168) S.Emory, S.Nie, *J. Phys. Chem. B.* **102** (1998), 493.
- (169) A.Haes, R.Van Duyne, *Mater. Res. Soc. Symp. Proc.*, 723 (2002).
- (170) G.Kataby, A.Ulman, R.Prozorov, A.Gedanken, *Langmuir* **14** (1998), 1512.
- (171) Y.Ohko, T.Tatsuma, T.Fujii, K.Naoi, C.Niwa, Y.Kubota, A.Fujishima, *Nature Materials* **2** (2003), 29.
- (172) J.Kreuter, Medinova medical Consulting GmbH, 6,117,454, 2000.
- (173) V.Sicaras, <http://www.rdmag.com/features/0208nano23.asp>, 2002.
- (174) A.petri, M.Chastellain, M.Hofmann, <http://ltp.epfl.ch/page17706.html>, 2003.
- (175) H.Gleiter, *Nanocrystalline Materials*, Pergamon Press, Oxford, 1989.
- (176) R.Siegel, *Synthesis and processing of nanostructured materials*, 233, Netherland, 1993.
- (177) D.McRae, E.Matijevic, E.J.Davis, *J. Colloidal Interface Sci.* **53** (1975), 411.
- (178) S.Vemury, S.Pratsinis, *Appl. Phys. Lett.* **66** (1995), 3275.
- (179) G.Ulrich, *J. Colloidal Interface Sci.* **87** (1982), 257.
- (180) M.El-Shal, S.Li, T.Turkki, D.Graiver, U.Pernisz, *J. Phys. Chem.* **99** (1995), 17807.

- (181) P.Mishra, B.Mohanty, B.Nayak, *Mater. Lett.* **23** (1995), 153.
- (182) J.Lee, G.Beaucage, S.Paratsinis, *Chem. Mater.* **9** (1997), 2400.
- (183) Jahresbericht, Jahresbericht, INM, Saarbruecken, (1995-2001)
- (184) D.Burgard, H.Ma, Synthesis of n- α -Al₂O₃, INM, Saarbruecken, (1996), 47.
- (185) M.Sameti, T.Sciestel, Surface modified nanoparticles for somatic gene therapy, INM, Saarbruecken, (1998), 35.
- (186) W.Lü, *Synthesis of nanosized BaSnO₃ powders*, Dissertation, Universität des Saarlandes, 2003.
- (187) A.Feiock, Al₂O₃/TiN nanocomposites, INM, Saarbruecken, (1998), 23.
- (188) S.Albayrak, *Kolloidale Verarbeitung und Sintern von nanoskaligem TiN-Pulver*, Dissertation, Universität des Saarlandes, 1997.
- (189) R.Nonniger, C.Goebbert, H.Schmidt, R.Drumm, S.Sepur, DE 19849048, 2000.
- (190) R.Naß, D.Burgard, H.Schmidt, *Eurogel 91*, Saarbruecken, Germany, 5 (1991), 243.
- (191) H.Schmidt, R.Naß, D.Sporn, S.Ray, *Materials Science Forum* **34-36** (1988), 833.
- (192) D.Burgard, C.Kropf, R.Naß, H.Schmidt, *Mat. Res. Soc. Symp. Proc.*, California, 346 (1994), 101.
- (193) O.Varghese, L.Malhotra, *J. Appl. Phys.* **87** (2000), 7457.
- (194) Ch.Beck, W.Härtl, R.Hempelmann, *J. Mater. Res.* **13** (1998), 3174.
- (195) G.De, A.Licciulli, C.Massarò, L.Tapfer, M.Catalano, G.Battaglin, C.Meneghini, P.Mazzoldi, *Journal of Noncrystalline Solids* **194** (1996), 225.
- (196) W.Sager, H.Eicke, W.Sun, *Colloids and Surfaces A: Physicochemical and Engineering Aspects*, Amsterdam, 79 (1993), 199.
- (197) J.Jolivet, L.Vayssieres, C.Chaneac, E.Tronc, *Mat. Res. Soc. Symp. Proc.*, 432 (1997), 145.
- (198) S.Sakka, H.Kozuka, G.Zhao, *SPIE* **2288** (1994), 108.
- (199) R.Salker, P.Jeevanadam, S.Aruna, Y.Koltypin, A.Gedanken, *J. Mater. Chem.* **9** (1999), 1333.
- (200) D.Kim, S.Oh, J.Lee, *Langmuir* **15** (1999), 1599.
- (201) M.Lopez-Quintela, J.Quiben-Salla, J.Rivas, *Use of microemulsions in the production of nanostructured Materials*, 66, 1997.
- (202) H.Schmidt, *Proceedings of the fourth International conference on ceramic powder processing science*, Nagoya, Japan, 22 (1991).

- (203) W.Ostwald, *Kolloid-Z.* **36** (1925), 380.
- (204) G.Lagaly, *Colloid stability, Ullmann's Encyclopedia of Industrial Chemistry*, Wiley-VCH Verlag GmbH & Co.KGAA, Kiel, 2002.
- (205) H.Müller, *Polymere Stabilisatoren in der Emulsionspolymerisation*, Doktorarbeit, Universität Potsdam, 1997.
- (206) R.Hunter, *Zeta Potential in Colloid Science*, Academic Press, New York, 1981.
- (207) R.Greenwood, K.Kendall, *Brit. Ceramic Trans.* **97** (1998), 174.
- (208) R.O'Brien,
http://www.ceramicindustry.com/CDA/ArticleInformation/features/BNP_Features_Item/0,2710,73678,00.html, 2002.
- (209) H.Schmidt, R.Naß, D.Burgard, R.Nonniger, *Materials Research Society Symposium Proceedings*, California, 520 (1998), 21.
- (210) S.Bhagwat, R.Howson, *Surface coatings and technology* **111** (1999), 163.
- (211) X.Meng, W.Zhen, J.Guo, X.Fan, *Appl. Phys. A* **70** (2000), 421.
- (212) K.Zhang, F.Zhu, C.Huan, A.We, *Thin solid films* **376** (2000), 255.
- (213) H.Nanto, T.Minami, S.Orito, S.Takata, *J. appl. Phys.* **63** (1988), 2711.
- (214) J.Chang, H.Wang, M.Hon, *Journal of crystal growth* **211** (2000), 93.
- (215) V.Korobov, M.Leibovitch, Y.Shapira, *Appl. Phys. Lett.* **65** (1994), 2290.
- (216) A.Amaral, P.Broqueira, C.Carvalho, G.Lavareda, *Surface and Coatings Technology* **125** (2000), 151.
- (217) N.Balasubramanian, A.Subrahmanyam, *J. Phys. D: appl. Phys.* **22** (1989), 206.
- (218) J.George, C.Menon, *Surface and Coatings Technology* **132** (2000), 45.
- (219) H.Randhawa, M.Matthews, R.Bunshah, *Thin solid films* **83** (1981), 267.
- (220) F.Adurodija, H.Izumi, T.Ishihara, H.Yoshioka, M.Motoyama, K.Murai, *Applied surface science* **177** (2001), 114.
- (221) H.Kim, A.Pique, J.Horwitz, H.Mattoussi, H:Murata, Z.Kafai, D.Chrisey, *Appl. Phys. Lett.* **74** (1999), 34443446.
- (222) S.Qadri, H.Kim, J.Horwitz, D.Chirsey, *J. Appl. Phys.* **88** (2000), 6564.
- (223) H.Kim, J.Horwitz, C.Golmore, D.Chrisey, *Appl. Phys. A* **69** (1999), 447.
- (224) N.Naghavi, C.Marcel, L.Dupont, A.Rougier, J.Leriche, C.Guery, *J. Mater. chem.* **10** (2000), 2315.

- (225) Y.Yadava, G.Denicolo, A.Arias, L.Roman, I.Huettel, *Mater. Chem. Phys.* **48** (1997), 263.
- (226) D.Zhang, H.Ma, *J. Mater. Sci. Technol.* **13** (1997), 50.
- (227) Z.Zhao, D.Morel, C.Ferekides, *Thin solid films* **413** (2002), 203.
- (228) Yung Jen-Lin, Ching-Jiunn Wu, *Surface and Coatings Technology* **88** (1996), 239.
- (229) S.Shanthi, C.Subramanian, P.Ramasamy, *Cryst. Res. Technol.* **34** (1999), 1037.
- (230) H.Bisht, H.Eun, A.Mehrtens, M.Aegerter, *Thin solid films* **351** (1999), 109.
- (231) E.Shanthi, A.Banerjee, V.Dutta, K.Chopra, *J. Appl. Phys.* **53** (1982), 1615.
- (232) J.Song, I.Park, K.Yoom, W.Cho, K.Lim, *J. Korean Phys. Soc.* **29** (1996), 219.
- (233) C.Lee, K.Lim, J.Song, *Solar Energy Materials and Solar Cells* **43** (1996), 37.
- (234) G.Blandenet, Y.Lagarde, J.Spitz, *Chemical Vapor Deposition Proceedings of the 5th Int. Conf.*, Princeton (1975), 190.
- (235) K.Nishio, T.Sei, T.Tsuchiya, *J. Mat. Sci.* **31** (1996), 1761.
- (236) R.Tahar, T.Ban, Y.Ohya, Y.Takahashi, *J. Am. Ceram. Soc.* **84** (2001), 85.
- (237) R.Tahar, T.Ban, Y.Ohya, Y.Takahashi, *J. Appl. Phys.* **83** (1998), 2139.
- (238) R.Ota, S.Seki, M.Ogawa, T.Nishide, A.Shida, M.Ide, Y.Sawada, *Thin solid films* **411** (2002), 42.
- (239) E.Shigeno, K.Shimizu, S.Seki, M.Ogawa, A.Shida, M.Ide, Y.Sawada, *Thin solid films* **411** (2002), 56.
- (240) M.Wakagi, K.Chahara, K.Onisawa, Y.Kawakubo, T.Kichikawa, T.Satoh, T.Minemura, *Thin solid films* **411** (2000), 46.
- (241) T.Kololuoma, J.Rantala, *Electronics Letters* **36** (2000), 172.
- (242) S.Park, J.Mackenzie, *J. Am. Ceram. Soc.* **78** (1995), 2669.
- (243) D.Gallagher, F.Scanlan, R.Houriet, H.Mathieu, *J. Mater. Res.* **8** (1993), 3135.
- (244) J.Aikens, H.Sarkas, R.Brotzman, *Mat. Res. Soc. Symp. Proc.* **536** (1999), 377.
- (245) J.Ederth, A.Hultaker, P.Heszler, G.Niklasson, A.Van Doorn, C.Granqvist, C.Van Haag, M.Jongorius, D.Burgard, *Smart Mater. Struc.* **11** (2002), 675.
- (246) D.Burgard, C.Goebbert, R.Nass, *Journal of Sol-Gel Science and Technology* **13** (1998), 789.
- (247) C.Goebert, R.Nonniger, M.Aegerter, H.Schmidt, *Thin solid films* **351** (1999), 79.

- (248) M.Kawata, M.Yukinobu, Sumitomo Metal Mining Company, Ltd., USA 5,662,962, 1997.
- (249) J.Dutta, S.Ray, *Thin solid films* **162** (1988), 119.
- (250) Y.Shigesato, D.Paine, *Thin solid films* **238** (1994), 44.
- (251) J.Zheng, H.Kwork, *Appl. Phys. Lett.* **63** (1993), 1.
- (252) D.Paine, T.Whitson, D.Janiac, R.Beresford, C.yang, B.Lewis, *J. Appl. Phys.* **85** (1999).
- (253) S.Muranaka, *Jpn. J. Appl. Phys.* **30** (1991), L2062.
- (254) Y.Akagi, K.Hanamoto, H.Suzuki, T.Katoh, M.Sasaki, S.Imai, M.Tsudagawa, H.Miki, *Jpn. J. Appl. Phys.* **38** (1999), 6846.
- (255) Y.Suzaki, T.Shikama, O.Tanaka, H.Higuchi, S.Nakamura, *Electronics and Communications in Japan* **82** (1999), 30.
- (256) J.Ma, S.Li, J.Zhao, H.Ma, *Thin solid films* **307** (1997), 200.
- (257) F.Niino, H.Hirsawa, K.Kondo, *Thin solid films* **411** (2002), 28.
- (258) F.Adurodija, H.Izumi, T.Ishihara, H.Yoshioka, M.Motoyama, *J. App. Phys.* **88** (2000), 4175.
- (259) V.Craciun, D.Craciun, Z.Chen, J.Hwang, R.Singh, *Applied Surface Science* **168** (2000), 118.
- (260) F.Adurodija, H.Izumi, T.Ishihar, H.Yoshiko, H.Matsui, M.Motoyama, *Jpn. J. Appl. Phys.* **38** (1999), 2710.
- (261) F.Adurodija, H.Izumi, T.Ishihara, H.Yoshioka, H.Matsui, M.Motoyama, *Appl. Phys. Lett.* **74** (1999), 3059.
- (262) M.Martino, A.Luches, M.Fernandes, P.Anobile, V.Petruzzelli, *J. Phys. D* **34** (2001), 2606.
- (263) H.Kim, J.Horwitz, G.Kushto, Z.Kafafi, D.Chrisey, *Appl. Phys. Lett.* **79** (2001), 284.
- (264) H.Izumi, T.Ishirhara, H.Yoshioka, M.Montoya, *Thin solid films* **411** (2002), 32.
- (265) T.Larsen, *40th Annual Technical Conference Proceedings*, 40 (1997), 365.
- (266) T.Minami, H.Sonohara, T.Kakuma, S.Takata, *Thin solid films* **270** (1995), 37.
- (267) H.Gurev, K.Bicking, *SPIE* **2262** (1994), 246.
- (268) Y.Hoshi, T.Kiyomura, *Thin solid films* **411** (2002), 36.
- (269) H.Ando, G.Haacke, US 4048372.
- (270) A.Kulkarni, K.Schulz, T.Lim, M.Khan, *Thin solid films* **308-309** (1997), 1.

- (271) P.Carcia, R.Mclean, M.Reilly, Z.Li, L.Pillione, R.Messier, *App. Phys. Lett.* **81** (2002), 1800.
- (272) B.Chiou, S.Hsieh, *Thin solid films* **229** (1993), 146.
- (273) S.Maniv, C.Miner, W.Westwood, *J. Vac. Sci. Technol. A* **1** (1983), 1370.
- (274) Y.Chen, D.Zhang, Q.Wang, J.Ma, T.Yang, *J. Mater. Sci. Technol.* **16** (2000), 23.
- (275) P.Foot, R.Singer, M.Sugrue, I.Joungs, The secratry state of defense, Ep 0887103A1, 1998.
- (276) M.Murouchi, T.Hayashi, A.Nishihara, M.Ishihara, Mitsubishi Materials Corporation & Dai Nippon Toryo Co., Ltd., US 5,504,133, 1996.
- (277) H.Imai, A.Tomianga, H.Hirashima, M.Toki, M.Aizawa, *J. Sol-Gel Sci. Technol.* **13** (1998), 991.
- (278) A.Heeger, *Synthetic Metals* **55-57** (1993), 3471.
- (279) C.Pratt, <http://homepage.dtn.ntl.com/colin.pratt/applcp.htm>, 2002.
- (280) A.Kaynak, L.Rintoul, G.George, *Material Research Bulletin* **35** (2000), 813.
- (281) Y.Lee, J.Kim, *Mol. Cryst. and Liq. Cryst.* **337** (1999), 213.
- (282) G.Gustaffson, Y.Cao, G.Treary, F.Klavetter, N.Colaneri, A.Heeger, *Nature* **357** (1992), 477.
- (283) Y.Cao, G.Treacy, P.Smith, A.Heeger, *Appl. Phys. Lett.* **60** (1992), 2711.
- (284) K.Yangisawa, C.Udwatte, S.Nasu, *J. Mater. Res.* **15** (2000), 1404.
- (285) G.Frank, H.Köstlin, *Appl. Phys. A* **27** (1982), 197.
- (286) N.Yamada, I.Yasui, Y.Shigesato, H.Li, Y.Ujihira, K.Nomura, *Jpn. J. Appl. Phys.* **38** (1999), 2856.
- (287) A.Segmüller, I.NNoyan, V.Sperious, *X-ray diffraction studies of thn films and multilayer structure*, 18, Pergamon Press, Oxford, 1989.
- (288) Dr. H. Krajiwisky, internal communication
- (289) H.Gleiter, *Proc. Makromol. Chem, Macromol. Symp.*, Basel, 50 (1991), 171.
- (290) D.Hoebbel, Praktische Anwendung der NMR-Spektroskopie zur Untersuchung von Sol-Gel-Reaktionen Charakterisierung des Aufbaus von Materialien, Institut für Neue Materialien (INM), Saarbruecken, (2001),35.
- (291) Y.Shigesato, Y.Hayashi, T.Haranoh, *Appl. Phys. Lett.* **61** (1992), 73.
- (292) C.Yi, I.Yasui, Y.Shigesato, *Jpn. J. Appl. Phys.* **34** (1995), 1638.
- (293) P.Thilakan, C.Minarini, S.Loreti, E.Terzini, *Thin solid films* **388** (2001), 34.

- (294) Y.Shigesato, D.Paine, *Appl. Phys. Lett.* **62** (1993), 1268.
- (295) T.Omata, H.Fujiwara, S.Matsuo, N.Ono, *Appl. Phys. A* **71** (2000), 609.
- (296) N.Balasubramanien, A.Subrahmanyam, *J. Phys. D: appl. Phys.* **22** (1989), 206.
- (297) N.Yamada, I.Yasui, Y.Shingesato, H.Liu, Y.Ujihira, K.Nomura, *Jpn. J. Appl. Phys.* **38** (1999), 2856.
- (298) G.Frank, E.Kauer, H.Köstlin, *Thin solid films* **77** (1981), 107.
- (299) N.Taga, M.Maekawa, M.Kamei, I.Yasui, Y.Shigesato, *Jpn. J. Appl. Phys.* **37** (1998), 6585.
- (300) S.Seki, Y.Sawada, T.Nishidi, *Thin solid films* **388** (2001), 22.
- (301) S.Honda, A.Tsujimoto, M.Watamori, K.Oura, *Jpn. J. Appl. Phys.* **34** (1995), 1386.
- (302) M.Mizuno, T.Miyamoto, T.Ohnishi, H.Hayashi, *Jpn. J. Appl. Phys.* **36** (1997), 3408.
- (303) S.Choi, J.Lee, *J. Vac. Sci. Technol. A* **19** (2001), 2043.
- (304) T.Minami, T.Yamamoto, Y.Toda, T.Miyata, *Thin solid films* **373** (2000), 189.
- (305) R.Tahar, T.Ban, Y.Ohya, Y.Takahashi, *J. Appl. Phys.* **82** (1997), 865.
- (306) A. Soliman, M. Aegerter, internal communication
- (307) W.Theiß, *Festkörperprobleme* **33** (1994), 149.
- (308) J.Ederth, *Electrical transport in nanoparticle thin films of gold and indium tin oxide*, Doctoral thesis, Uppsala University, 2003.
- (309) P.Innocenzi, G.Brusatin, R.Bertani, *Chem. Mater.* **11** (1999), 1672.
- (310) J.Gilberts, A.Tinnemans, M.Hogerheide, T.Koster, *J. Sol-Gel Sci. Technol.* **11** (1998), 153.
- (311) G.Hernandez, R.Rodriguez, *Journal of Noncrystalline Solids* **246** (1999), 209.
- (312) T.Gunji, Y.Makabe, N.Takamura, Y.Abe, *Applied Organometallic Chemistry* **15** (2001), 683.
- (313) T.Kololuoma, L.Johansson, J.Cambell, A.Tolonen, M.Halttunen, *Chem. Mater.* **14** (2002), 4443.
- (314) L.Scalvi, F.Messias, A.Souza, M.Li, C.Santilli, S.Pulcinelli, *Journal of Sol-Gel Science and Technology* **13** (1998), 793.
- (315) H.Imai, M.Yasumori, h.Hirashima, K.awazu, H.Onuki, *J. Appl. phys.* **79** (1996), 8304.
- (316) M.Kanamori, K.Suzuki, T.Yamada, Y.Ohya, Y.Takahashi, *Journal of the ceramic society of Japan Int.Edition* **103** (1995), 1244.

- (317) R.Tahar, T.Ban, Y.Ohya, Y.Takahashi, *J. Appl. Phys.* **83** (1998), 2631.
- (318) A.Lopes, E.Fortunato, P.Nunes, P.Vilarinho, R.Martins, *International Journal of Inorganic Materials* **3** (2001), 1349.
- (319) H.Fritzsche, B.Pashmakov, B.Claflin, *Solar Energy Materials and Solar Cells* **32** (1994), 383.
- (320) A.Hultåker, G.Niklasson, *Mat. Res. Symp. Proc.*, 581 (2000), 491.
- (321) F.Barlow, M.Naby, A.Joshi, A.Elshabini, *Solar Energy Mater. Solar Cells* **33** (1994), 63.
- (322) O.Park, J.Jung, B.Bae, *J. Mater. Res.* **16** (2001), 2143.
- (323) C.Lee, J.Hsu, C.Jaing, *Thin solid films* **295** (1997), 122.
- (324) H.Krug, N.Merl, H.Schmidt, *Journal of Noncrystalline Solids* **147** (1992), 447.
- (325) K.Tadanaga, T.Owan, J.Morinaga, S.Urbaneck, T.Minami, *J. Sol. Gel Sci. Technology* **2000** (2000), 791.
- (326) H.Yu, X.Feng, D.Grozea, Z.Lu, R.Sodhi, A-M. Hor, H.Aziz, *Appl. Phys. Lett.* **78** (2001), 2595.
- (327) J.Kim, R.Friend, F.Cacialli, *J. Appl. Phys.* **86** (1999), 2774.
- (328) J.Chaney, P.Pehrsson, *Applied Surface Science* **180** (2001), 214.
- (329) J.Kim, F.Cacialli, M.Gransröm, R.Friend, N.Johansson, W.Salaneck, R.Daik, W.Feast, *Synthetic Metals* **101** (1999), 111.
- (330) D.Milliron, I.Hill, C.Shen, A.Kahn, J.Schwartz, *J. Appl. Phys.* **87** (2000), 572.
- (331) K.Sugiyama, H.Ishii, Y.Ouchi, *J. Appl. Phys.* **87** (2000), 295.
- (332) M.Mazon, L.Hung, C.Tang, S.Lee, K.Wong, M.Wang, *J. Appl. Phys.* **86** (1999), 1688.
- (333) B.Vasil'ev, M.Kanganov, V.Lyuboshits, *Physics-Uspokhi* **37** (1994), 353.
- (334) J.Fan, J.Goodenough, *J. Appl. Phys.* **48** (1977), 3524.
- (335) T.Minami, T.Miyata, T.Yamamoto, *Surface coating and technology* **108-109** (1998), 583.
- (336) T.Ishida, H.Kobayashi, Y.Nakato, *J. Appl. Phys.* **73** (1993), 4344.
- (337) J.Kim, F.Cacialli, A.Cola, G.Gigli, R.Cingolani, *Synthetic Metals* **111-112** (2000), 363.
- (338) V.Henrich, P.Cox, *The Surface Science of Metal Oxides*, Cambridge Univ. Press., Cambridge, 1994.

- (339) J.Kim, B.Lägel, E.Moons, N.Johansson, I.Baikie, W.Salaneck, R.Friend, F.Cacialli, *Synthetic Metals* **111-112** (2000), 311.
- (340) Krüss-GmbH, *Kontaktwinkel-Messsystem Benutzerhandbuch* (1999), 138.
- (341) Z.Zhong, S-Yin, C.Liu, Y.Zhong, W.Zhang, D.Shi, C.Wang, *Applied Surface Science* **207** (2003), 183.
- (342) .MicrofabricationTechnology, http://www-inst.eecs.berkeley.edu/~ee143/f2002/Lab/four_point_probe.pdf, 2002.
- (343) B.Yoldas, *Applied Optics* **19** (1980), 1425.
- (344) R.Cahn, P.Hassen, E.Kramer, *Materials Science and Technology: A comprehensive Treatment*, 2A, VCH, New York, 1992.
- (345) G.Park, *Surface coating and technology* **115** (1999), 52.
- (346) I.Baikie, E.Venderbosch, J.Mayer, P.Estrup, *Rev. Sci. Instrum.* **62** (1991), 725.

List of Publications

1. C. GOEBBERT, H. BISHT, N. AL-DAHOUDI, R. NONNINGER, M. A. AEGERTER, H. SCHMIDT, *Journal of Sol-Gel Science and Technology*, 201-204 (2000).
2. C. GÖBBERT*, H. BISHT, N. AL-DAHOUDI, M. A. AEGERTER, Kurzreferate 74. Glastechnische Tagung, Ulm, 29./31.05.2000, Deutsche Glastechnische Gesellschaft e. V., pp 294-297.
3. N. AL-DAHOUDI, H. BISHT, C. GOEBBERT, T. KRAJEWSKI, M. A. AEGERTER*, in: Proc. of the 3rd International Conference on Coatings on Glass (3rd-ICCG), ed. H. A. Meinema, C.I.M.A. Spee, M. A. Aegerter, October 29-November 2, 2000, Maastricht, pp. 555-564.
4. N. AL-DAHOUDI, H. BISHT, C. GOEBBERT, T. KRAJEWSKI, M. A. AEGERTER, *Thin Solid Film*, 392, 299-304, 2001.
5. N. AL-DAHOUDI, M. A. AEGERTER*, in: Proc. of the Sixth International Conference on Frontiers of Polymers and Advanced Materials ICFPAM, 4-9 March, 2001, Recife/Brazil, in: *Mol. Cryst. Liq. Cryst.*, volume 374, 91-100, 2001.
6. N. AL-DAHOUDI, M. A. AEGERTER*, in: Proceedings of the 1st International Materials Symposium MATERIAIS 2001, 9.-11. April 2001, Coimbra/Portugal, in: *Key Engineering Materials*, volume 230-232, 555-558, 2002.
7. N. AL-DAHOUDI, M.A. AEGERTER*, in: Proceedings of the Sol-Gel Materials Conference 2001, 13.-16. Juni 2001, Rokosowo/Polen, in: *Materials Science*, volume 29 (1), 71-79, 2001.
8. N. AL-DAHOUDI, M.A. AEGERTER*, in: Proceedings of the Sol-Gel 2001, 11th International Workshop on Glasses, Ceramics, Hybrids and Nanocomposites from Gels, 16.-21.09.2001, Abano Terme, Italy, *Journal of Sol-Gel Science and Technology*, 26, 693-697, 2003.
9. N. Al-Dahoudi*, M.A. Aegerter, in: Kurzreferate 76. Glastechnische Tagung, Deutsche Glastechnische Gesellschaft – DGG, Bad Soden im Taunus, 27.-29. Mai 2002.

10. J. Puetz, F.N. Chalvet, G. Gapsarro, N. Al-Dahoudi, M.A. Aegerter*, in: Proceedings of the XI. International Materials Research Congress, Cancun/Mexiko, 25.29.08.2002, in print.
11. N. Al-Dahoudi; M. Aegerter; Journal of Sol-Gel Science and Technology, 26, 2003, 693-697.
12. M.A. Aegerter, N. Al-Dahoudi, in: Sol-Gel Coating of Plastic Substrate, Special issue of Journal of Sol-Gel Science and Technology, 27,2003, 81-89.

* *Presenting author*